Manukau Harbour Numerical Modelling

Metocean Study Report

Report prepared for Tonkin + Taylor

May 2024

MetOcean SOLUTIONS

Document History

Versions

Version	Revision Date	Summary	Reviewed by
0.1	08/06/2023	Draft document for internal review	Cussioli/Gardiner/Meirelles/Watson
0.2	08/06/2023	Draft document for client review	Berthot
0.3	12/06/2023	Revised draft	Watson/Thiebaut/Berthot
1.1	07/09/2023	Draft document for next stage of study for internal review	Watson
1.2	31/10/2023	Draft document for internal review	Watson/Thiebaut/Meirelles
1.3	10/11/2023	Draft document for client review	Berthot/Watson
1.4	02/02/2024	Revised draft	Watson/Thiebaut/Berthot
1.5	09/02/2024	Revised draft	Watson/Thiebaut/Berthot
1.6	13/02/2024	Revised draft	Watson/Thiebaut/Berthot
2.1	25/03/2024	Draft document for internal review	Watson/Berthot
3.0	02/05/2024	Final Version	Watson/Berthot

Distribution

Version	Date	Distribution
1.0	14/06/2023	Tonkin & Taylor
2.0	16/02/2024	Tonkin & Taylor
3.0	02/05/2024	Tonkin & Taylor

Document ID: P597-01

Authors

Berthot A., Watson H., Thiebaut S., Meirelles S., Cussioli M., Gardiner S.

MetOcean Solutions is a Division of Meteorological Services of New Zealand Ltd, MetraWeather (Australia) Pty Ltd [ACN 126 850 904], MetraWeather (UK) Ltd [No. 04833498] and MetraWeather (Thailand) Ltd [No. 0105558115059] are wholly owned subsidiaries of Meteorological Service of New Zealand Ltd (MetService).

Executive Summary

Earlier studies identified that the current Ports of Auckland Ltd (POAL) freight operation in the Waitematā Harbour is likely to run out of capacity to cater for Auckland's long-term freight needs. The Manukau Harbour has previously been identified as a potential port location, however there are unanswered questions around the technical feasibility of this given the complex and dynamic nature of the harbour entrance along with other factors associated with greenfield port development.

Te Manatū Waka / the New Zealand Ministry of Transport has appointed Tonkin & Taylor Ltd and their subconsultants (Royal HaskoningDHV, MetOcean Solutions (MOS), Pacific Marine Management, the University of Auckland, Discovery Marine Limited, and RMA Science) to undertake a feasibility study to understand whether it would be technically possible to locate a port in the Manukau Harbour from a navigation and operational reliability perspective. Environmental, social, and economic factors are not part of the current scope of work.

MetOcean Solutions has undertaken a numerical modelling study to support this feasibility study. The modelling work is presented in two reports:

1. TWP03b (MOS) - Numerical modelling - Metocean study report - MOS Report P0597-01
2. TWP03c (MOS) - Numerical modelling - Sediment Transport report – MOS Report P0597-02

This report is presenting the Metocean study (i.e. first report).

A review of all available global model dataset and measured data near or within Manukau Harbour, as well as the field data collection undertaken for this project (presented in TWP02a - (TT) -Fieldwork), was undertaken to identify data to use as input, calibration or validation of the numerical models.

A digital elevation model for the present morphology of the entrance bar based on the 2023 bathymetry survey collected for this project was prepared (see Figure 1). Another digital elevation model was prepared with the proposed concept navigation channel (see Figure 2) within the natural South West channel of Manukau Harbour entrance.

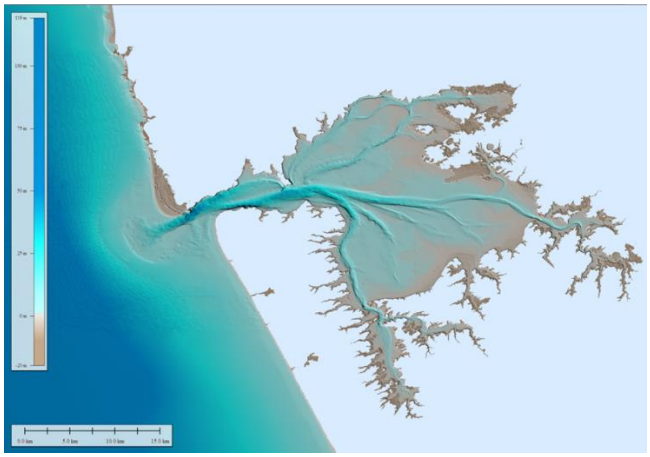

Figure 1: Final bathymetry dataset (bar region based on 2023 survey data (DML 2023)).

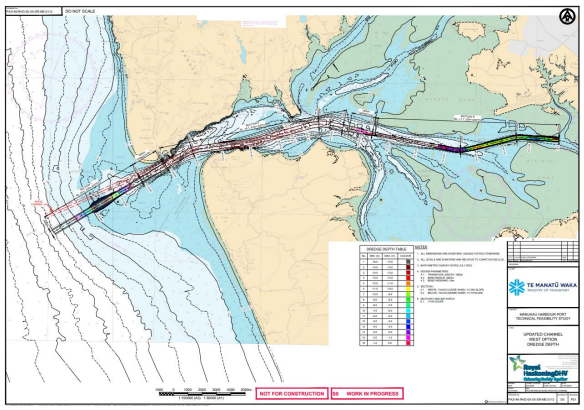

Figure 2 Concept navigation channel within Manukau Harbour.

A SWAN Wave model for the Manukau Harbour, entrance and coastal area was setup and validated (see Figure 3) . A DelftFM coupled Wave /Hydrodynamic model was also setup and validated (see Figure 4). The validations were undertaken using existing global data sets, available measured data and in situ data collected as part of this project and presented in the TWP02a - (TT) - Fieldwork. The models were validated in terms of water level, waves and currents and showed good agreements with the measured data. This provided confidence in the model ability to reproduce the hydrodynamic, wave and sedimentr transport processes on the Manukau entrance bar and within the Manukau Harbour

The SWAN model was run to prepare a 41- year hindcast on the existing bathymetry and a 10-year hindcast on the concept channel bathymetry (South West Channel). The model was also used to provide wave boundary input to the DelftFM model.

The DelftFM model was run for a full year on both the existing bathymetry and the concept channel design bathymetry of the South West Channel.

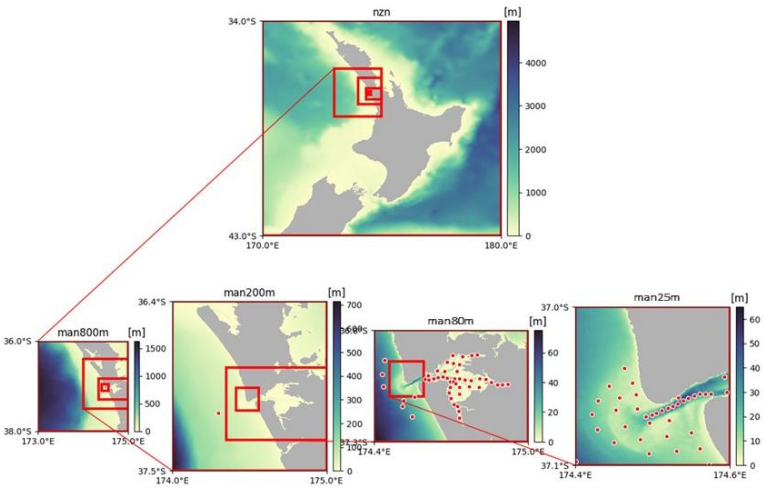

Figure 3 Bathymetry map showing the area of interest and the successive wave model nests including the model output locations.

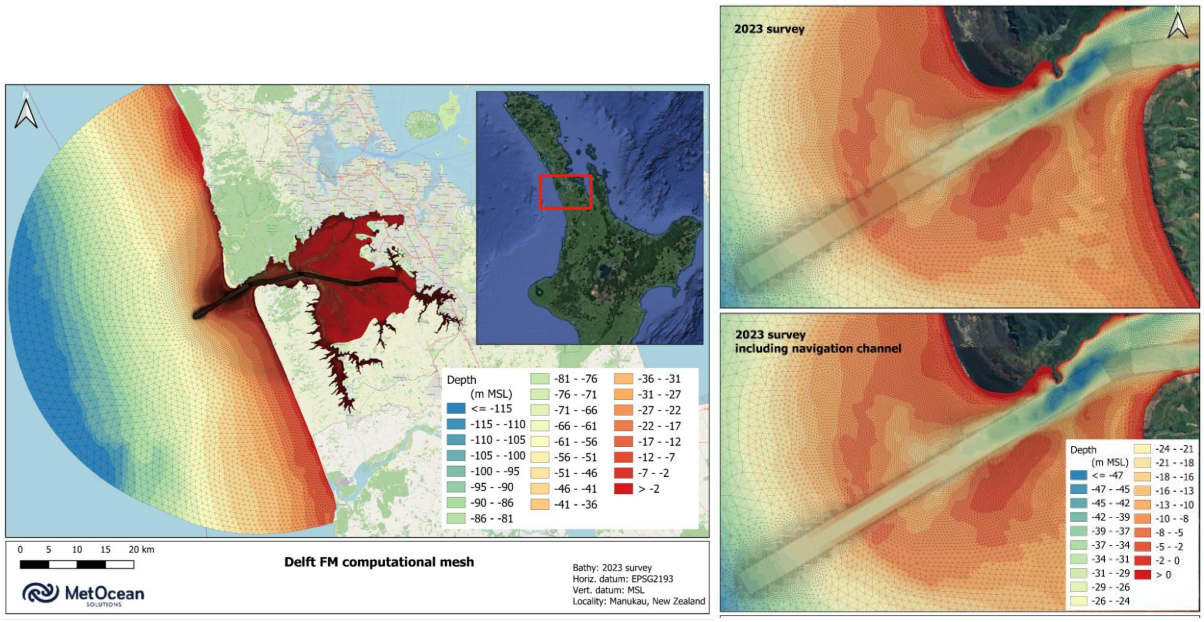

Figure 4: Delft FM computational mesh of Manukau Harbour (left). The model bathymetry near the Manukau entrance bar for the 'existing' simulation is shown on top right panel and for the channel 'design' simulations on the bottom right panel.

The model hindcast datasets were used to define ambient/operational wave and current conditions, extreme wave conditions on the bar, harbour entrance and along the proposed navigation channel, assess the potential impact of the proposed channel on water level, current and wave conditions.

An example of the ebb and flood currents for the 'existing' and channel 'design' from the DelftFM model simulations are show on Figure 5. Tidal currents are strong within the Manukau entrance and close to 2.5 $m.s^{-1}$ during peak spring tide. An example of the wave patterns near the entrance bar is shown on Figure 6.

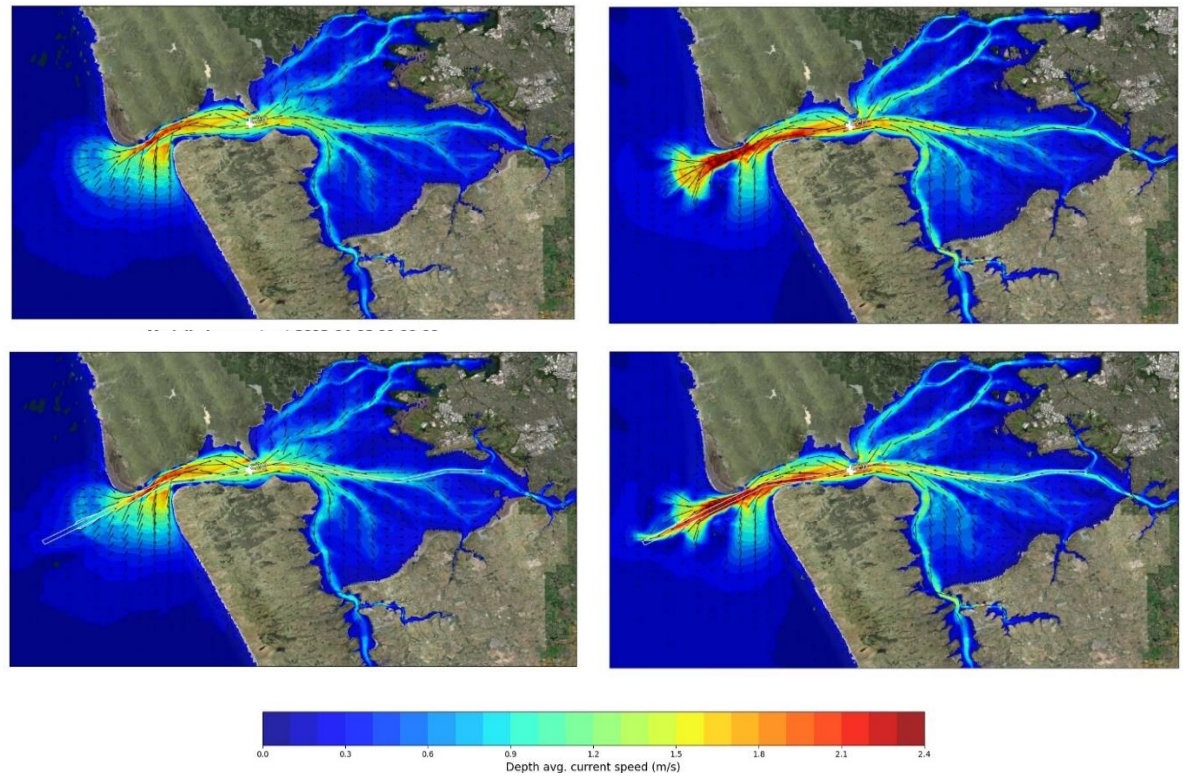

Figure 5 Modelled spring tidal current magnitudes and vectors for the 'existing' simulation at peak flood tide (top left) and peak ebb tide (top right) and for the channel design simulation at peak flood tide (bottom left) and peak ebb tide (bottom right).

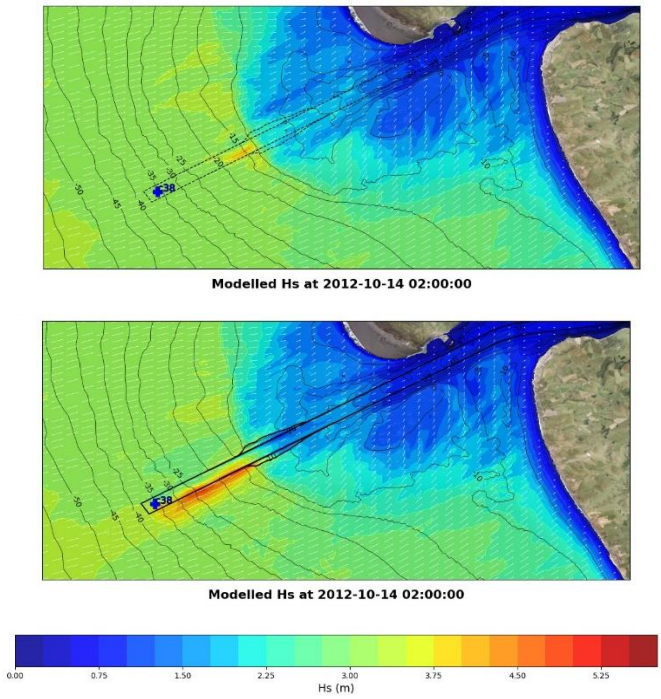

Figure 6 Modelled wave heights for the existing (top) and channel 'design' (bottom) simulation over Manukau bar during a wave event.

Results showed that the mean wave height offshore Manukau is about 2.5 m with waves exceeding 3 m for 20% of the time. Peak wave periods are typically between 10 and 16 seconds. The waves are mostly from the southwest to west sector, with waves from the northwest sector only occuring about 2% of the time. The 1-year and 100-year Return Period wave height is about 6.9 m and 10.6 m, respectively.

Modelling results were provided as data file, maps and tabulated values to the other project work stream teams. The data has been used for the analysis presented in the coastal processes assessment (TW03 (TT) – Coastal Processes) the navigation and channel design assessment (TW04 (RH) – Navigation and Channel Design and TW05 (PMM) – Navigational Operability).

A high level assessment of the potential change in water levels, waves and currents with the proposed South West navigation channel compared to the existing case was undertaken. Small changes in currents (less than 0.2 $m.s^{-1}$) are observed within the harbour however they are likely mostly related to a change in phasing of the flood and ebb currents with the channel in place compared to the existing. The channel also led to a small increase in the tidal prism and a potential for higher water level in the upstream branches of the harbour. Potential changes in wave height were minimal and mostly confined to the entrance bar and channel.

In addition to the detailed metocean assessment for the prefered concept navigation channel within the natural South West Channel, a high level assessment of a concept navigation channel in the South Channel was also undertaken. This may be further developed if this option is considered at a later stage.

Contents

List of Figures

List of Tables

1.Introduction

Earlier studies identified that the current Ports of Auckland Ltd (POAL) freight operation in the Waitematā Harbour is likely to run out of capacity to cater for Auckland's long-term freight needs.

The Manukau Harbour has previously been identified as a potential port location, however there are unanswered questions around the technical feasibility of this given the complex and dynamic nature of the harbour entrance along with other factors associated with greenfield port development.

Te Manatū Waka / the New Zealand Ministry of Transport has appointed Tonkin & Taylor Ltd and their subconsultants (Royal HaskoningDHV, MetOcean Solutions (MOS), Pacific Marine Management, the University of Auckland, Discovery Marine Limited, and RMA Science) to undertake a feasibility study to understand whether it would be technically possible to locate a port in the Manukau Harbour from a navigation and operational reliability perspective. Environmental, social, and economic factors are not part of the current scope of work.

This study will support on-going work by the Ministry on the National Freight and Supply Chain Strategy, which is examining New Zealand's freight system for the next 30 years.

MetOcean Solutions scope include developing calibrated wave (spectral), hydrodynamic and sediment transport models of the harbour and entrance to inform navigation and maintenance dredging requirements.

The modelling work is presented in two reports:

3. TWP03b (MOS) - Numerical modelling - Metocean study report - MOS Report P0597-01
4. TWP03c (MOS) - Numerical modelling - Sediment Transport report – MOS Report P0597-02

This report is the first of the two and present the data, wave and hydrodynamic model setup, validation and simulations, the hindcast results and metocean analysis.

This report covers a description of modelling approach in Section 3. The available data and datums and projections used are presented in Section 3. In Section 4 a description of the numerical models used, setup and the completed and planned validation of the models is provided, this includes the global wind hindcast, SWAN wave hindcast and coupled Delft FM hydrodynamic wave and sediment transport model. Section 5 presents the results from the modelling. References are given in Section 6.

2.Modelling Approach Overview

Our modelling methodology for defining the metocean conditions (water level, waves, and current) offshore, in the entrance and within Manukau Harbour, understanding the complex coastal and entrance bar processes and estimating the potential sedimentation in a navigational channel is shown in Figure 2-1.

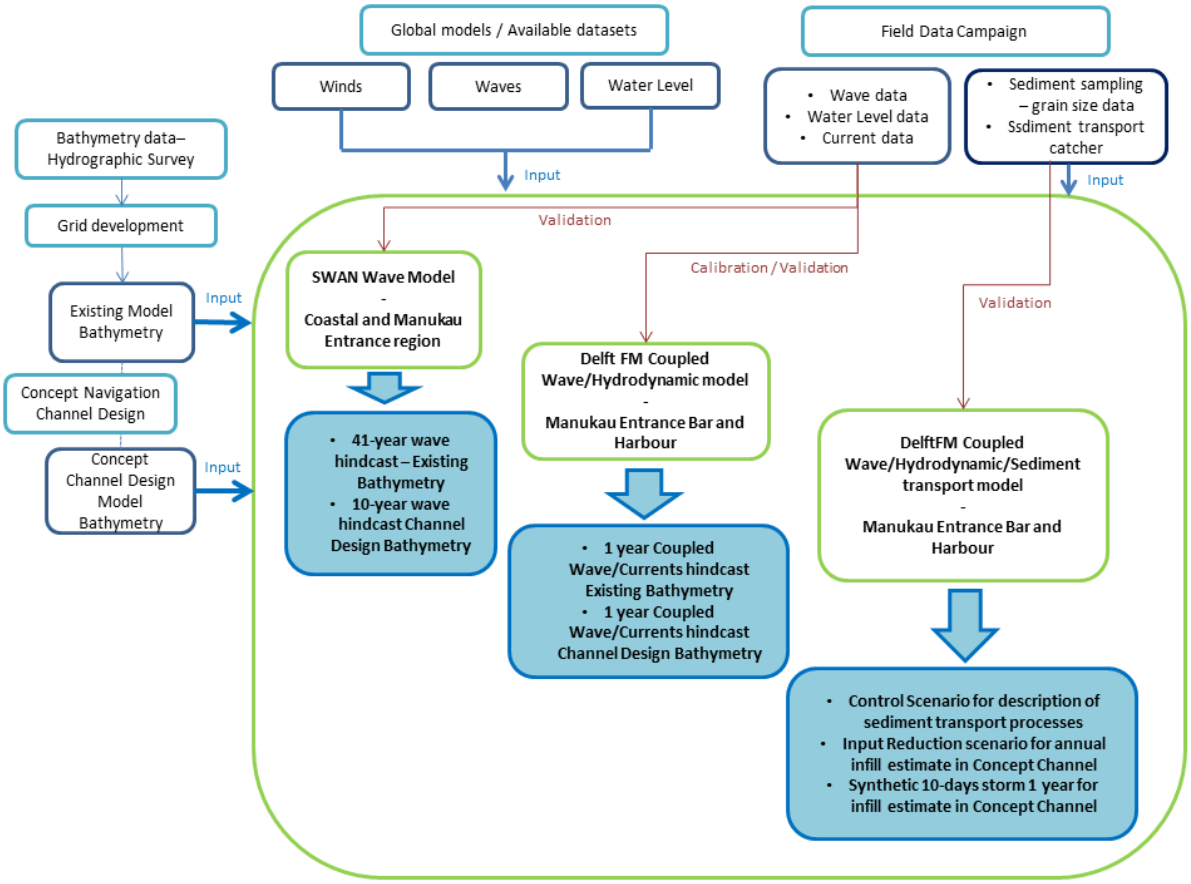

Figure 2-1: Numerical modelling methodology

The numerical modelling methodology consists of the following steps:

- Model domain bathymetry preparation: A range of existing bathymetry data was sourced and compiled into a digital elevation model. The hydrographic survey collected for this project was added to the initial bathymetry composite to have a contemporary representation of the entrance bar (see TWP02 (TT) – Fieldwork). This was used to prepare our numerical model bathymetry. The navigation and channel design team provided a concept design drawing for the navigational channel which was implemented in the existing digital terrain model to prepare a model bathymetry with the proposed South West Channel in place.

- Metocean input: Winds, wave and water levels dataset were sourced from global reanalysis dataset as well as in house New Zealand wide hindcast dataset and used as forcings for all the proposed numerical models.
- Field data Campaign: A field data campaign was undertaken specifically for this project by Tonkin + Taylor. The data collection included measurement of water level, wave, currents, sediment transport as well as seabed sediment sampling and particle size distribution analysis. This data was either used for validation or as input parameters (e.g. sediment grain size) for the numerical models.
- Numerical models description:
    - A SWAN Wave model was setup, validated and run for a 41- year hindcast on the existing bathymetry and a 10-year hindcast on the concept channel bathymetry (South West Channel). This dataset was used to define long term wave climate offshore and near the entrance of Manukau Harbour.
    - DelftFM Coupled Wave /Hydrodynamic model was setup, validated and run for a full year on both the existing bathymetry and the concept channel design bathymetry of the South West Channel. The model simulates current and waves forced by wind, tide, oceanographic currents and river discharge.
    - DelftFM Coupled Wave /Hydrodynamic/Sediment transport model was setup, validated and run for a selection of metocean forcing scenario. The model simulations were separated in two groups: control scenarios (i.e. 17 scenarios of various tide, wave and wind forcing conditions) used to better understand the sediment transport patterns over the entrance bar, and input reduction scenarios (i.e. 34 scenarios representative of main offshore waves conditions) used to provide a detailed baseline of sediment erosion/ deposition data used for the estimate of annual infill in the concept navigation channel design. The methodology for the calculation of the annual infill used a combination of the offshore wave climate from the 40-years wave hindcast and the sediment infill rate for each input reduction scenario. The methodology is further described in the (separate) Sediment Transport report. The model was also run for a 10-days storm to confirm the suitability of the annual estimate modelling approach and identify morphological change that could occurs in a single event.

3.Input Data Overview

3.1 Datums and projections

The project datum and coordinate system adopted for this study are as follows:

- Vertical Datum: Chart Datum (CD) Onehunga
- Coordinate: NZTM2000 (EPSG: 2193)

Mean sea level at Onehunga is 2.43 m above CD (based on the LINZ tide tables) but some data is referenced to the Paratutae Datum which is 2.33 m above CD. The NZVD2016 is 2.5 m above Onehunga.

For the vertical datums used in the numerical models in this study, all model bathymetry and water levels are relative to MSL (CD + 2.43 m).

Both cartesian and spherical projections were used for the site. Delft FM modelling used cartesian coordinates using the NZGD2000 / New Zealand Transverse Mercator 2000 with EPSG 2193. The wave hindcast ran on the spherical projection WGS 84 (World Geodetic System 1984 ensemble) with EPSG 4326.

3.2 Bathymetry

Bathymetry data sources for the Manukau region (Table 3-1 and Table 3-2) include scanned sounding sheets obtained from LINZ, however the west coast of this region has not been historically surveyed in much detail and most of the data is relatively old. Single beam data has been collected by Ports of Auckland (POAL) (Table 3-2) and LiDAR (Light detection and ranging) data has been collected by Auckland Council for substantial areas of the coast and intertidal areas. This data can be accessed through the LINZ data service (https://data.linz.govt.nz/).

An initial composite bathymetry was constructed in Global Mapper, combining the 2020 single beam survey from POAL, available LiDAR, ENCs and digitised fairsheets. The latest fairsheet for the bar area dated from 1989 (Figure 3-1). This initial composite was prepared considering the priority order of the data as follow:

1989 Composite Bathymetry:

1. LIDAR (2016-2018) Auckland north and LiDAR (2016-2017) Auckland south
2. Digitised Fair sheets (mostly 1989 over bar and 1962 offshore)
3. LINZ ENC charts.

A final composite bathymetry was collated using the DML 2023 survey completed as part of this project. The survey undertaken in May to June 2023 by Tonkin & Taylor and Discovery Marine Ltd (DML) involved a hydrographic survey using a single beam echo sounder across the study area, with supplementary spot depths using a helicopter dipping with a pressure transducer to cover shallow areas. A full description of this dataset is described in Section 3.1 of the Tonkin & Taylor fieldwork report (Tonkin & Taylor Ltd, 2024).

The priority order of the data for this composite bathymetry was as follow:

2023 Composite Bathymetry (Figure 3-2):

1. LIDAR (2016-2018) Auckland north and LiDAR (2016-2017) Auckland south (blue)
2. DML 2023 survey (green)
3. Helicopter dip bathy points (red points)
4. Other POA bathy
5. 1961 sounding sheets (closest matched the current 2023 bar configuration) (pinks)
6. LINZ ENCs (white)
7. Contours produced by hand to aid gridding between survey run lines.

The 1989 and 2023 composite bathymetry are presented in Figure 3-3 and Figure 3-4.

Table 3-1 Bathymetry data and sources for the Auckland Region west coast

Data	Source	Comments
Fairsheets (43, 4315, 4314)	LINZ data service	Coverage good in Manukau harbour, patchy on the coast
ENCs (Electronic Navigation Charts)	LINZ data service	Fills in gaps
LIDAR (2016-2018) Auckland north LiDAR (2016-2017) Auckland south	LINZ data service (Auckland Council)	Good coverage for the coastal region and intertidal for the whole of the west coast. Quality can be patchy.
Multibeam/singlebeam survey data	Ports of Auckland (POAL)	Manukau Harbour mouth/south channel, navigation survey.
Singlebeam survey data of the Manukau Harbour entrance and main channels March 2023	DML	Survey data collected for this project

Table 3-2 Multiple bathymetry datasets have previously been collected by POAL (Ports of Auckland)

Year	Area	Date	Info
2001	SW Channel	28/09/2001	POAL
2002	SW Channel	10/10/2002	POAL
2003	SW & S Channel	13/01/2003, 17/01/2003, 10/07/2003, 11/11/2003	POAL
2004	SW Channel	27/01/2004, 21/05/2004, 30/09/2004	POAL
2005	SW Channel	12/04/2005, 01/09/2005, 14/10/2005	POAL
2006	SW Channel	20/04/2006, 16/08/2006	POAL
2007	SW Channel	24/01/2007, 29/11/2007	POAL
2008	SW Channel	11/04/2008, 07/08/2008, 03/12/2008	POAL
2009	SW Channel	04/04/2009, 27/07/2009	POAL
2010	SW Channel	04/02/2010, 19/05/2010, 29/09/2010	POAL
2011	SW Channel	11/01/2011, 12/04/2011, 17/07/2011	POAL
2012	SW & S Channel	09/02/2012, 28/04/2012, 15/06/2012, 10/07/2012, 10/12/2012	POAL
2013	SW & S Channel	22/01/2013, 15/05/2013, 03/09/2013, 05/11/2013, 27/11/2013	POAL
2014	SW & S Channel	21/02/2014, 01/05/2014, 27/08/2014, 09/12/2014	POAL
2015	SW Channel	04/03/2015, 18/06/2015, 03/12/2015	POAL
2016	SW Channel	24/02/2016, 03/06/2016, 02/09/2016, 04/12/2016	POAL
2017	NIL		
2018	SW Channel	26/04/2018, 17/12/2018 – Sanfords own the data	Sanfords
2019	NIL		
2020	SW Channel	27/02/2020 – Sanfords own the data	Sanfords
2021	NIL		
2022	NIL		

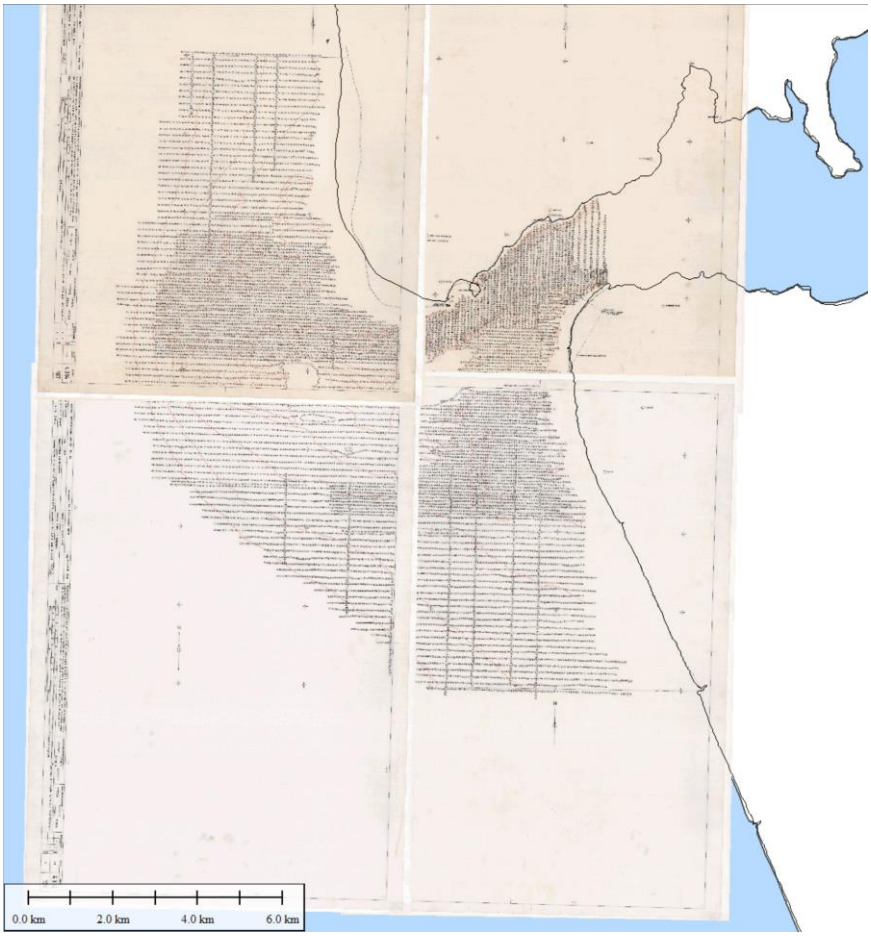

Figure 3-1 LINZ scanned sounding sheets number 4314 – Manukau Harbour mouth 1989.

Table 3-3 Bathymetry data and sources for the Auckland Region west coast

Data	Source	Comments
Fairsheets (43, 4315, 4314)	LINZ data service	Coverage good in Manukau harbour, patchy on the coast
ENCs (Electronic Navigation Charts)	LINZ data service	Fills in gaps
LIDAR (2016-2018) Auckland north LiDAR (2016-2017) Auckland south	LINZ data service (Auckland Council)	Good coverage for the coastal region and intertidal for the whole of the west coast. Quality can be patchy.
Multibeam/singlebeam survey data	Ports of Auckland (POAL)	Manukau Harbour mouth/south channel, navigation survey.
Singlebeam survey data of the Manukau Harbour entrance and main channels March 2023	DML	Survey data collected for this project

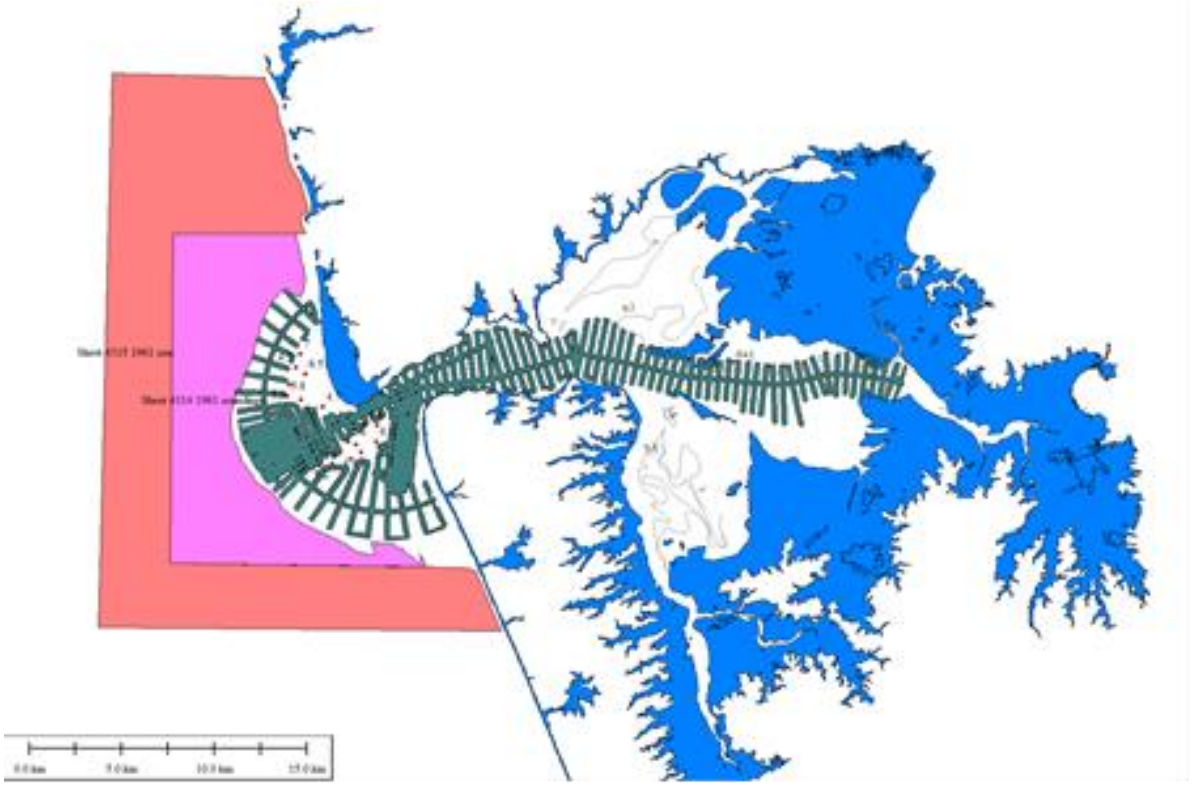

Figure 3-2 Bathymetry dataset used in the preparation of the 2023 composite bathymetry. LIDAR data (blue), Tonkin & Taylor/DML 2023 survey (green), Helicopter dip bathy points (red points),1961 sounding sheets (closest matched the current bar configuration) (pinks) and LINZ ENCs (white)

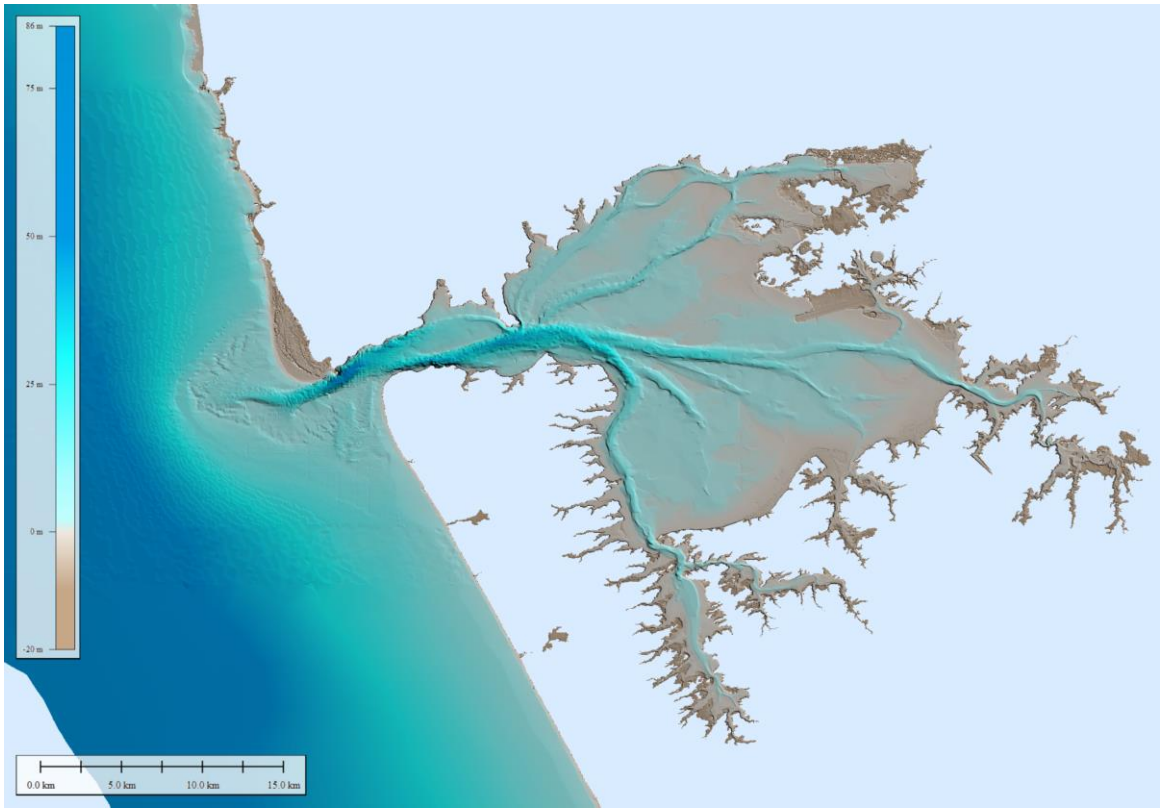

Figure 3-3 Initial composite bathymetry constructed over Manukau Harbour (bar region based on 1989 soundings).

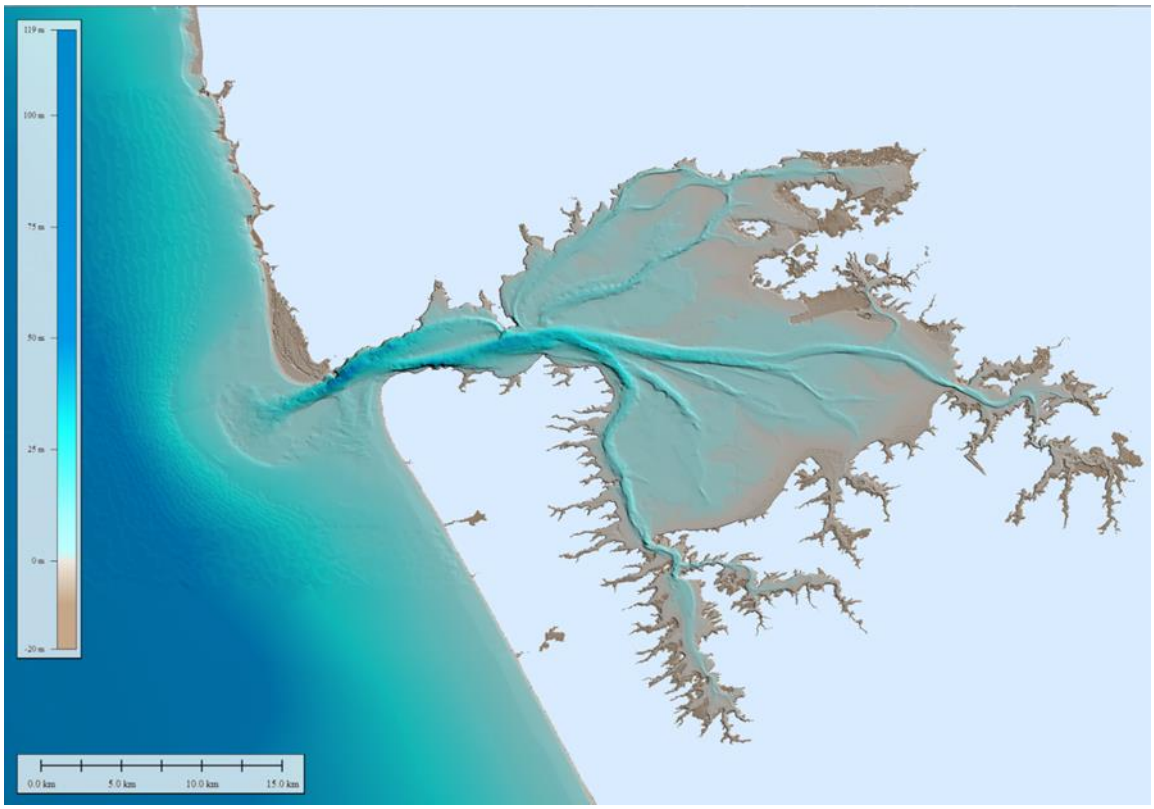

Figure 3-4 Final bathymetry dataset (bar region based on 2023 survey data (DML 2023)).

In order to assess the morphology of the bar region, fairsheets that had sufficient coverage of the region were examined and contours taken from the data. These included data from 1961, 1965, 1977, 1982 and 1989. Data from 1961 and 1965 were recorded in feet and fathoms and this was converted to meters. Figure 3-5 shows how the main channel can shift from and more north-westerly alignment, such as in 1961 and 1965 to a more south-westerly alignment in 1977 and 1982 and then back more north-westerly again in 1989 (see a more detailed assessment in TWP03a (UOA) - Historic bar and channel dynamics).

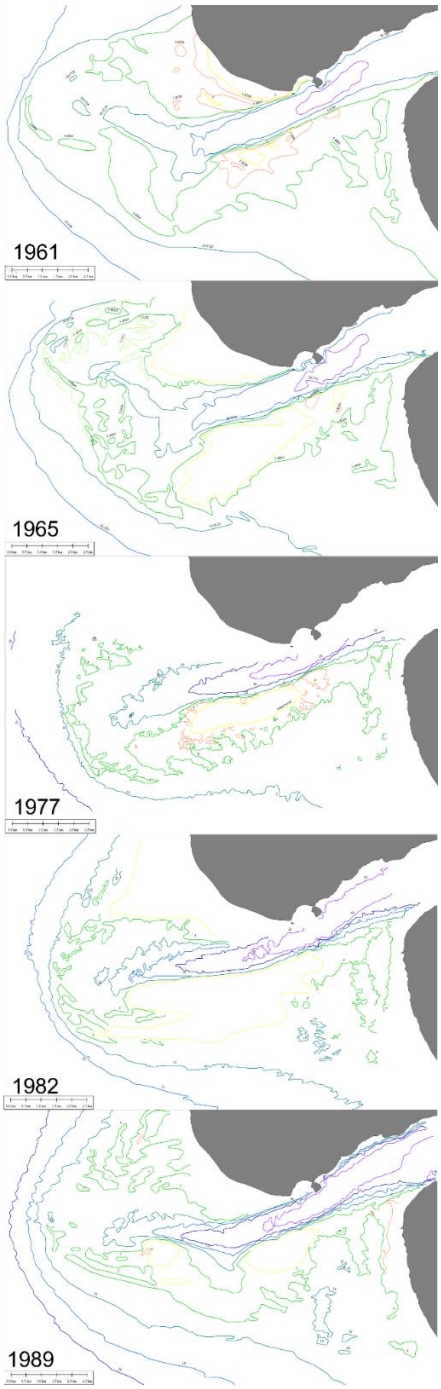

Figure 3-5 Bar morphology from multiple fairsheet surveys.

3.3 Concept navigation channel

The concept navigation channel for Manukau Harbour is shown in Figure 3-6(TWP04 (RH) - Navigation and Channel Design). The design was incorporated into the model mesh for Delft FM and the dredge design was incorporated into the 2023 bathymetry survey. The dredge depth require to incorporate the concept navigation channel design depths into the 2023 survey is displayed in Figure 3-7 where a negative value is the amount of sediment needed to be dredged to achieve design depth.

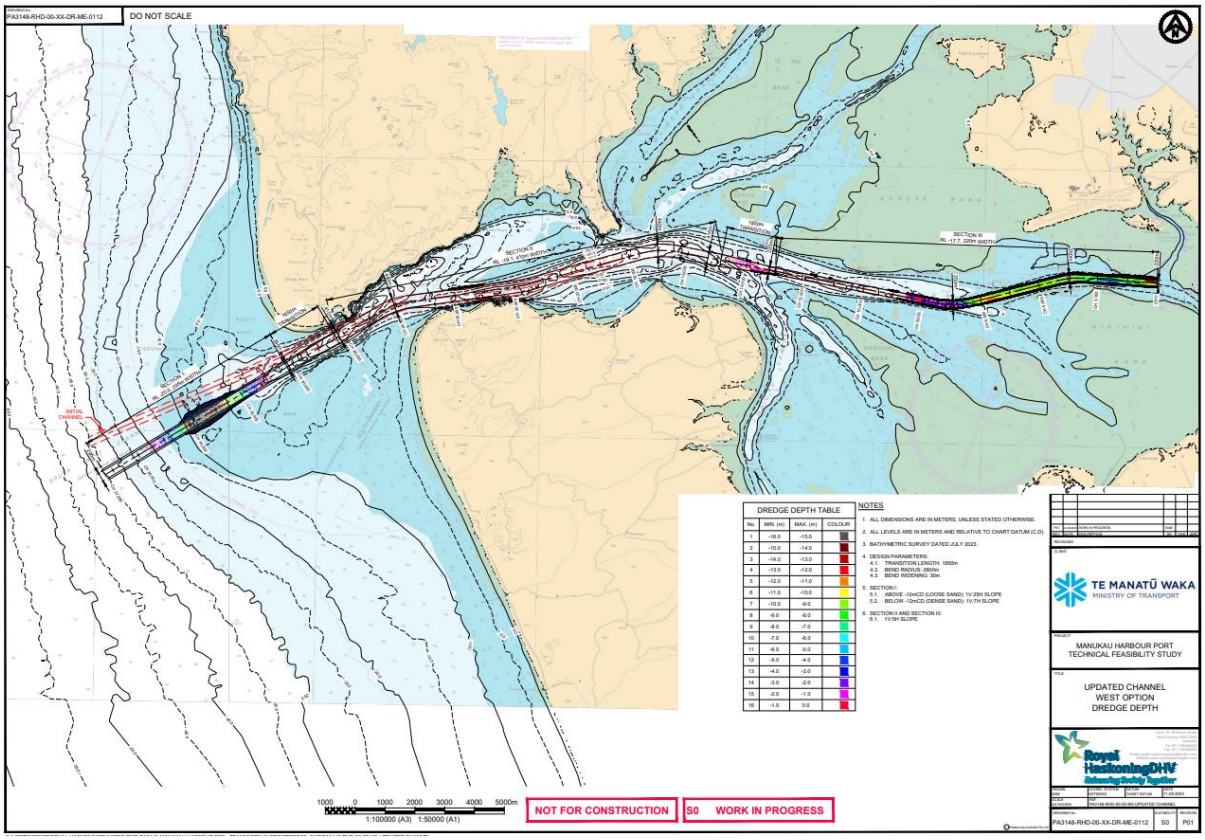

Figure 3-6: Concept navigation channel within Manukau Harbour.

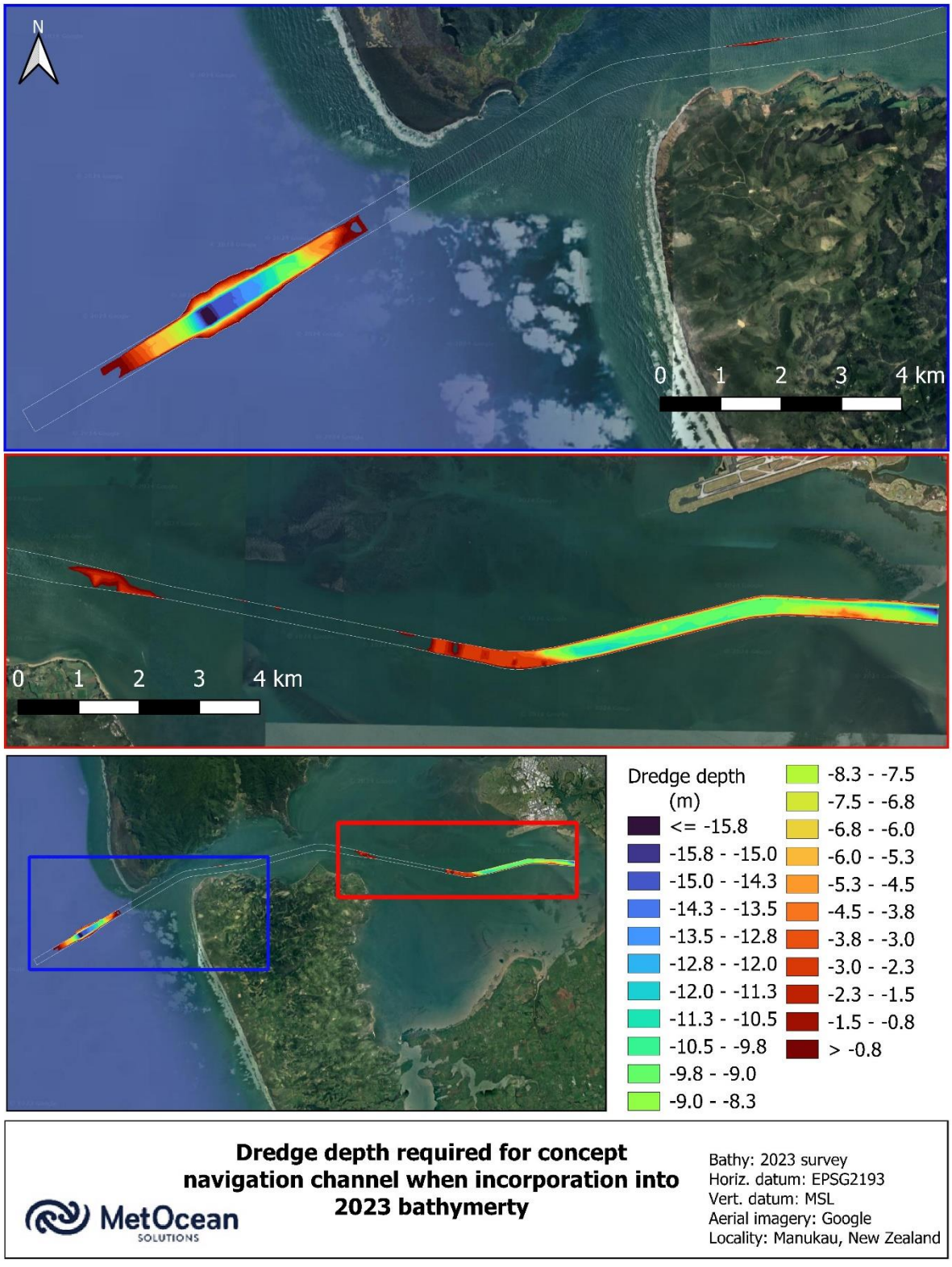

Figure 3-7: Dredge depth required to incorporate the concept navigation channel within Manukau Harbour 2023 bathymetry.

3.4 Metocean data

3.4.1 Project field data collection campaign

A fieldwork campaign has been designed to acquire data specifically for this project. This is providing data that did not presently exist or provides up-to-date information to complement or compare to existing data. Tonkin & Taylor managed and delivered the measured data, the full descriptions of the fieldwork instruments, data collection and processing is available in the TWP02 (TT) – Fieldwork. A map of the instrument locations already available or deployed for this project are presented in Figure 3-8.

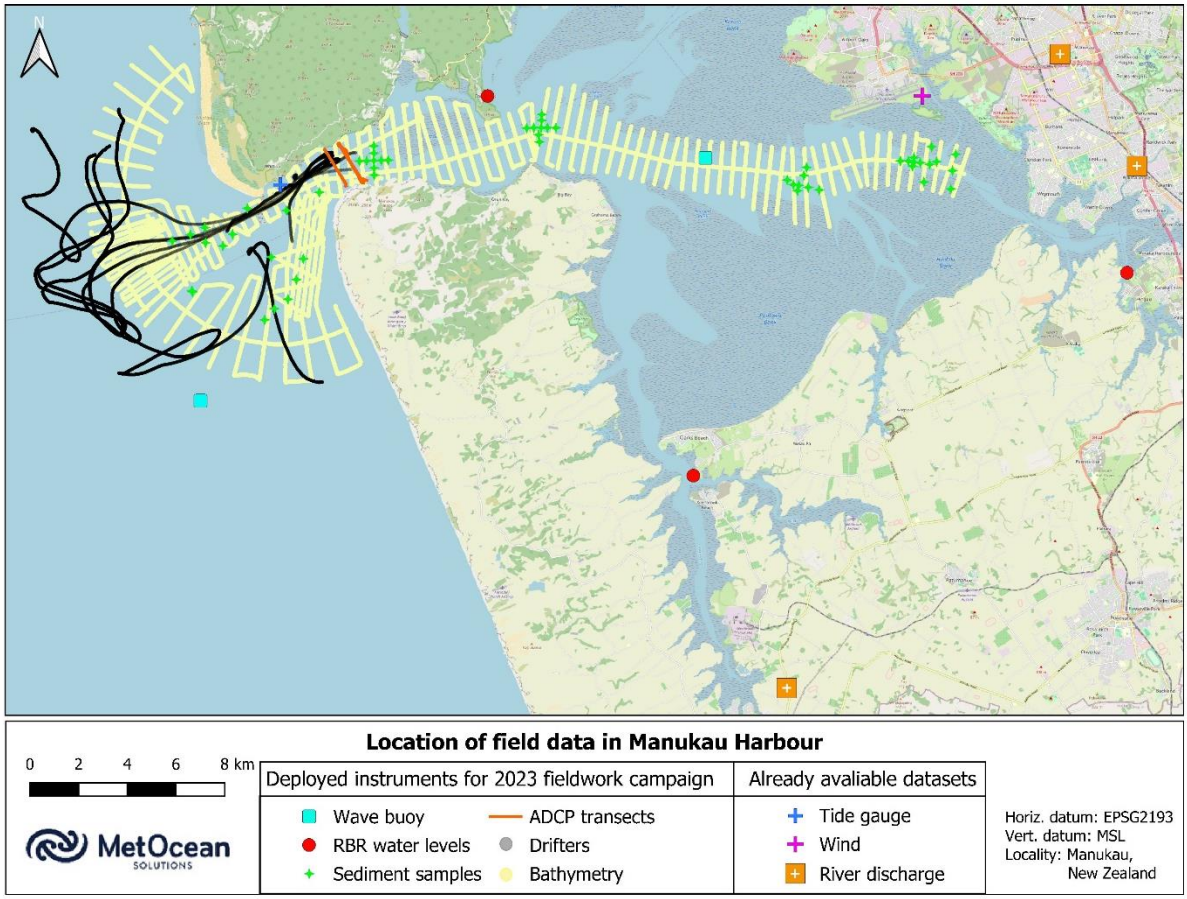

Figure 3-8: Field data map showing instruments and deployment locations.

3.4.2 Water level

Three RBR instruments measuring water levels were deployed within Manukau Harbour for the field data collection campaign by Tonkin & Taylor. Measurements at Cornwallis and Waiuku were over 117 days, the depths are displayed in Figure 3-9. Measurements at Karaka cover 16 days as shown in Figure 3-10. The raw measurements were provided in metres above gauge zero with no reference to a datum.. The water level measurements were adjusted to be around MSL by taking the mean water level over the period.

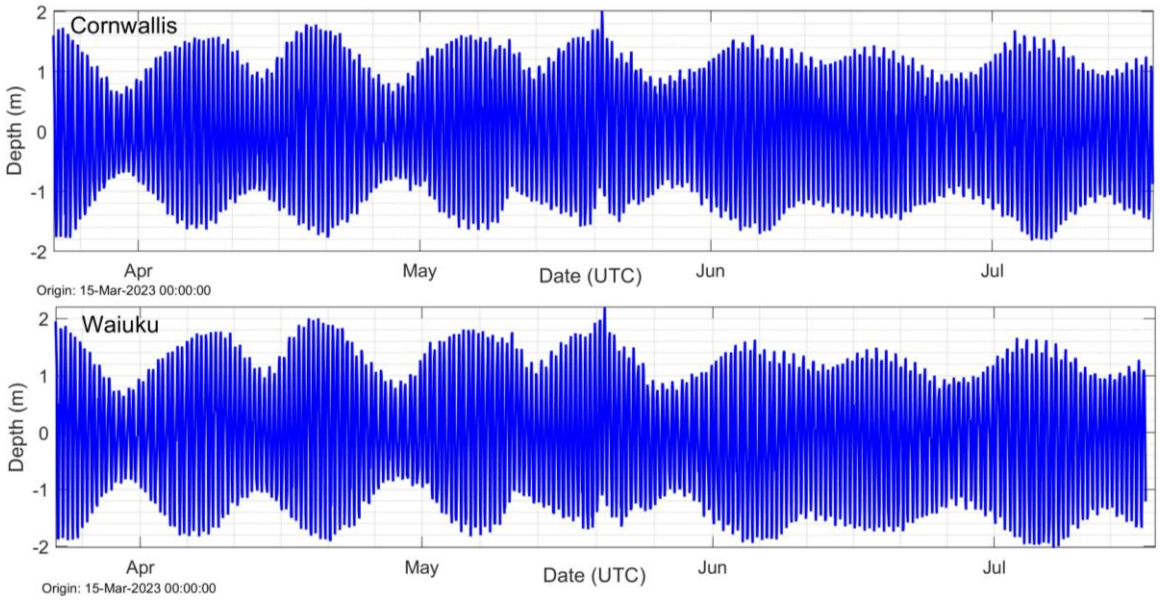

Figure 3-9 Measured water levels (MSL) at Cornwallis and Waiuku.

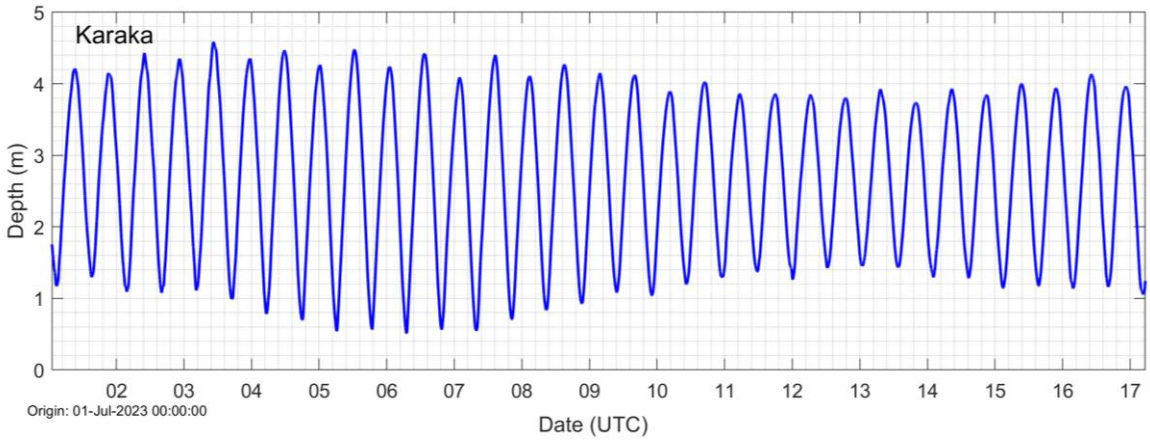

Figure 3-10 Measured water levels (MSL) at Karaka.

Water level data is also available from the tide gauge at Paratutae Island which is located on the northern side of the Manukau entrance and on the western side of the island (-37.0466, 174.5113). The gauge is maintained by LINZ (Land Information New Zealand) but since its installation (July 2010) it does not measure against any referenced datum; the station information states that the levels are referenced to an arbitrary point above gauge zero. According to LINZ Nautical cartographer, *"the sensors are liable to drift and caution is advised when using them for scientific analysis*". The data is also available via the IOC (Intergovernmental Oceanographic Commission) of UNESCO hosted sea level station monitoring facilities as Manukau station. The data was extracted directly from the LINZ access which has two sensors for the site (sensor 40 and sensor 41) for redundancy purposes.

The water levels for the full period available are displayed in Figure 3-11. The data is displayed in metres above gauge zero with no reference to a datum. The Paratutae Sounding Datum of 2.33 m may be used to correct the measured data to be around MSL. The Sounding Datum was derived by POAL and used from 2011 onwards, shortly after the tide gauge had been installed. There is noticeable upward shift in the water levels after September 2020 which is not explained in any of the station information. Due to this and the caution from LINZ, this dataset was only used as a comparison water level in the initial setup and running of the model.

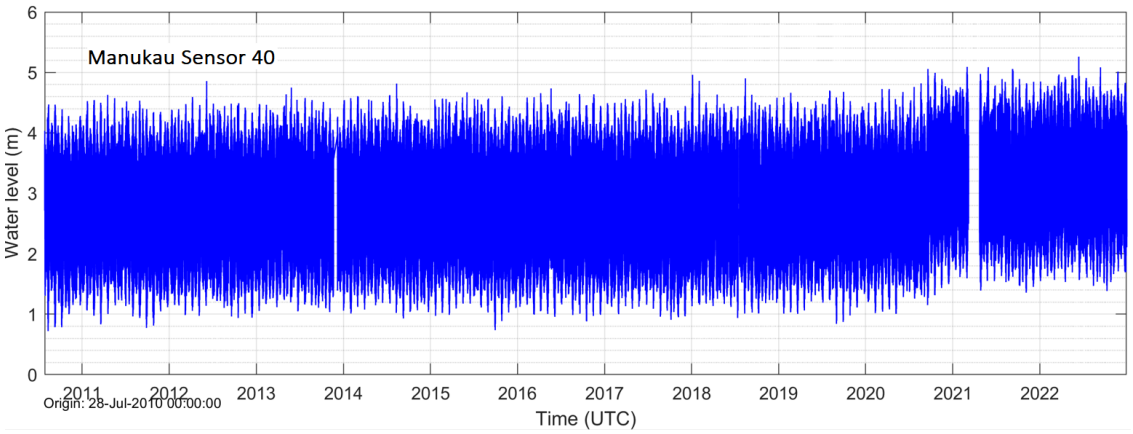

Figure 3-11 Measured water levels at Paratutae Island Manukau.

3.4.3 Waves

Two wave buoys were deployed by Tonkin & Taylor, one offshore and one in the inner harbour. The measured wave parameters for both instruments are displayed in Figure 3-12 and Figure 3-13. For comparisons mean wave period was used as peak period measurements seemed to be overestimated and used set period bins.

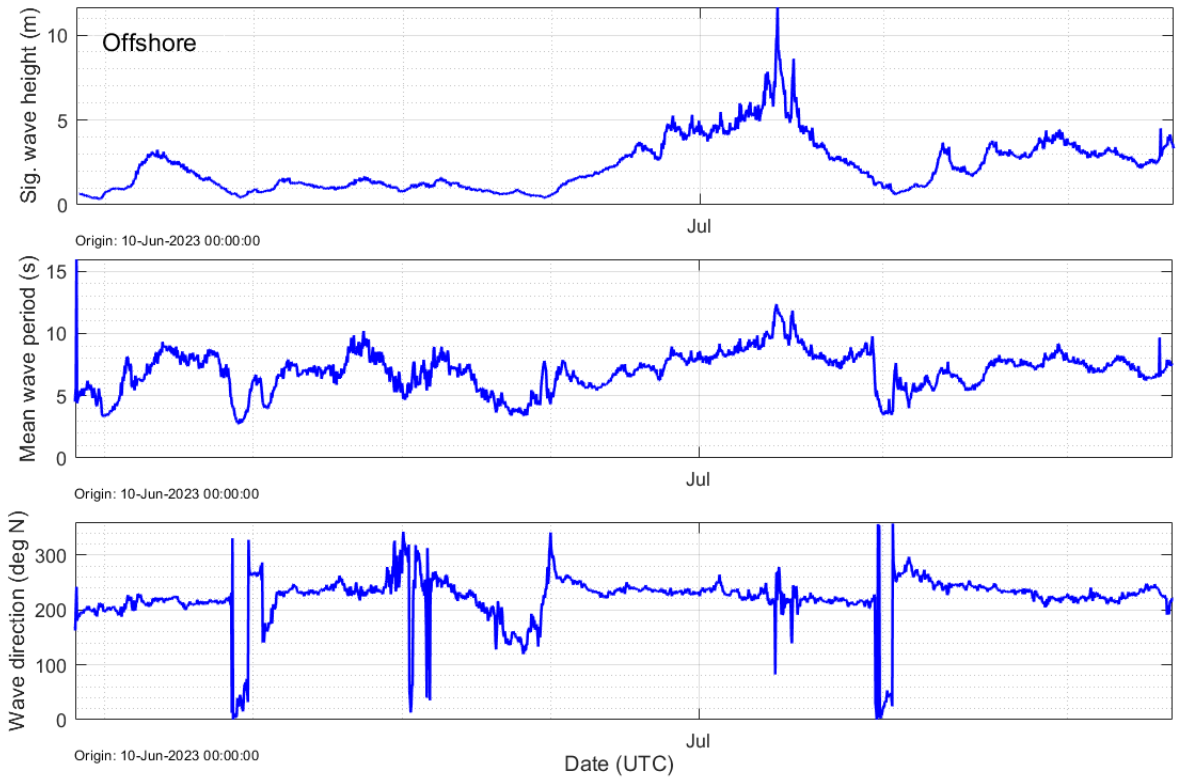

Figure 3-12 Measured wave parameters at the offshore wave buoy.

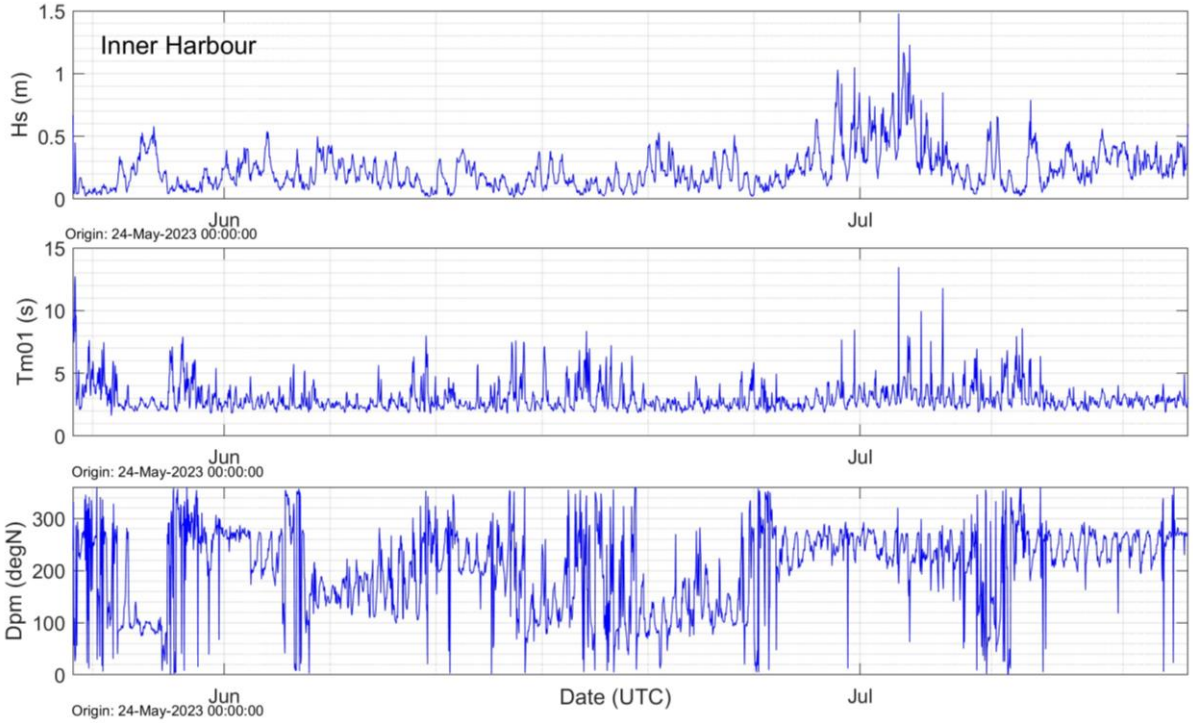

Figure 3-13 Measured wave parameters at the inner harbour wave buoy.

3.4.4 Currents

3.4.4.1 Drifters

Five surface current drifters were deployed and retrieved by Tonkin & Taylor in the Manukau Harbour entrance over the 10th-11th June 2023. The instruments recorded location and time at regular intervals from which a speed could be calculated. Figure 3-14 displays the current speeds for each drifter track.

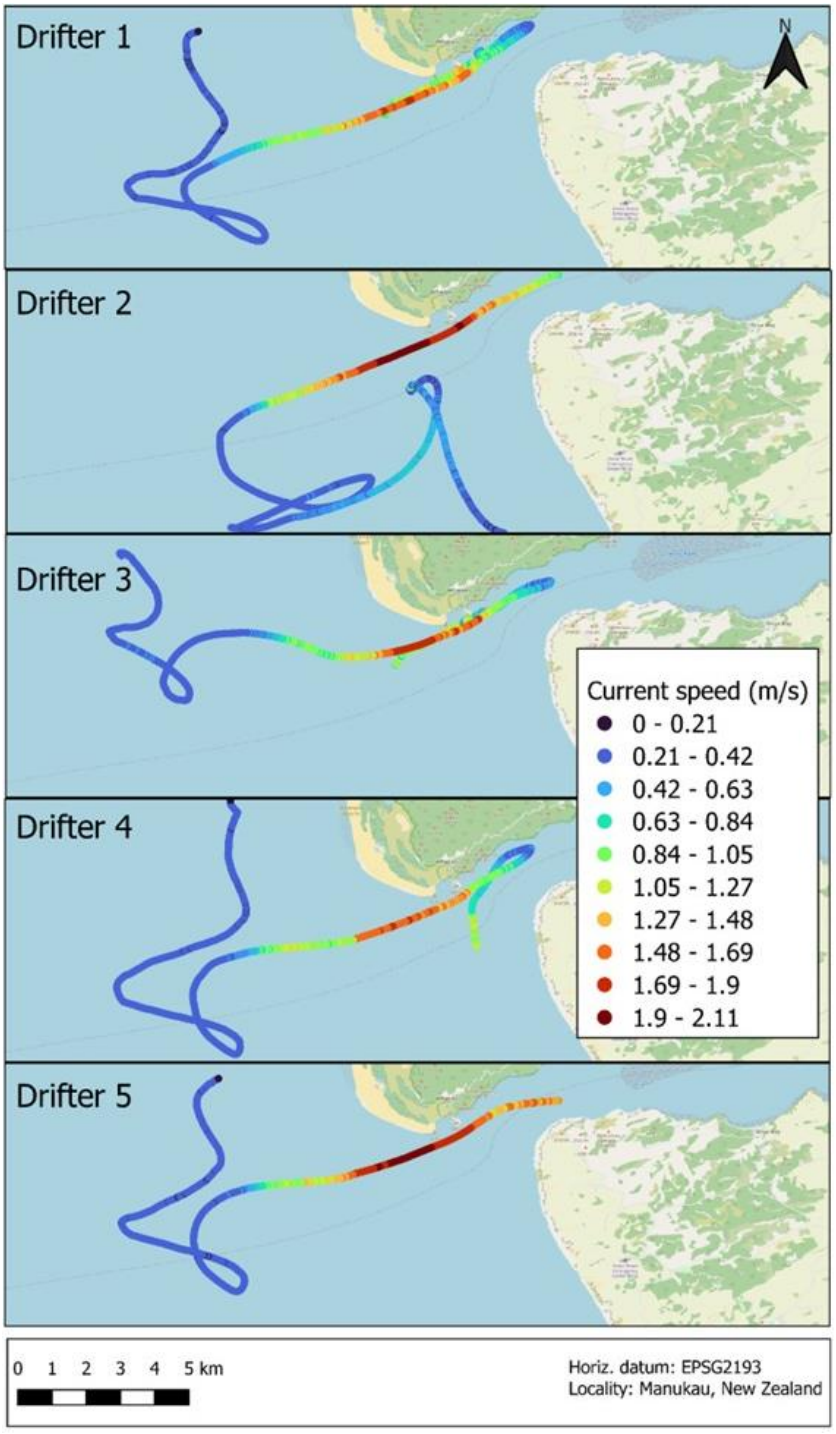

Figure 3-14: Drifters deployed in Manukau harbour on 10th June 2023.

3.4.4.2 ADCP Transects

Current measurements were carried out by DML Pty Ltd and Tonkin & Taylor across the channel using a boat mounted ADCP. A total of 30 transects were completed on the 23rd March 2023. The campaign covered just over 13 hours (between approximately 7am and 9pm - NZDT) covering a complete tidal cycle.

The transects were carried out across the channel off Manukau Heads. The first four transects were located between -37.0326775°S; 174.53151433°E and -37.045933°S; 174.54171467°E and the remaining 26 transects were located between -37.03046133°S; 174.5378965°E and -37.044628°S; 174.54938867°E. The two sets of survey were approximately 600 m apart (Figure 3-15).

The ADCP current speed for different stages of the tidal cycle are presented in Figure 3-16 and Figure 3-17.

Current magnitudes show a close correlation with tidal variation, indicating the dominant effect of the tide in this area. The currents indicate that the main flow is along the northern margin of the channel during the incoming tide (flood). Mean speed along transect 007 was 1.4 m/s and the highest speed recorded was 2.5 m/s. In contrast, stronger currents flowed along the southern margin at the outgoing tide (ebb). Mean current speed along transect 019 were 1.5 m/s and peak speed was 3.2 m/s.

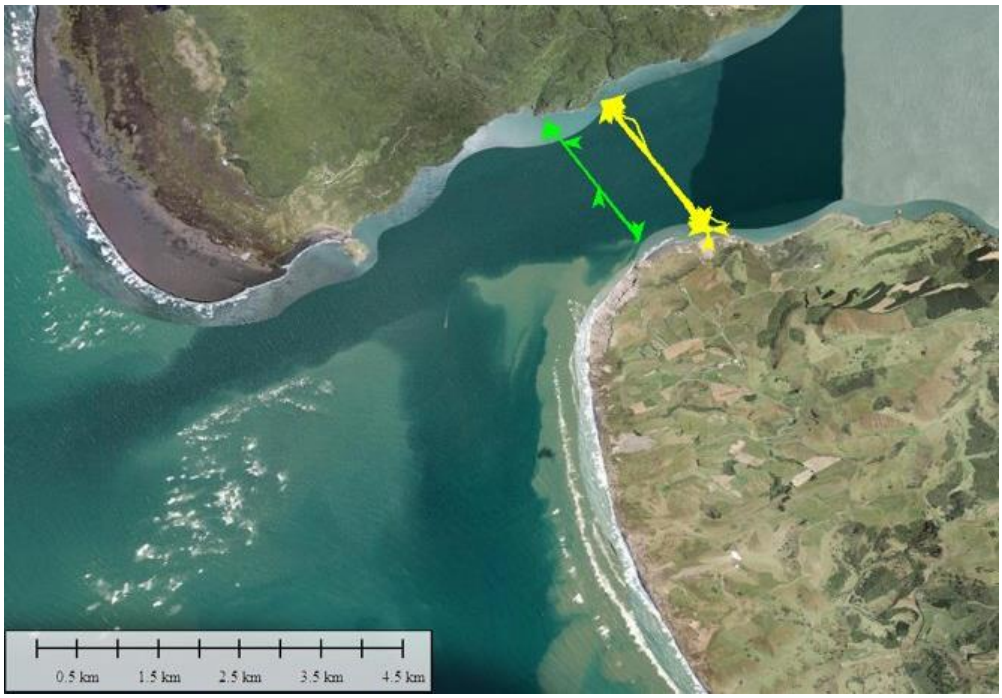

Figure 3-15 Location of ADCP transects. Green lines represent transects 000 to 004 and yellow lines represent transects 005 to 029.

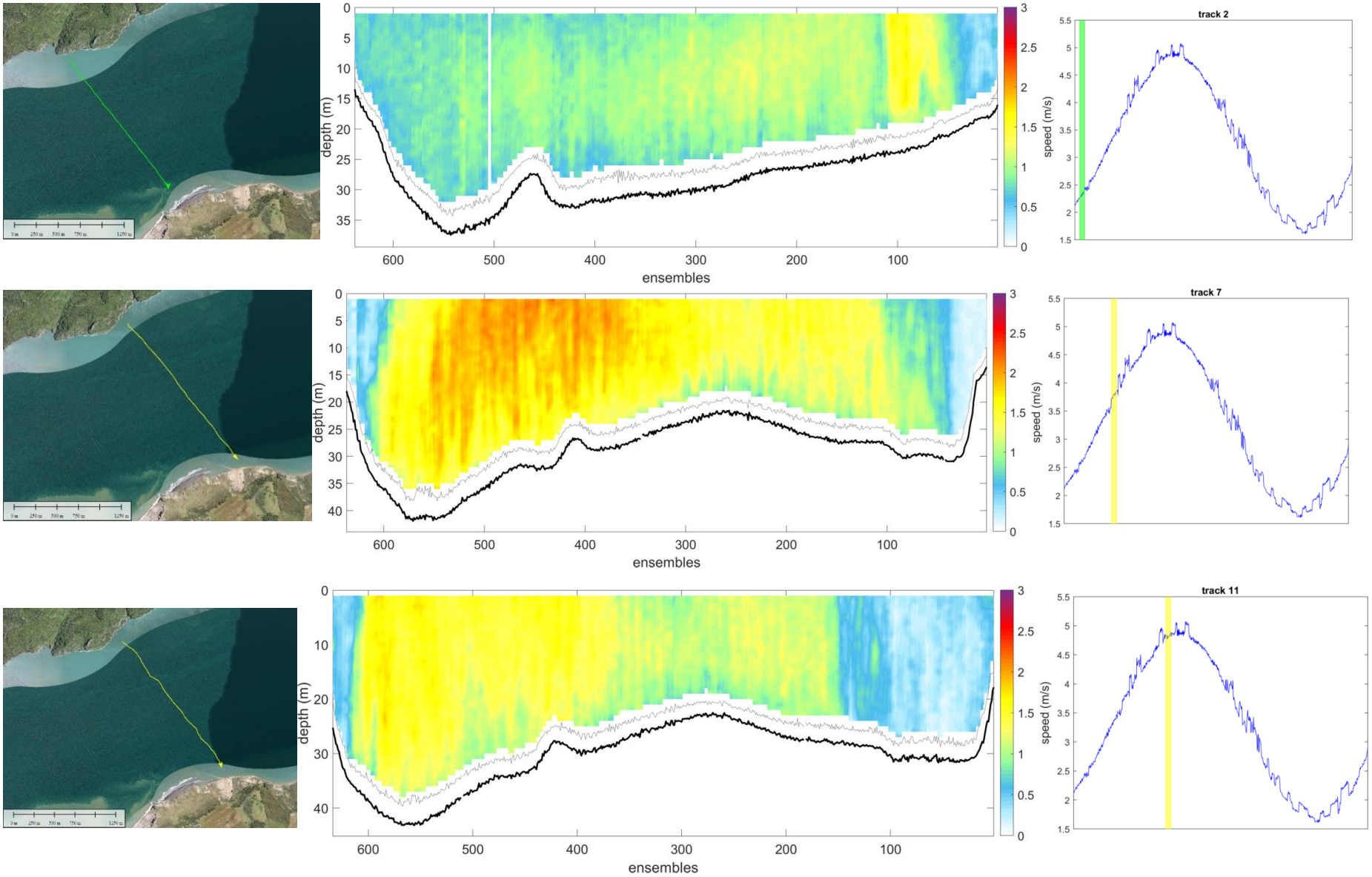

Figure 3-16: Example of ADCP transects (Transect 02, 07, 11) during the flood showing transect location (top left), water level at time of transect (top right) and current velocity through the water column (bottom).

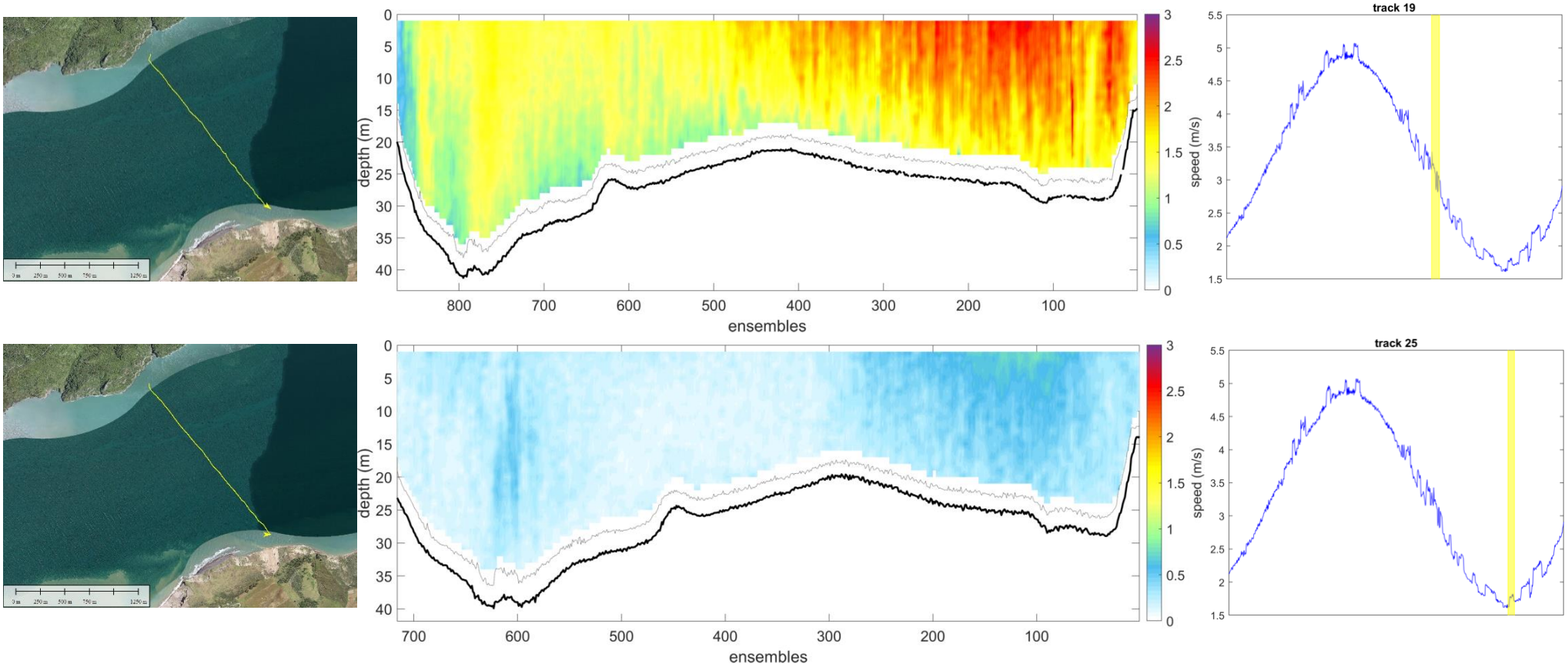

Figure 3-17: Example of ADCP transects (Transect 19 and 25) during the ebb showing transect location (top left), water level at time of transect (top right) and current velocity through the water column (bottom).

4. Numerical Model Description and Setup

4.1 CFSR wind reanalysis

Near-surface wind conditions (at 10 m above MSL) were extracted from the hourly Climate Forecast System Reanalysis CFSR and CFSv2 products (Saha et al., 2010) from the National Centres for Environmental Prediction (NCEP). The data spans 43 years (Jan 1979 – Sep 2022) at hourly intervals and has a spatial resolution of 0.31° (approximately 30 km) until March 2011 and 0.20° (approximately 20 km) beyond April 2011. The wind speeds are 10-minute means. The MSLP was also extracted from the gridded dataset to be used for the atmospheric forcing in the Delft FM model. The CFSR is available from Jan 1979 to December 2010 and the CFSRv2 data is available from January 2011.

4.1.1 Validation

Measured data from the Auckland Aerodrome weather station (174.807°E, 37.009°S in Figure 3-8), in the vicinity of the Manukau Harbour, were considered for the CFSR model input from 2010-2022. There is a good agreement between hindcast and observed wind speed (Wspd) and direction (Wdir) at Auckland Aerodrome, as shown in the following subsection. Both measured and modelled data correspond to 10-min averaged wind data at 10-m elevation.

Auckland Aerodrome:

The quantitative measures of hindcast accuracy (Table 4-1) show the hindcast wind speed is biased slightly high (0.21 $m.s^{-1}$) at Auckland Aerodrome. The hindcast wind direction is biased slightly low by 7.51 degrees.

The time series of measured and hindcast wind speed are provided in Figure 4-1, while the scatter and quantile-quantile (Q-Q) plots for wind speed are presented on Figure 4-2, showing good consistency between the measured and hindcast wind speed data, although a slight under-prediction is noted for the upper quantiles. The distributions of wind directions are shown as histograms (Figure 4-3) instead of Q-Q plots, which is more suitable for directional comparisons. The predominance of winds coming from the SW sector is consistent between the measured and hindcast data. The NE sector winds are also well replicated by the hindcast model.

Statistical metrics, including bias, mean absolute error and scatter index, demonstrate good agreement between model and measured wind data. A scatter index of 0.39 is

considered relatively low when comparing global wind data with onshore measured wind data that are subject to local topographic effects and turbulence.

The measured and hindcast storm peaks are also compared in Figure 4-4 and Figure 4-5, along with a fitted linear regression. The results indicate an overall under prediction of storm peaks. Consequently, an adjustment factor of 1.16 is considered for the extreme value analysis. By applying this factor to the entire modelled wind speed time series, the estimated return period values are consequently consistent with real storm events.

Table 4-1 Accuracy measures of the hindcast wind speed and direction at Auckland Aerodrome.

Parameter	Modelled – measured comparison statistics				
	MAE	RMSE	MRAE	Bias	Scatter Ind
Wspd	1.46 $m.s^{-1}$	1.86 $m.s^{-1}$	0.66	0.21 $m.s^{-1}$	0.39
Wdir	28.57 deg	45.12 deg	N.A.	-7.51 deg	0.26

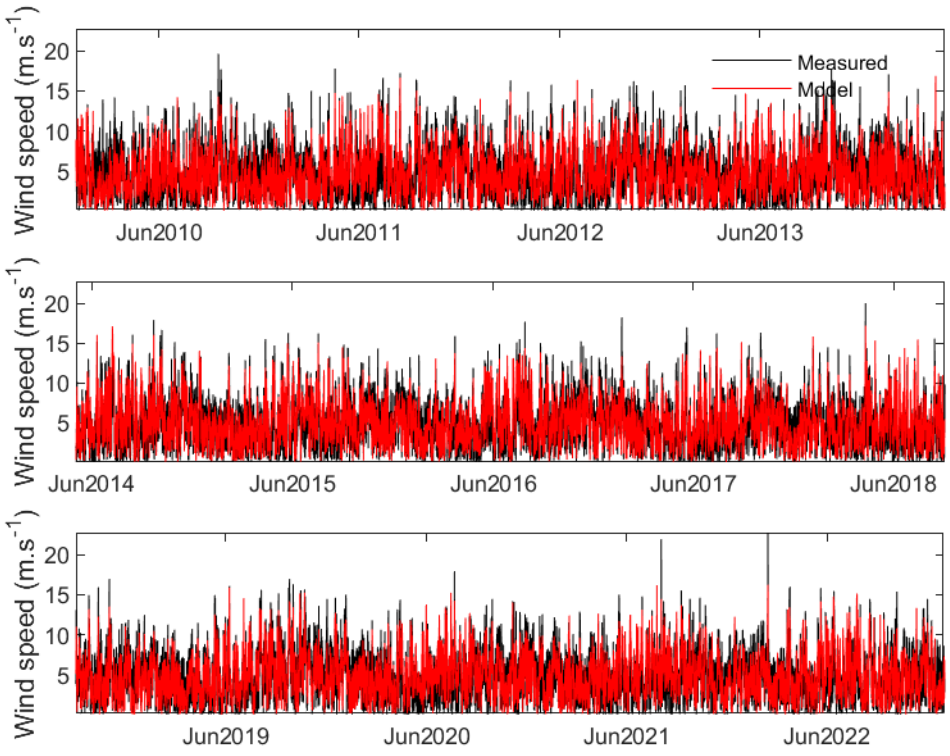

Figure 4-1 Measured and hindcast time series of wind speed at Auckland Aerodrome.

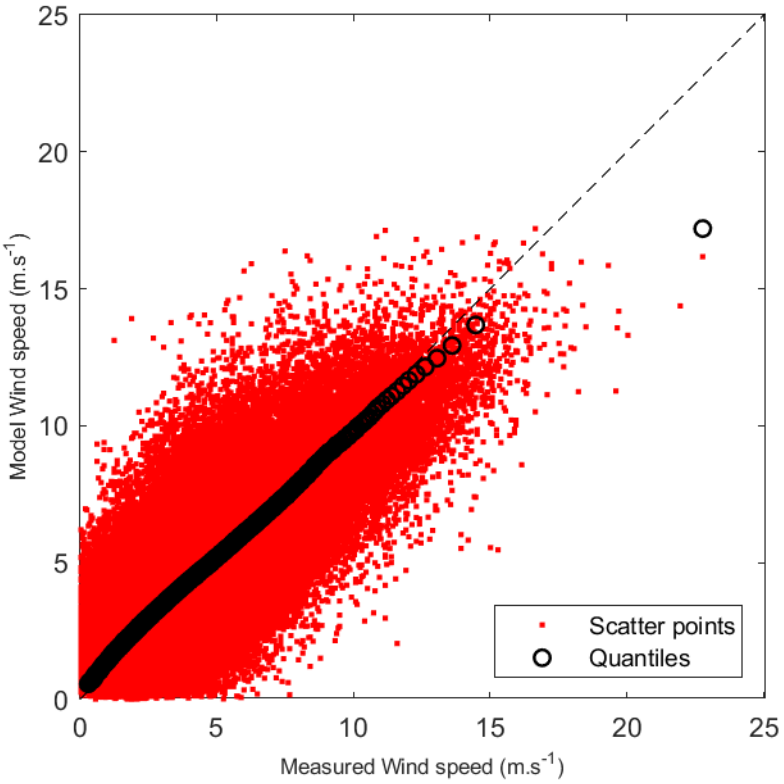

Figure 4-2 Scatter plot (red dots) and Quantile-Quantile plot (dark circles) comparing hindcast and measured wind speed at Auckland Aerodrome. Also shown is the line of equivalence (dark dashed line).

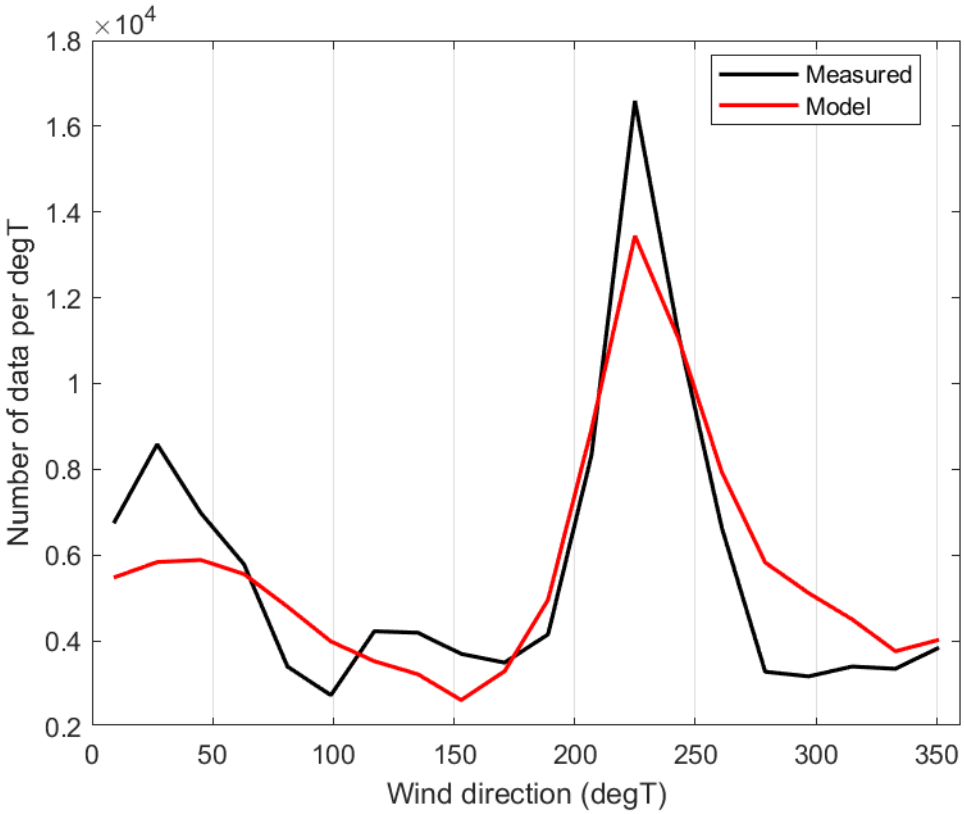

Figure 4-3 Histograms of measured and hindcast wind directions (in degree true north) at Auckland Aerodrome.

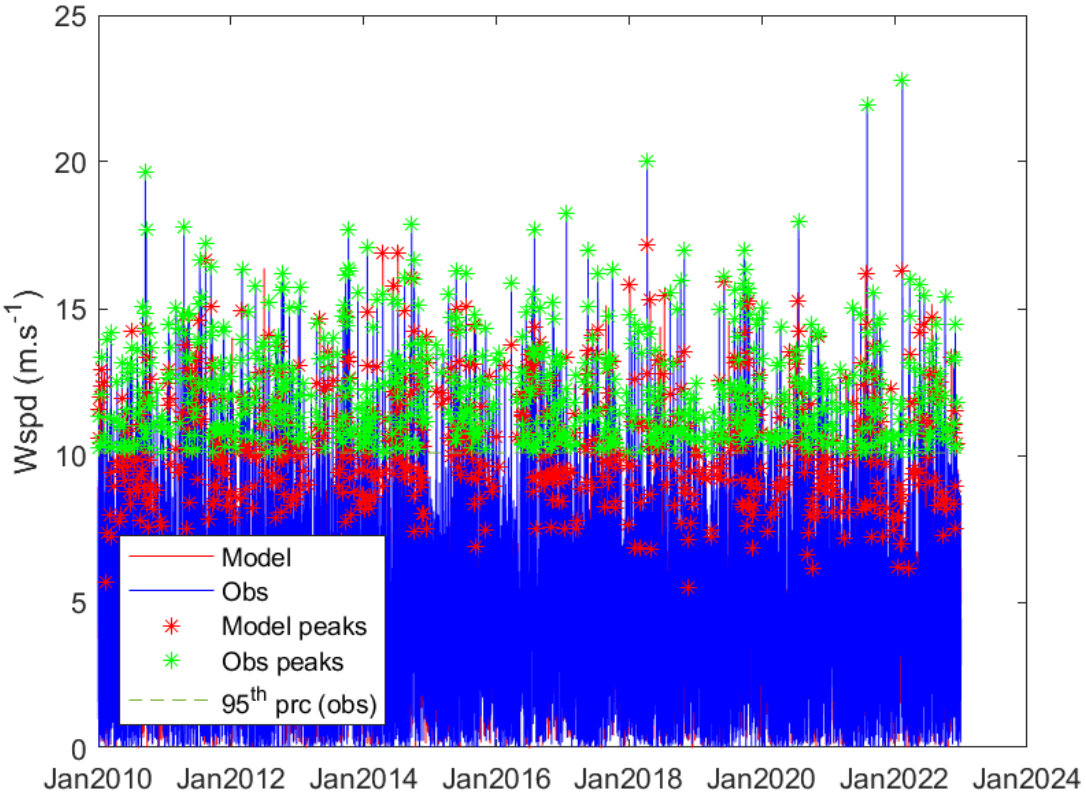

Figure 4-4 Measured wind speed (Wspd) peaks over 95th percentile level and corresponding Hindcast wind speed (Wspd) peaks within a +/- 6-hour window at Auckland Aerodrome from Jan 2010 – Dec 2022 (top).

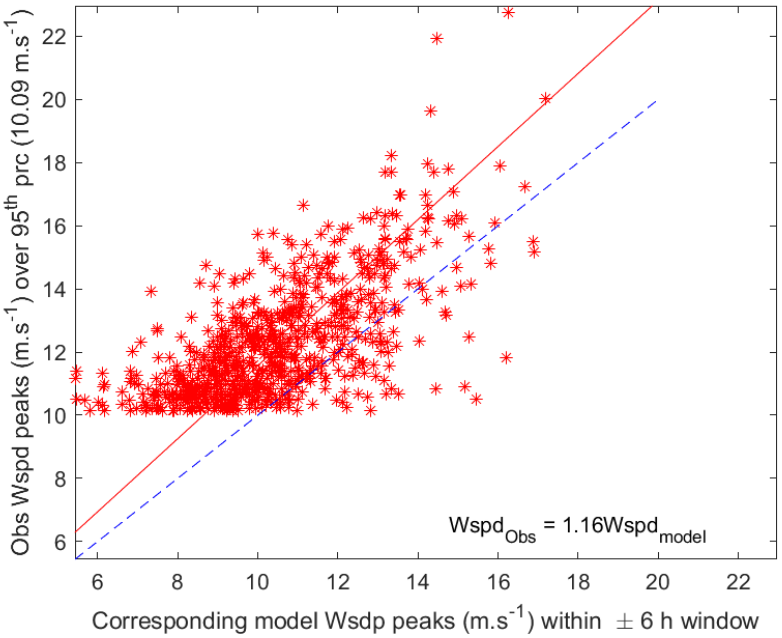

Figure 4-5 Measured and modelled wind speed (Wspd) peaks over the 95th percentile level and linear regression line (red) at Auckland Aerodrome from Jan 2013 – Dec 2022. Also shown is the equation of the linear regression line ($Wspd_{Obs}$ = 1.16$Wspd_{model}$) and line of equivalence (dashed line).

4.2 SWAN wave model

The long-term hindcast wave modelling was performed using a modified version of Simulating WAve Nearshore (SWAN)1. This section describes details of the wave model and the technique employed in the simulations.

4.2.1 Model description

SWAN is a third-generation ocean wave propagation model which solves the spectral action density balance equation (Booij et al., 1999). The model simulates the growth, refraction and decay of each frequency-direction component of the complete sea state, providing a realistic description of the wave field as it changes in time and space. Physical processes that can be modelled include the generation of waves by surface wind, dissipation by white-capping, resonant nonlinear interaction between the wave components, bottom friction and depth-induced wave breaking dissipation. A detailed description of the model equations, parametrisations and numerical schemes can be found in Holthuijsen et al. (2007) and in the SWAN documentation[2].

4.2.2 Setup

The wave hindcast was set and run for a 43-year period, from 1980 to 2022 (inclusive). The model was configured in non-stationary mode including all third-generation physics. The Westhuysen physics and the bottom friction scheme of Collins (1972) with coefficient of 0.015 were applied based on previous calibrations carried out by MetOcean Solutions. These calibrations involved adjusting the physics of the model for different regional grids around New Zealand aiming at a better representation of the different wave climates found. Depth-induced wave breaking dissipation was modelled according to Battjes and Janssen (1978). The wave spectra were discretised with 36 directional bins (10-deg directional resolution) and up to 38 frequencies logarithmically spaced between 0.041 and 1.54 Hz at 10% increments.

A dynamical downscaling nesting approach was applied to resolve the nearshore region around the sites of interest. To fully capture the details of the coastal line and bathymetry in the area, 5 regular SWAN nests were defined with resolutions of ~4 km, 800 m, 200 m, 80 m and 25 m to resolve the small-scale bathymetric features of the area (Figure 4-6).

[1] Modified from SWAN version of the 40.91 release.
[2] http://swanmodel.sourceforge.net/

Full spectral boundaries for the parent SWAN hindcast domain were prescribed from a global implementation of the WAVEWATCHIII (WW3) spectral wave model (Tolman, 1991), run at 0.5 deg resolution with the source terms of Ardhuin et al. (2010). Therefore, sea and swell waves are included in the modelling boundary conditions. The model was forced with CFSR surface winds.

4.2.3 Validation

The offshore wave model nests were validated against data from IMOS satellite altimeter (Ribal & Young, 2019). This dataset is binned into 1° by 1° bins globally. As presented in Ribal and Young (2019), in-situ measurement and altimeter wave height data show very good correlation (coefficient close to one). The statistical parameters used to analyse the model performance in the model domain are presented in Figure 4-7. In general, the bias is slightly positive. The averaged Root Mean Squared (RMSD) is 0.39 m and the scatter index (SI) is 0.07. The mean r^2 value is 0.9.

The quantile-quantile (Q-Q) plot of the modelled and measured (IMOS satellite altimeter) wave (Figure 4-8) shows that the model performance was in general good with bias and scatter index averages of 0.07 and 19 cm, respectively. The lower-quartile indicate the model tends overestimate smaller values of H_s. A slight overestimation is also observed in the upper-quartile.

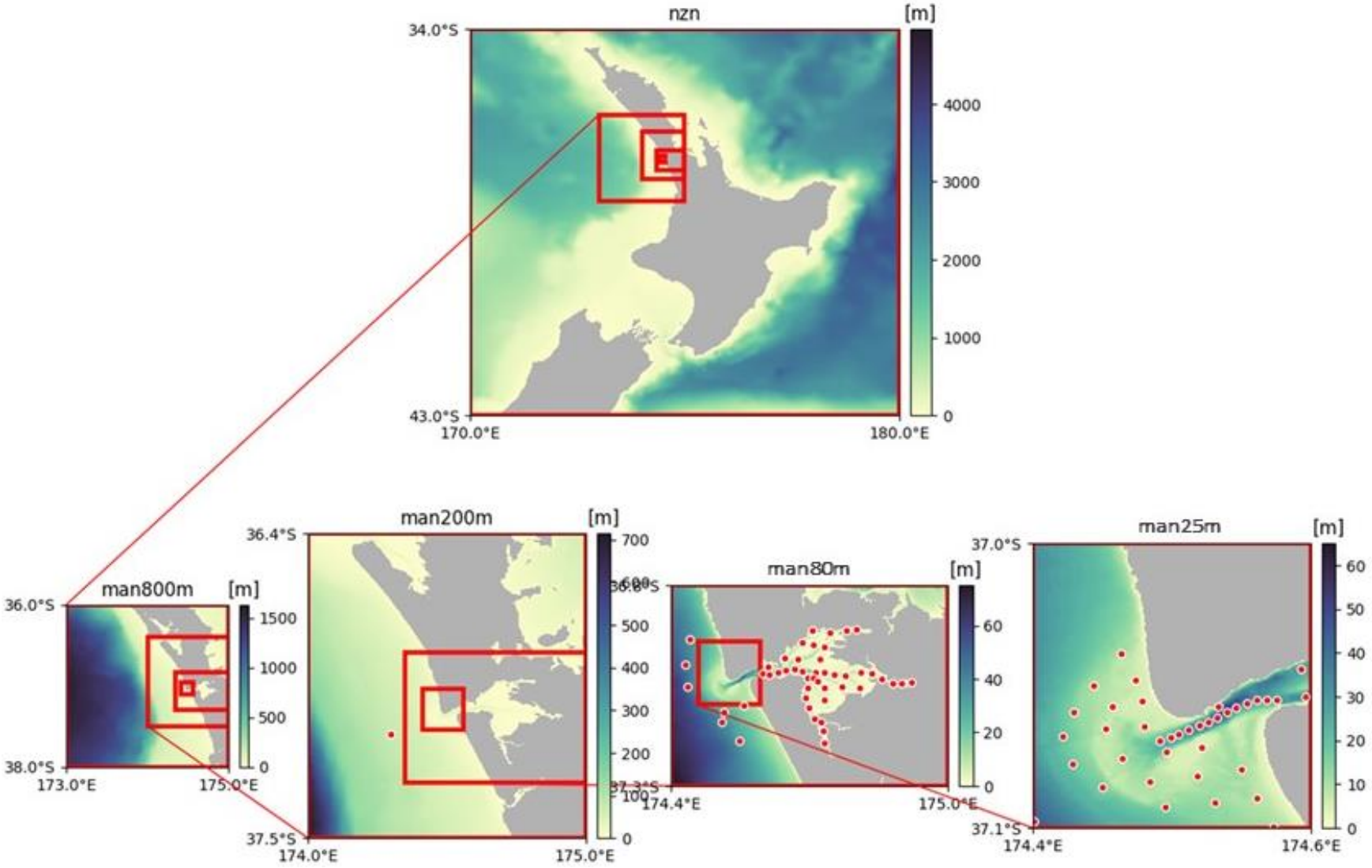

Figure 4-6: Bathymetry map showing the area of interest and the successive wave model nests including the data output locations.

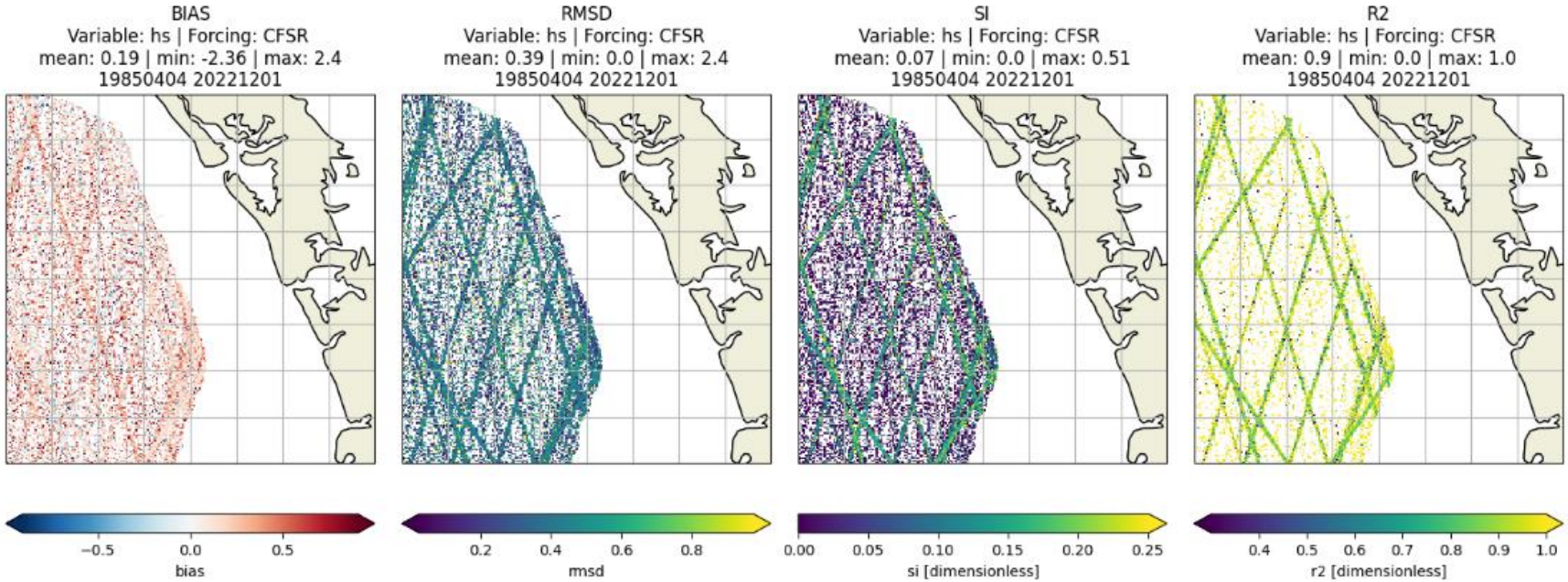

Figure 4-7: Statistical parameters from the offshore model validation.

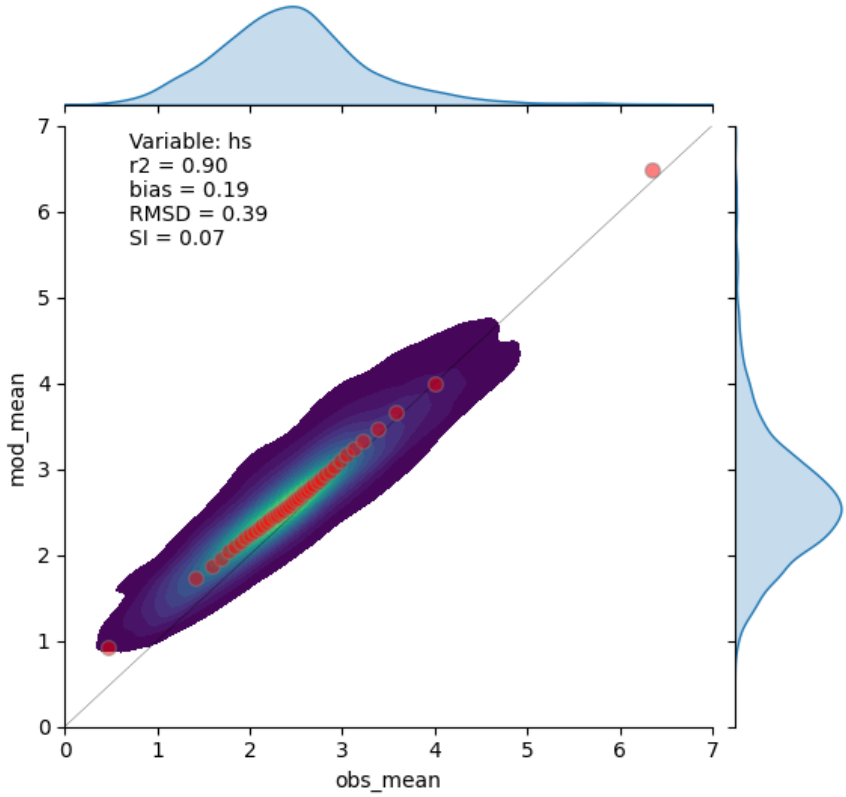

Figure 4-8: Q-Q plot of mean wave heights between SWAN model and IMOS satellite altimeter observations.

Validation of the wave model nearshore was undertaken against the wave buoys data deployed offshore and inside the Manukau Harbour. The model validation for the offshore site spanned approximately two weeks, encompassing two periods of more intense wave activity, both of which were effectively captured by the SWAN model as depicted in Figure 4-9. During periods characterized by smaller waves, the RMSD displayed a slight increase. In a broader context, the model exhibited a tendency to slightly overestimate H_s as indicated by a Bias value of 0.27.

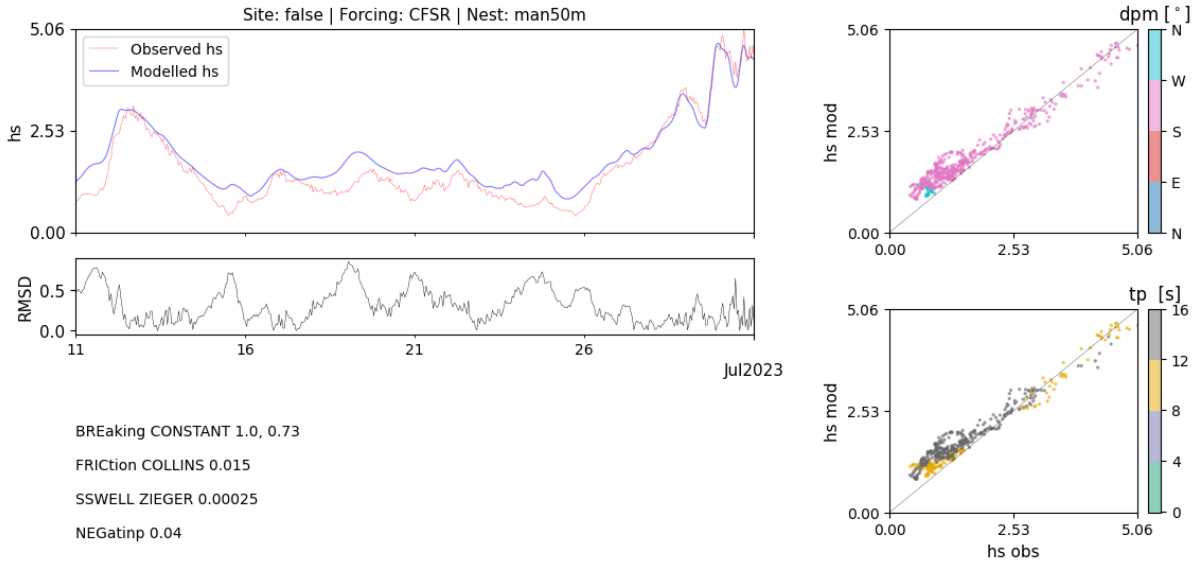

Figure 4-9: Offshore Site H_s Validation Results - Upper left panel shows a time series comparison between observed H_s (in red) and modelled H_s (in blue) over the buoy deployment time period. Lower left panel displays the time series of RMSD in H_s between observed and modelled values. Upper right panel presents a scatter plot comparing modelled H_s to observed H_s, color-coded by wave peak direction (dpm). Lower right panel is a similar scatter plot but color-coded by wave peak period (T_p).

Figure 4-10 highlights these overestimations in the lower tail of the Q-Q plot. Additionally, the Scatter Index (SI) was 0.16. Although low, it must be considered together with the limited dataset available for validation, suggesting that a longer time series might yield a more comprehensive evaluation.

Despite these considerations, the model's overall performance was good, with an r^2 value of 0.96, showing the ability of the model to accurately simulate the observed wave conditions at the offshore site.

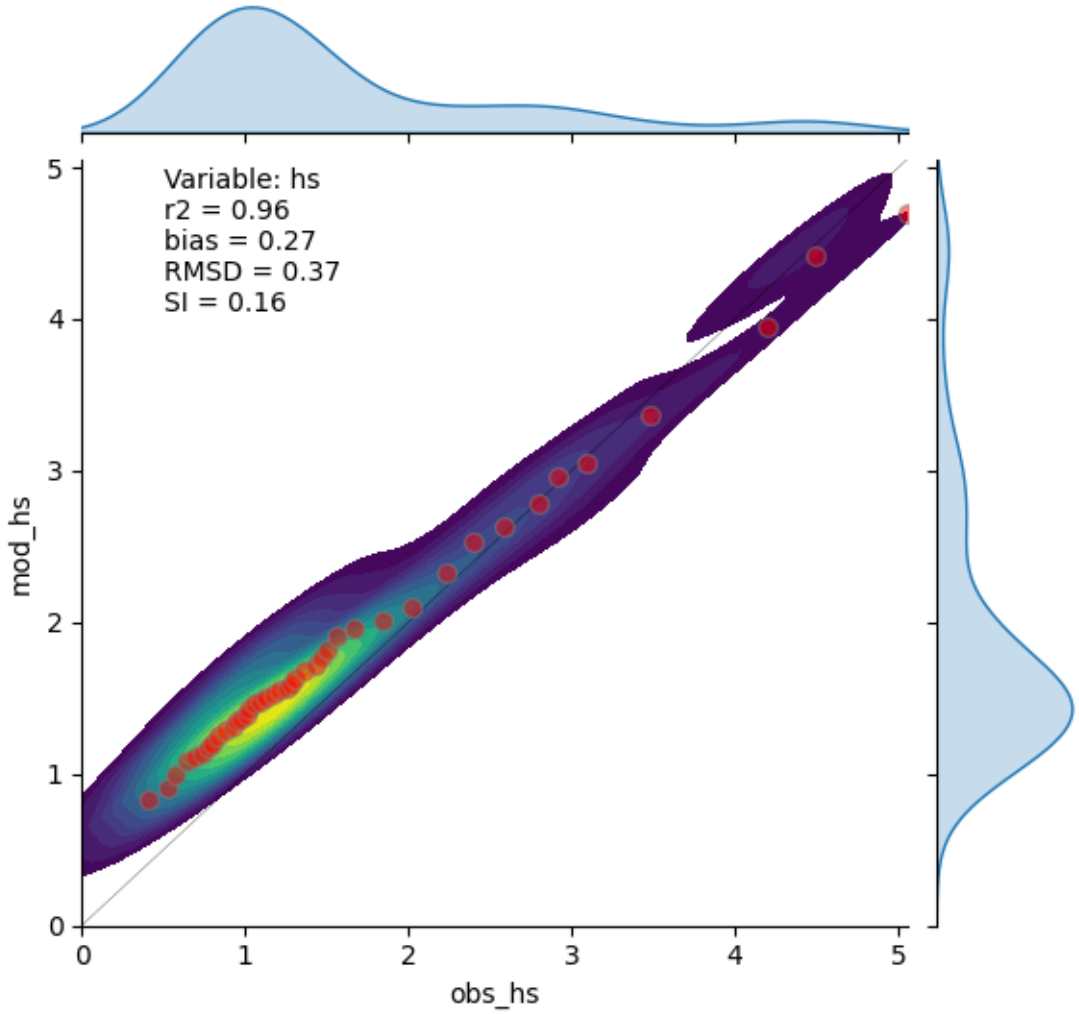

Figure 4-10: Q-Q plot and density plot of H_s comparing the SWAN model to the offshore wave buoy observations.

The validation of the Inner Harbour site is presented in Figure 4-11and Figure 4-12. The wave series spans approximately one month for this site, overlapping with measurements from the offshore site. While the modelled Hs generally followed the observed Hs patterns, it consistently exhibited a slight overestimation, with an average bias of 0.06. The tidal signal in the H_s measurements appeared more pronounced than in the model, potentially contributing to the observed overestimation, as increased friction during low tides could dampen wave energy.

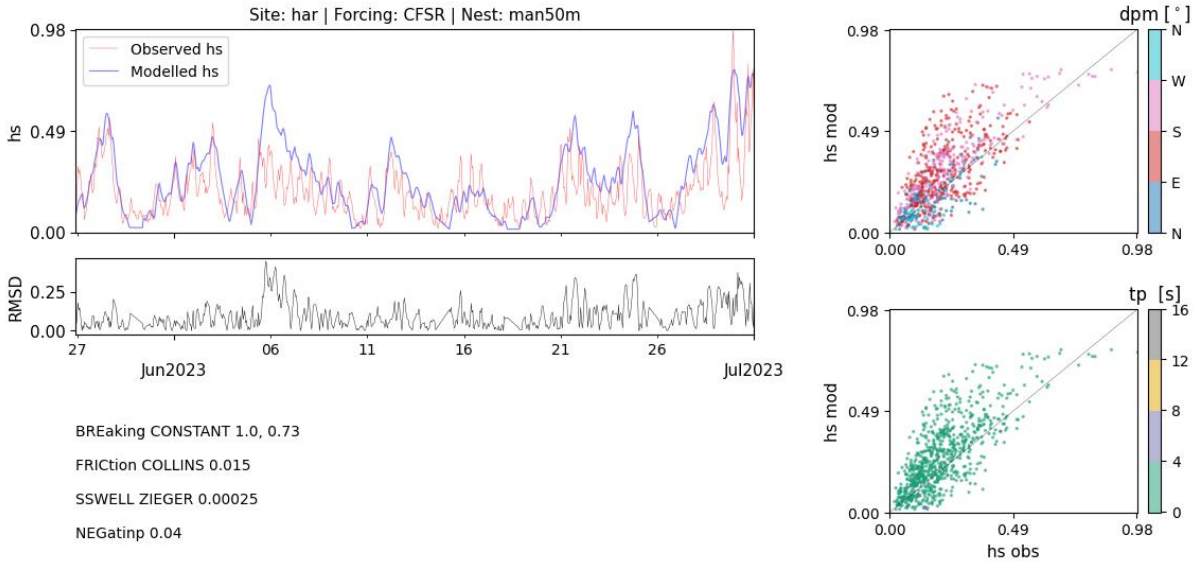

Figure 4-11: Inner Harbour Site H_s Validation Results - Upper left panel shows a time series comparison between observed H_s (in red) and modelled H_s (in blue) over the buoy deployment time period. Lower left panel displays the time series of RMSD in H_s between observed and modelled values. Upper right panel presents a scatter plot comparing modelled H_s to observed H_s, color-coded by wave peak direction (D_{pm}). Lower right panel is a similar scatter plot but color-coded by wave peak period (T_p).

The Q-Q plot and density plot revealed that the overestimation tended to be more significant for higher Hs values. The Scatter Index (SI) value of 0.54 indicated a relatively high level of variability in the model's predictions compared to the measurements, suggesting that the extent of overestimation varied widely across different Hs values. This variability was reflected in the r^2 of 0.57.

In summary, while the model generally captured the overall trends in the measurements, caution is advised when using the modelled H_s values where interaction with tidal currents is expected to be significant (e.g. main ebb channel). Further detail and explanation on the H_s, T_p and tidal current interaction in the channel is provided in Section 4.3.3.3.1 in relation to the outputs from the fully coupled Delft FM and SWAN wave model.

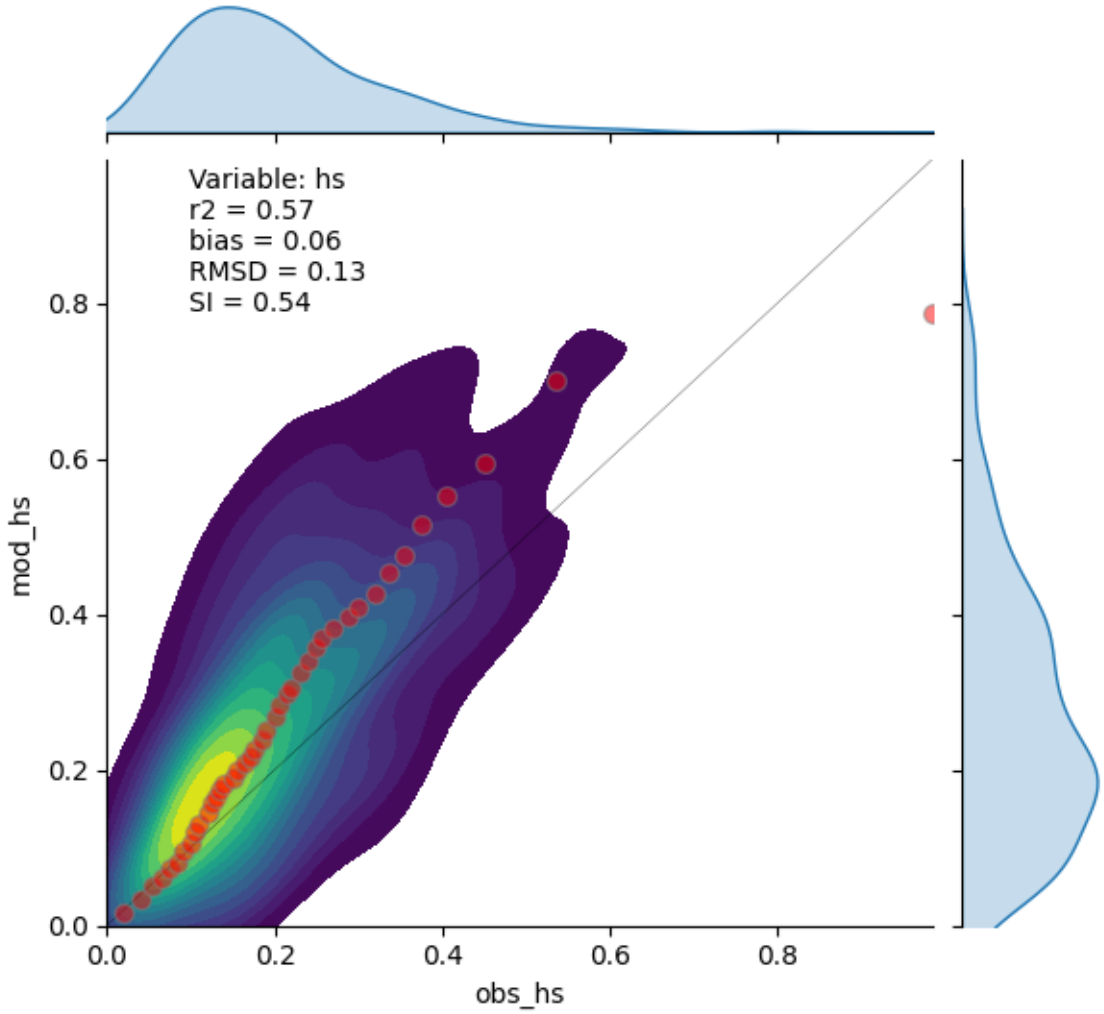

Figure 4-12: Q-Q plot and density plot of Hs comparing the SWAN model to the wave buoy observations in the Inner Harbour.

4.3 Delft FM hydrodynamic and wave model

The modelling of the hydrodynamic and wave followed an approach that aimed at capturing the complete range of possible forcing expected near the site to provide a robust picture of the likely transport and deposition patterns. Sediment transport modelling is presented in the second report TWP03c (MOS) - Numerical modelling - Sediment Transport report.

4.3.1 Model description

The modelling system Delft3D Flexible Mesh (FM) (Deltares, 2020b, 2020a, 2020c, 2022) was used in this study. The software is based on interlinking three separate components that together simulate flows, waves and sediment transport. The hydrodynamic and wave components are fully coupled, i.e. water level and currents are used in the wave module and the wave parameters are then in turn affecting the hydrodynamic. The unstructured mesh provides the optimal degree of flexibility in representing complex coastlines and bathymetries.

The hydrodynamic module is a 2D or 3D hydrodynamic model which calculates non-steady flows and transport processes resulting from tidal and meteorological forcing. The system solves the horizontal equations of motion, the continuity equation, the transport equations for conservative constituents and a turbulence closure scheme (Deltares, 2020b).

The third-generation SWAN model (Simulating WAves Nearshore) is used in the wave module (Booij et al., 1999; Deltares, 2020c; Ris et al., 1999). SWAN computes the evolution of random, short-crested waves in coastal regions with deep, intermediate and shallow water depths. Wave forces computed by the wave module based on radiation shear stress gradients are used as a driving force to compute the wave-induced currents and set-up in the flow module.

4.3.2 Setup

4.3.2.1 Hydrodynamic mesh

The Delft FM model domain is defined by the finite-element triangular grid shown in Figure 4-13 which enables resolution and scale benefits over other regular or curvilinear based hydrodynamic models. The model mesh extends approximately 40 km north and south of the entrance and 40 km offshore. The inner harbour is resolved up to +4-5 m MSL of vertical elevation to ensure the full tidal prism is represented. The flexible mesh is composed of a network of triangular and quadrilateral elements constructed from nodes to increase computational efficiency and to align with the main harbour channels

and dominant flow directions. The varying 2D mesh resolution was established in SMS (Surface-water Modelling System) mesh generation software from a combination of the bathymetry, seabed gradient and also weighed on distance to site. The resulting mesh varies from a coarse size of approximately 1.5 km at the open boundary to the fine size of approximately 20 m in the main entrance channel and upstream tributaries. A resolution of at least 25 m covers the entire concept navigation channel out to 100 m from the top of the batter slope. Figure 4-14 displays the mesh resolution within the entrance channel and bar.

The hydrodynamic model is configured in depth-averaged (2D) model. The choice between a 2D depth-averaged and 3D model depends on several factors, including the complexity of the flow field, computational resources available, and the specific objectives of the modelling study. In many practical applications, especially for long-term studies or large-scale assessments, the simplification provided by a 2D depth-averaged model may be sufficient. These models can accurately represent the main flow patterns, sediment transport, and water quality processes while reducing the computational overhead associated with simulating the third dimension. The justifications for choosing a 2D depth-averaged Delft FM model at Manukau Harbour include:

- Computational efficiency - 2D depth-averaged models are computationally less intensive compared to 3D models. They require fewer computational resources, especially for long-term studies or large-scale simulations where the computational time increase exponentially when coupled waves and sediment transport are added. A longer 2D simulation was favoured over significantly shorter-term 3D model as annual model outputs were needed to justify the statical analysis and probability assessments of the metocean conditions needed for the study.
- Variation in depth - The flow in Manukau Harbour is primarily driven by variations in the horizontal plane and depth changes are minimal and predictable, therefore a 2D depth-averaged model can adequately capture the flow dynamics. This is often the case in rivers, estuaries, and coastal areas where the variations in depth are much smaller compared to the horizontal extent of the domain.
- Temperature and salinity – Manukau Harbour has three notable creeks or streams that discharge into the inlet, all with low flow rates, and no major river systems. The vertical stratification in salinity and temperature are not expected to have notable impact at Manukau Harbour.
- Flow driven processes - the primarily focus of the modelling was on variables or processes that are primarily influenced by horizontal flow patterns, such as sediment transport in estuaries or coastal areas. The simplification provided by a

2D depth-averaged model is sufficient, and in some cases a 2D depth-averaged model may be more appropriate.

- Model resolution – as 2D models are computationally less intensive, this allows the model mesh to have enhanced resolution in areas of wave/flow interaction, that if included in a 3D model, would result in not viable computational time.

Modelling is undertaken in cartesian coordinates using the NZGD2000 / New Zealand Transverse Mercator 2000 with EPSG 2193. The model is run in UTC.

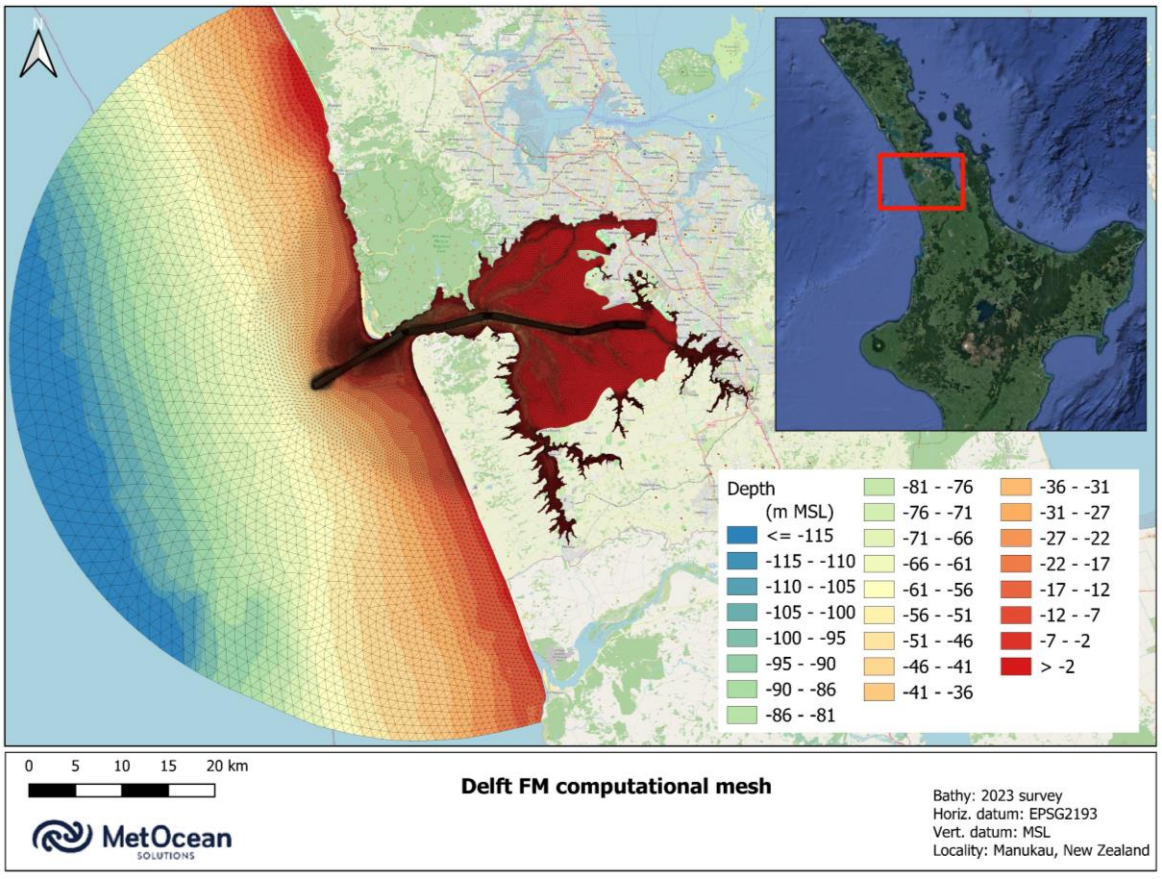

Figure 4-13 Delft FM computational mesh of Manukau Harbour with the 2023 existing bathymetry.

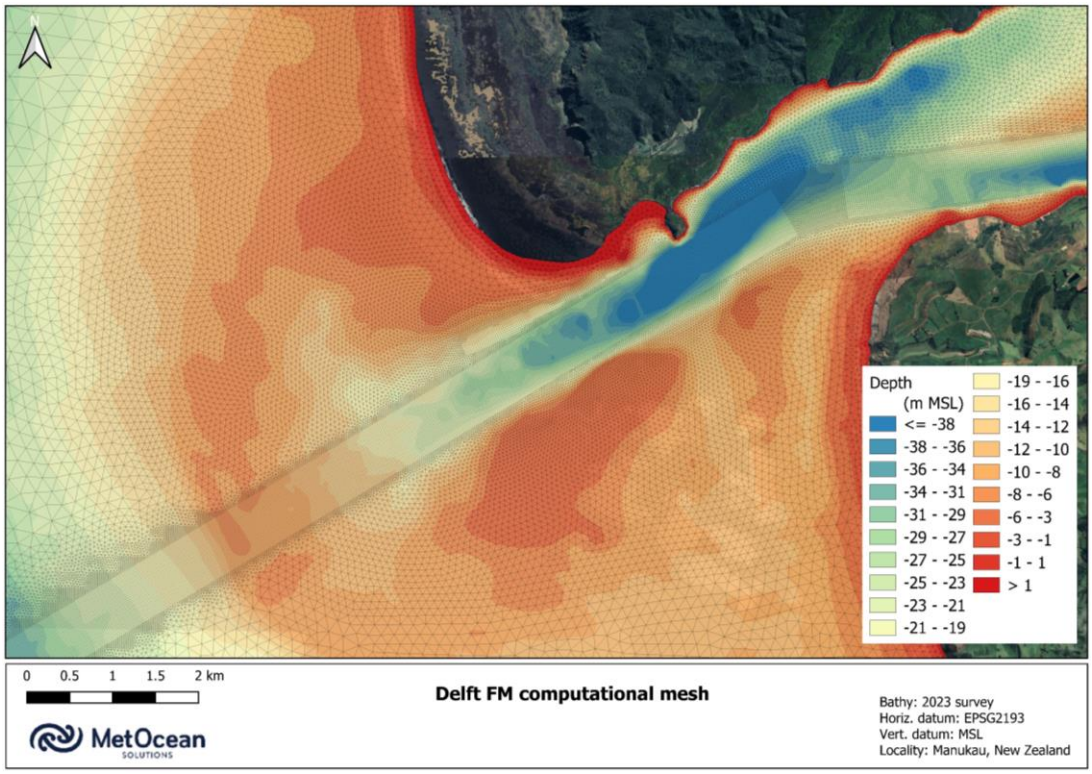

Figure 4-14 Delft FM computational mesh of Manukau Harbour entrance with the existing 2023 bathymetry of the entrance bar and channel.

4.3.2.2 Hydrodynamic model forcing

The Delft FM open boundary was forced with water levels extracted from OTIS TPXO model (Egbert & Erofeeva, 2002). Water levels were specified at 35 points spaced along the open boundary. The wind forcing used in the coupled Delft FM and SWAN model is from the CFSR (Climate Forecast System Reanalysis) dataset distributed by NOAA (Saha et al., 2010). Model forcing was developed during the validation of the hydrodynamic and wave model. A description of the other datasets that were tested for model forcing is provided in Section 4.3.3.1.

Discharge forcing was included for the three main river systems discharging into the harbour. The flow rates for Puhinui Creek, Papakura Stream and Waitangi Falls were sourced from Auckland Council Environmental Data Portal. The locations of the discharge measurements are displayed in Figure 3-8. The model inputs are provided as point source discharge timeseries in m^3.s. The flow rates from all three river systems are low, in 2012 there were maximum measured discharges of 24 m^3.s 10 m^3.s and 8 m^3.s and mean measured discharges of 0.9 m^3.s 0.2 m^3.s and 0.3 m^3.s for Papakura Stream, Puhinui Creek and Waitangi Falls respectively.

4.3.2.3 Bed roughness

Sensitivity analysis of the bed roughness was undertaken to improve the model predictions and a varying bed roughness map was developed during the calibration of the hydrodynamic model. A description of the datasets and literature sources used in the development of the bed roughness map are provided Section 4.3.3.1. The bed roughness map using Manning roughness is displayed in Figure 4-15.

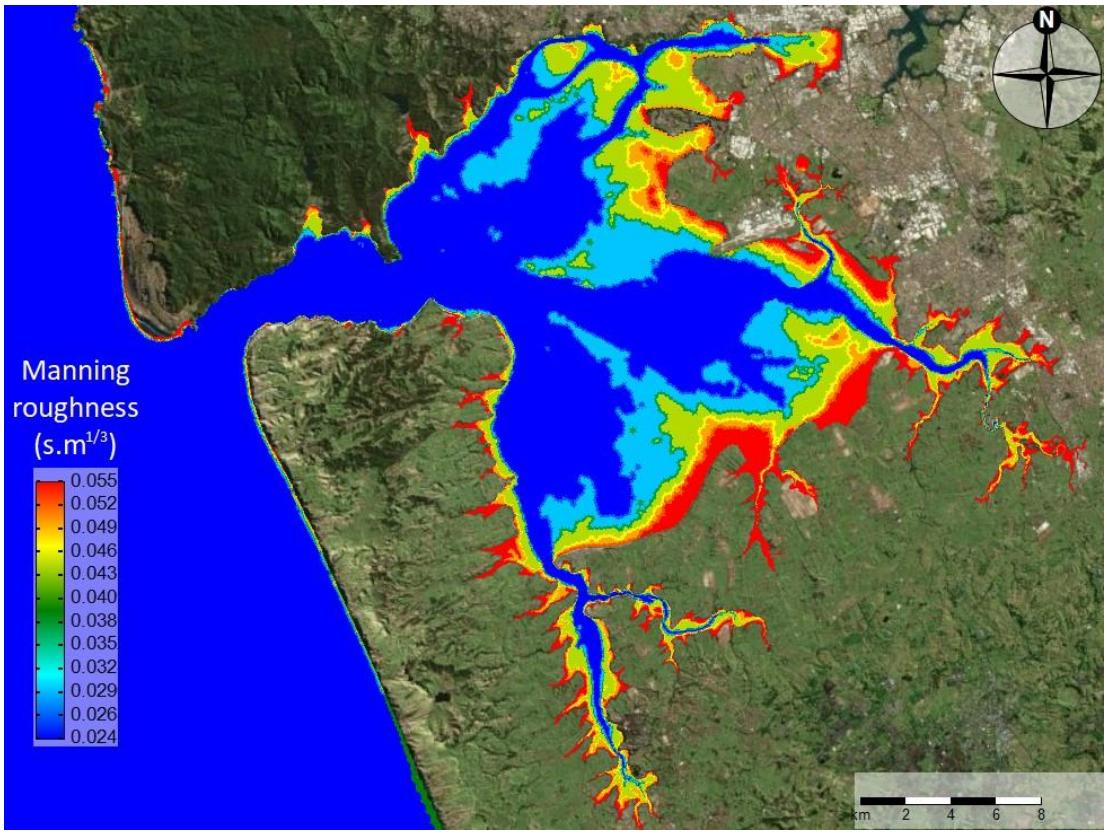

Figure 4-15 Bed roughness map applied to the Delft FM model of Manukau Harbour.

4.3.2.4 Wave model

The coupled SWAN wave model is comprised of four nested grids covering the entire Delft FM domain. The nested grids are displayed in Figure 4-16. The 200 m extent is the same as that used in the SWAN hindcast and the outer 80 m, 25 m grids and inner 80 m were rotated to be aligned with the coastline. The inner harbour 80 m grid is nested in the 25 m grid to ensure the waves though the entrance transfer to the inner harbour grid.

The wave boundary is defined as hourly wave spectra extracted from the SWAN model described in Section 4.1. The model is forced around all sides of the 200 m.

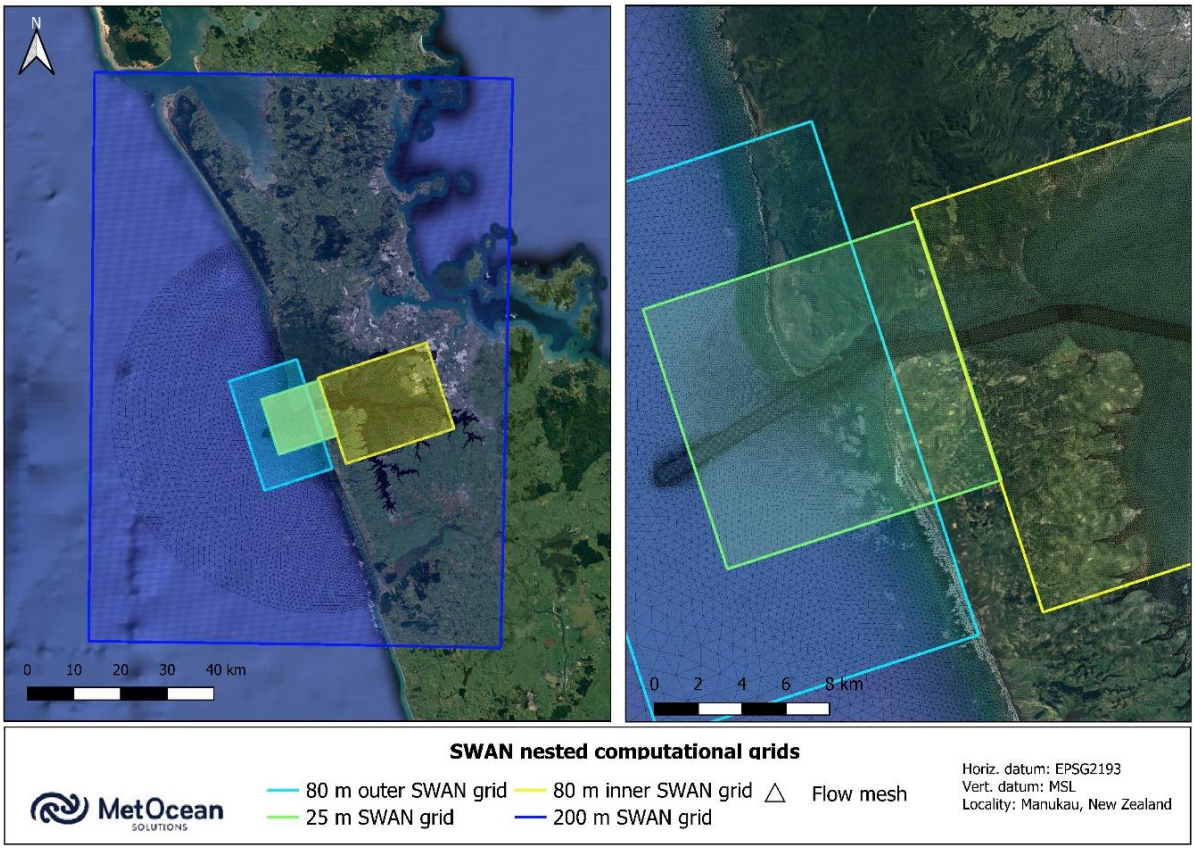

Figure 4-16 Model domains used in the coupled Delft FM/SWAN model runs.

4.3.3 Calibration and Validation

Model calibration is the process of setting physically realistic values for model parameters so that the model reproduces observed values to the desired level of accuracy. Model validation is used to confirm that the calibrated model continues to consistently represent the natural processes to the required level of accuracy in periods other than the calibration period without any additional adjustment to the model parameter settings. The coupled Delft FM and SWAN model was calibrated and validated against measured data at several locations throughout the model domain for the project including current drifters, water level measurements, ADCP transects across the entrance and wave measurements, all of which are described in Section 3.3. The location of the deployed instruments is displayed in Figure 4-17.

The two calibration and a validation comparison period for the hydrodynamics, one calibration period for the waves, and the datasets used in each are displayed in Figure 4-18. The calibration and validation periods were:

- In the first phase of model calibration, modifications to the schematisation and resolution of the model mesh, bathymetry, bed roughness and boundary forcing were undertaken until a good agreement with the measured data was reached. The ADCP transects for currents and tidal discharge and two water levels measurements were used for the calibration period one (between 22nd March and 21st April).
- A second calibration period was undertaken where the bed roughness map was developed further, and upstream areas of constricted bathymetry were corrected and checked. Model statistics were compared for two water level measurements (between 21st April and 30th May).
- Validation to ensure the model continues to consistently represent the natural processes to the required level of accuracy without any additional adjustment to the model parameter settings. This was undertaken with the current drifters and three water level measurements (between 1st June and 17th July).
- The waves were calibrated at two measurement locations during the 1st June and 17th July period.

This process provides confidence in the model results and is essential for the accurate representation of coastal hydrodynamics and wave processes. Confirming the numerical modelling systems are representative of the natural environment also provides a level of confidence that the models can be used as a predictive tool to inform design decisions and assess impacts.

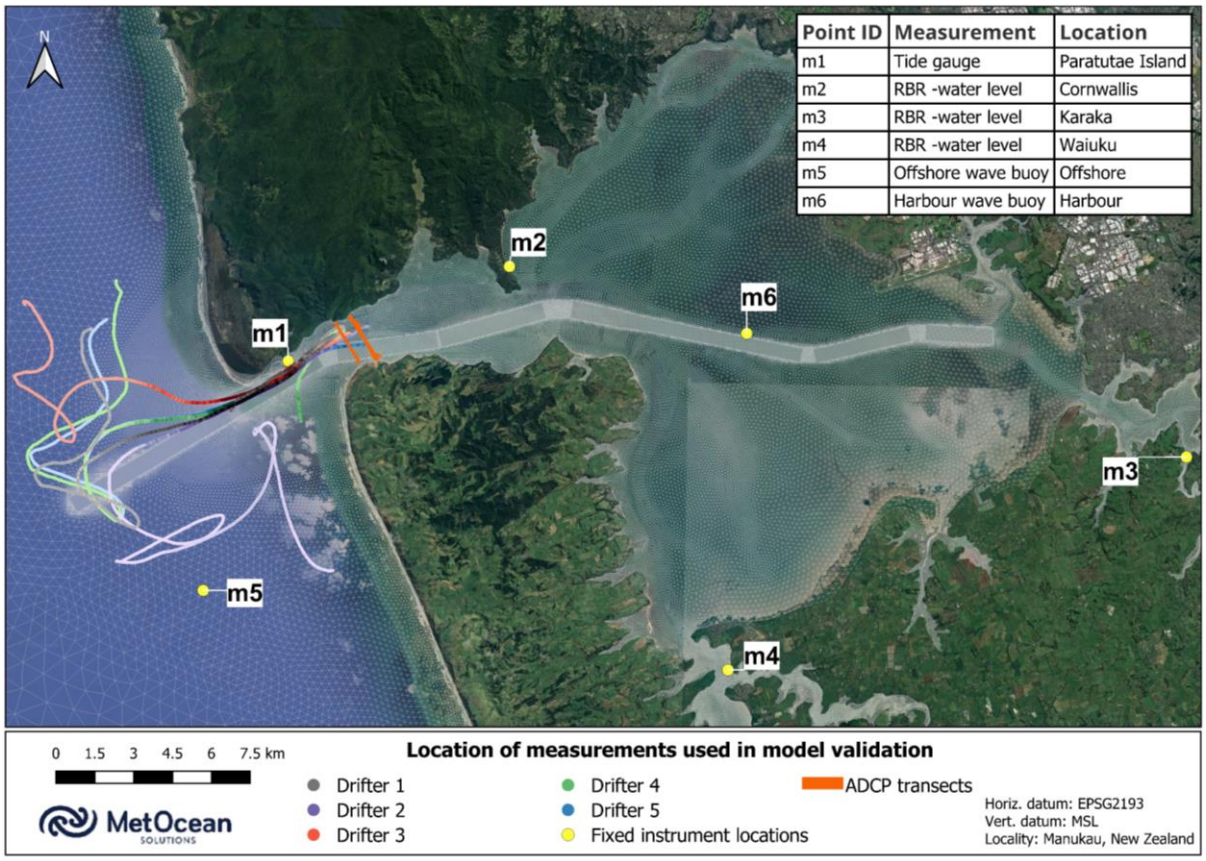

Figure 4-17 Location of measured water levels, currents, discharges and waves collected in 2023 used in the calibration and validation of the coupled Delft FM and SWAN model.

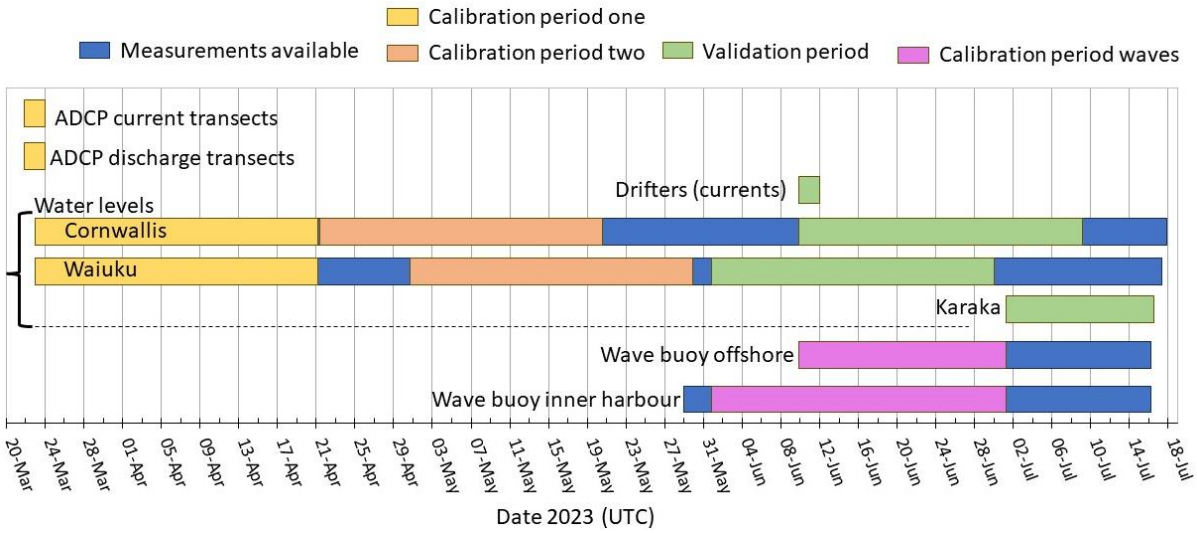

Figure 4-18 Summary of the comparison periods and field data used in the calibration and validation of the coupled Delft FM and SWAN model.

4.3.3.1 Calibration - Hydrodynamics

In the first phase of model calibration, modifications to the schematisation and resolution of the model mesh, bathymetry, bed roughness and eddy viscosity were undertaken until a good agreement with the measured data was reached. Testing of various boundary forcing was also undertaken. A second calibration period was undertaken where the bed roughness map was developed further. These periods were between 22nd March and 21st April, and 21st April and 30th May respectively.

The main parameters altered in the calibration of the model were bed roughness, model boundary forcing and an optimisation of upstream bathymetry.

A varying bed roughness map was developed to reproduce the physical processes in the harbour particularly the upper estuary where there are areas of mangroves and salt marsh. The Department of Conservation 2011 habitat mapping layers of mangroves and salt marsh along with aerials were used to define the roughness zones. Mapping of the mangrove and saltmarsh areas are closely correlated with depth.

Using Manning roughness coefficients to define mangrove areas in tidal inlets is widely used by the scientific community for a range of applications. The default Manning roughness coefficient in Delft-FM is 0.023 s.m$^{-1/3}$ which is typical for a sandy tidally dominated inlet. Studies which were informed by measurements of the Manning friction coefficient in mangrove areas gave values between 0.02-0.05 s.m$^{-1/3}$ (Hoogeveen, 2020; Wolanski et al., 1992). The final bed roughness map used in the simulations is displayed in Figure 4-15.

Water level variations within the model were driven with tidal water levels generated from the OTIS TPXO global tide model (Egbert & Erofeeva, 2002). Tidal constituents (amplitude and phase) were extracted from the TPXO global tide model at over 40 locations along the Delft FM open boundary, and then reconstrued to give water level time series at each of the boundary points. The Moana Backbone model was also tested during calibration which consists of a 25+ years 3D hydrodynamic hindcast for New Zealand waters from a high-resolution 3D ROMS model, however a better calibration was achieved with from the OTIS TPXO model.

Optimisation of upstream bathymetry was also undertaken during calibration. Upstream areas like Karaka and Waiuku were optimised to ensure flow and hydro-connectivity into these areas and to capture the full tidal prism of the inlet. This was done by ensuring there were three wet grid cells across the streams by altering the grid resolution and bathymetry.

4.3.3.1.1 Water levels

The Delft FM model has been used to assess the conveyance and exchange of tidal waters within the Manukau Harbour as the tide propagates into the harbour and up to the tidal limit. Simulations were compared during calibration at two water level measurement locations. As the inlet is tidally dominated, calibration was undertaken over 29-day lunar cycles. For the Cornwallis and Waiuku which were deployed for 117 and 116 days respectively, two separate 29 -day lunar cycles were compared for each calibration phase. During calibration phase two, different 29-day periods were selected for Cornwallis and Waiuku. This was to increase robustness in calibration phase two by comparing different conditions in the two measured water level datasets as they were the only datasets available during the period.

Model statistics are presented for the two calibration phases in Table 4-2. Comparisons of modelled and measured water levels are presented in Figure 4-19 for calibration phase one and Figure 4-20 for calibration phase two.

Table 4-2 Model performance statistics against measured water levels during the two calibration periods.

Location	Model period	Comparison period (2023)	Model skill	Bias (m)	MAE (m)	RMSE (m)	R^2
Cornwallis	Calibration 1	23 Mar- 21 Apr	0.99	-0.04	0.11	0.13	0.99
	Calibration 2	21Apr – 20 May	0.99	-0.04	0.12	0.14	0.99
Waiuku	Calibration 1	23 Mar - 21 Apr	0.99	-0.03	0.12	0.14	0.99
	Calibration 2	1 May - 30 May	0.99	-0.07	0.14	0.18	0.99

The model statistics shows that modelled water levels agree generally well with the measured data throughout the lunar cycle in calibration period 1 with model skill scores and R^2 values of 0.99 and bias of -0.04 m or less. In calibration period two there is a higher bias of underpredicting at Waiuku, this is evident in the Figure 4-20 where an increase in water levels occurred on the 20th May that is not reflected in the model. This is likely due to the effect of periodic non-tidal water level variations that were not described by the tidal boundary or the CFSR winds and MSLP forcing such as localised weather events.

The Paratutae Island tide gauge dataset is also available and was used in the initial model development before measurements from the 2023 data collection campaign were available. However as was noted in Section 3.4.2 caution is advised when using this station for scientific analysis as it is liable to drift and is not measured against any referenced datum so was not used in the final validation.

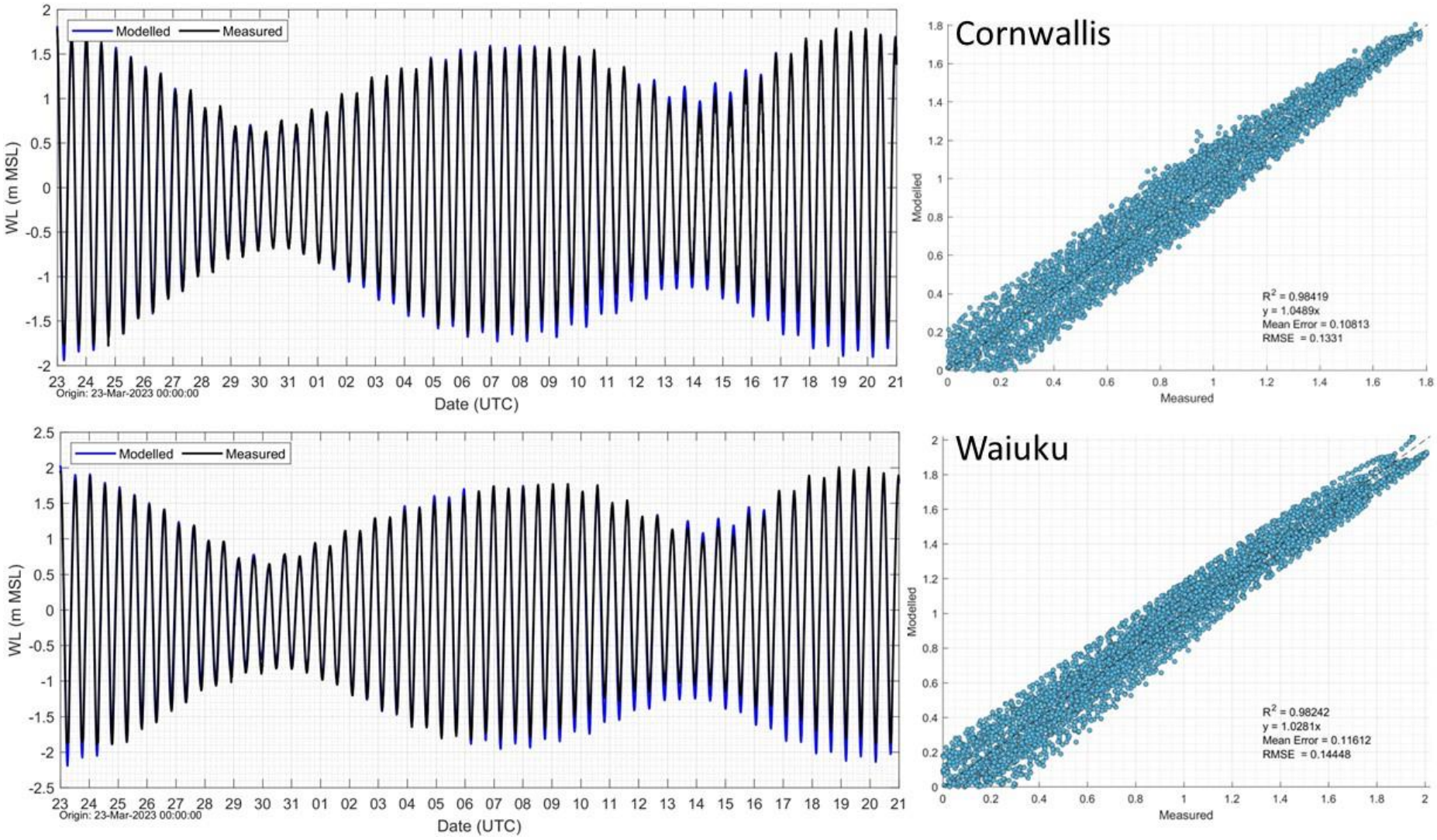

Figure 4-19 Modelled and measured water level timeseries (left) and Q-Q plots (right) at Cornwallis and Waiuku over the same 29-day lunar cycle period for calibration phase one.

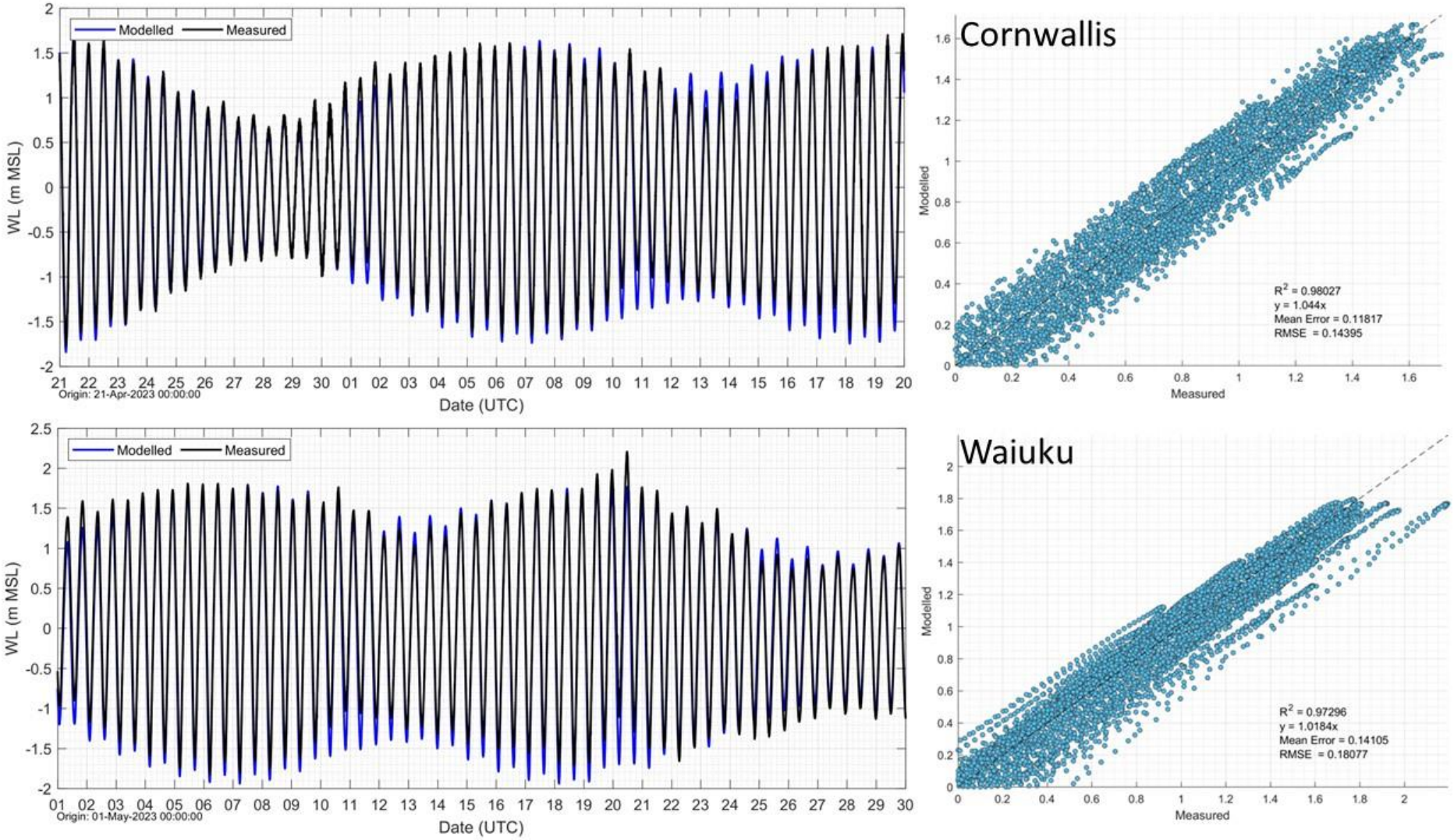

Figure 4-20 Modelled and measured water level timeseries (left) and Q-Q plots (right) at Cornwallis and Waiuku over separate 29-day lunar cycle periods for calibration phase two.

4.3.3.1.2 ADCP current transects

Current transects measuring 3D flow velocities across the Manukau entrance channel were undertaken throughout the tidal cycle on 22nd March 2023 to provide measurements of current velocities along the transects. The depth averaged velocities of the measurements were used for model comparisons. Model outputs of depth averaged current velocities were extracted from the map outputs which were saved at 5-minute intervals. A representative transect at peak flood, slack water and peak ebb tide are presented in Figure 4-21, Figure 4-22 and Figure 4-23 respectively.

Model performance statistics against measured velocities though ADCP transects are presented in Table 4-3. A moving mean was applied to the measurements to smooth any unrealistic variations or spikes that were visible in the dataset. The lower skill score at some transects can be attributed to differences at the ends of the cross sections on both the north and south bank of the channel, which is expected due to model resolution and bathymetry interpolation on the edges of the channel/domain. Current speeds and direction through the middle portion of the transects are well represented. The flood and ebb tides have a better calibration than transects undertaken on a slack tide, however the directions in Figure 4-22 show the opposing directions measured along the transects during slack tide are replicated within the modelled channel.

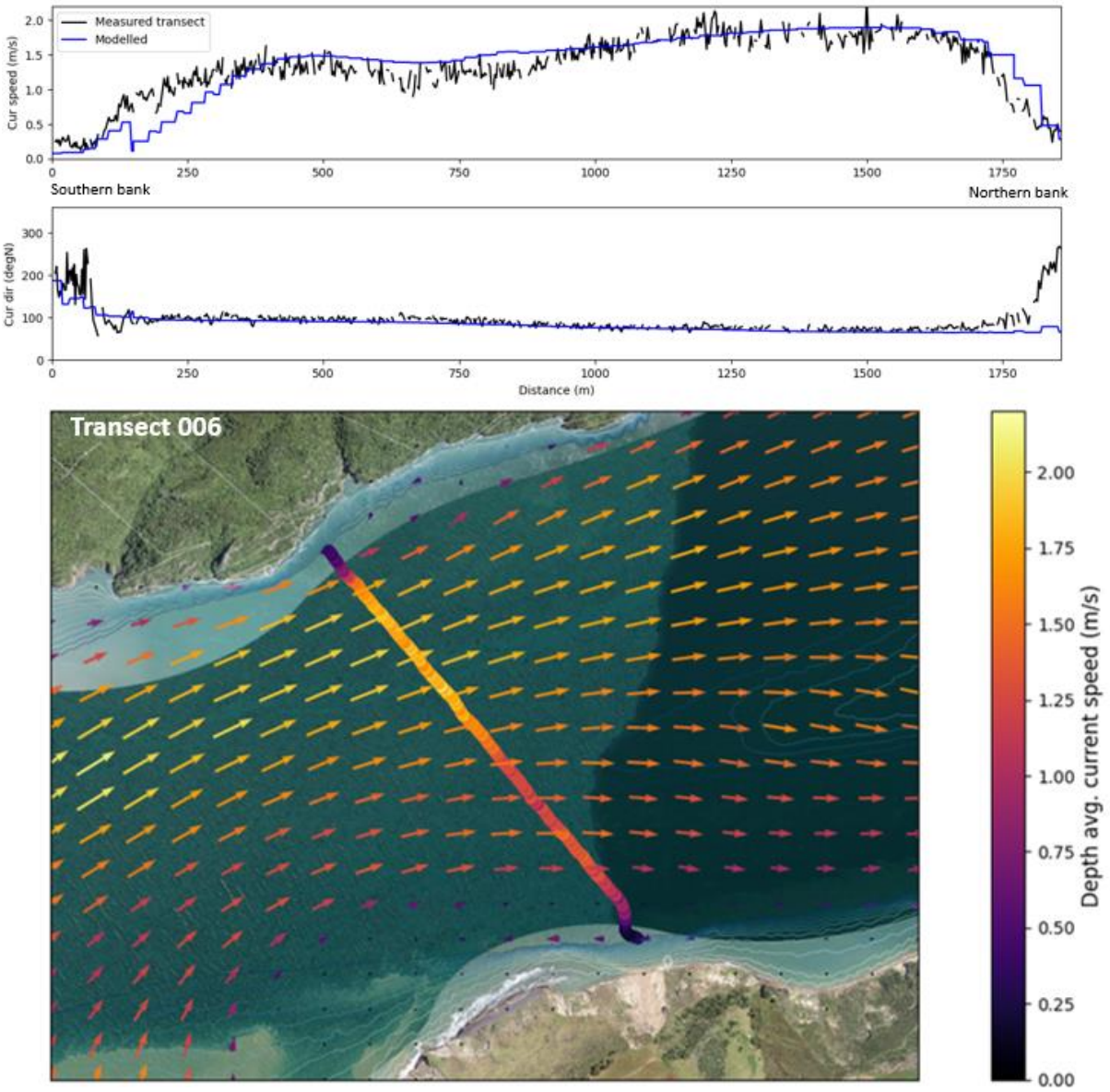

Figure 4-21 Modelled and measured current velocities and directions through transect 006 on a flood tide between 20:13 and 20:29 on the 22nd of March 2023 (UTC) for calibration phase one.

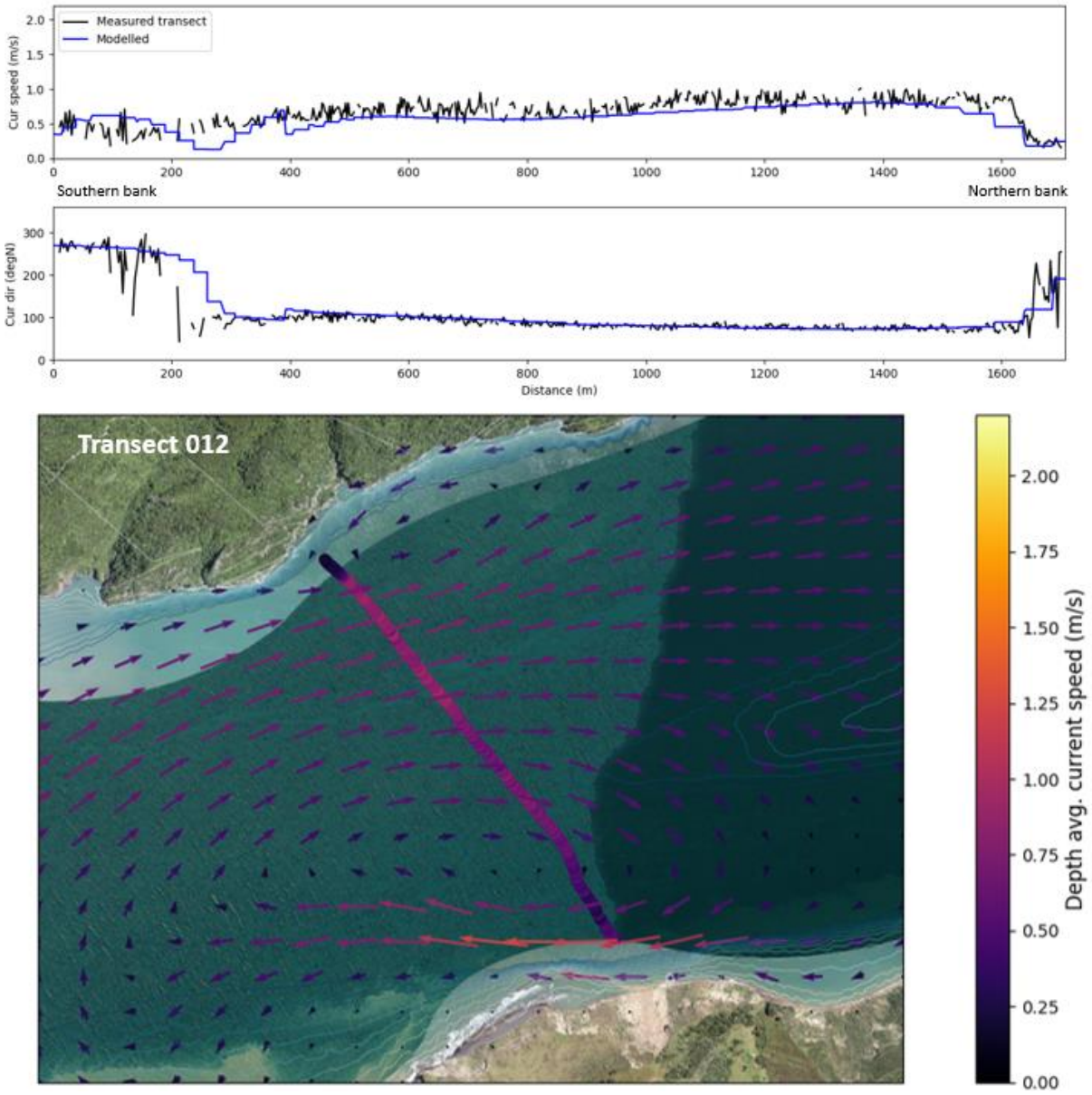

Figure 4-22 Modelled and measured current velocities and directions through transect 012 on a slack tide between 23:12 and 23:25 on the 22nd of March 2023 (UTC) for calibration phase one.

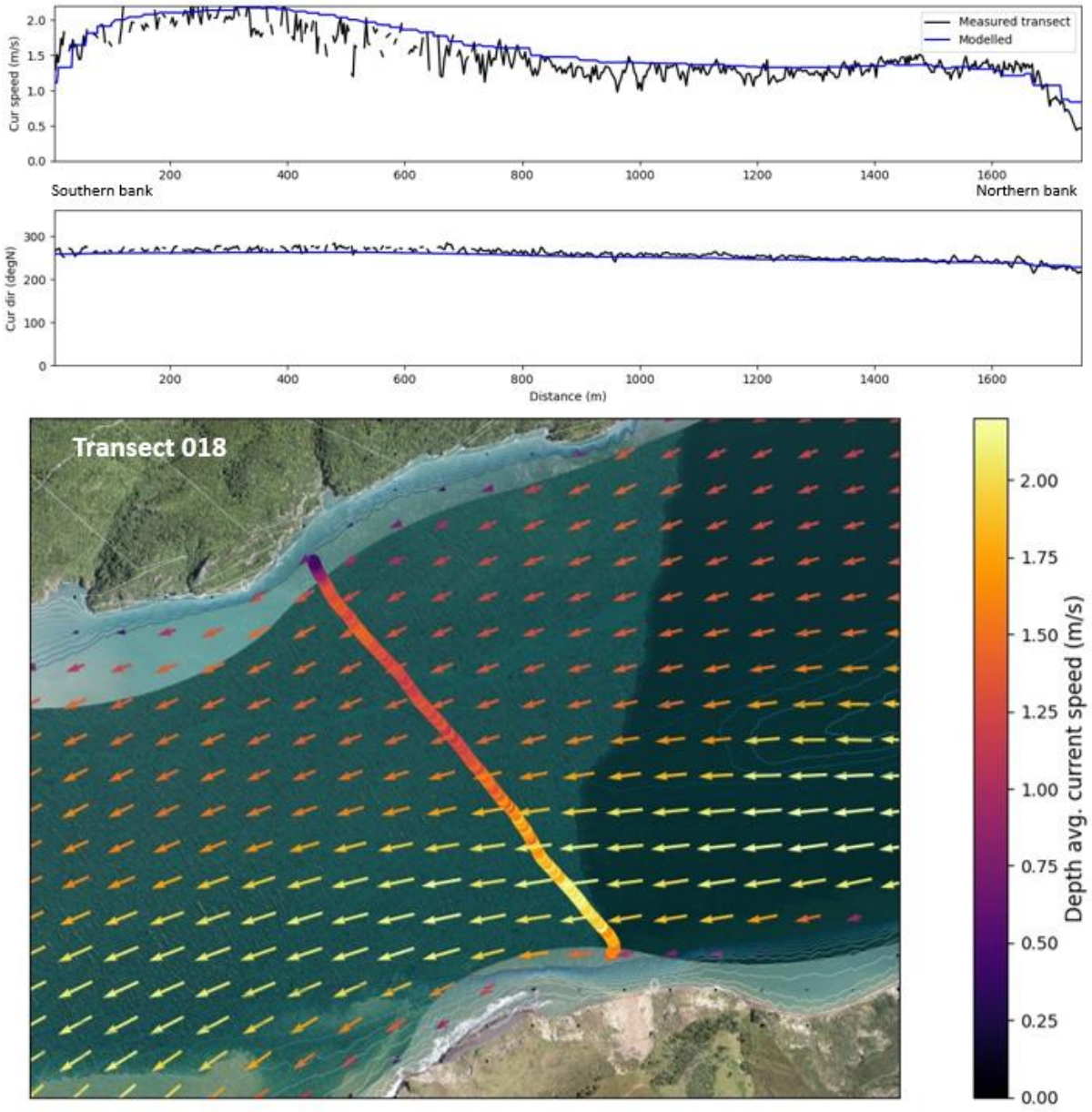

Figure 4-23 Modelled and measured current velocities and directions through transect 018 on an ebb tide between 2:16 and 2:29 on the 23rd of March 2023 (UTC) for calibration phase one.

Table 4-3 Model performance statistics against measured velocities though ADCP transects during calibration.

Transect	Tidal stage	Current speed					Current direction		
		Model skill	Bias ($m.s^{-1}$)	MAE ($m.s^{-1}$)	Meas mean ($m.s^{-1}$)	Model mean ($m.s^{-1}$)	Bias (˚N)	Meas mean (˚N)	Model mean (˚N)
002	Flood	0.73	0.05	0.16	0.97	0.92	-6.43	74.25	80.67
003	Flood	0.76	0.01	0.15	1.4	1.39	-3.44	73.41	76.85
006	Flood	0.96	0.05	0.13	1.42	1.37	-4.87	85.39	90.26
007	Flood	0.92	0.06	0.19	1.4	1.34	4.47	93.64	89.17
008	Flood	0.94	0.06	0.15	1.41	1.35	3.35	87.05	83.7
009	Flood	0.95	-0.02	0.16	1.26	1.28	1.53	95.4	93.87
010	Flood	0.96	-0.03	0.11	1.06	1.09	5.08	105.59	100.52
011	Flood	0.95	-0.03	0.14	1	1.03	4.33	104.32	100
012	Slack	0.75	0.01	0.1	0.68	0.67	8.05	111.32	103.27
013	Slack	0.66	0.09	0.13	0.61	0.52	-7.36	125.68	133.04
014	Slack	0.76	0.09	0.12	0.63	0.54	-10.57	252.22	262.79
015	Ebb	0.9	0.08	0.11	0.9	0.82	-6.87	250.13	257
016	Ebb	0.91	0.09	0.11	1.42	1.33	-8.16	251.72	259.88
017	Ebb	0.92	0.11	0.13	1.56	1.44	-7.4	251.69	259.09
018	Ebb	0.94	0.11	0.14	1.61	1.5	-6.39	252.24	258.63
019	Ebb	0.87	0.1	0.18	1.56	1.46	-6.24	251.83	258.07
020	Ebb	0.83	0.01	0.2	1.38	1.37	-5.12	252.61	257.73

021	Ebb	0.85	0.05	0.18	1.34	1.28	-6.86	252.91	259.77
022	Ebb	0.93	0	0.12	1.03	1.03	-7.26	253.2	260.46
023	Ebb	0.88	-0.03	0.13	0.89	0.92	-6.37	252.85	259.23
024	Slack	0.91	-0.1	0.12	0.37	0.48	-25.79	228.56	254.34
025	Slack	0.68	-0.11	0.12	0.16	0.27	-54.65	184.37	239.01
026	Slack	0.82	0.09	0.12	0.5	0.41	-11.53	69.13	80.66
027	Flood	0.54	0.09	0.14	0.72	0.63	-8.8	70.74	79.54
028	Flood	0.55	0.02	0.12	1.14	1.12	-8.09	78.5	86.59
029	Flood	0.85	0	0.11	1.18	1.18	-8.08	79.22	87.3

4.3.3.1.3 ADCP tidal discharge

From the 30 current transects across the Manukau entrance channel, 24 covered a similar location and distance (transect 006-029). Tidal discharge (m^3.s) through the transect was calculated at each of these 24 comparable transects. The flood and ebb tidal prisms were also calculated which is the total volume of water discharging into and out of the harbour on the rising and falling tide, respectively.

The modelled and measured discharges throughout the tidal cycle across the entrance channel are shown in Figure 4-24. An average across all 24 transects was used for the modelled discharge, the model cross-section outputs are at five-minute intervals. There is a good agreement between modelled and measured tidal discharge curves across the transects indicating the model performs well at representing the magnitude and timing of tidal flows in the Manukau Harbour.

For calculation of the measured tidal prism there was not a complete flood tide measured, therefore an estimate of a complete flood tide was extrapolated from the measured values available. These extrapolations are displayed in Figure 4-24 and give the estimates of the flood tidal prism. The measured and modelled water levels at Cornwallis are also displayed in Figure 4-24, only half of the transect measurement period has coinciding water levels measurements at Cornwallis. The modelled and measured tidal prism during the flood and ebb tidal stage are provided in Table 4-4.

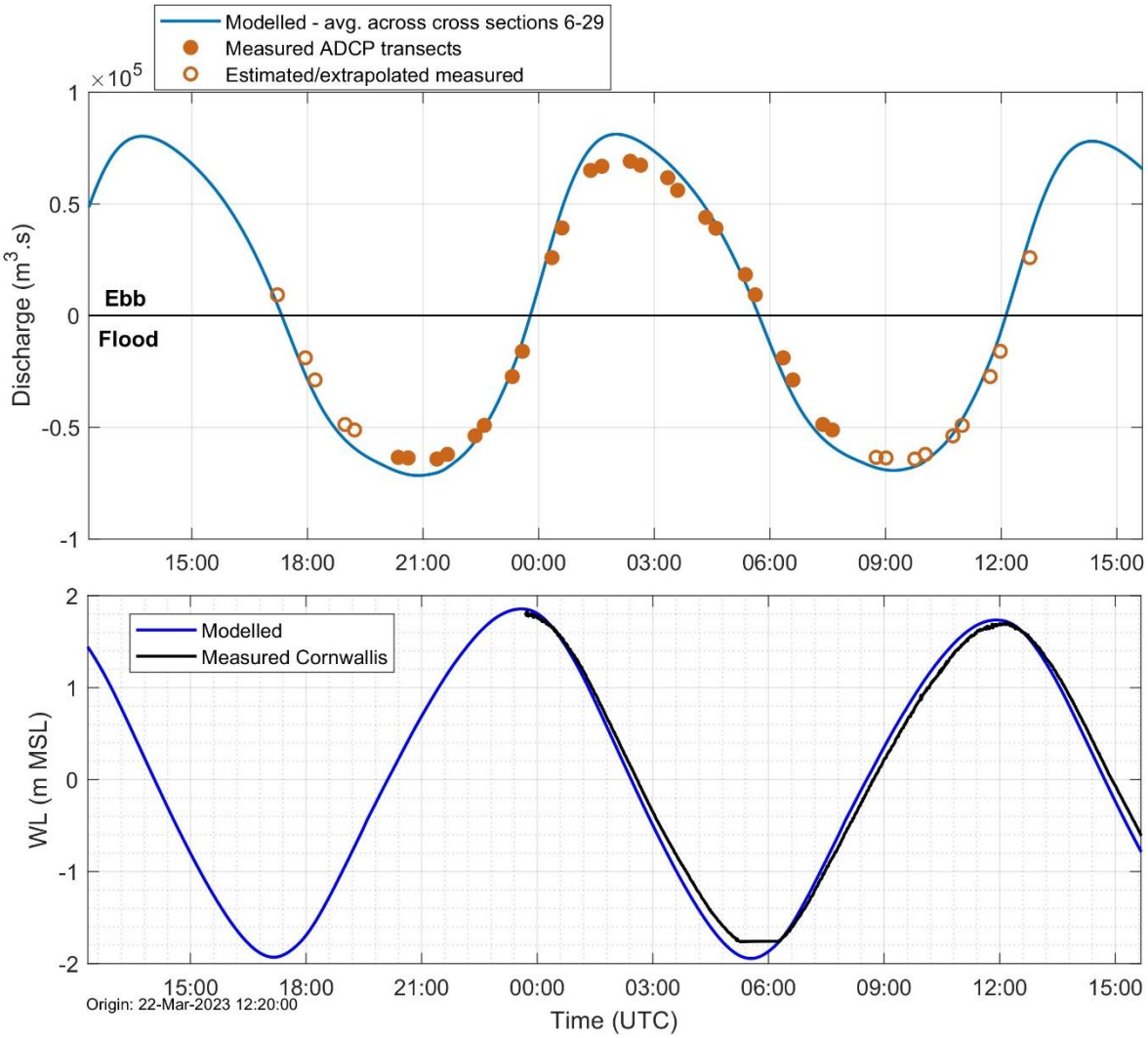

Figure 4-24 Modelled and measured discharge volumes for calibration phase one (top), note that the estimated/extrapolated measured values on the two flood tidal discharges were used to give estimates of the flood tidal prism and bottom. And concurrent measured and modelled water levels at Cornwallis during the time of ADCP transects (bottom).

Table 4-4 Calculated flood and ebb tidal prism values for measured and modelled transects across Manukau entrance, note that both measured flood tidal prisms were calculated using extrapolated data.

Data set	Tidal prism		
	Flood	Ebb	Flood
Modelled (m^3)	-1,161,393,662	1,140,742,643	-1,119,087,871
Measured (m^3)	-1,041,322,416	992,629,373	-1,041,430,428
Difference	10.9 %	13.9 %	7.2 %

4.3.3.2 Validation – Hydrodynamics

Validation is undertaken to ensure the model continues to consistently represent the natural processes to the required level of accuracy without any additional adjustment to the model parameter settings. Validation was between 1st June and 17th July.

4.3.3.2.1 Water levels

Simulations were compared during validation at three water level measurement locations. For Cornwallis and Waiuku 29 -day lunar cycles were compared. Analysis at Karaka was undertaken for the full 16-day period available at the location. Model performance statistics during the validation period is presented in Table 4-5. Comparisons of modelled and measured water levels for validation are presented in Figure 4-26 for Karaka Figure 4-26 Figure 4-25 for Cornwallis and Waiuku. The model skill at all three locations was 0.99 or above as was the R^2. Unlike the two calibration periods where there was a negative bias for all comparisons, the three locations all had a positive bias over the comparison periods.

Table 4-5 Model performance statistics against measured water levels during the validation period.

Location	Model period	Comparison period (2023)	Model skill	Bias (m)	MAE (m)	RMSE (m)	R^2
Cornwallis	Validation	10.Jun - 9.Jul	1.00	0.04	0.10	0.12	0.99
Waiuku	Validation	1.Jun - 30.Jun	0.99	0.15	0.16	0.18	0.99
Karaka	Validation	1.Jul - 17.Jul	0.99	0.05	0.15	0.19	0.99

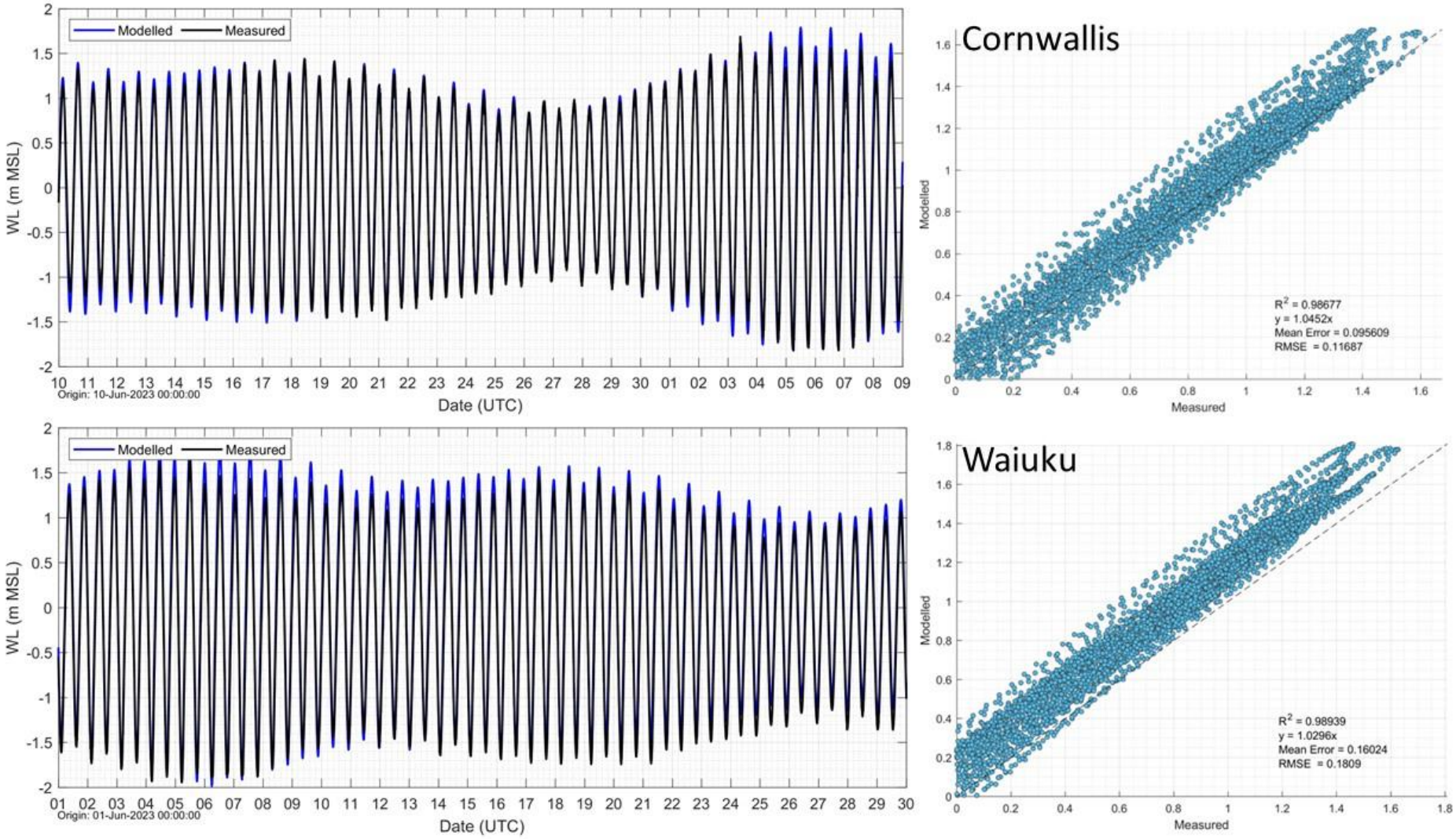

Figure 4-25 Modelled and measured water level timeseries (left) and Q-Q plots (right) at Cornwallis and Waiuku over separate 29-day lunar cycle periods for the validation phase.

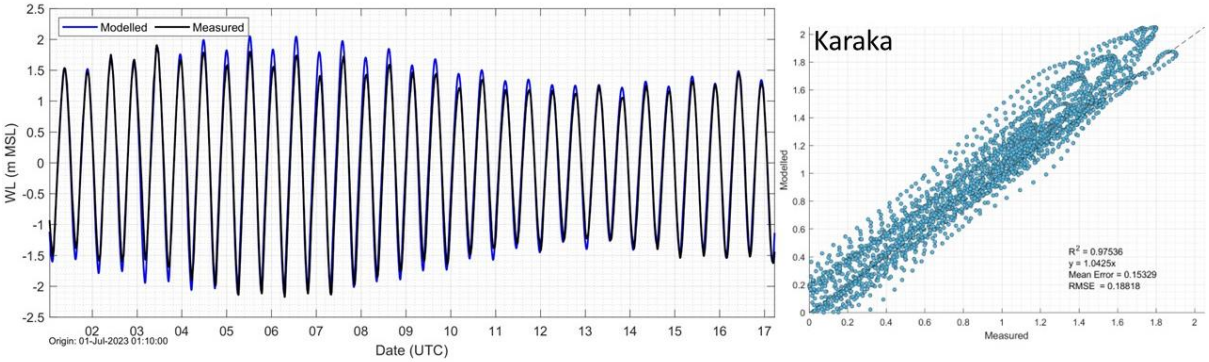

Figure 4-26 Modelled and measured water level timeseries (left) and Q-Q plots (right) at Karaka over the full 16-day period during the validation phase.

4.3.3.2.2 Drifter currents

Five drifters were deployed within the Manukau entrance channel on the 10th June 2023 (UTC). The drifters remained in the water for at least 28 hours and over two full tidal cycles. Measured current speeds across the drifter track were compared to modelled currents extracted from the map outputs which were saved at 15-minute intervals. Comparison of modelled and measured current speeds at the five drifters are presented from Figure 4-27 to Figure 4-31. Measured wave heights at the offshore wave buoy were less than 1 m at the time of drifter deployment.

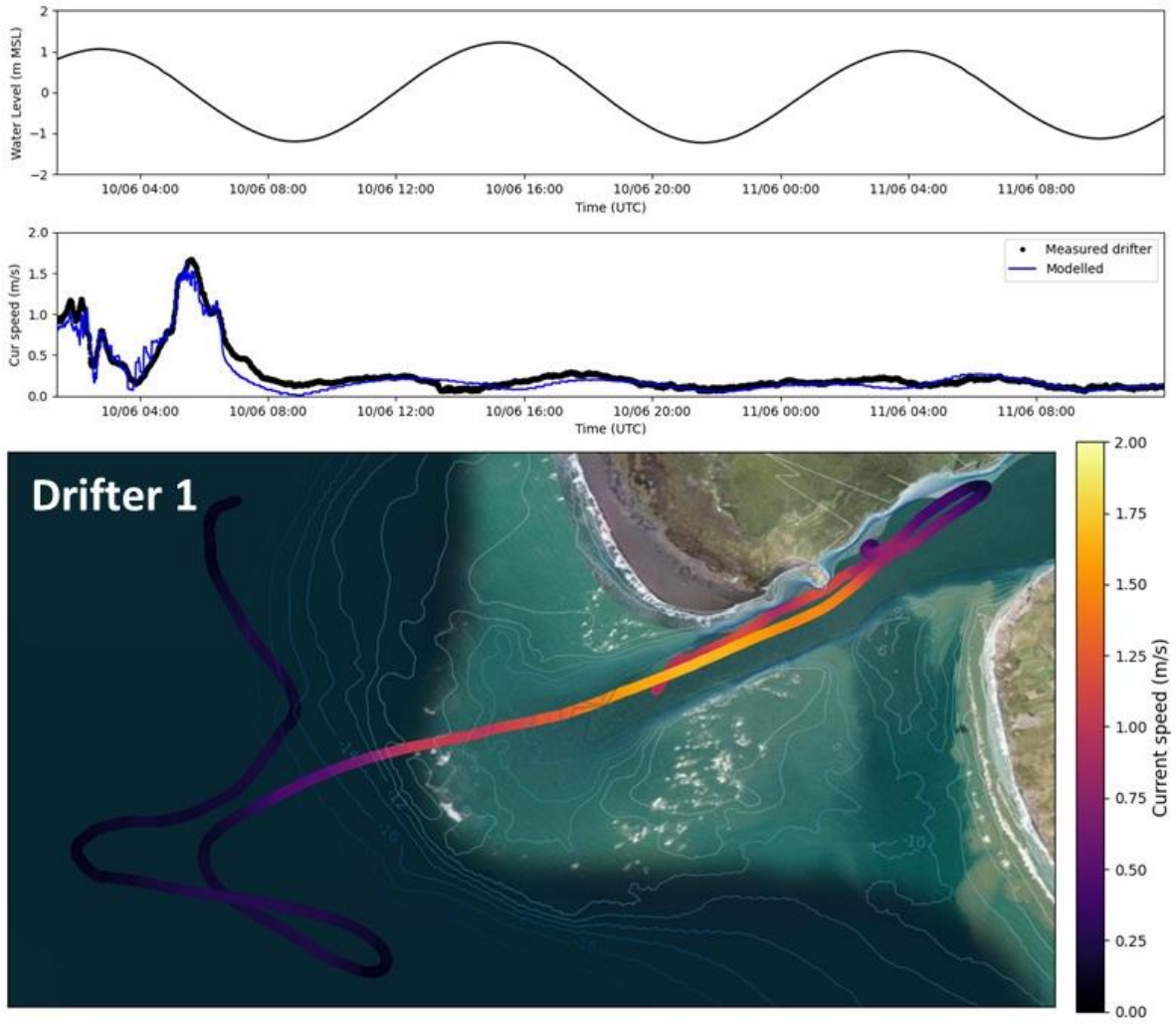

Figure 4-27 Modelled and measured current speeds from drifter one deployed on 10th June 2023 and used in the validation phase.

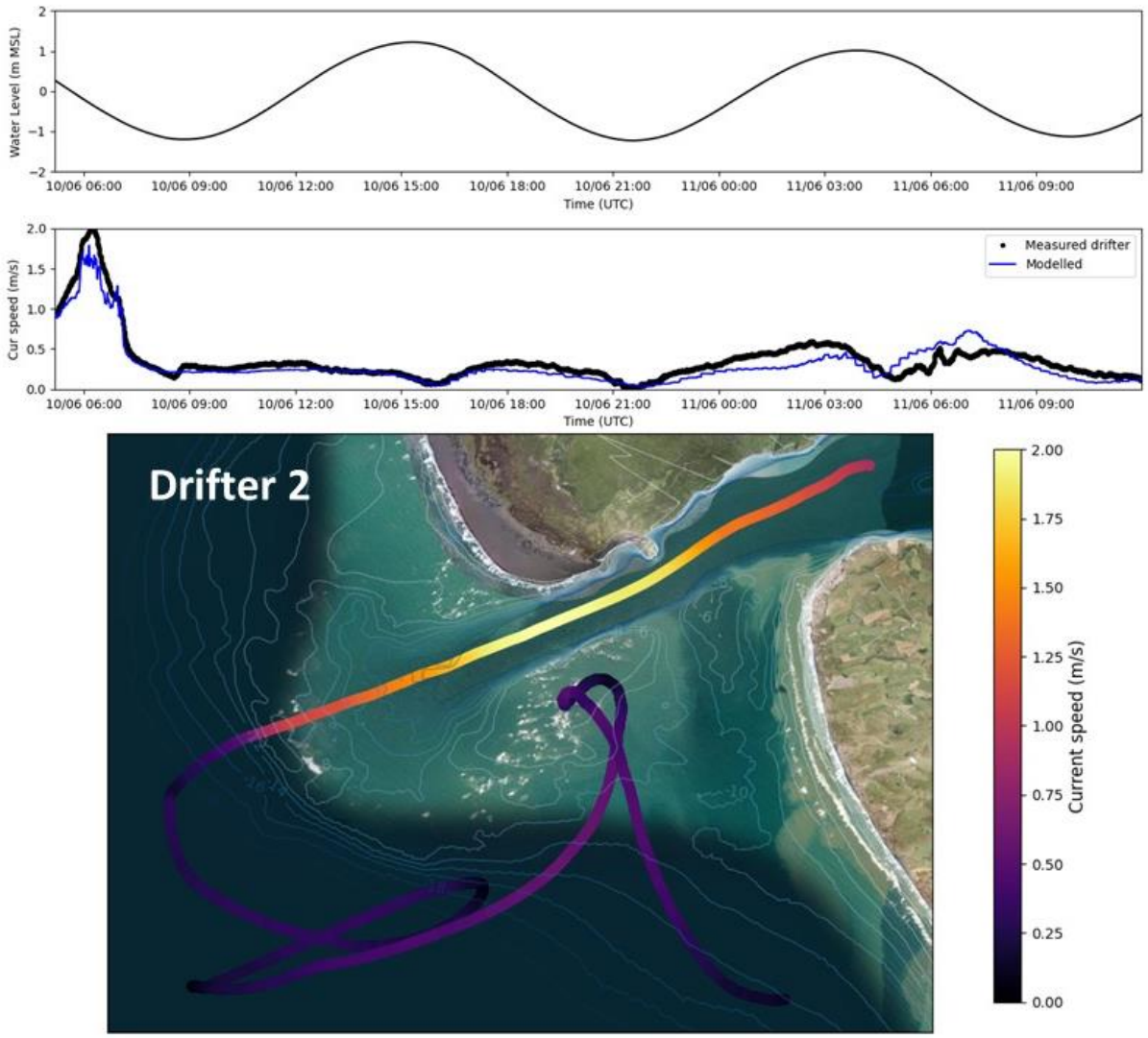

Figure 4-28 Modelled and measured current speeds from drifter two deployed on 10th June 2023 and used in the validation phase.

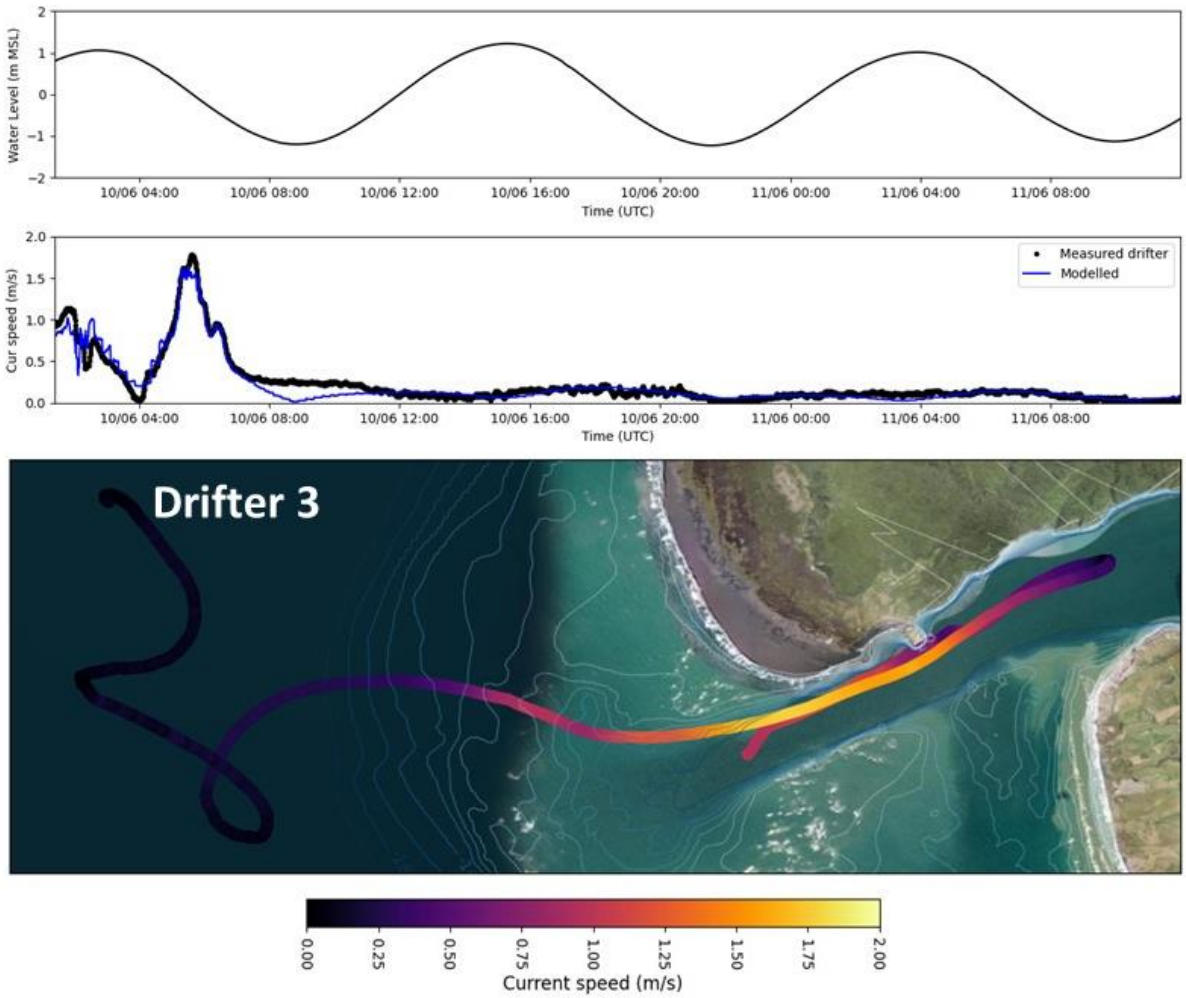

Figure 4-29 Modelled and measured current speeds from drifter three deployed on 10th June 2023 and used in the validation phase.

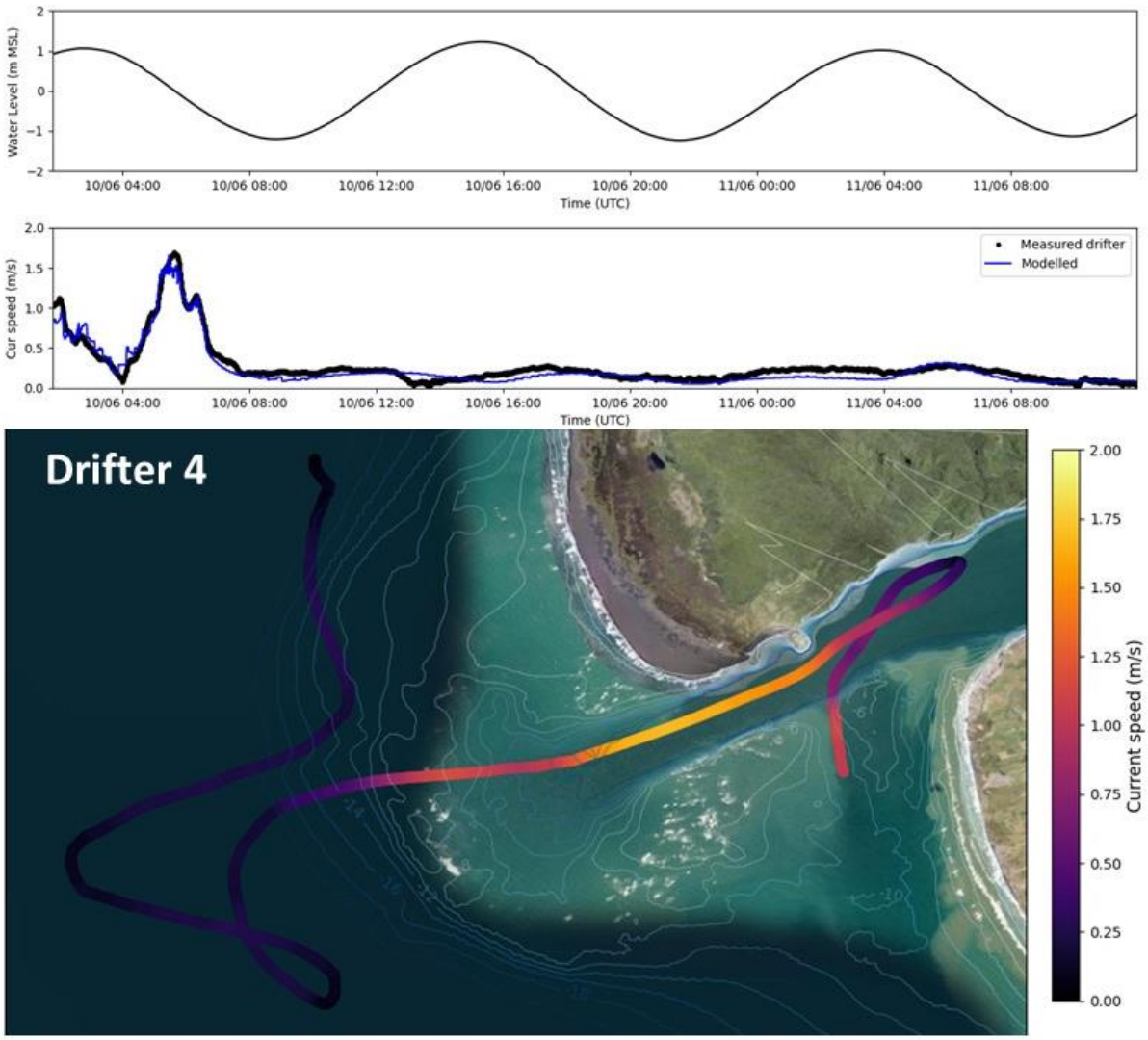

Figure 4-30 Modelled and measured current speeds from drifter four deployed on 10th June 2023 and used in the validation phase.

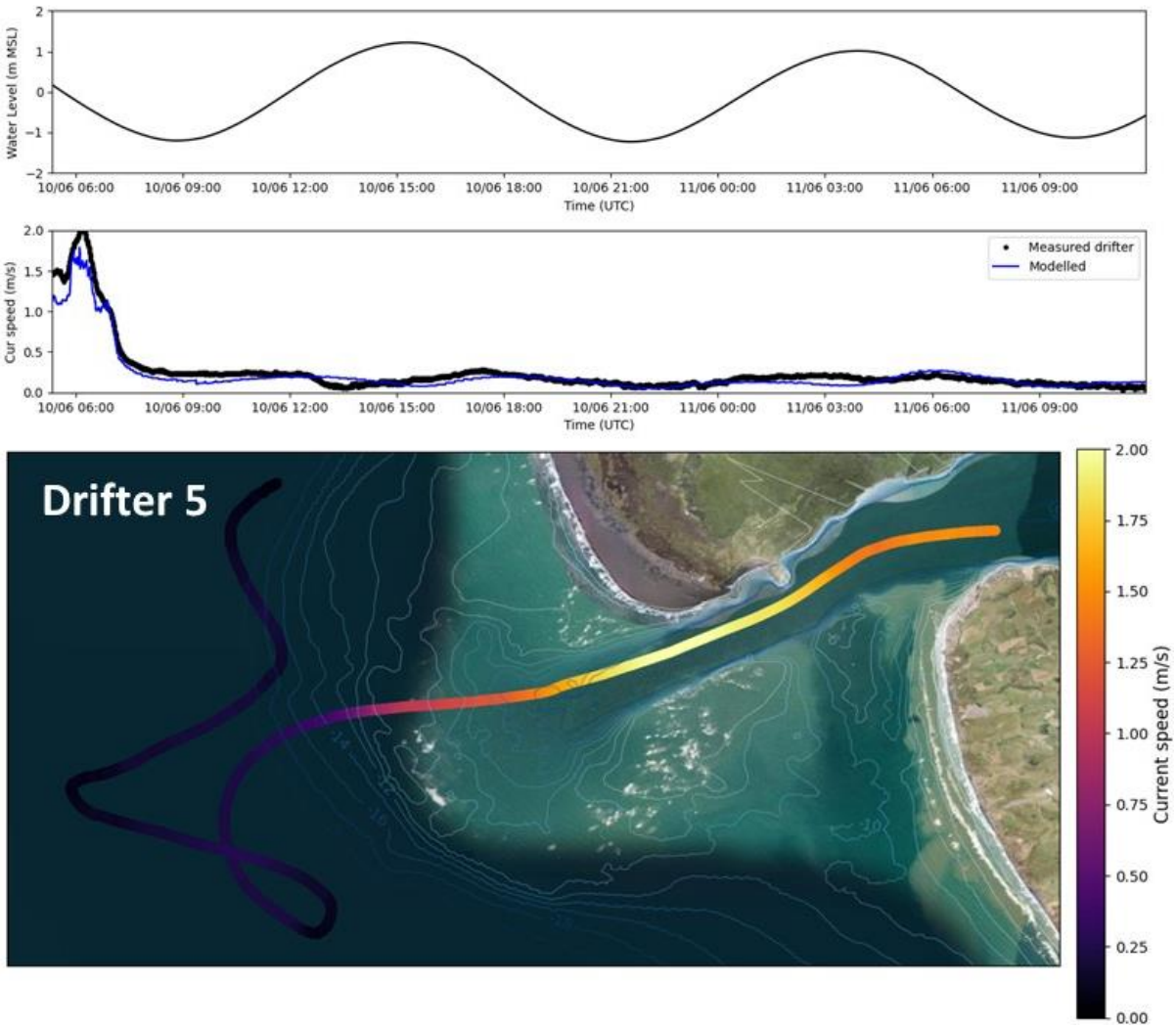

Figure 4-31 Modelled and measured current speeds from drifter five deployed on 10th June 2023 and used in the validation phase.

4.3.3.3 Calibration - Waves

The Delft FM wave module has been calibrated with the wave data from the two buoys deployed offshore and inside Manukau Harbour. Comparisons of the wave parameters output from the Delft FM and SWAN components of the coupled model was undertaken to determine the most accurate/suitable parameters to use in the analysis.

4.3.3.3.1 Descriptions of wave period

A comparison of the wave parameters from the Delft FM model to those output in the coupled SWAN wave model was undertaken. Modelled wave parameters are described for each output location in the Delft FM model (at five-minute intervals) and SWAN model (computed every hour). There are several interpolations carried out between these models, the SWAN wave grids to the Delft FM mesh, time interpolation, and coupling time where information is passed between the models (which in these simulations was every

60 minutes). In principle, it is inevitable to see differences when comparing outputs of the Delft FM and SWAN models, but overall comparisons of the wave height and wave directions are not significantly different.

Wave period output from the Delft FM flow model were lower than expected when compared to outputs from the Wave module. The wave period in Delft FM is described as the wave peak period, T_p. The coupled Delft FM model converts SWAN mean wave period T_{m01} to a peak wave period T_p with a proportionality factor between the mean period of a spectrum and its peak period, assuming a theoretical JONSWAP shape. Studies have found that Delft FM wave period was underpredicted when compared to laboratory measurements (Dingemans, 1987). T_p from the SWAN model was extracted from the hourly 2D wave spectra (only T_{m01} is written at the output locations). T_p from the wave spectra and from the wave hindcast at a similar location offshore of the bar were of a similar magnitude (see Figure 4-32) and were approximately 20%-30% larger than the T_p described in Delft FM.

Further analysis showed that the effect of strong ebb currents on waves at the entrance lead to some instability in the wave data at some locations. This was particularly clear in the section of the entrance channel with the strongest ebb currents where during a peak ebb tide the peak spectra frequency drops from a low frequency to high frequency. This is evident in both the 1D spectra, T_p extracted from the 2D spectra, and the maps of SWAN smooth peak period T_{ps} in Figure 4-33. T_{ps} is a SWAN output, the value according to the SWAN manual is the maximum of a parabolic fitting through the highest bin and two bins on either side the highest one of the discrete wave spectrum. This 'non-discrete' or 'smoothed' value is a better estimate of the 'real' peak period compared to the quantity RTP.

These instabilities did not occur during any other tidal stage. This is likely due to the limitation of the model in dealing with strong currents with opposing waves, which in reality tend to increase wave breaking but is not particularly well described in numerical models (Rapizo et al., 2017). Care should be taken using the model outputs at these isolated locations where the instabilities occur (mostly C30 and C31).

For the timeseries at each output location, wave height and direction from Delft FM was used and wave period (T_p) was extracted from the 2D spectra. For the wave maps, SWAN outputs of smoothed peak wave period (T_{ps}) over the entire domain were used along with the wave heights and directions from the Delft FM. These wave periods were used as they were determined to be the most representative and stable for each output type.

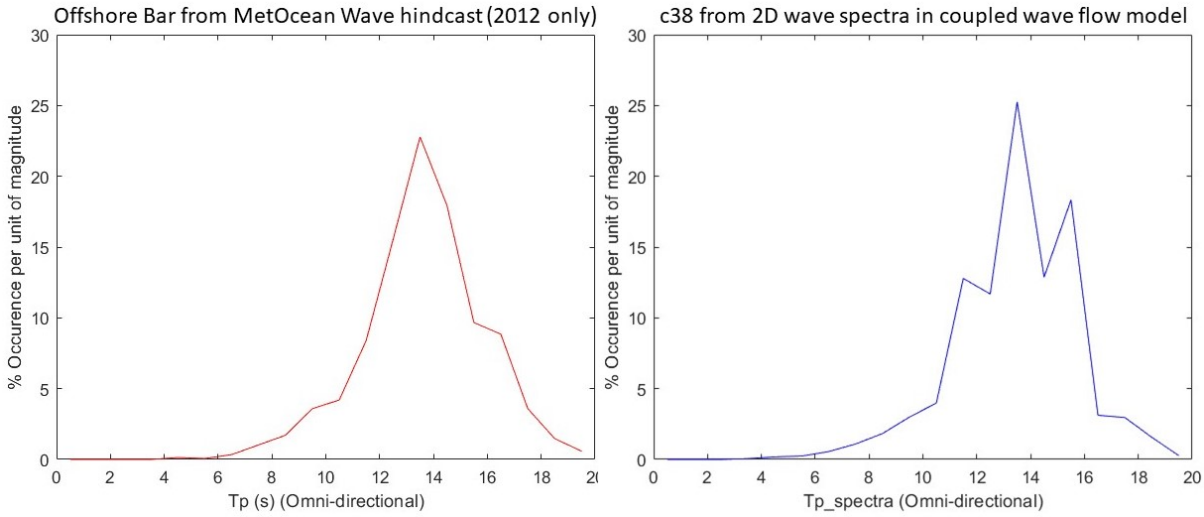

Figure 4-32 Probability of occurrence of peak wave period over 2012 from the wave hindcast 200 m grid offshore of the bar (left) and extracted from the 2D wave spectra (right) at c38.

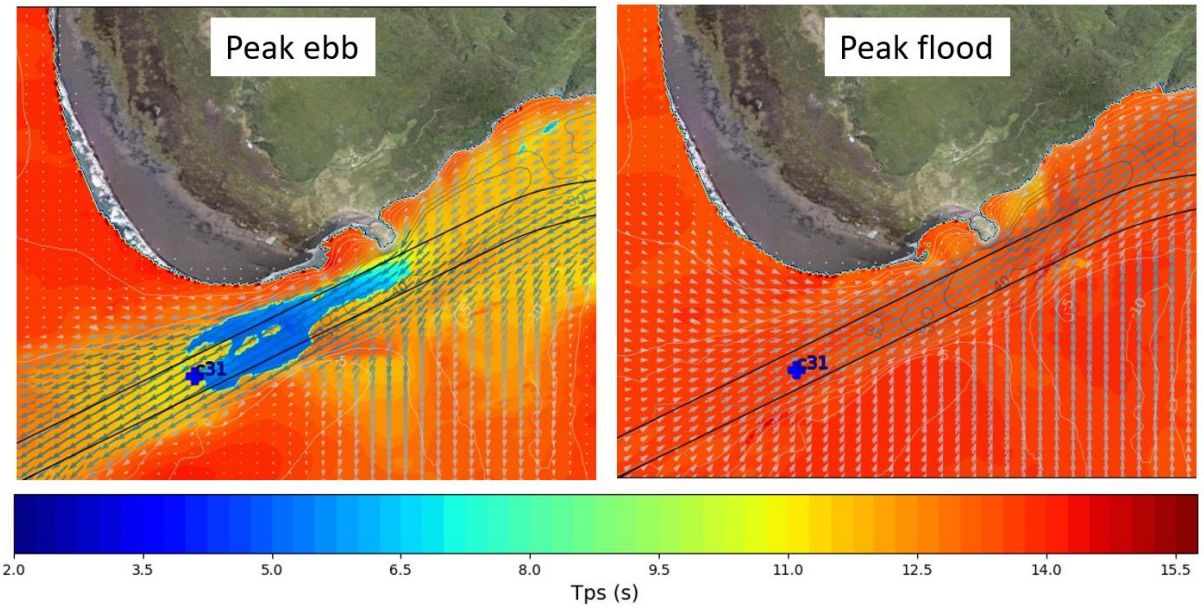

Figure 4-33 Smoothed peak wave period (SWAN) during a peak ebb and peak flood tide within Manukau entrance.

4.3.3.3.2 Wave buoys

Model performance statistics are presented in Table 4-6. Wave parameter figures with significant wave height, mean period (from the SWAN model) and mean direction are presented at the offshore and inner harbour wave buoys in Figure 4-34 and Figure 4-35 respectively. The peak wave period (T_p) measurements were deemed inaccurate as the data appeared to be binned, therefore for validation comparisons were made between modelled and measured peak mean period (T_{m01}).

Table 4-6 Model performance statistics against measured significant wave height.

Location	Comparison period (2023)	Meas mean (m)	Model mean (m)	Meas 90th %ile (m)	Model 90th %ile (m)	Model skill	Bias (m)	MAE (m)	RMSE (m)
Offshore	10.Jul -1.Aug	1.56	1.81	3.05	2.91	0.95	0.25	0.33	0.40
Inner harbour	1.Jul – 1.Aug	0.20	0.29	0.37	0.48	0.79	0.09	0.10	0.13

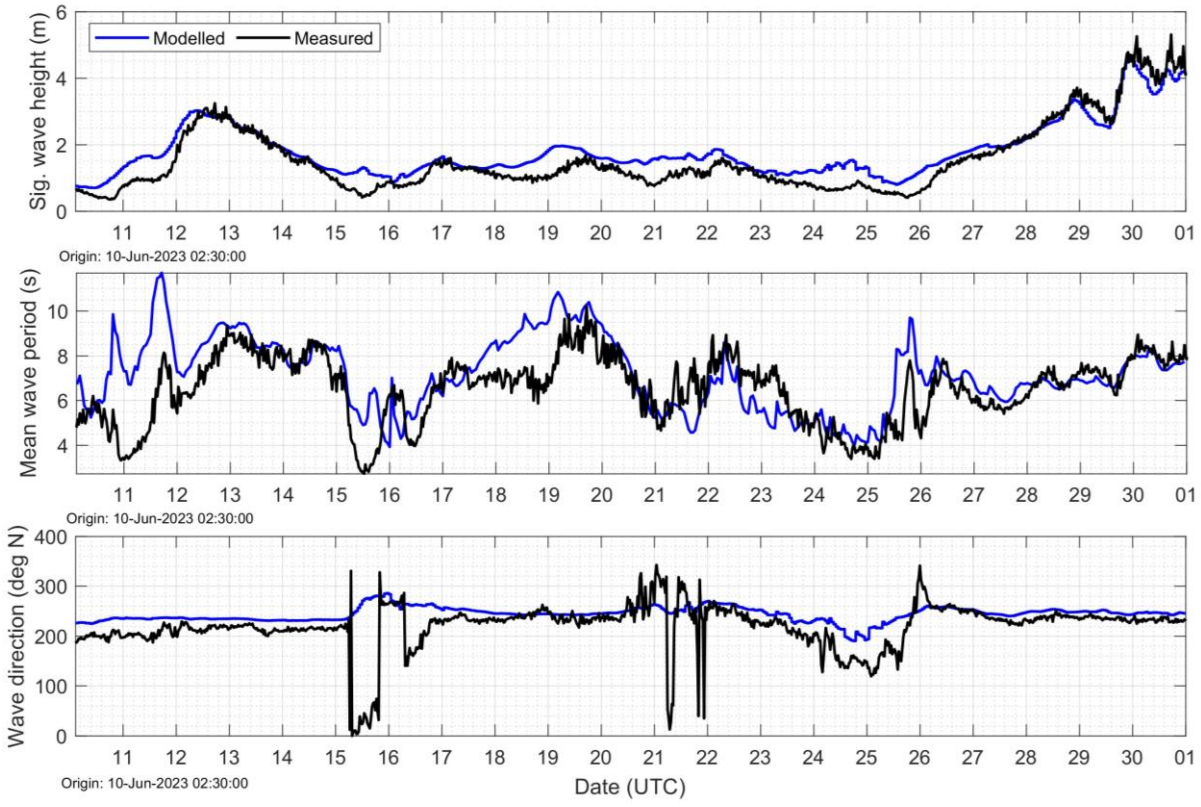

Figure 4-34 Modelled and measured significant wave height at the offshore wave buoy during the wave calibration phase.

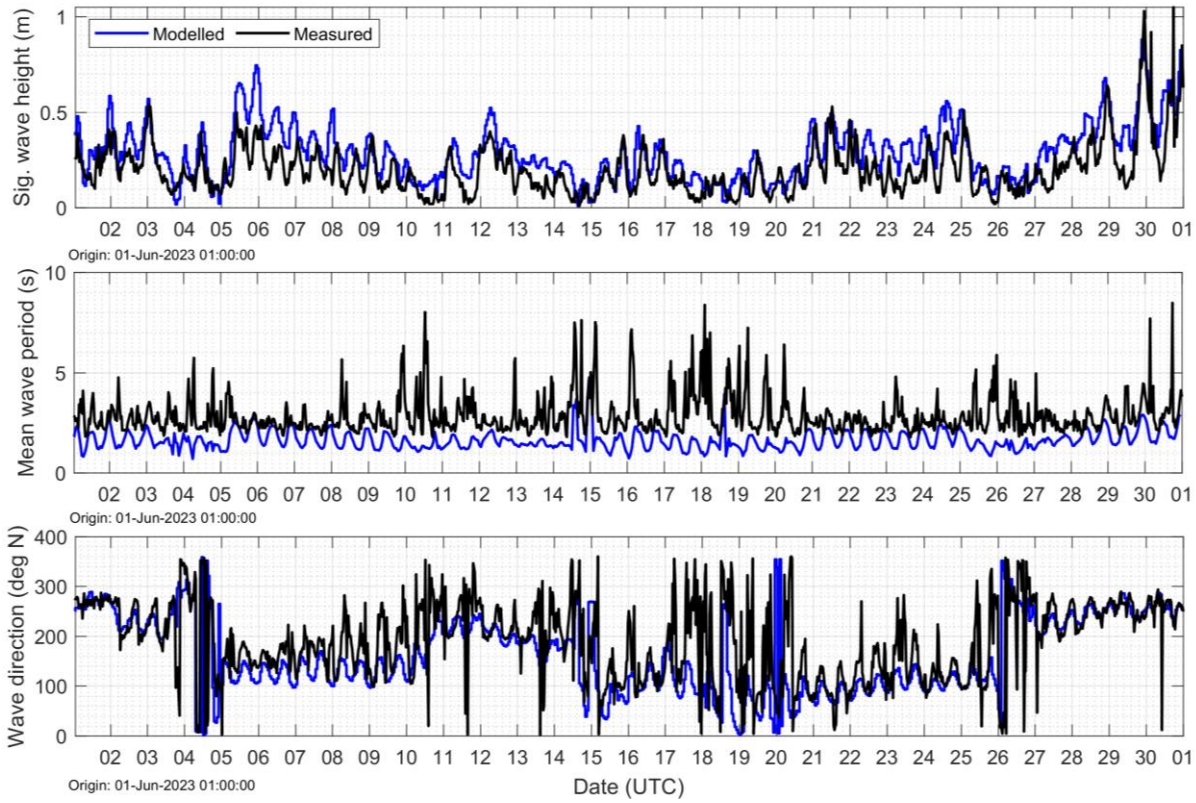

Figure 4-35 Modelled and measured significant wave height at the inner harbour wave buoy during the wave calibration phase.

5. Results

5.1 Model output locations

Model output locations were selected in collaboration with the Project team. The positions of the output locations were selected to cover key locations for the overall project and include measured data locations, reporting locations over the entrance bar and within the channel, and locations of the potential port structures.

A nomenclature referring to locations has been adopted to delineate between those Offshore (o), on the Bar (b), at 1 km intervals along the Channel (c), in the Harbour (h) and at Measured data sites (m). The complete set of model output locations are displayed in Figure 5-1. For reporting of model results, all 38 channel output locations spaced at 1 km intervals along the concept design channel were used. The channel output locations (C1 – C38) referred to in the following sections are displayed in Figure 5-2 and Figure 5-3.

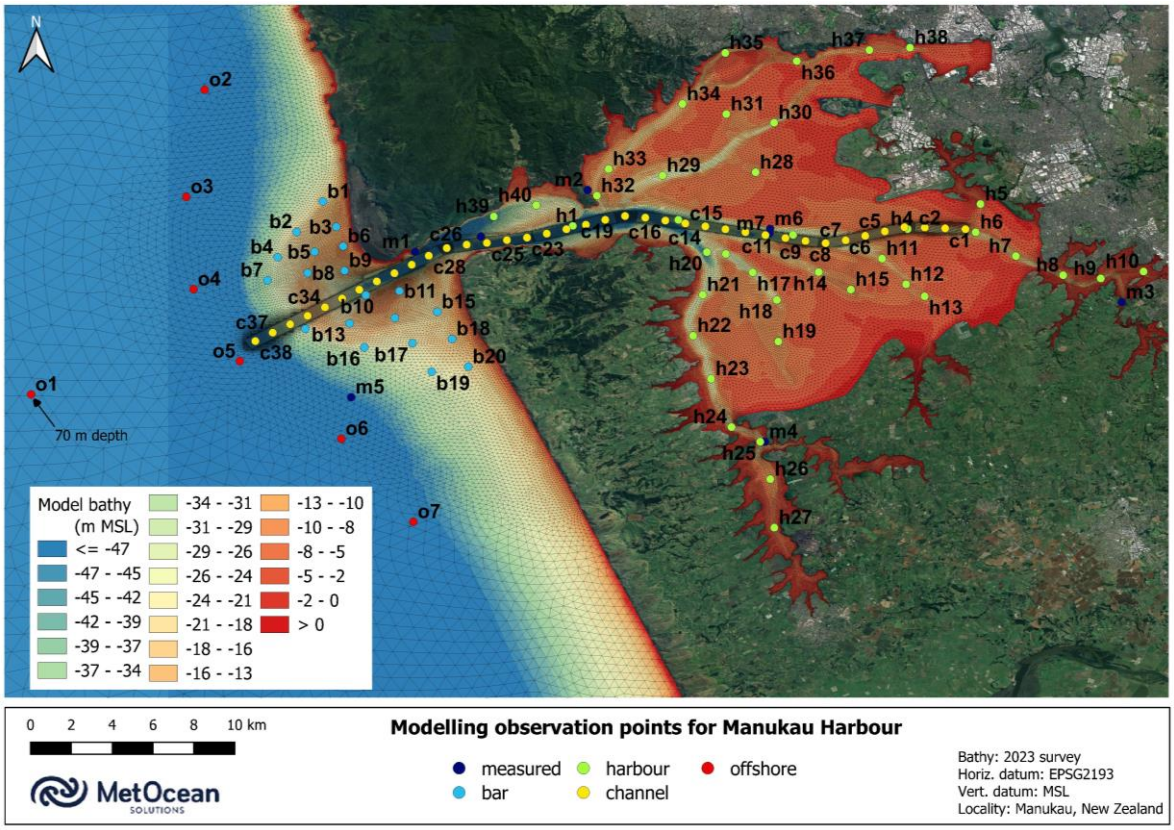

Figure 5-1 Model output locations used in the numerical models of Manukau Harbour with 'existing' model mesh.

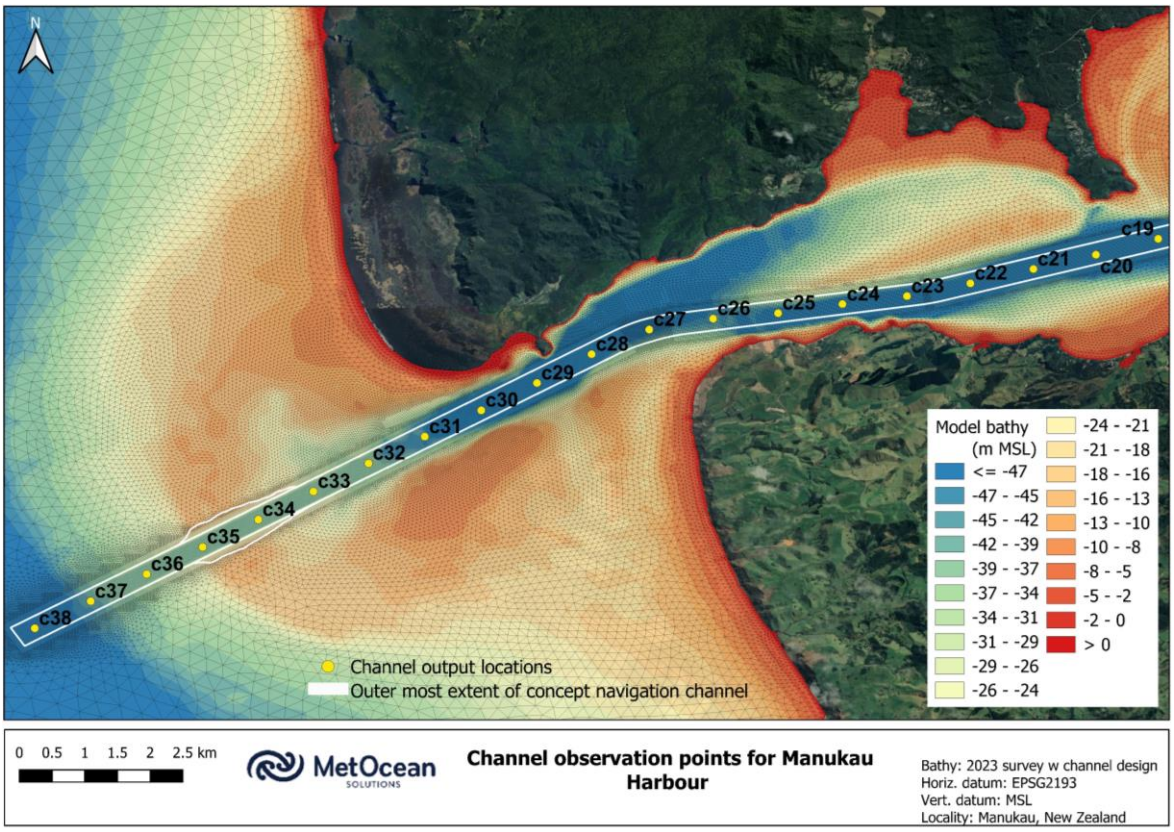

Figure 5-2 Channel output locations within the entrance and bar of Manukau Harbour with channel 'design' mesh.

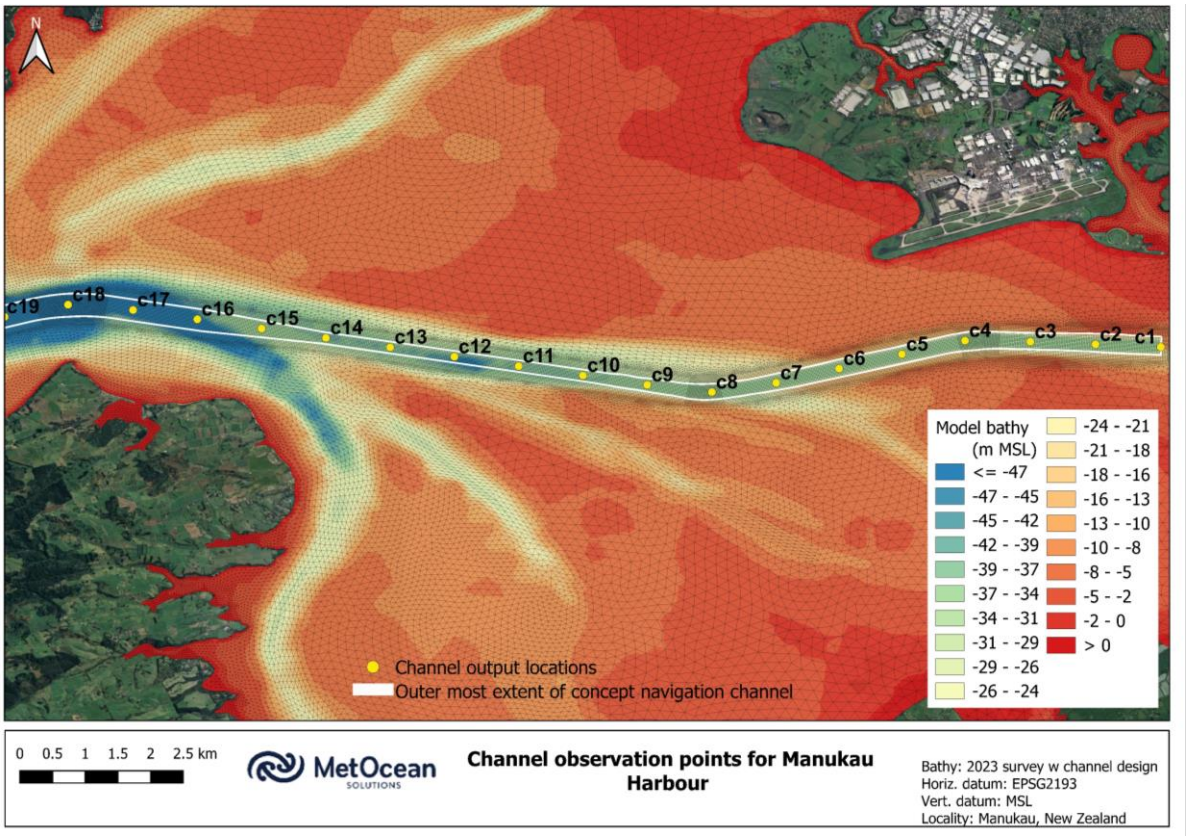

Figure 5-3 Channel output locations within Manukau Harbour with channel 'design' mesh.

5.2 SWAN model – 41 years wave hindcast

A 41-years (1980-2020) SWAN wave hindcast (with existing bathymetry) has been completed using over four domain nests with the following grid resolution: 4 km, 800 m, 200 m, 80 m and 20 m.

Hindcast wave data have been extracted and provided to the channel design and navigation team. Note a 10-year (2010-2020) SWAN simulation with the channel 'design' bathymetry which was the existing 2023 bathymetry with the addition of the South West Channel dredged design for the concept navigation channel over the 20-m nest has also been completed and site output data were provided.

In this section, we present the wave results of the 41-year existing simulation at site O1 (off the bar).

A summary of the total (i.e., sea plus swell) significant wave height statistics (H_s) at O1 is provided in Table 5-1.

The annual joint probability distribution of the total significant wave height and peak period (T_p) are presented in Table 5-2. The annual joint probability distribution of the total significant wave height and mean wave direction at peak energy are presented in Table 5-3.

Monthly and annual exceedance statistics for H_s and T_p are presented in Table 5-4 and Table 5-5, respectively.

The annual and seasonal non-exceedance persistence probabilities for total significant wave height at O1 (Table 5-6 to Table 5-11) can be used to estimate the operational uptime for tasks with wind speed limitations of variable duration. For example, at O1 on average in summer, total significant wave heights are less than 2.0 m for durations of 36 hours and greater for 50.21% of the time (Table 5-6).

The wave rose for annual total significant wave height is presented in Figure 5-4, showing the predominance of waves incoming from the SW sector.

The directional return period values for wave extremes are given in Table 5-12 for 1, 10, 25, 50 and 100-year return periods (see Appendix A for details on the extreme value analysis). Note a continuing trend of increasing wave (energy) is predicted in response to climate change, particularly in the Southern Ocean (Hemer et al., 2013; Rouse et al., 2017). Increases of order 5% in wave height are suggested for 2070–2099 for parts of New Zealand exposed to Southern Ocean swell, but less and variable elsewhere (Rouse et al., 2017). Although the studied area is not directly exposed to Southern Ocean swell, the

conservative estimate of 5% increase in extreme wave heights is indicated as a reference in the extreme wave table presented in this section for omni-directional conditions (Table 5-12).

Contour plot of omni-directional bi-variate return period values for significant wave height and peak wave period are presented in Figure 5-5.

Table 5-1 Annual and monthly total significant wave height statistics at O1 for the 'existing' scenario.

Period (01 Jan 1980 – 31 Dec 2020)	Total significant wave height statistics [1]															
	Total significant wave height (m)				Exceedance percentile for total significant wave height (m)											Main [2] Direction(s)
	min	max	mean	std	p1	p5	p10	p50	p70	p75	p80	p90	p95	p98	p99	
January	0.46	7.43	2.04	0.77	0.83	1.06	1.22	1.89	2.29	2.44	2.61	3.05	3.50	4.06	4.42	SW
February	0.65	6.00	1.97	0.70	0.90	1.08	1.22	1.84	2.19	2.32	2.47	2.91	3.30	3.79	4.14	SW
March	0.57	6.94	2.16	0.80	0.88	1.16	1.30	2.00	2.44	2.58	2.75	3.24	3.68	4.22	4.56	SW
April	0.67	8.40	2.32	0.88	0.92	1.17	1.36	2.16	2.63	2.79	2.98	3.53	3.98	4.57	5.04	SW
May	0.59	8.97	2.62	1.05	1.00	1.26	1.46	2.42	3.02	3.23	3.46	4.09	4.67	5.27	5.62	SW
June	0.69	7.97	2.63	1.02	0.99	1.31	1.52	2.45	2.97	3.16	3.36	3.98	4.62	5.33	5.85	SW
July	0.37	8.22	2.60	1.08	0.69	1.23	1.48	2.39	2.91	3.10	3.34	4.04	4.78	5.55	6.00	SW
August	0.77	9.76	2.69	0.96	1.08	1.40	1.63	2.53	3.02	3.19	3.41	4.02	4.52	5.04	5.50	SW
September	0.63	8.34	2.69	0.99	1.08	1.40	1.57	2.54	3.05	3.21	3.42	3.97	4.56	5.28	5.80	SW
October	0.59	8.13	2.66	0.92	1.04	1.43	1.62	2.54	3.00	3.13	3.30	3.84	4.36	5.05	5.52	SW
November	0.64	7.22	2.32	0.81	0.95	1.23	1.39	2.21	2.64	2.77	2.92	3.37	3.85	4.38	4.76	SW
December	0.57	5.80	2.05	0.70	0.88	1.10	1.25	1.93	2.30	2.42	2.57	3.02	3.41	3.84	4.13	SW
Winter	0.37	9.76	2.64	1.02	0.94	1.31	1.54	2.46	2.97	3.15	3.37	4.02	4.64	5.32	5.81	SW
Spring	0.59	8.34	2.56	0.92	1.00	1.33	1.53	2.43	2.90	3.04	3.22	3.76	4.29	4.94	5.45	SW
Summer	0.46	7.43	2.02	0.73	0.87	1.08	1.23	1.89	2.26	2.39	2.55	3.00	3.41	3.89	4.25	SW
Autumn	0.57	8.97	2.37	0.93	0.93	1.19	1.36	2.18	2.68	2.86	3.06	3.65	4.18	4.83	5.27	SW
All	0.37	9.76	2.40	0.94	0.92	1.20	1.38	2.23	2.72	2.88	3.07	3.64	4.19	4.87	5.37	SW

Notes: (1) All statistics derived from hindcast wave data for the period 01 January 1980 to 31 December 2020.

(2) Main directions are those with greater than 15% occurrence and represent directions from which the waves approach.

Table 5-2 Annual joint probability distribution (in %) of the total significant wave height and peak period at O1 for the 'existing' scenario.

H_s (m)	Peak period (s)											
	2-4	4-6	6-8	8-10	10-12	12-14	14-16	16-18	18-20	20-22	Total	Exceed%
0-0.5	-	-	-	-	0.01	0.04	-	*	*	-	0.05	100.00
0.5-1	0.06	0.03	*	0.03	0.47	0.75	0.21	0.10	0.04	*	1.69	99.95
1-1.5	0.02	0.13	0.13	0.35	2.87	6.05	2.01	0.87	0.30	0.05	12.78	98.25
1.5-2	*	0.20	0.39	1.08	3.76	11.21	4.92	1.91	0.66	0.11	24.24	85.46
2-2.5	-	0.06	0.46	1.25	3.12	9.35	5.92	2.10	0.58	0.11	22.95	61.22
2.5-3	-	*	0.32	1.16	2.24	5.82	4.92	1.65	0.34	0.05	16.50	38.27
3-3.5	-	-	0.11	0.87	1.27	3.06	3.21	1.12	0.17	0.01	9.82	21.77
3.5-4	-	-	0.01	0.53	0.69	1.61	1.69	0.90	0.13	0.01	5.57	11.95
4-4.5	-	-	*	0.27	0.44	0.79	0.94	0.53	0.06	*	3.03	6.37
4.5-5	-	-	-	0.09	0.33	0.44	0.50	0.29	0.03	*	1.68	3.35
5-5.5	-	-	-	0.02	0.22	0.23	0.23	0.14	0.02	-	0.86	1.67
5.5-6	-	-	-	*	0.11	0.14	0.13	0.06	0.01	-	0.45	0.82
6-6.5	-	-	-	-	0.05	0.05	0.07	0.03	*	-	0.20	0.37
6.5-7	-	-	-	-	0.02	0.04	0.03	0.02	*	-	0.11	0.17
7-7.5	-	-	-	-	*	0.02	0.01	0.01	-	-	0.04	0.07
7.5-8	-	-	-	-	*	0.01	*	*	-	-	0.01	0.03
8-8.5	-	-	-	-	*	*	*	*	-	-		0.01
8.5-9	-	-	-	-	-	*	*	*	-	-		
9-9.5	-	-	-	-	-	-	*	*	-	-		
9.5-10	-	-	-	-	-	-	*	-	-	-		
Total	0.08	0.42	1.42	5.65	15.60	39.61	24.79	9.73	2.34	0.34	100.00	
Exceed%	100.00	99.93	99.50	98.08	92.43	76.83	37.22	12.43	2.69	0.34		

Notes: * represents less than 0.005%.

Table 5-3 Annual joint probability distribution (in %) of the total significant wave height and mean wave direction at peak energy at O1 for the 'existing' scenario.

H_s (m)	Mean wave direction at peak energy (degree True North, coming from)									
	337.5-22.5	22.5-67.5	67.5-112.5	112.5-157.5	157.5-202.5	202.5-247.5	247.5-292.5	292.5-337.5	Total	Exceed%
0-0.5	-	-	-	-	-	0.05	-	-	0.05	100.00
0.5-1	0.03	*	*	0.01	0.01	1.57	0.05	0.04	1.71	99.95
1-1.5	0.02	0.04	0.02	0.01	0.01	12.17	0.40	0.11	12.78	98.25
1.5-2	0.02	0.04	0.05	0.04	0.02	22.52	1.27	0.27	24.23	85.46
2-2.5	*	0.01	0.03	0.02	0.03	20.77	1.84	0.25	22.95	61.22
2.5-3	-	-	-	0.01	0.02	14.59	1.74	0.15	16.51	38.27
3-3.5	-	-	-	*	0.01	8.40	1.34	0.07	9.82	21.77
3.5-4	-	-	-	-	0.01	4.74	0.79	0.04	5.58	11.95
4-4.5	-	-	-	-	*	2.48	0.52	0.02	3.02	6.37
4.5-5	-	-	-	-	*	1.36	0.31	0.01	1.68	3.35
5-5.5	-	-	-	-	-	0.69	0.15	0.01	0.85	1.67
5.5-6	-	-	-	-	-	0.34	0.10	*	0.44	0.82
6-6.5	-	-	-	-	-	0.16	0.04	*	0.20	0.37
6.5-7	-	-	-	-	-	0.07	0.03	*	0.10	0.17
7-7.5	-	-	-	-	-	0.03	0.01	*	0.04	0.07
7.5-8	-	-	-	-	-	0.01	0.01	*	0.02	0.03
8-8.5	-	-	-	-	-	*	*	*		0.01
8.5-9	-	-	-	-	-	*	*	-		
9-9.5	-	-	-	-	-	*	-	-		
9.5-10	-	-	-	-	-	*	-	-		
Total	0.07	0.09	0.10	0.09	0.11	89.95	8.60	0.97	100.00	

*Notes: * represents less than 0.005%.*

Table 5-4 Monthly and annual total significant wave height exceedance probabilities (%) at O1 for the 'existing' scenario.

H_S (m)	Exceedance (%)												
	Jan	Feb	Mar	Apr	May	Jun	Jul	Aug	Sep	Oct	Nov	Dec	annual
>0	100.00	100.00	100.00	100.00	100.00	100.00	100.00	100.00	100.00	100.00	100.00	100.00	100.00
>0.5	99.94	100.00	100.00	100.00	100.00	100.00	99.51	100.00	100.00	100.00	100.00	100.00	99.95
>1	96.55	97.19	97.91	97.96	98.96	98.93	97.57	99.47	99.46	99.14	98.43	97.38	98.25
>1.5	75.30	71.65	80.41	84.74	88.98	90.52	89.41	93.20	92.35	93.40	86.41	78.38	85.46
>2	43.99	40.69	49.82	58.95	68.00	71.01	69.38	75.53	74.48	75.34	60.87	45.48	61.22
>2.5	23.17	19.30	27.78	34.84	46.80	47.71	44.91	51.72	51.75	51.99	35.93	22.23	38.27
>3	10.94	8.59	14.06	19.52	30.50	29.11	27.39	30.68	31.66	29.81	17.80	10.36	21.77
>3.5	4.99	3.47	6.88	10.41	19.08	16.93	17.08	18.18	18.24	15.16	8.19	4.26	11.95
>4	2.22	1.23	2.92	4.86	11.17	9.83	10.43	10.32	9.67	8.16	3.92	1.41	6.37
>4.5	0.82	0.60	1.13	2.24	6.29	5.78	6.54	5.14	5.50	3.99	1.66	0.33	3.35
>5	0.35	0.24	0.48	1.08	3.08	3.15	3.85	2.16	2.77	2.11	0.61	0.09	1.67
>5.5	0.20	0.04	0.27	0.45	1.27	1.59	2.15	1.01	1.54	1.05	0.19	0.03	0.82
>6	0.12	0.00	0.14	0.21	0.41	0.84	1.00	0.48	0.70	0.47	0.07	0.00	0.37
>6.5	0.04	0.00	0.06	0.09	0.19	0.38	0.43	0.25	0.31	0.24	0.04	0.00	0.17
>7	0.01	0.00	0.00	0.07	0.04	0.13	0.19	0.11	0.14	0.10	0.02	0.00	0.07
>7.5	0.00	0.00	0.00	0.03	0.03	0.03	0.07	0.09	0.05	0.04	0.00	0.00	0.03
>8	0.00	0.00	0.00	0.02	0.03	0.00	0.01	0.05	0.02	0.00	0.00	0.00	0.01
>8.5	0.00	0.00	0.00	0.00	0.02	0.00	0.00	0.04	0.00	0.00	0.00	0.00	0.00
>9	0.00	0.00	0.00	0.00	0.00	0.00	0.00	0.02	0.00	0.00	0.00	0.00	0.00
>9.5	0.00	0.00	0.00	0.00	0.00	0.00	0.00	0.01	0.00	0.00	0.00	0.00	0.00

Table 5-5 Monthly and annual total peak period exceedance probabilities (%) at O1 for the 'existing' scenario.

T_p (s)	Exceedance (%)												
	Jan	Feb	Mar	Apr	May	Jun	Jul	Aug	Sep	Oct	Nov	Dec	annual
>2	100.00	100.00	100.00	100.00	100.00	100.00	100.00	100.00	100.00	100.00	100.00	100.00	100.00
>3	100.00	100.00	100.00	100.00	100.00	100.00	99.99	100.00	100.00	100.00	100.00	100.00	100.00
>4	99.97	99.95	100.00	100.00	100.00	99.97	99.35	99.95	99.96	100.00	99.99	100.00	99.93
>5	99.87	99.84	99.80	99.85	99.85	99.60	98.43	99.65	99.70	99.98	99.83	99.96	99.69
>6	99.69	99.58	99.68	99.79	99.78	99.34	97.72	99.61	99.64	99.92	99.54	99.70	99.50
>7	99.30	99.22	99.18	99.63	99.57	98.94	97.34	99.46	99.46	99.66	99.01	99.17	99.16
>8	97.94	98.27	98.41	98.74	98.45	97.66	96.38	98.54	98.96	98.75	97.55	97.32	98.08
>9	95.63	96.94	97.13	96.90	96.61	94.62	93.74	96.45	97.09	96.33	94.43	94.44	95.85
>10	92.24	94.60	95.71	94.73	93.17	89.81	89.10	92.57	93.38	92.20	91.20	90.63	92.43
>11	85.07	88.62	92.58	91.89	88.90	84.52	83.55	87.29	88.91	86.80	85.41	81.88	87.10
>12	67.12	72.77	81.21	85.08	82.99	77.37	76.35	80.86	83.24	78.66	73.13	63.15	76.83
>13	43.12	47.75	59.96	68.86	68.36	65.09	64.59	70.40	72.63	63.94	50.49	39.42	59.59
>14	21.85	24.40	33.61	42.13	44.98	44.92	45.37	51.28	51.42	40.35	25.59	20.11	37.22
>15	11.11	11.93	17.72	21.82	25.10	26.68	26.93	30.73	30.27	21.68	12.14	9.85	20.54
>16	6.58	7.11	10.86	13.06	14.48	16.99	16.46	18.25	18.70	13.13	7.08	6.13	12.43
>17	1.95	2.48	4.55	5.40	6.08	7.71	7.12	7.43	8.17	6.14	2.91	2.48	5.21
>18	0.89	1.31	2.30	2.79	3.01	4.24	3.78	3.35	4.33	3.27	1.53	1.37	2.69
>19	0.22	0.38	0.95	1.16	1.20	1.85	1.71	1.40	1.97	1.54	0.59	0.47	1.12
>20	0.06	0.08	0.36	0.35	0.32	0.56	0.59	0.43	0.60	0.43	0.22	0.11	0.34
>21	0.00	0.01	0.14	0.11	0.11	0.19	0.25	0.13	0.19	0.12	0.08	0.03	0.11

Table 5-6 Annual and seasonal non-exceedance persistence (%) for significant wave height below 2.0 m at O1 for the 'existing' scenario.

Hs (m)	Duration (hours)											
	3	6	9	12	15	18	21	24	30	36	42	48
Summer	56.43	56.20	55.90	55.49	55.04	54.54	54.04	53.50	51.98	50.21	48.61	47.10
Autumn	40.94	40.67	40.33	39.93	39.34	38.60	38.00	37.47	35.81	34.44	33.36	31.87
Winter	27.90	27.62	27.05	26.58	25.90	25.29	24.72	24.16	22.65	21.58	20.52	19.55
Spring	29.58	29.35	28.87	28.44	27.71	27.24	26.39	25.73	24.57	23.30	21.99	20.64
Annual	38.66	38.43	38.03	37.61	37.03	36.47	35.86	35.30	33.88	32.57	31.34	30.09

Table 5-7 Annual and seasonal non-exceedance persistence (%) for significant wave height below 2.5 m at O1 for the 'existing' scenario.

Hs (m)	Duration (hours)											
	3	6	9	12	15	18	21	24	30	36	42	48
Summer	78.30	78.14	77.94	77.73	77.47	77.15	76.84	76.44	75.88	75.25	74.23	72.88
Autumn	63.39	63.21	63.02	62.78	62.44	61.83	61.29	60.74	59.96	58.74	57.57	56.55
Winter	51.71	51.46	51.14	50.70	50.19	49.57	48.55	47.65	46.00	44.75	42.77	40.99
Spring	53.18	52.86	52.52	52.03	51.22	50.44	49.81	49.00	47.62	46.02	44.61	43.32
Annual	61.60	61.38	61.13	60.79	60.35	59.80	59.21	58.59	57.58	56.45	55.07	53.79

Table 5-8 Annual and seasonal non-exceedance persistence (%) for significant wave height below 3.0 m at O1 for the 'existing' scenario.

Hs (m)	Duration (hours)											
	3	6	9	12	15	18	21	24	30	36	42	48
Summer	89.97	89.85	89.73	89.62	89.43	89.27	89.01	88.83	88.51	88.16	87.70	87.18
Autumn	78.53	78.37	78.23	78.04	77.84	77.50	77.31	76.99	76.21	75.53	74.44	73.52
Winter	70.83	70.64	70.34	70.08	69.75	69.30	69.04	68.56	67.52	66.38	65.23	63.74
Spring	73.42	73.19	72.83	72.44	72.12	71.68	71.14	70.60	69.22	67.73	66.38	65.29
Annual	78.15	77.98	77.76	77.53	77.30	76.99	76.69	76.35	75.54	74.69	73.73	72.83

Table 5-9 Annual and seasonal non-exceedance persistence (%) for significant wave height below 3.5 m at O1 for the 'existing' scenario.

Hs (m)	Duration (hours)											
	3	6	9	12	15	18	21	24	30	36	42	48
Summer	95.72	95.71	95.69	95.62	95.59	95.55	95.50	95.45	95.27	95.04	94.76	94.39
Autumn	87.75	87.60	87.48	87.26	87.13	86.99	86.73	86.57	86.03	85.54	85.09	84.62
Winter	82.49	82.35	82.13	81.86	81.52	81.34	81.06	80.84	80.09	79.48	78.89	78.07
Spring	86.04	85.94	85.78	85.58	85.34	85.17	84.92	84.65	84.05	83.60	82.73	81.74
Annual	87.97	87.88	87.76	87.57	87.38	87.26	87.06	86.91	86.46	86.06	85.61	85.01

Table 5-10 Annual and seasonal non-exceedance persistence (%) for significant wave height below 4.0 m at O1 for the 'existing' scenario.

Hs (m)	Duration (hours)											
	3	6	9	12	15	18	21	24	30	36	42	48
Summer	98.36	98.33	98.31	98.30	98.28	98.26	98.26	98.26	98.23	98.11	98.02	98.02
Autumn	93.64	93.57	93.48	93.37	93.30	93.16	93.05	92.94	92.81	92.44	91.77	91.52
Winter	89.73	89.62	89.53	89.38	89.18	89.05	88.91	88.78	88.38	87.85	87.40	86.95
Spring	92.70	92.66	92.56	92.48	92.37	92.16	91.95	91.90	91.39	91.12	90.72	90.36
Annual	93.59	93.53	93.45	93.37	93.28	93.16	93.05	92.99	92.76	92.48	92.15	91.89

Table 5-11 Annual and seasonal non-exceedance persistence (%) for significant wave height below 4.5 m at O1 for the 'existing' scenario.

Hs (m)	Duration (hours)											
	3	6	9	12	15	18	21	24	30	36	42	48
Summer	99.41	99.41	99.40	99.40	99.38	99.36	99.36	99.33	99.33	99.29	99.24	99.19
Autumn	96.74	96.71	96.64	96.63	96.58	96.54	96.50	96.44	96.41	96.25	96.08	95.76
Winter	94.12	94.08	93.96	93.92	93.81	93.67	93.53	93.50	93.22	93.07	92.71	92.60
Spring	96.24	96.20	96.17	96.16	96.14	96.08	95.99	95.91	95.74	95.55	95.32	95.17
Annual	96.62	96.59	96.54	96.52	96.48	96.42	96.36	96.32	96.20	96.11	95.94	95.81

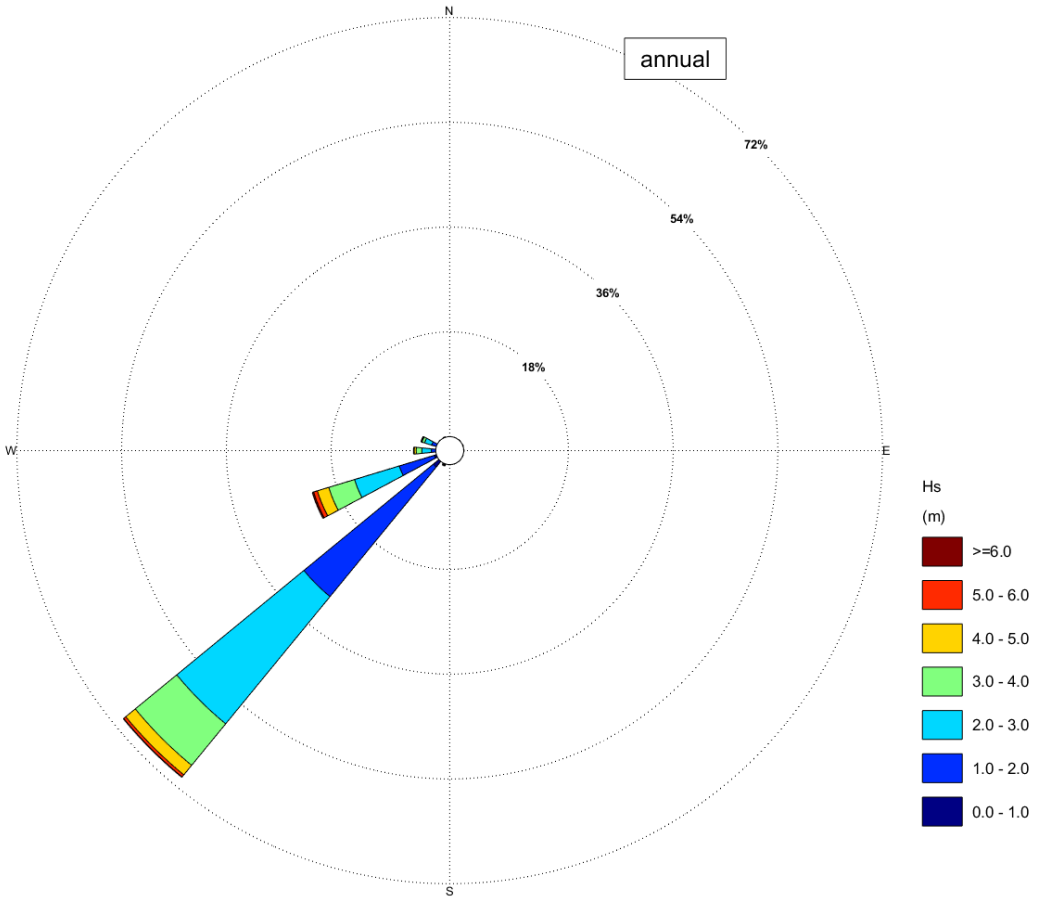

Figure 5-4 Annual wave rose plot for the total significant wave height at O1 for the 'existing' scenario given in 22.5-degree bins. Sectors indicate the direction from which waves approach.

Table 5-12 Directional and omni-directional extreme waves at O1 for the 'existing' scenario.

	Mean wave direction at peak energy (degree True North, coming from)								omni	Omni +5% (climate change projection)
Hs (m)	**337.5-22.5**	**22.5-67.5**	**67.5-112.5**	**112.5-157.5**	**157.5-202.5**	**202.5-247.5**	**247.5-292.5**	**292.5-337.5**		
1 yr	0.87	-	1.39	1.52	1.18	6.59	5.82	3.88	6.92	7.27
10 yr	2.07	-	2.25	2.62	4.32	8.37	7.94	5.66	8.78	9.22
25 yr	2.50	-	2.48	2.95	5.18	9.06	8.79	7.04	9.51	9.98
50 yr	2.80	-	2.63	3.17	5.76	9.58	9.43	8.18	10.05	10.55
100 yr	3.07	-	2.77	3.38	6.30	10.09	10.08	9.37	10.58	11.11
Tp (s)										
1 yr	3.75	-	3.37	4.88	5.01	13.88	11.99	9.74	13.72	-
10 yr	5.79	-	6.01	6.23	8.63	14.20	13.58	11.38	14.38	-
25 yr	6.37	-	7.32	6.56	9.22	14.30	14.13	12.45	14.59	-
50 yr	6.74	-	8.59	6.76	9.57	14.36	14.53	13.23	14.73	-
100 yr	7.07	-	10.37	6.94	9.87	14.42	14.91	13.98	14.86	-
95th conf lower Hs (m)										
1 yr	0.13	-	0.34	0.33	0.29	6.11	4.84	0.14	6.46	6.78
10 yr	1.53	-	1.79	2.03	3.41	7.63	6.41	3.25	8.06	8.46
25 yr	1.77	-	1.91	2.21	3.95	8.21	6.95	3.87	8.67	9.10
50 yr	1.91	-	1.97	2.32	4.29	8.64	7.35	4.27	9.13	9.58
100 yr	2.02	-	2.03	2.40	4.58	9.06	7.74	4.64	9.58	10.06
95th conf upper Hs (m)										
1 yr	5.93	-	5.68	7.05	4.83	7.10	7.00	109.65	7.43	7.80
10 yr	2.79	-	2.83	3.38	5.49	9.19	9.84	9.84	9.58	10.06
25 yr	3.53	-	3.22	3.93	6.79	10.01	11.12	12.82	10.42	10.94
50 yr	4.10	-	3.51	4.34	7.74	10.62	12.11	15.67	11.06	11.61
100 yr	4.66	-	3.79	4.74	8.66	11.23	13.11	18.90	11.69	12.28
Hmax (m)										
1 yr	1.62	-	2.58	3.18	3.71	12.39	11.25	7.09	12.78	13.41
10 yr	3.84	-	4.18	4.78	7.09	15.00	14.22	10.34	15.15	15.90
25 yr	4.65	-	4.61	5.21	7.89	15.92	15.19	11.81	15.98	16.77
50 yr	5.20	-	4.89	5.47	8.32	16.55	15.83	12.71	16.57	17.39
100 yr	5.71	-	5.15	5.68	8.68	17.13	16.39	13.41	17.12	17.97
Cmax (m)										
1 yr	0.88	-	1.19	1.97	2.27	7.55	6.89	4.35	7.87	8.26
10 yr	1.43	-	1.87	3.01	4.43	8.98	8.84	6.38	9.39	9.85
25 yr	2.03	-	2.47	3.28	4.95	9.48	9.48	7.30	9.92	10.41
50 yr	2.38	-	2.80	3.44	5.23	9.85	9.88	7.88	10.30	10.81
100 yr	2.61	-	3.01	3.57	5.45	10.20	10.24	8.32	10.64	11.17

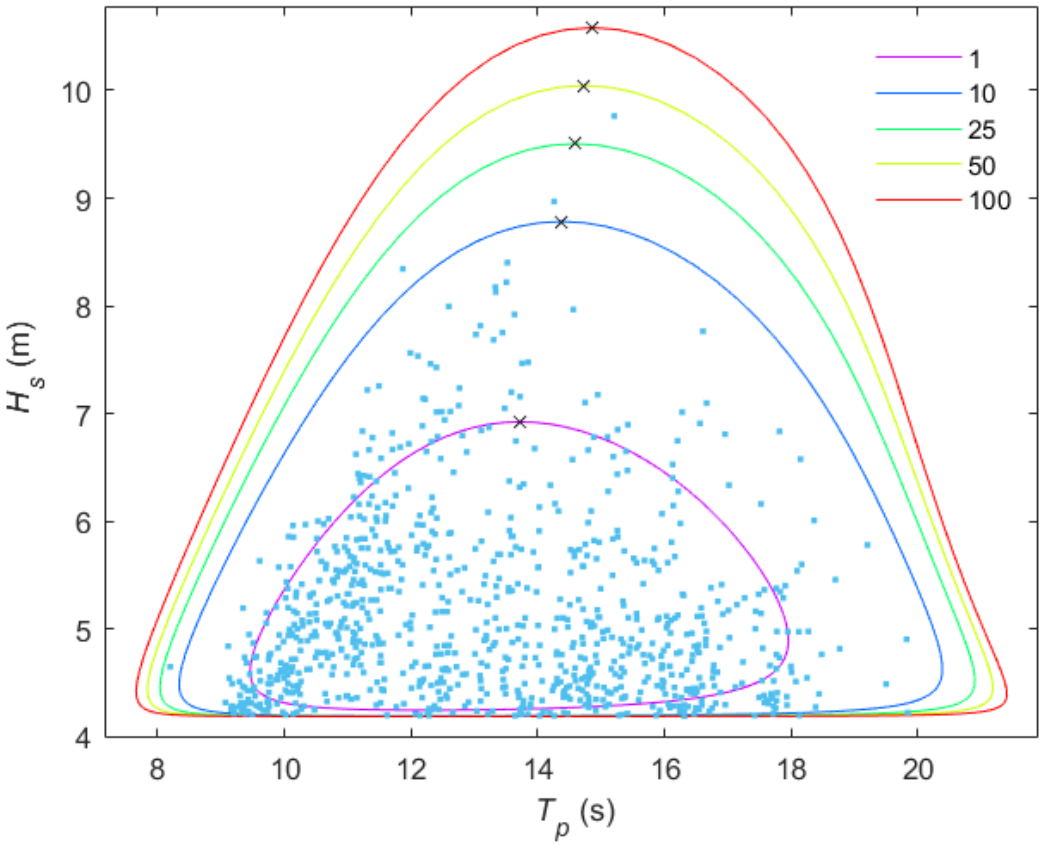

Figure 5-5 *Contour plot of omni-directional bi-variate (Hs-Tp) return period values for 1, 10, 25, 50 and 100-year ARIs for the 'existing' scenario. The dark crosses correspond to the Hs contour maxima and associated Tp return period values for each ARI indicated in the legend at O1.*

5.3 Delft FM coupled wave / hydrodynamic simulations

The calibrated and validated coupled Delft FM and SWAN wave model was used to simulate a full year of coupled wave and currents over a year representative of an average wave climate. The 43-year wave hindcast was assessed, extracting annual mean and percentile statistics of H_s at an offshore location for comparison. From these tabulated statistics, 2012 was selected for the representative year simulation, noting that it was slightly more energetic than an average year.

The model forcing and parameters developed during the calibration and validation was used in the annual runs and included tidal water levels derived from OTIS TPXO model, CFSR winds, measured river discharges and hourly wave spectra extracted from the SWAN hindcast model. Model outputs were processed at 1 km intervals along the concept navigation channel.

5.3.1 Bathymetry

The simulations were run for two bathymetry configurations:

- The 'existing' bathymetry which was developed from the 2023 survey and used during calibration.
- The channel 'design' bathymetry which was the existing 2023 bathymetry with the addition of the concept navigation channel within the natural South West Channel

Figure 5-1, Figure 5-2 and Figure 5-3 show the bathymetry used along the concept navigation channel (South West Channel) in the two annual simulations.

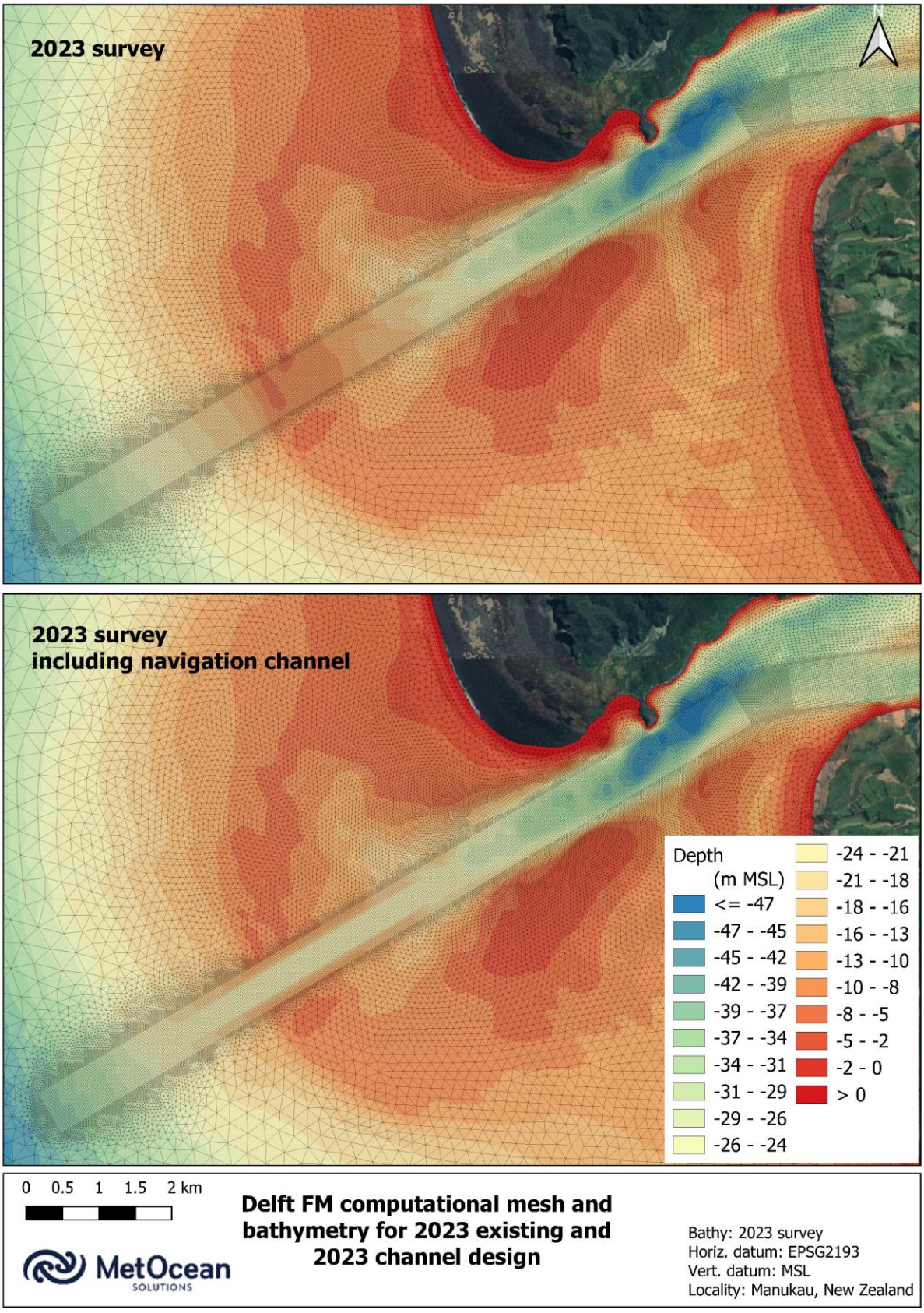

Figure 5-6 Bathymetry used in the 'existing' and channel 'design' model simulations within the entrance channel and bar at Manukau Harbour.

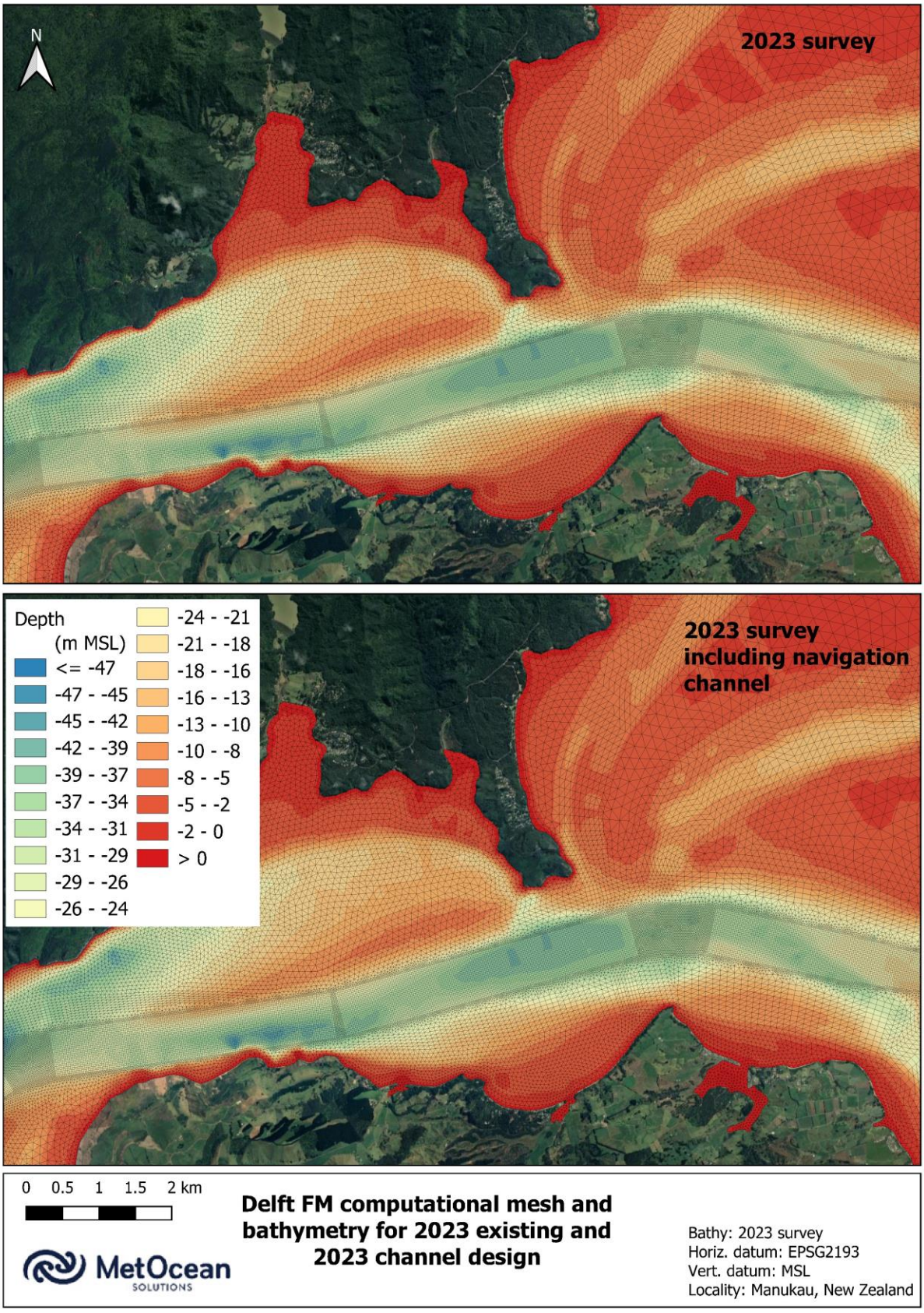

Figure 5-7 Bathymetry used in the 'existing' and channel 'design' model simulations within the entrance channel at Manukau Harbour.

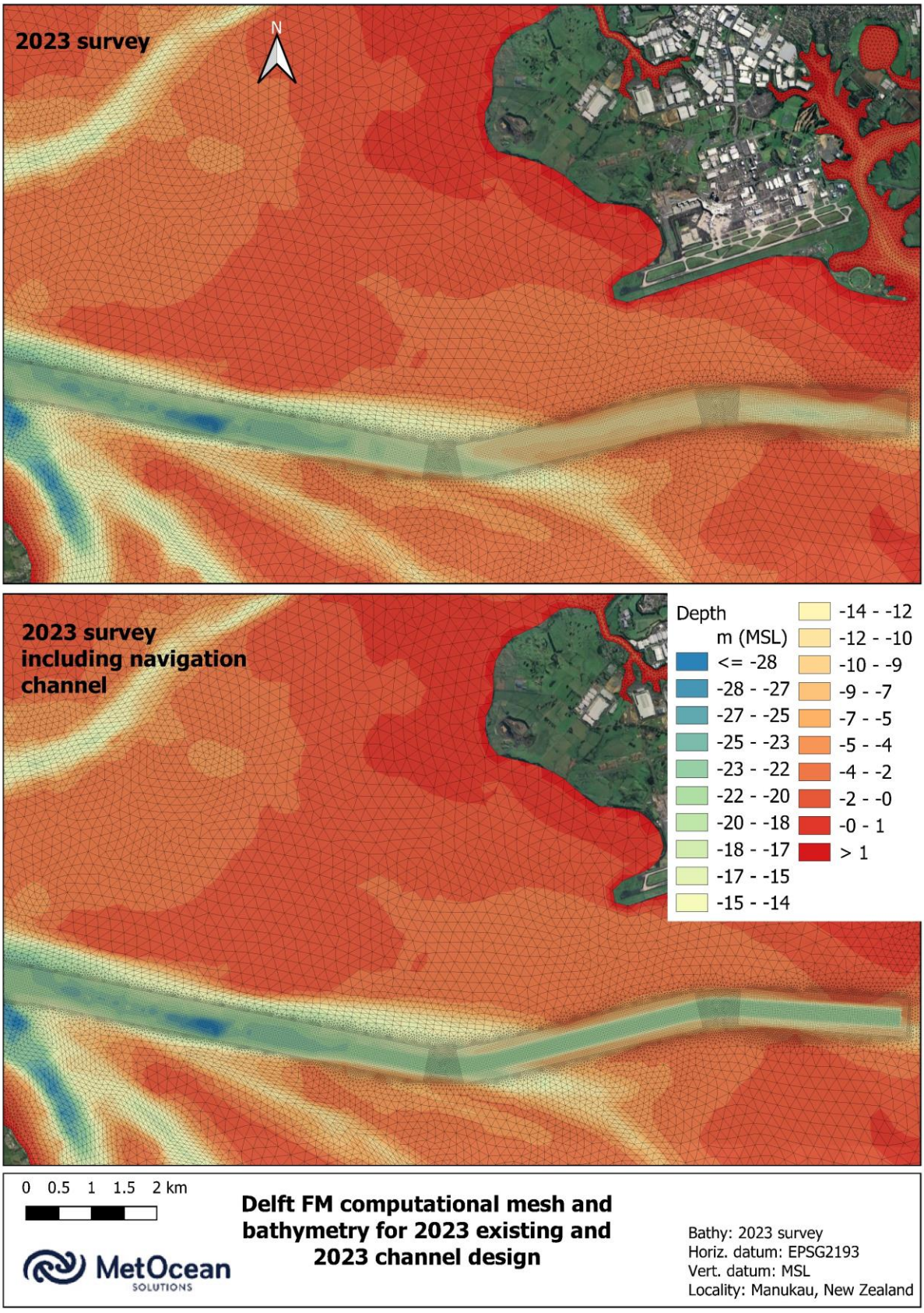

Figure 5-8 Bathymetry used in the 'existing' and channel 'design' model simulations within Manukau Harbour.

5.3.2 Spring tidal current maps

The modelled depth averaged currents for the 'existing' simulation for the peak flood and peak ebb current vectors during a spring tide within Manukau Harbour are presented in Figure 5-9 to Figure 5-14.

The modelled depth averaged currents for the channel 'design' simulation (South West Channel) for the peak flood and peak ebb current vectors during a spring tide within Manukau Harbour are presented in Figure 5-15 to Figure 5-20

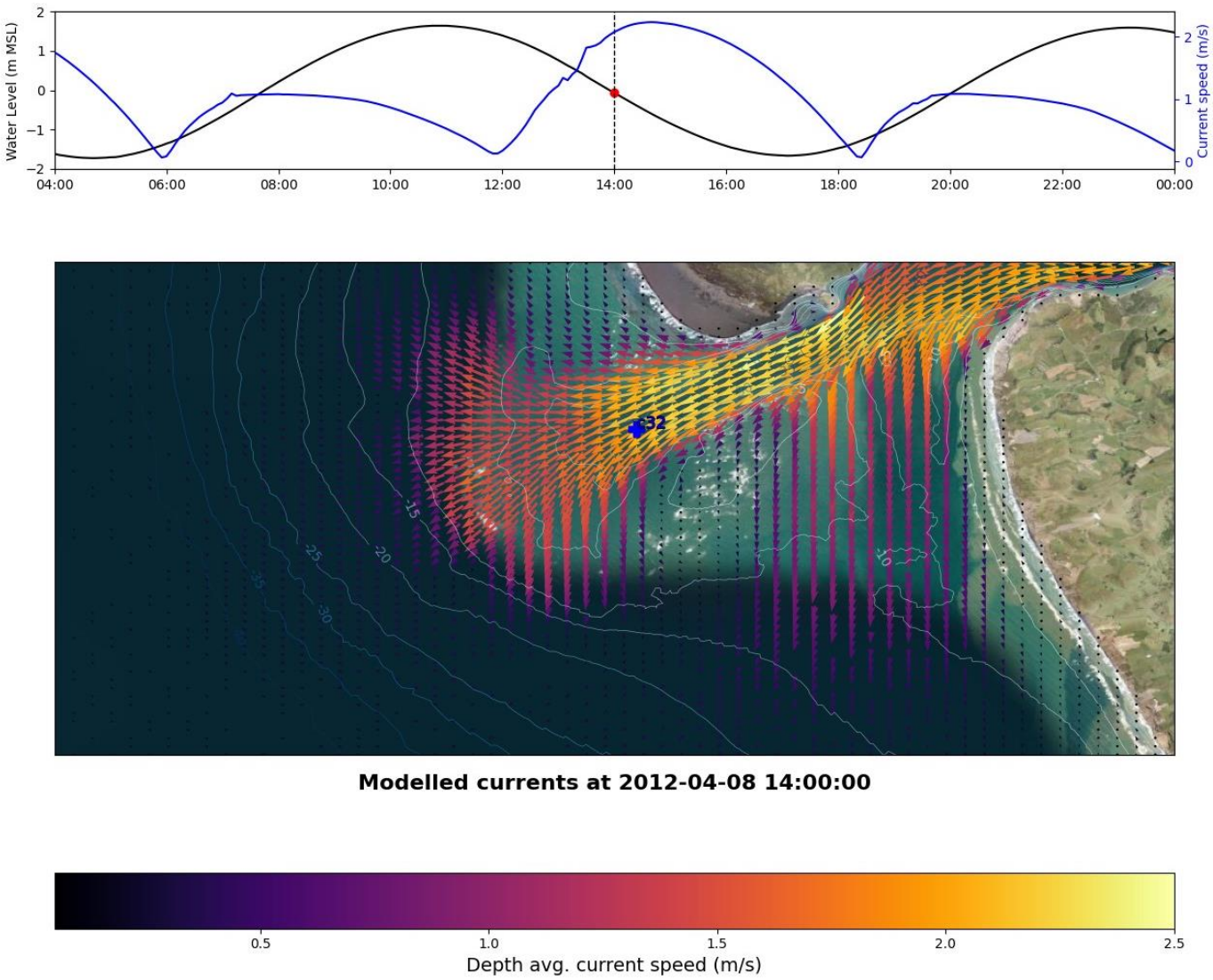

Figure 5-9 Modelled spring tidal current vectors for the 'existing' simulation over Manukau bar at peak ebb tide. The top panel presents the water level and depth averaged currents timeseries at the location shown as a blue cross on the map.

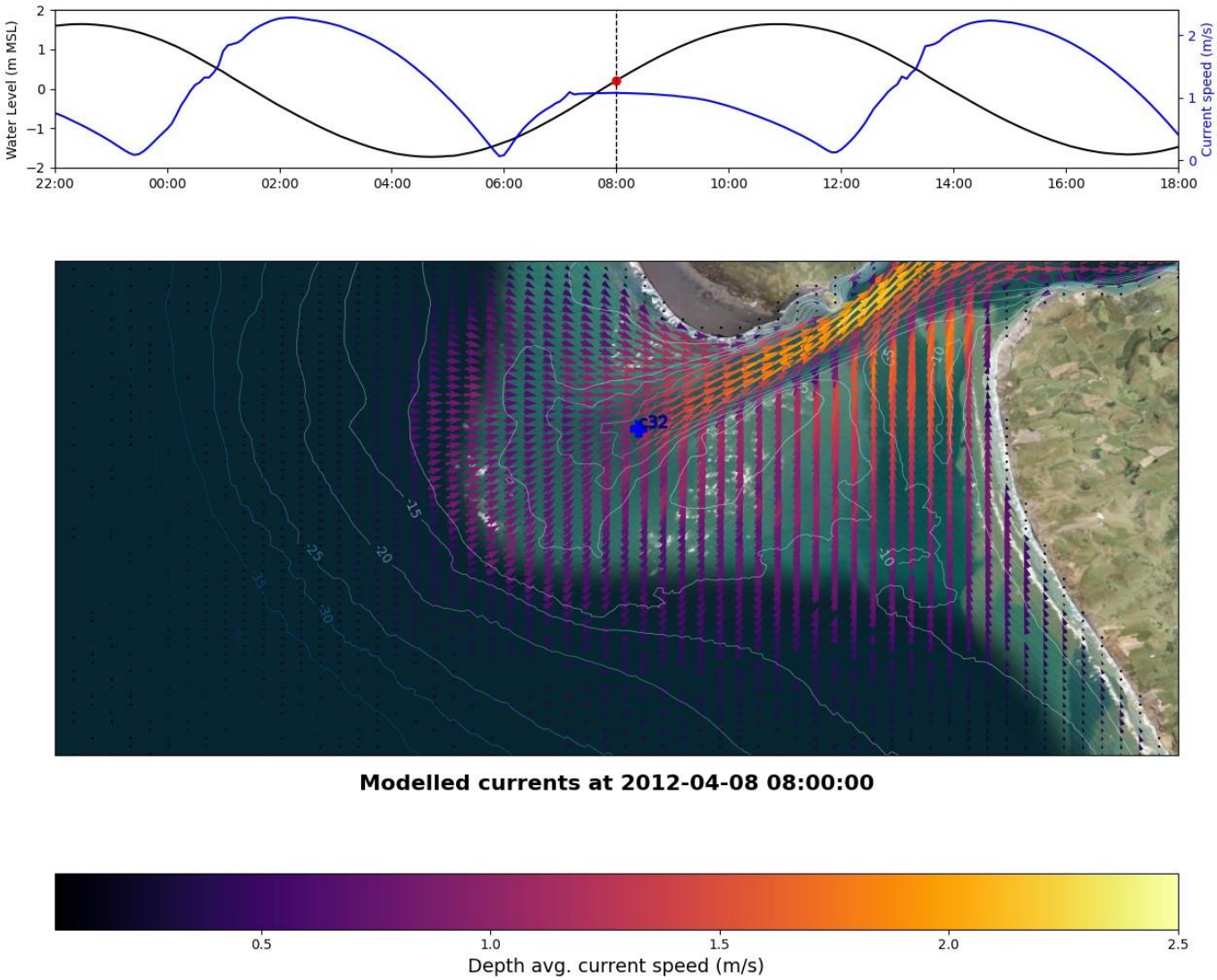

Figure 5-10 Modelled spring tidal current vectors for the 'existing' simulation over Manukau bar at peak flood tide. The top panel presents the water level and depth averaged currents timeseries at the location shown as a blue cross on the map.

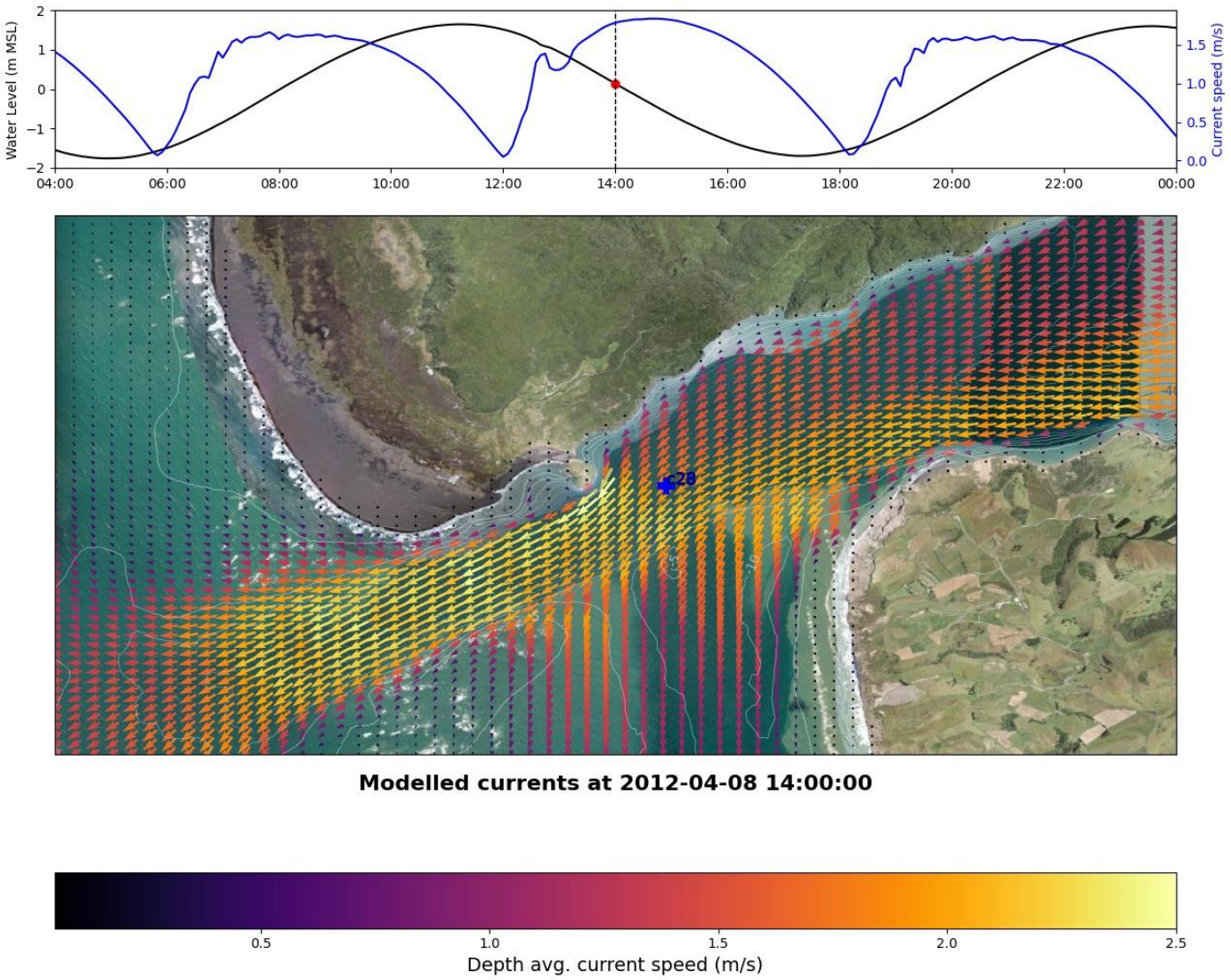

Figure 5-11 Modelled spring tidal current vectors for the 'existing' simulation over Manukau entrance at peak ebb tide. The top panel presents the water level and depth averaged currents timeseries at the location shown as a blue cross on the map.

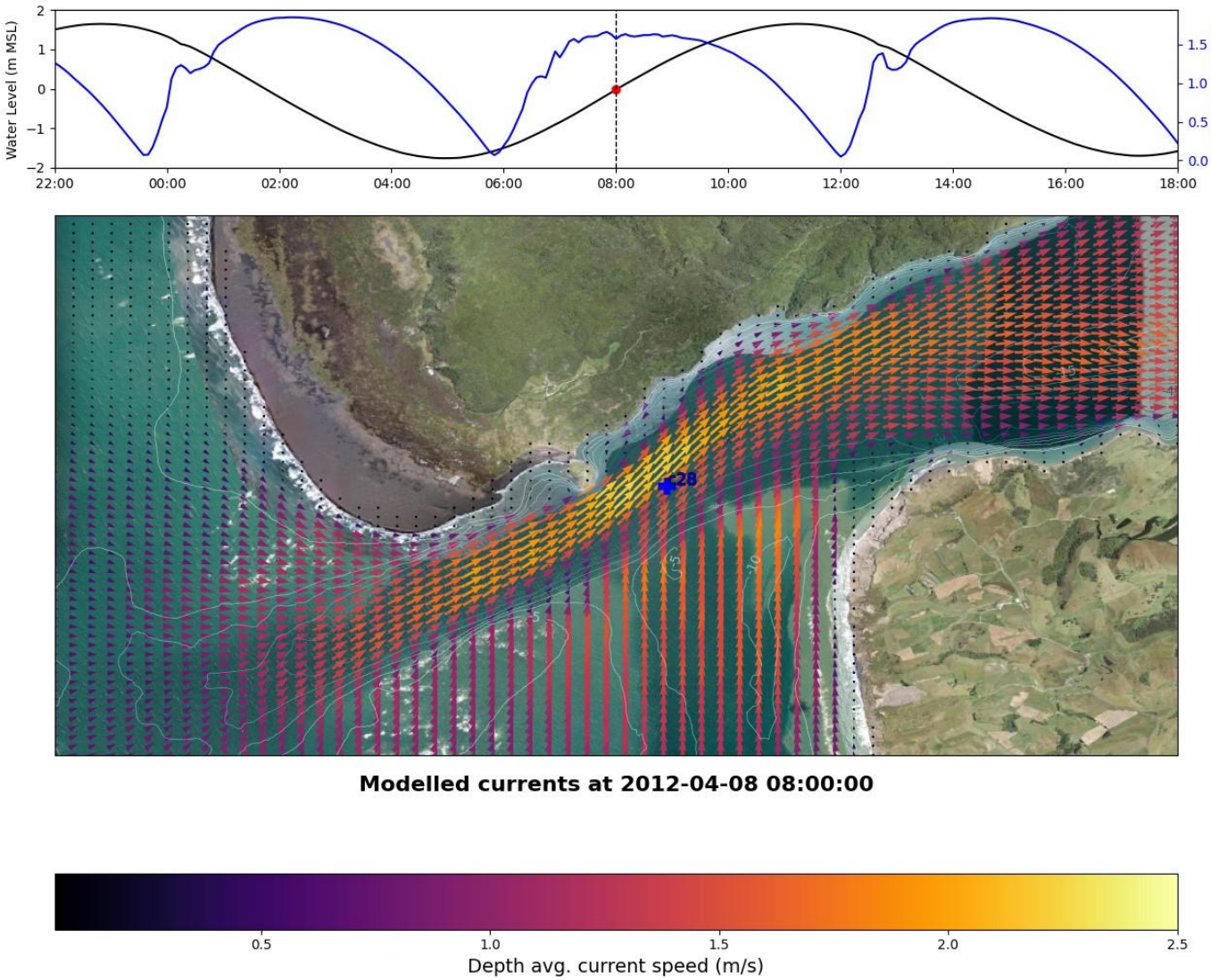

Figure 5-12 Modelled spring tidal current vectors for the 'existing' simulation over Manukau entrance at peak flood tide. The top panel presents the water level and depth averaged currents timeseries at the location shown as a blue cross on the map.

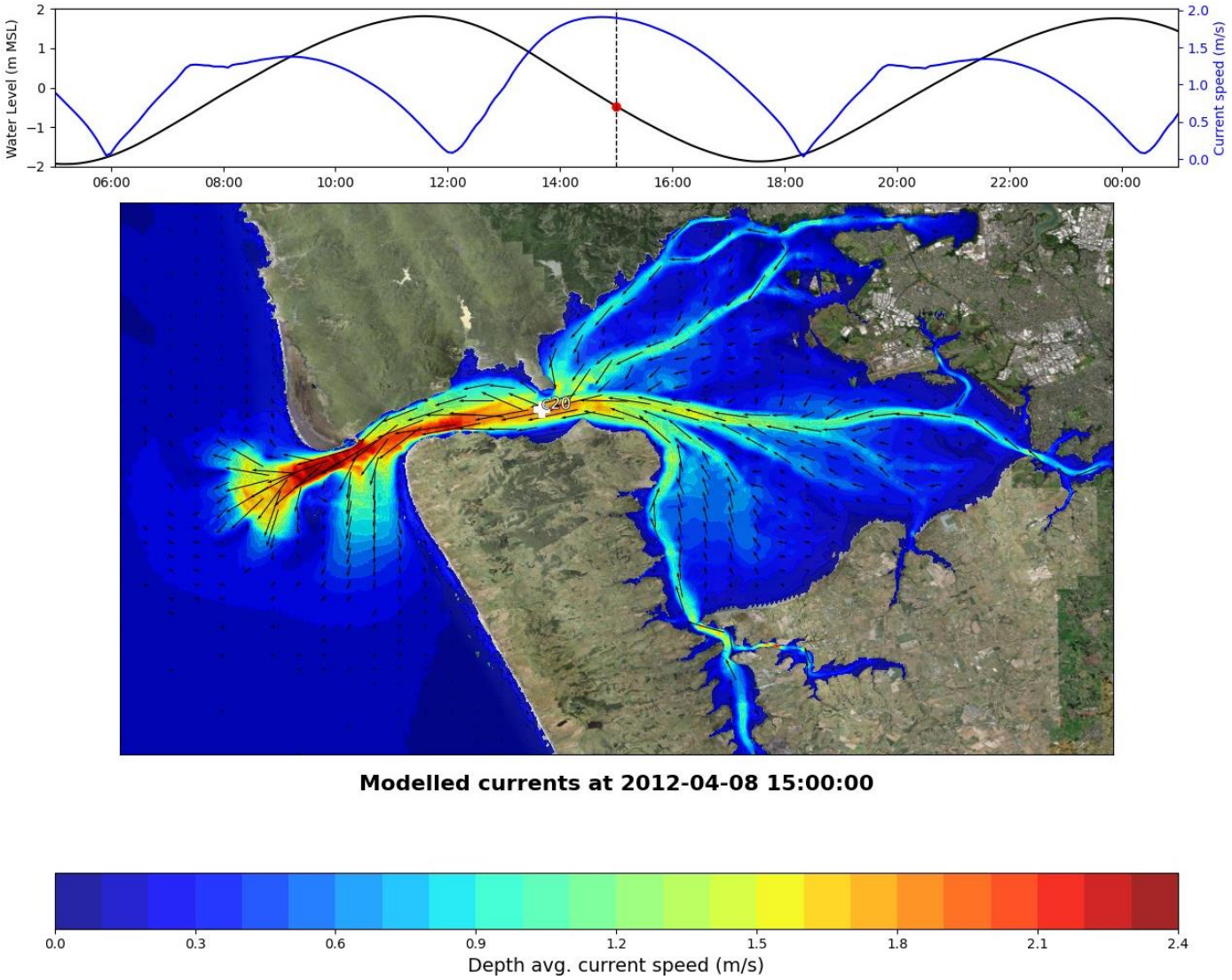

Figure 5-13 Modelled spring tidal current magnitudes and vectors for the 'existing' simulation within Manukau Harbour at peak ebb tide. The top panel presents the water level and depth averaged currents timeseries at the location shown as a white cross on the map.

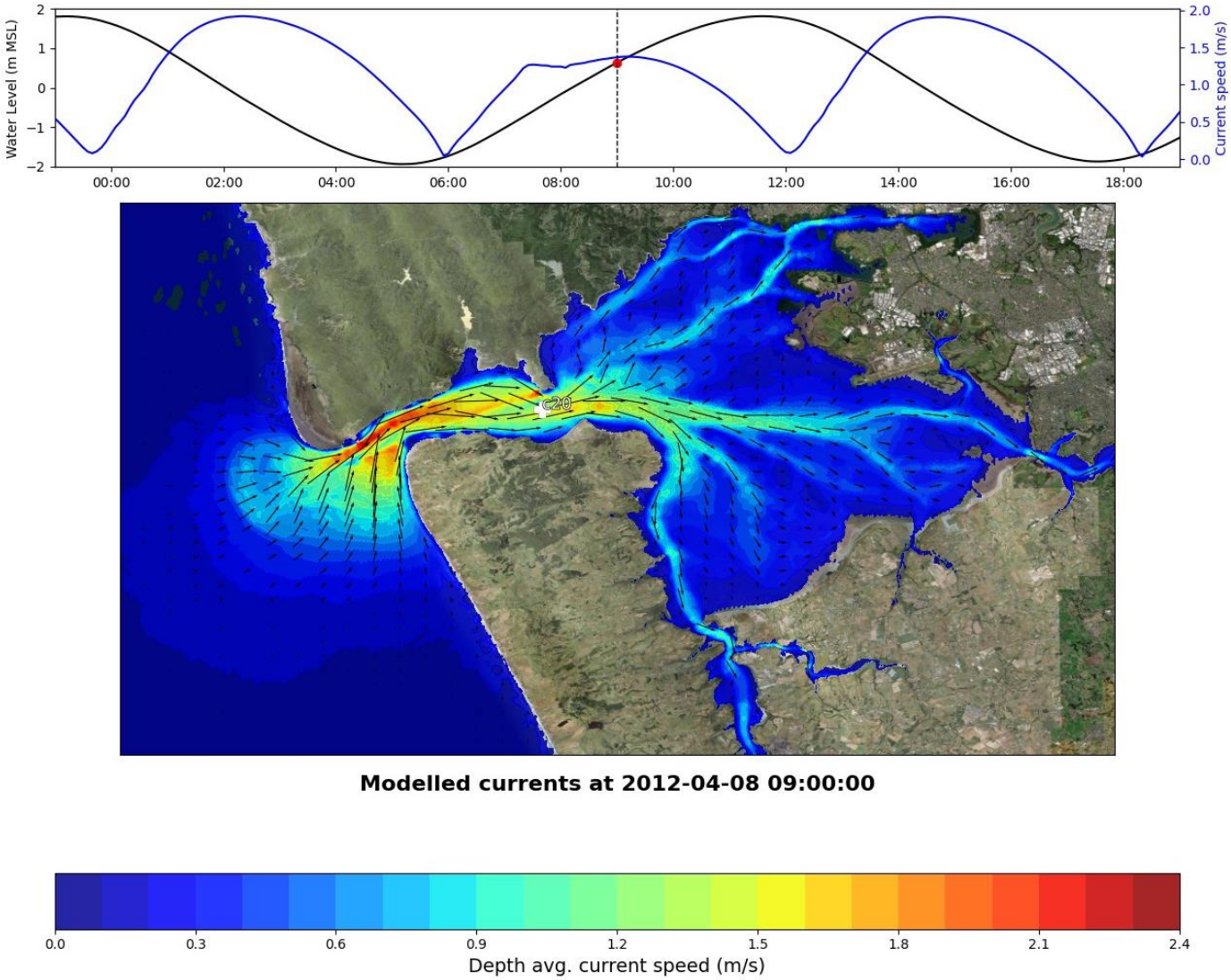

Figure 5-14 Modelled spring tidal current magnitudes and vectors for the 'existing' simulation within Manukau Harbour at peak flood tide. The top panel presents the water level and depth averaged currents timeseries at the location shown as a white cross on the map.

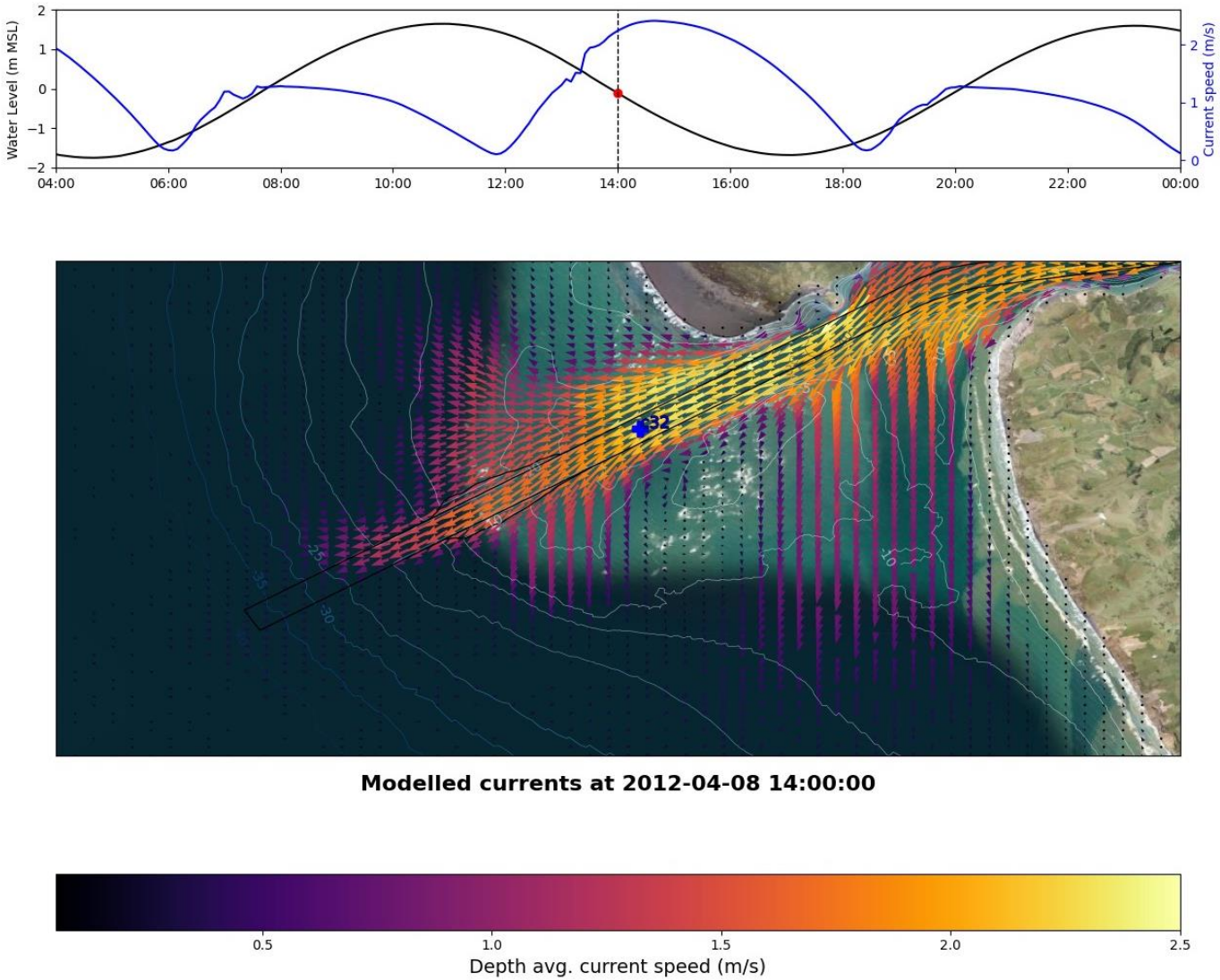

Figure 5-15 Modelled spring tidal current vectors for the channel 'design' simulation over Manukau bar at peak ebb tide. The top panel presents the water level and depth averaged currents timeseries at the location shown as a blue cross on the map.

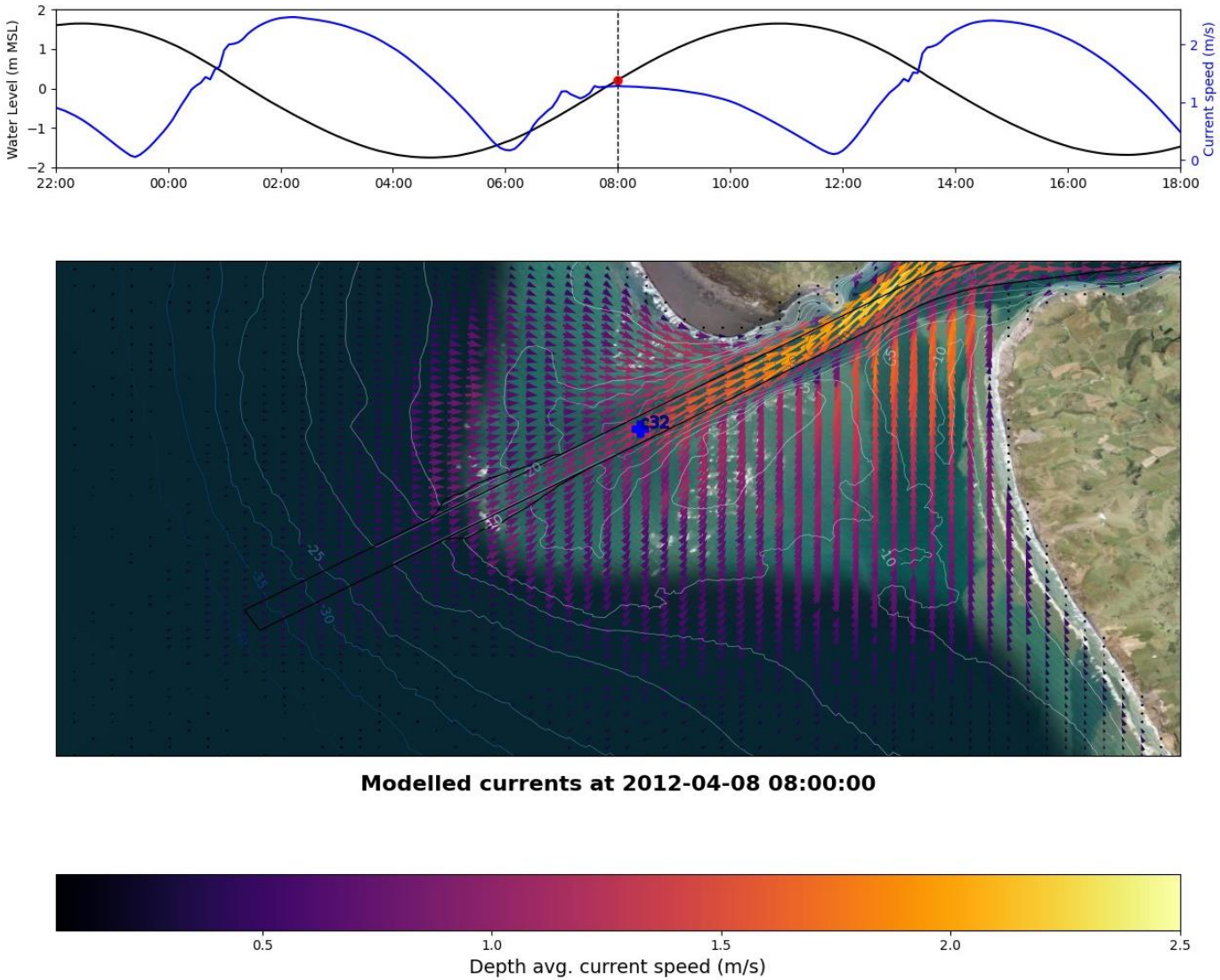

Figure 5-16 Modelled spring tidal current vectors for the channel 'design' simulation over Manukau bar at peak flood tide. The top panel presents the water level and depth averaged currents timeseries at the location shown as a blue cross on the map.

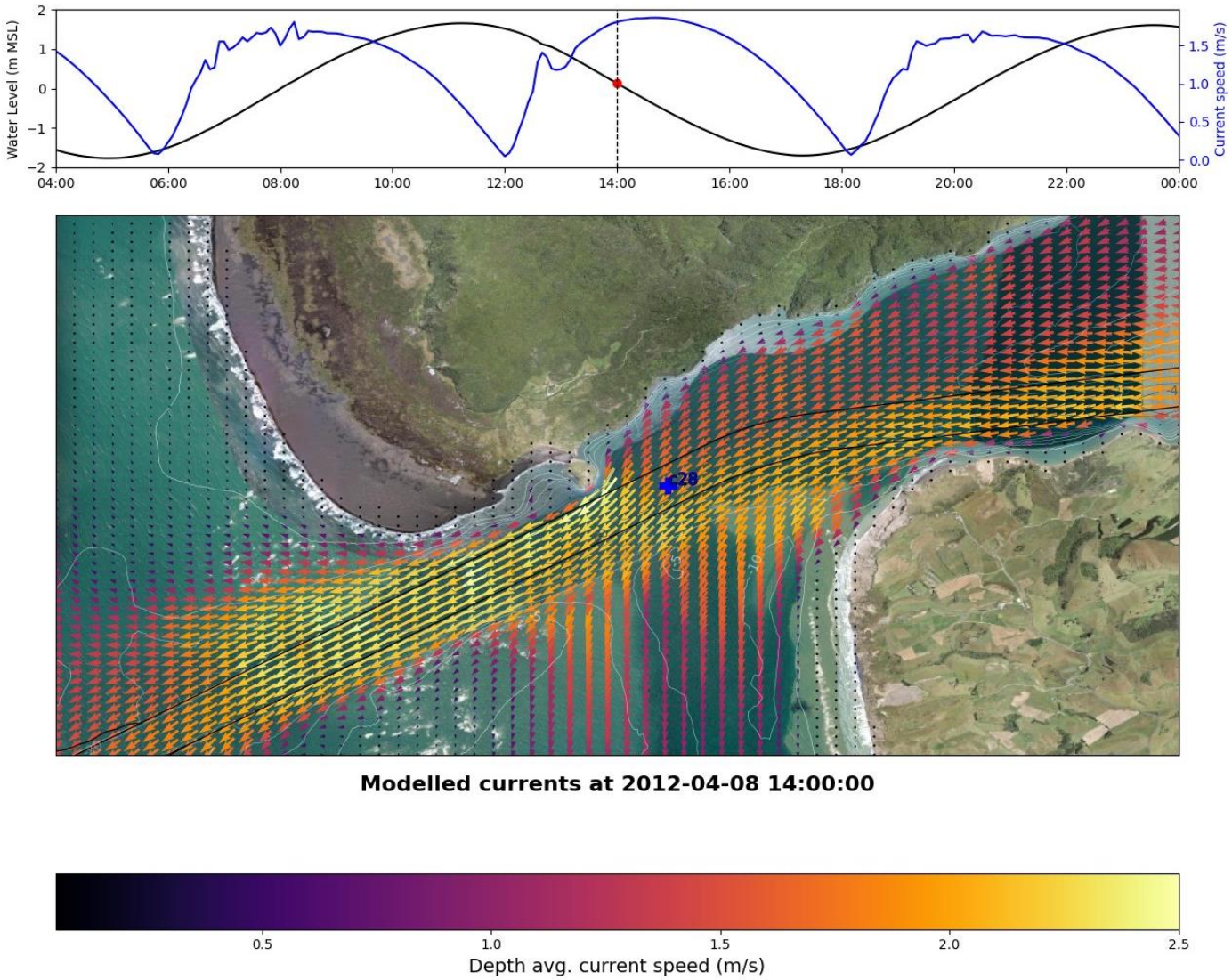

Figure 5-17 Modelled spring tidal current vectors for the channel 'design' simulation over Manukau entrance at peak ebb tide. The top panel presents the water level and depth averaged currents timeseries at the location shown as a blue cross on the map.

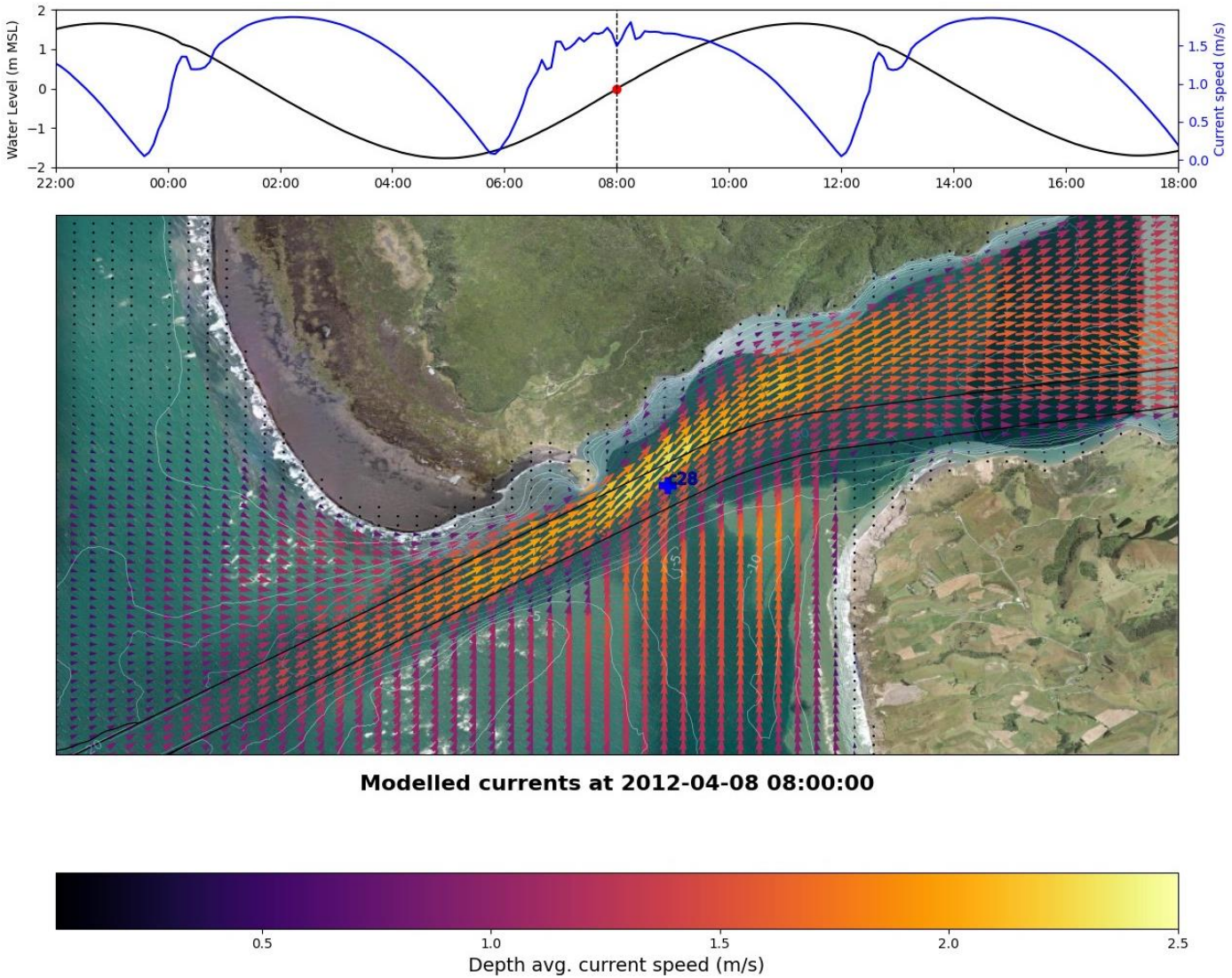

Figure 5-18 Modelled spring tidal current vectors for the channel 'design' simulation over Manukau entrance at peak flood tide. The top panel presents the water level and depth averaged currents timeseries at the location shown as a blue cross on the map.

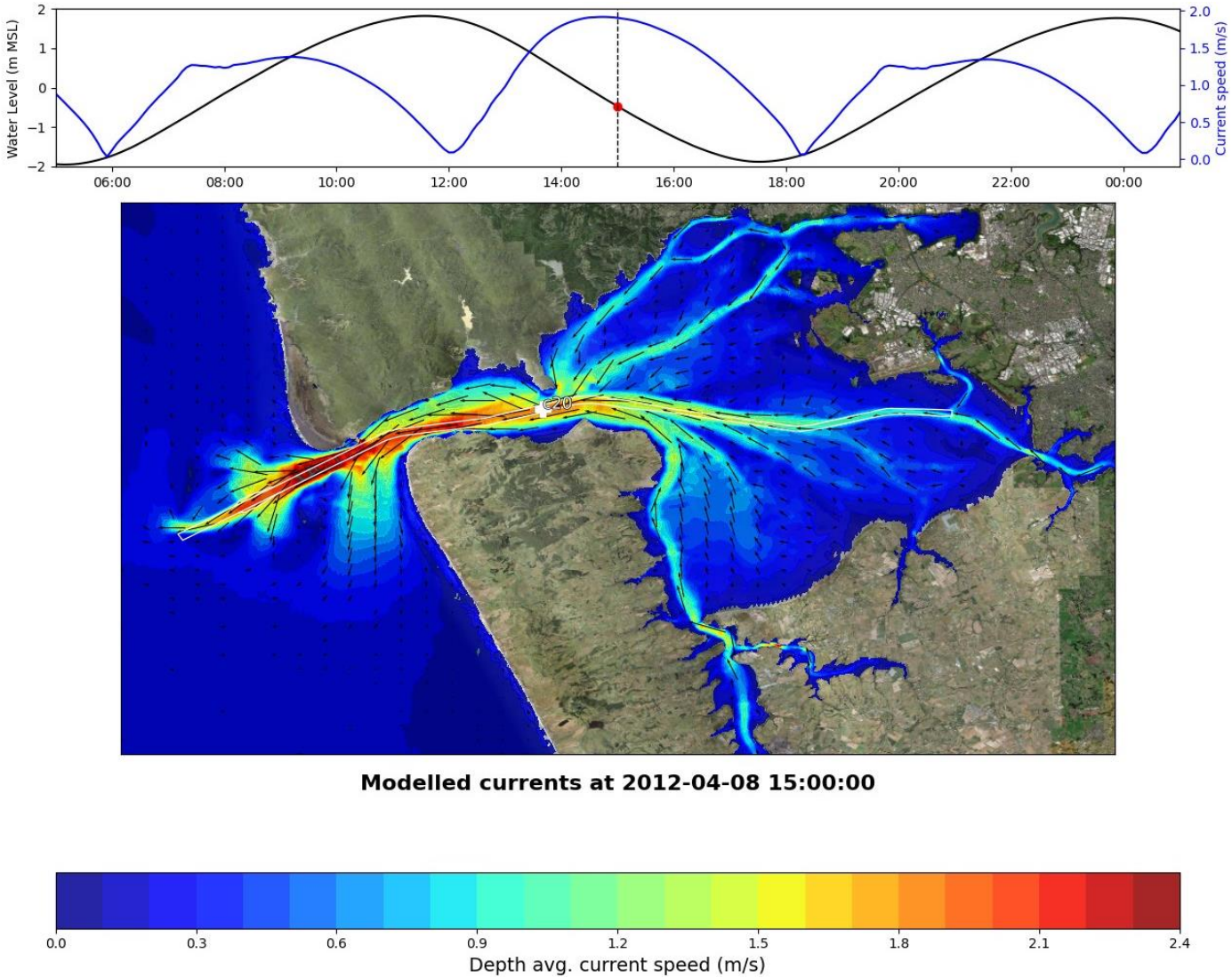

Figure 5-19 Modelled spring tidal current magnitudes and vectors for the channel 'design' simulation within Manukau Harbour at peak ebb tide. The top panel presents the water level and depth averaged currents timeseries at the location shown as a white cross on the map.

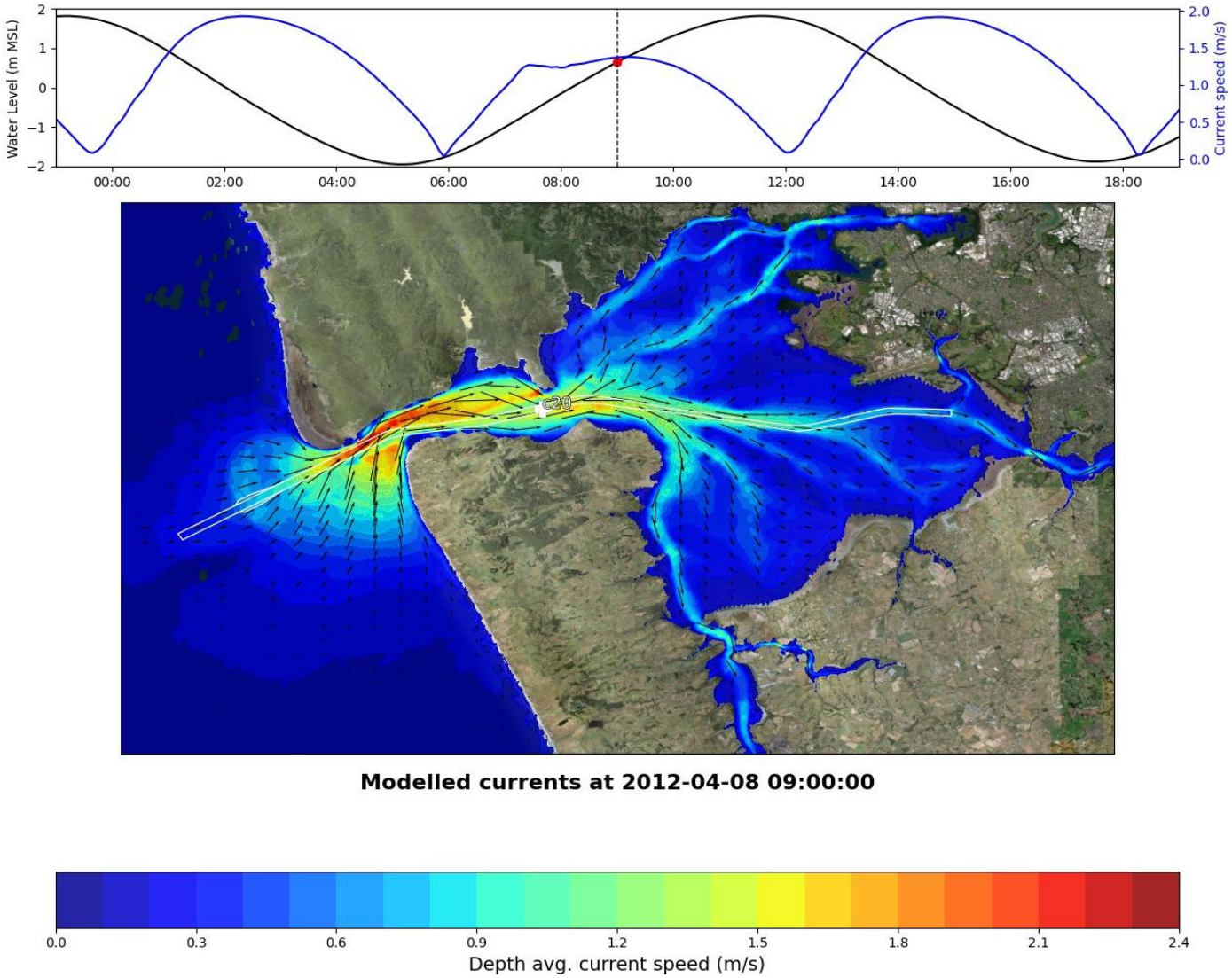

Figure 5-20 Modelled spring tidal current magnitudes and vectors for the channel 'design' simulation within Manukau Harbour at peak flood tide. The top panel presents the water level and depth averaged currents timeseries at the location shown as a white cross on the map.

5.3.3 Tidal currents difference maps

The difference between the modelled depth averaged currents during the 'existing' and channel 'design' simulation (existing minus design) at various stages of the tidal cycle during a spring tide within Manukau Harbour are presented in Figure 5-21 to Figure 5-24. Red (positive speeds) indicates and area of increased current speeds and blue (negative speeds) indicates a decrease in current speeds from 'existing' conditions.

At all stages of the tide, current speeds increase at the end of the dredged concept navigation channel due to focusing of the currents through the channel rather than dispersing more evenly across the whole bar. The current increase is particularly evident on an ebb tide. The change in timing of the ebb tidal currents at C35 indicates that there may also be an increase in the volume of water moving into the harbour over the tidal cycle.

Differences in currents are usually isolated to be around the dredged navigation channel, with limited change in currents in the southern and northern parts of the harbour.

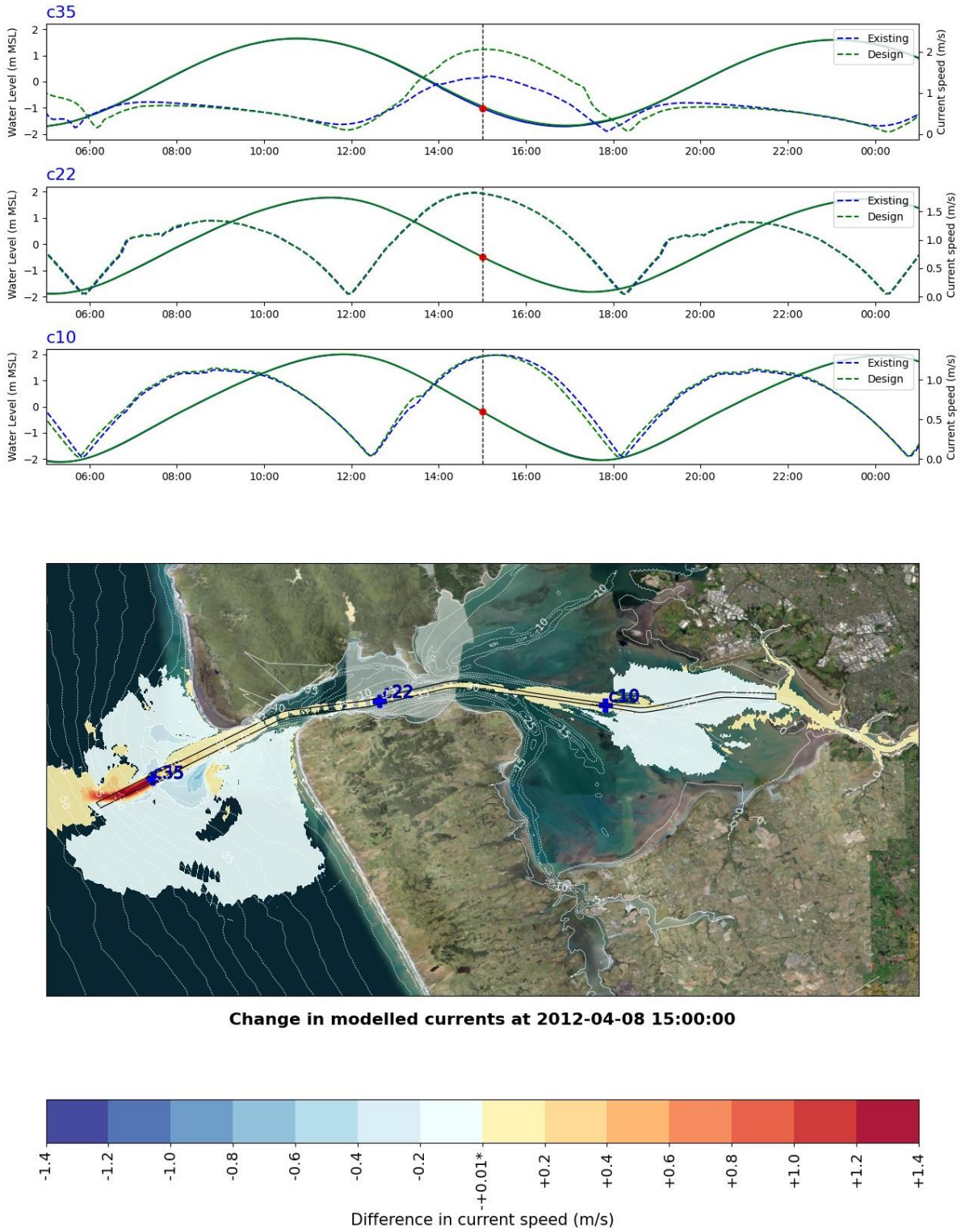

Figure 5-21 Difference in modelled spring tidal current magnitudes between the 'existing' and channel 'design' simulation within Manukau Harbour during a peak ebb tide. Red indicates and area of increased current speeds and blue indicates an area of decreased current speeds from 'existing' conditions. The top panel presents the water level and depth averaged currents timeseries at the locations shown as blue crosses on the map.

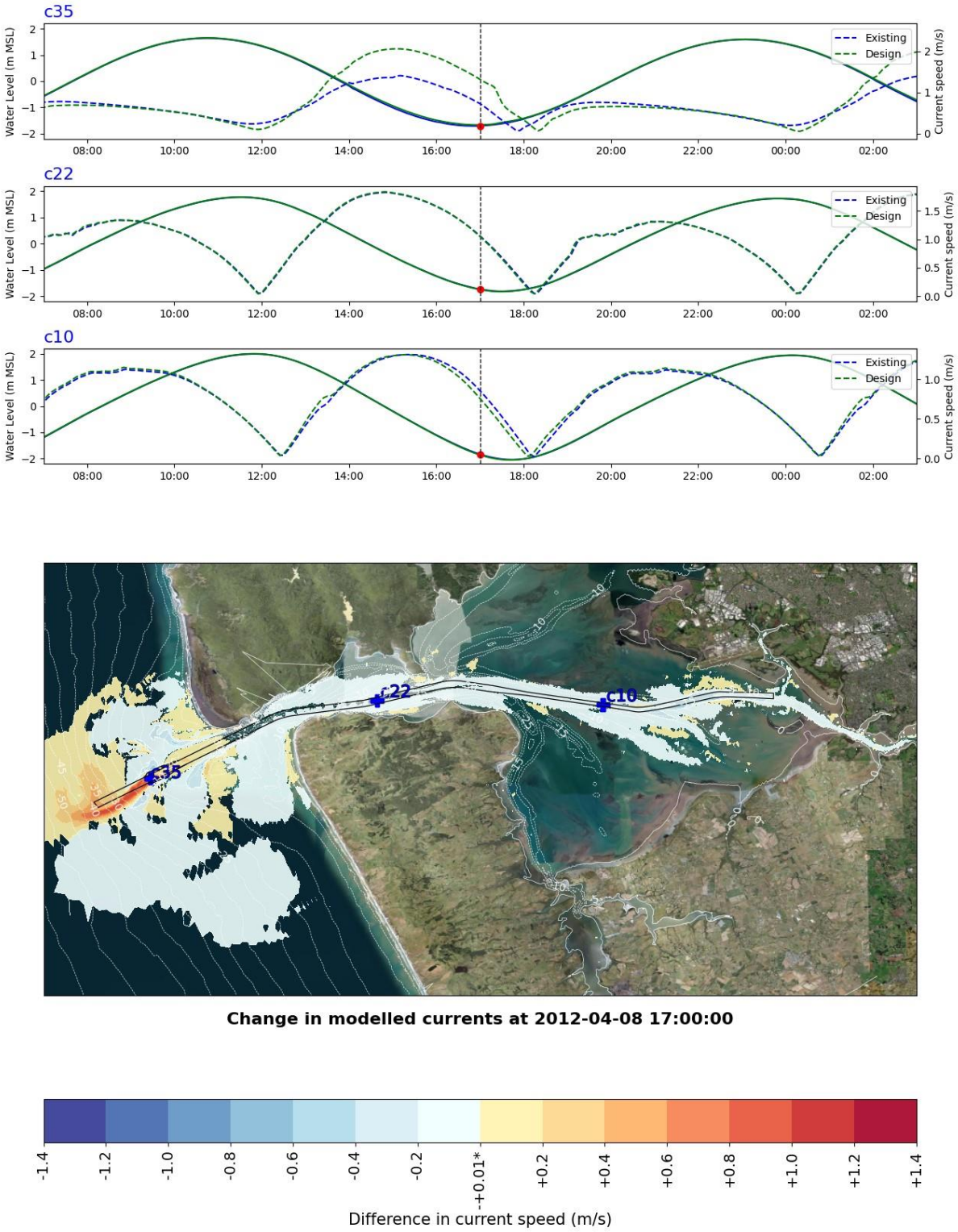

Figure 5-22 Difference in modelled spring tidal current magnitudes between the 'existing' and channel 'design' simulation within Manukau Harbour during an ebb tide. Red indicates and area of increased current speeds and blue indicates an area of decreased current speeds from 'existing' conditions. The top panel presents the water level and depth averaged currents timeseries at the locations shown as blue crosses on the map.

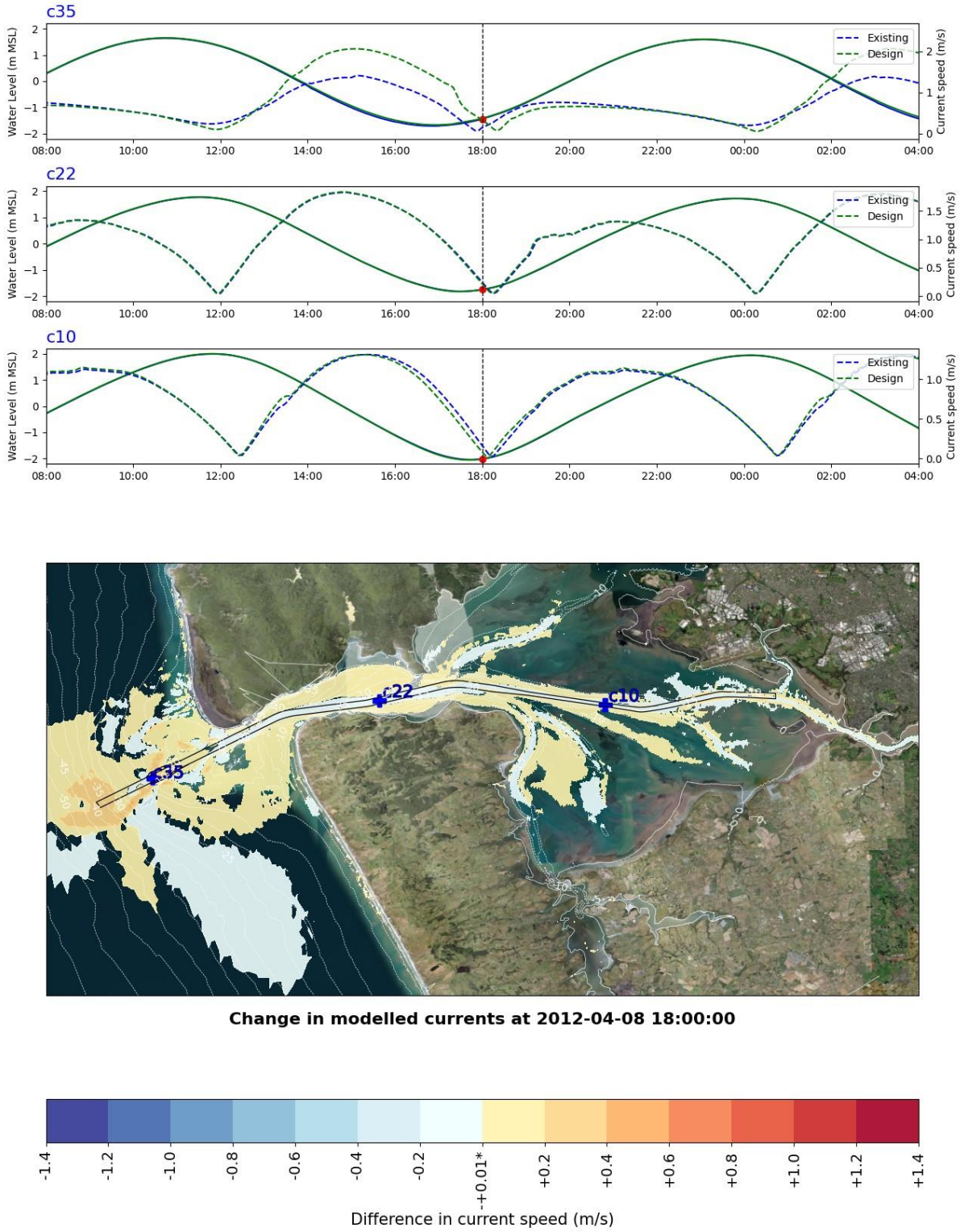

Figure 5-23 Difference in modelled spring tidal current magnitudes between the 'existing' and channel 'design' simulation within Manukau Harbour during a slack tide. Red indicates and area of increased current speeds and blue indicates an area of decreased current speeds from 'existing' conditions. The top panel presents the water level and depth averaged currents timeseries at the locations shown as blue crosses on the map.

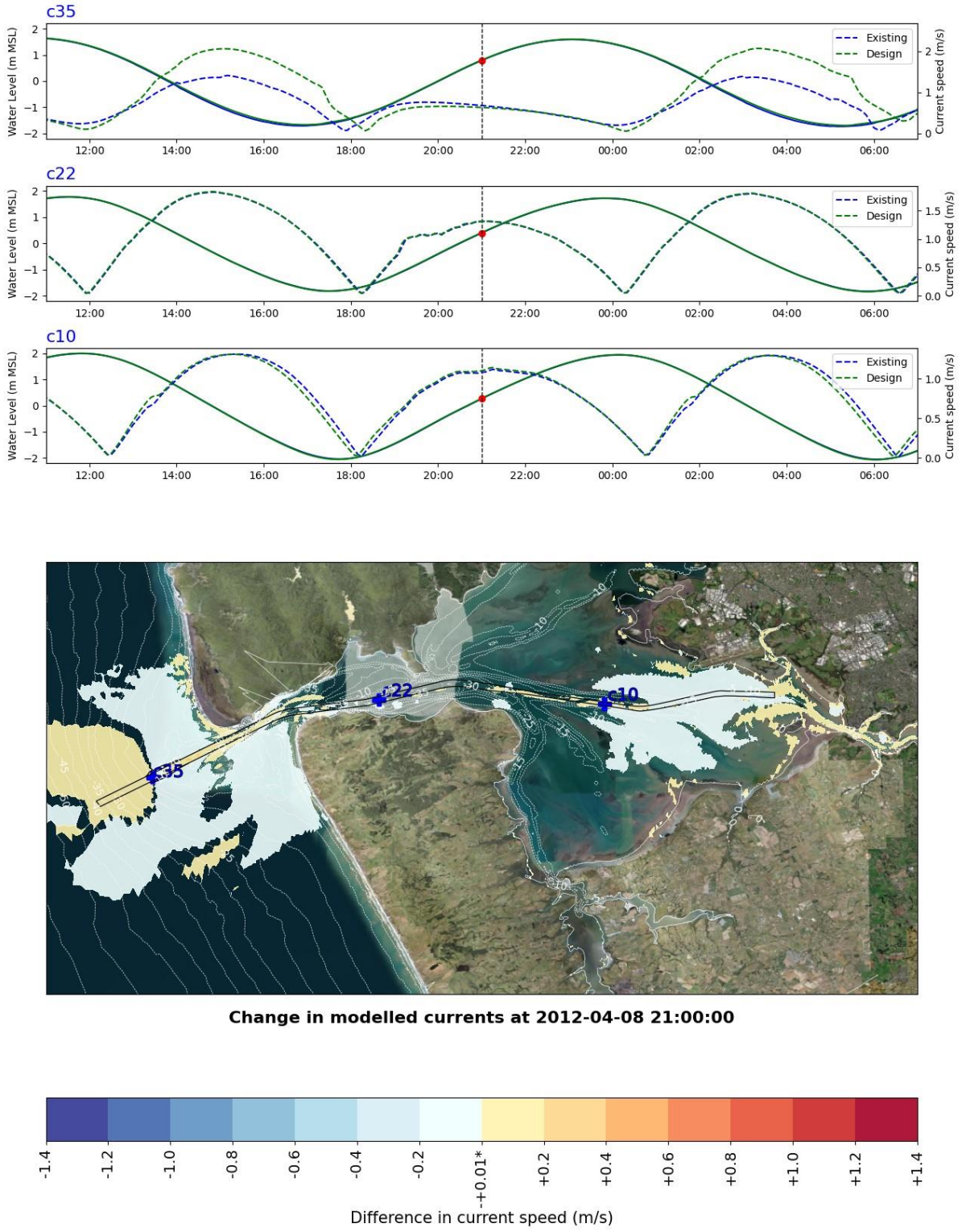

Figure 5-24 Difference in modelled spring tidal current magnitudes between the 'existing' and channel 'design' simulation within Manukau Harbour during a peak flood tide. Red indicates and area of increased current speeds and blue indicates an area of decreased current speeds from 'existing' conditions. The top panel presents the water level and depth averaged currents timeseries at the locations shown as blue crosses on the map.

5.3.4 Water level maps

The modelled water levels around high tide within the harbour for the 'existing' simulation during a spring tide are presented in Figure 5-25. The modelled water levels around high tide within the harbour for the channel 'design' simulation (South West Channel) during a spring tide are presented in Figure 5-26. Both simulations show the slowing of the propagation of the tide (lag) as well as the amplification of the tide as it propagates into the harbour.

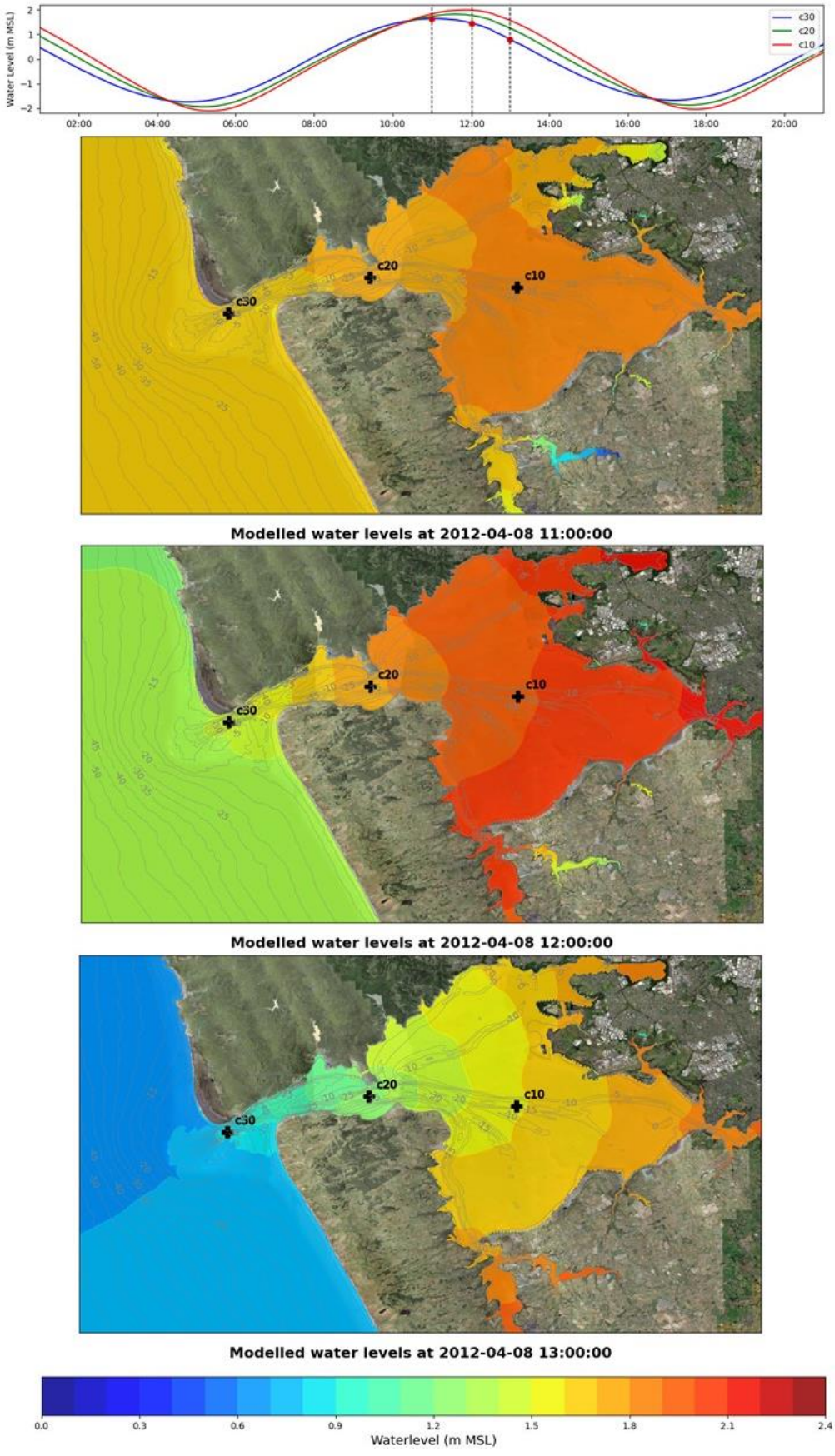

Figure 5-25 Modelled spring water levels around high tide within the harbour for the 'existing' simulation. The top panel presents the water level timeseries at the locations shown as a black cross on the map.

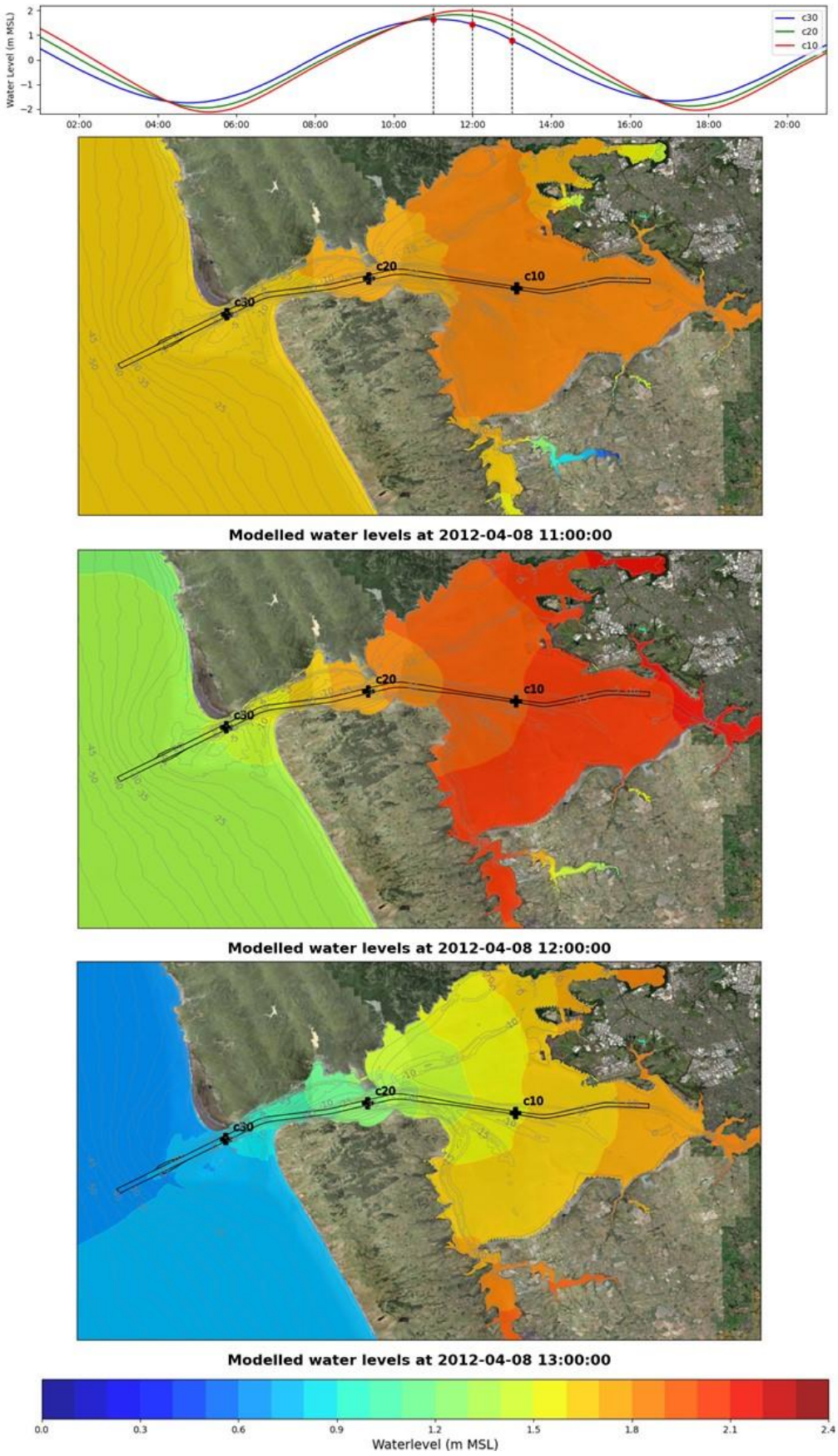

Figure 5-26 Modelled spring water levels around high tide within the harbour for the channel 'design' simulation. The top panel presents the water level timeseries at the locations shown as a black cross on the map.

5.3.5 Water level difference maps

The difference between the modelled water levels during the 'existing' and channel 'design' simulation (existing minus design) at various stages of the tidal cycle during a spring tide within Manukau Harbour are presented in Figure 5-27 to Figure 5-30. Red (positive levels) indicates an area of increased water levels and blue (negative levels) indicates a decrease in water levels from 'existing' conditions. Water levels increase on a flood tide (Figure 5-21 and Figure 5-22) and decrease on an ebb tide (Figure 5-23 and Figure 5-24) with the inclusion of the concept navigation channel, indicating that there is an increase in the volume of water moving into the harbour over the tidal cycle.

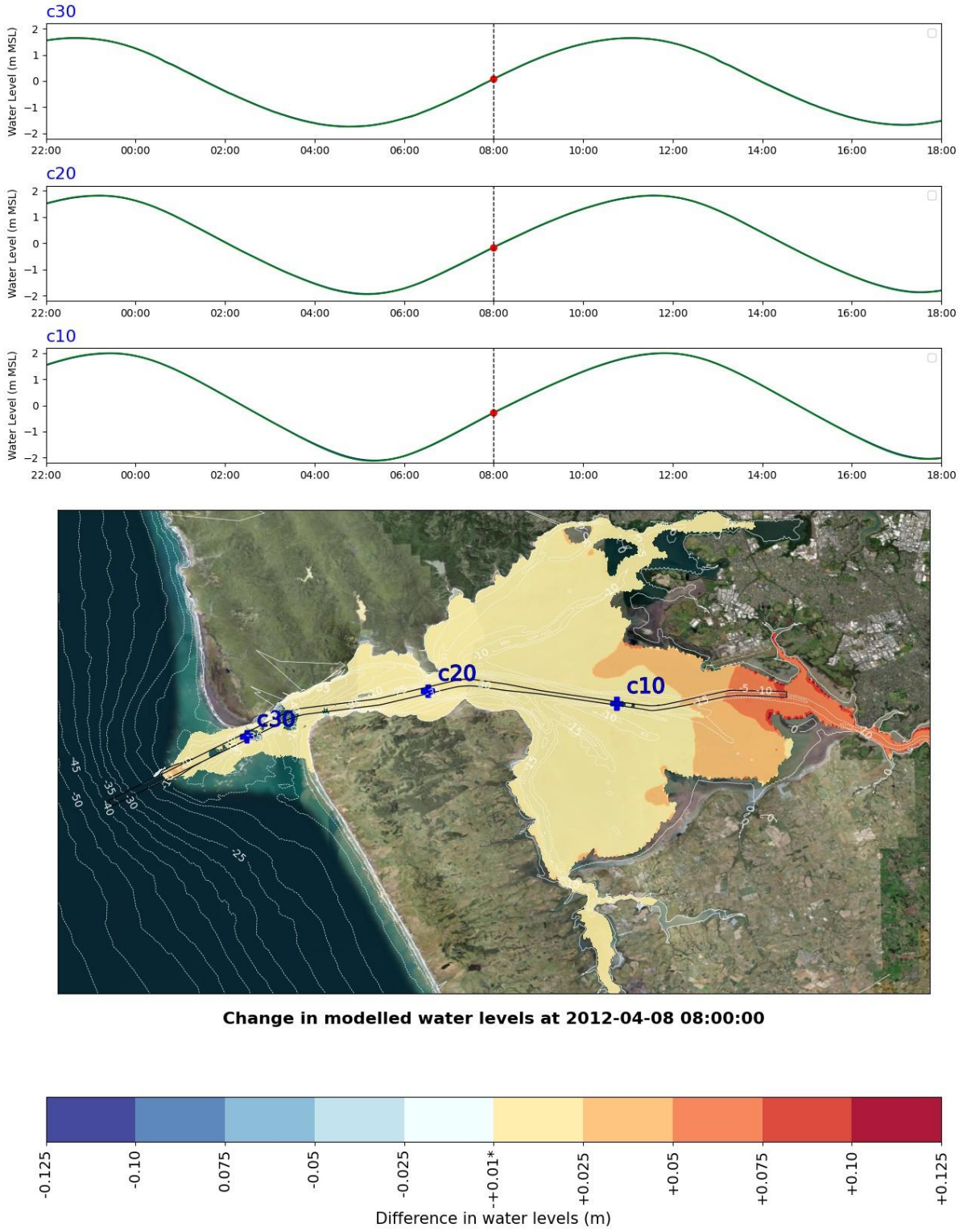

Figure 5-27 Difference in modelled spring water levels between the 'existing' and channel 'design' simulation within Manukau Harbour during a flood tide. Red indicates and area of increased water levels and blue indicates an area of decreased water levels from 'existing' conditions. The top panel presents the water level timeseries at the locations shown as blue crosses on the map.

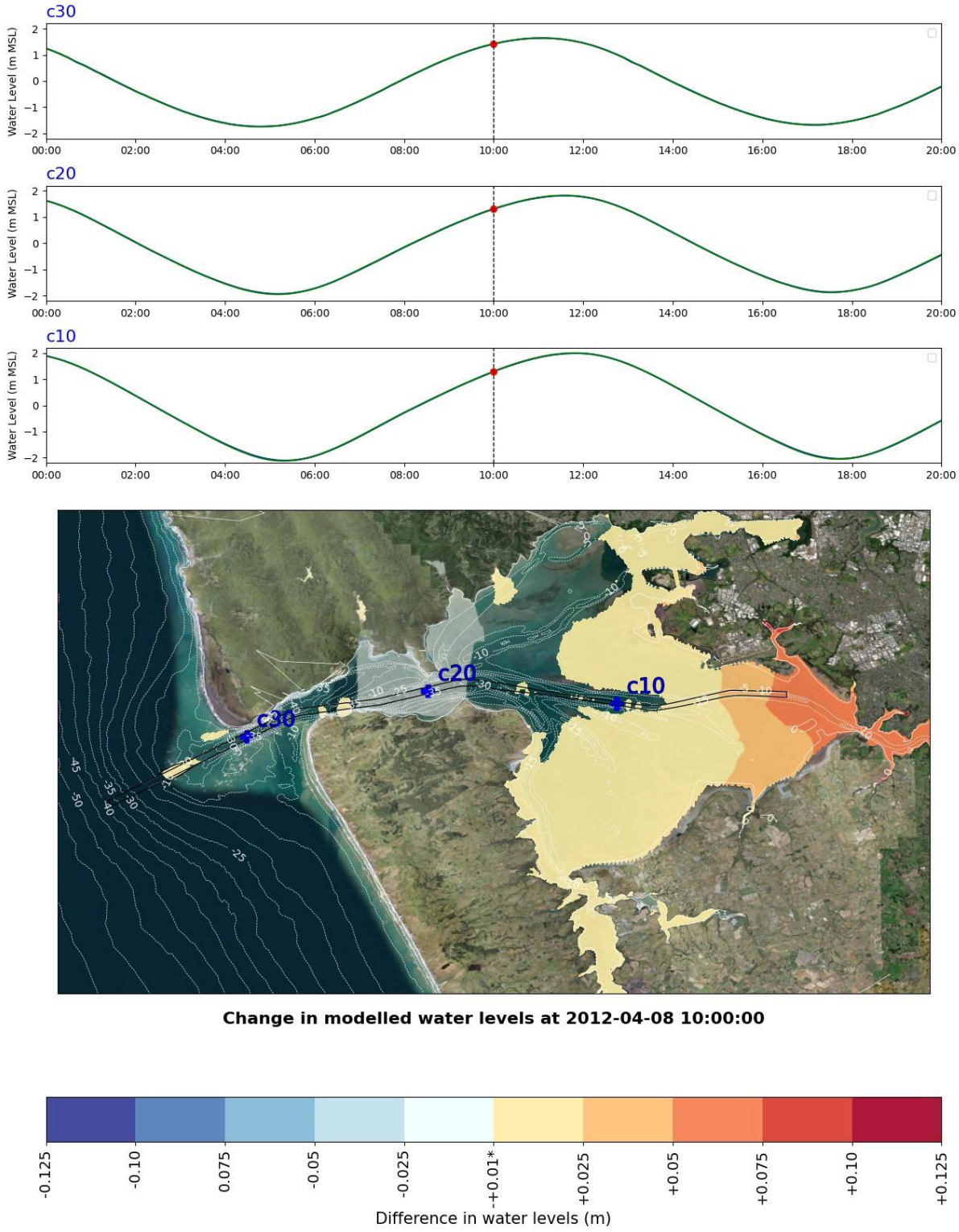

Figure 5-28 Difference in modelled spring water levels between the 'existing' and channel 'design' simulation within Manukau Harbour during a flood tide. Red indicates and area of increased water levels and blue indicates an area of decreased water levels from 'existing' conditions. The top panel presents the water level timeseries at the locations shown as blue crosses on the map.

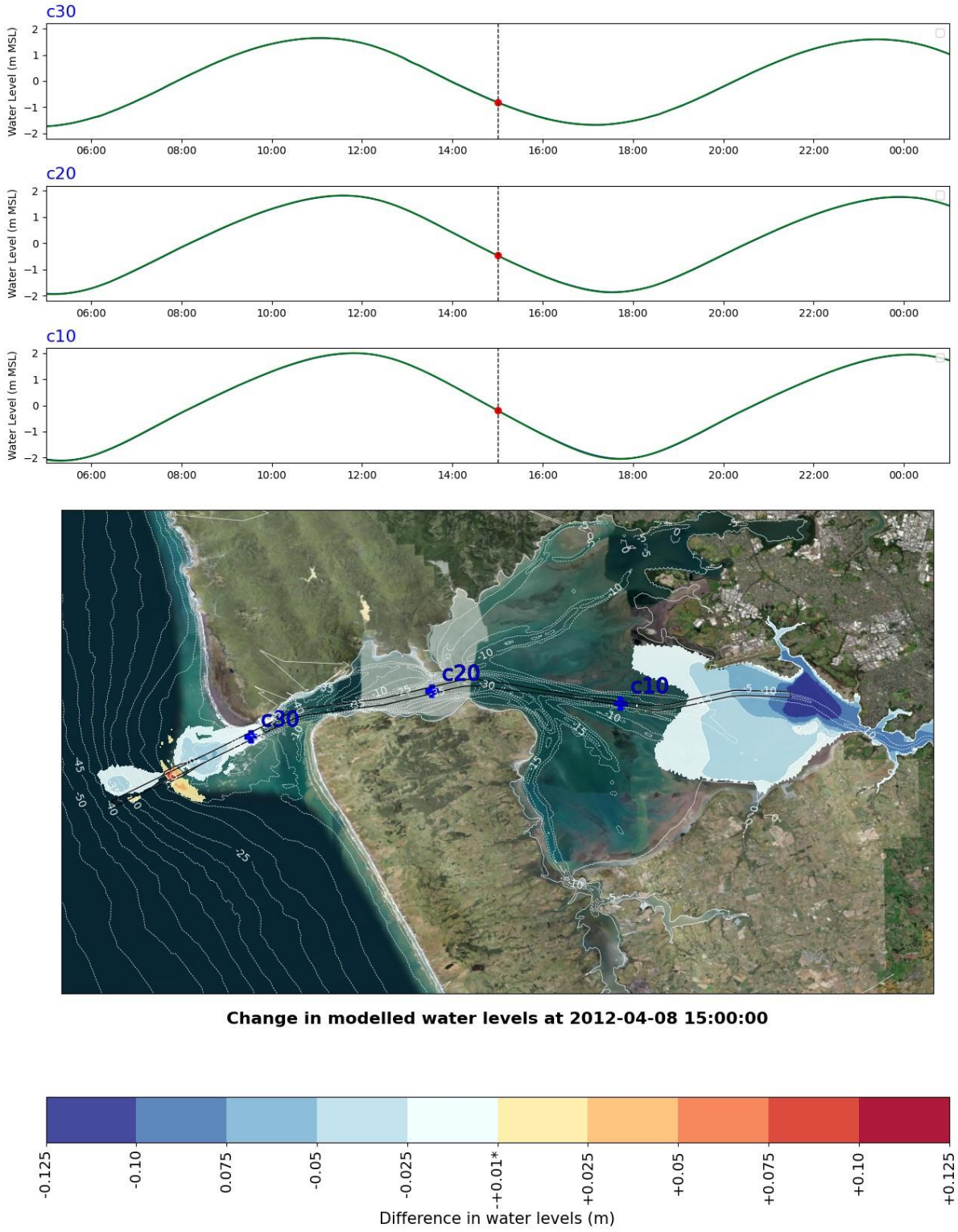

Figure 5-29 Difference in modelled spring water levels between the 'existing' and channel 'design' simulation within Manukau Harbour during an ebb tide. Red indicates and area of increased water levels and blue indicates an area of decreased water levels from 'existing' conditions. The top panel presents the water level timeseries at the locations shown as blue crosses on the map.

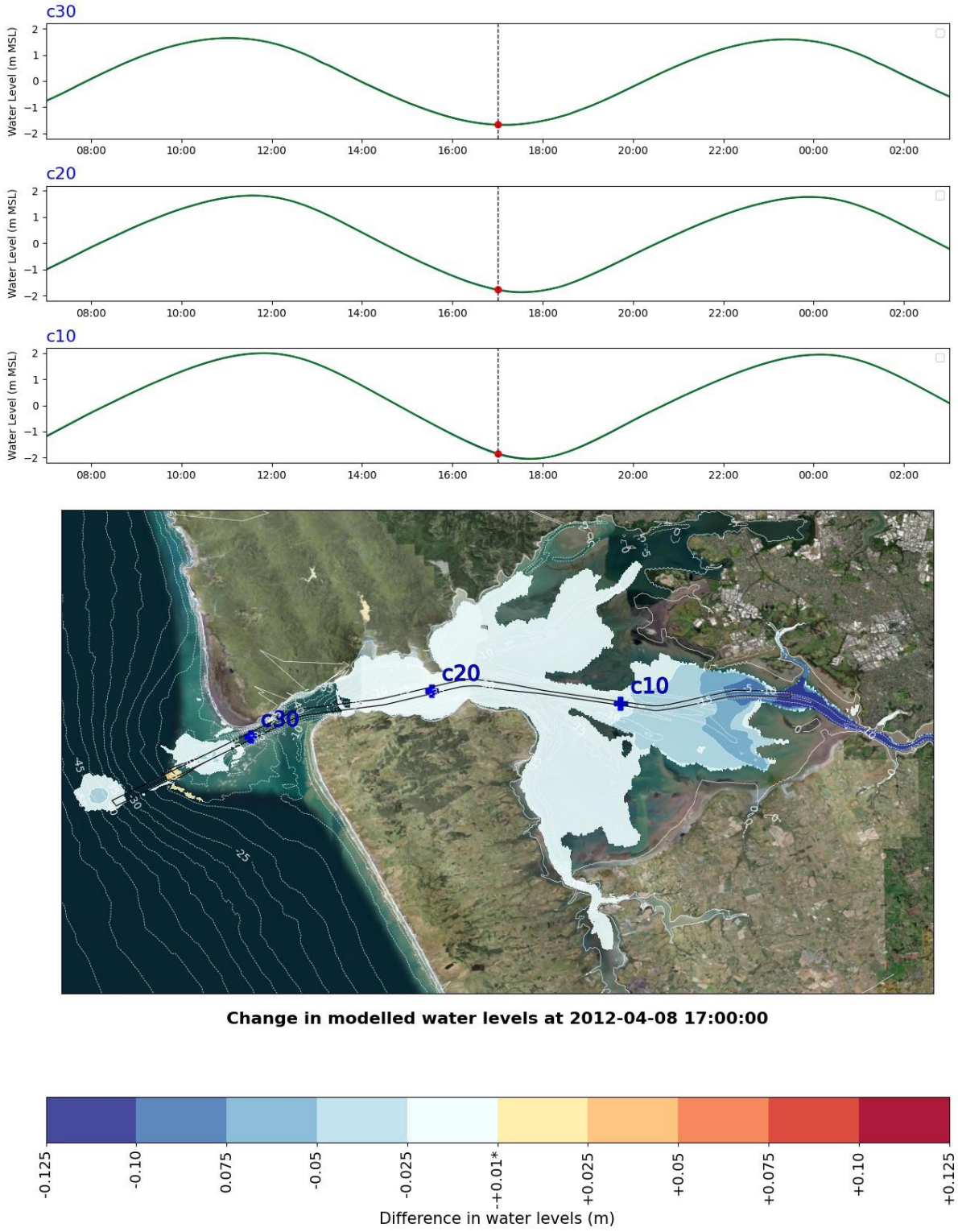

Figure 5-30 Difference in modelled spring water levels between the 'existing' and channel 'design' simulation within Manukau Harbour during an ebb tide. Red indicates and area of increased water levels and blue indicates an area of decreased water levels from 'existing' conditions. The top panel presents the water level timeseries at the locations shown as blue crosses on the map.

5.3.6 Tidal prism

A representative current transect across the Manukau entrance channel was selected, transect 026. The modelled tidal discharge (m^3.s) through the transect was extracted and the tidal prism was then calculated from the discharge. The tidal prism is the total volume of water discharging into and out of the harbour on the rising and falling tide, respectively.

The largest tidal prism from the 'existing' and channel 'design' simulations during a typical spring tide and neap tide are provided in Table 5-13. On a spring tide there is a 0.42% and 0.49% increase in tidal prism on the ebb and flood tide respectively for the design simulation. On a neap tide there is also a small increase (less than 0.07%) in the ebb and flood tides. The duration of the modelled flood tidal discharge is longer than that of the ebb tidal discharge.

The statistics of the calculated tidal prisms over a 29-day lunar cycle are displayed in Table 5-14. The statistics were undertaken on the 55 flood and 56 ebb tidal prisms over this period. The increase in tidal prism between the 'existing' and channel 'design' is consistent with the conclusions from the water levels and current difference maps presented.

In both 'existing' and channel 'design' simulations the flood tidal prism is larger than the ebb tidal prism, however this difference is a 2.1% increase in the mean and 1.3% increase in the maximum tidal prism over the 29-day period. For the representative spring and neap tides in Table 5-13, differences in the tidal prism between the flood and ebb tide are less than 0.2% on a spring tide and less than 1.4% on a neap tide. These small differences between flood and ebb tidal prism may be attributed to the transect location as well as the averaging of model discharges to a five-minute output (especially around slack tide). Transect 026 (and all transects from the measured dataset) is 80m shy of the shoreline on the southwestern edge and may be not capturing the discharges through this section. The main ebb volume gets discharged through the deeper southwestern side of the channel (see Figure 4-23) and there is return ebb flow on the southwestern side during a slack tide (see Figure 4-22).

Table 5-13 Calculated flood and ebb tidal prism values for 'existing' and channel 'design' transect across Manukau entrance for a typical spring and neap tide.

Cycle (date)	Model run	Flood		Ebb	
		Maximum tidal prism (m^3)	Start time and duration	Maximum tidal prism (m^3)	Start time and duration
Spring (7/4/2012)	**'Existing'**	-1,160,906,332	17:11 (6:20hrs)	1,160,316,509	23:31(6:00 hrs)
	'Design'	-1,166,589,247	17:09 (6:21hrs)	1,165,238,908	23:30 (5:59hrs)
Neap (28/4/2012)	**'Existing'**	-633,503,177	9:04 (6:26 hrs)	624,862,399	15:33 (6:13hrs)
	'Design'	-633,920,291	9:03 (6:27 hrs)	625,171,616	15:30 (6:13hrs)

Table 5-14 Statistical analysis from the calculated flood and ebb tidal prism at Manukau entrance over a 29-day lunar cycle for the 'existing' and channel 'design' simulations.

Stats parameter	Flood (m^3)		Ebb (m^3)	
	'Existing'	'Design'	'Existing'	'Design'
Mean	-860,290,265	-862,112,641	842,426,106	844,194,820
Maximum	-1,175,925,200	-1,180,413,001	1,160,316,509	1,165,238,908
25th %ile	-721,366,409	-722,383,384	717,455,894	717,941,468
50th %ile	-859,511,821	-861,140,908	843,127,893	844,395,309
75th %ile	-969,045,759	-971,230,309	925,034,807	927,001,844
85th %ile	-1,081,324,371	-1,085,371,585	1,070,232,322	1,073,579,530
90th %ile	-1,140,019,772	-1,145,436,082	1,111,069,640	1,115,286,986
95th %ile	-1,156,264,407	-1,162,650,711	1,140,469,365	1,146,439,596
99th %ile	-1,166,913,879	-1,172,118,749	1,153,667,400	1,158,124,178

5.3.7 Wave maps

The modelled wave parameters for the 'existing' simulation over the Manukau bar at during a high energy period are presented in Figure 5-31 and Figure 5-32. Wave parameters for the channel 'design' simulation (South West Channel) over the Manukau bar during the same high energy period are presented in Figure 5-33 and Figure 5-34. Maps of wave heights show a focusing along the southern side of the dredged concept navigation channel, increasing H_s in these areas.

For the same high energy period, the difference between the modelled H_s during the 'existing' and channel 'design' simulation (existing minus design) at a few representative timesteps within Manukau Harbour are presented in Figure 5-35. Red (positive levels) indicates an area of increased H_s and blue (negative levels) indicates a decrease in H_s from 'existing' conditions. An increase in H_s along the southern side of the dredged concept navigation channel is evident, along with an increase on the northern side which occurs earlier in the event (top map in Figure 5-35). There are small differences in H_s at the inner harbour end of the dredged concept navigation channel, these areas coincide with the areas that is dredged to reach design depth in Figure 3-7.

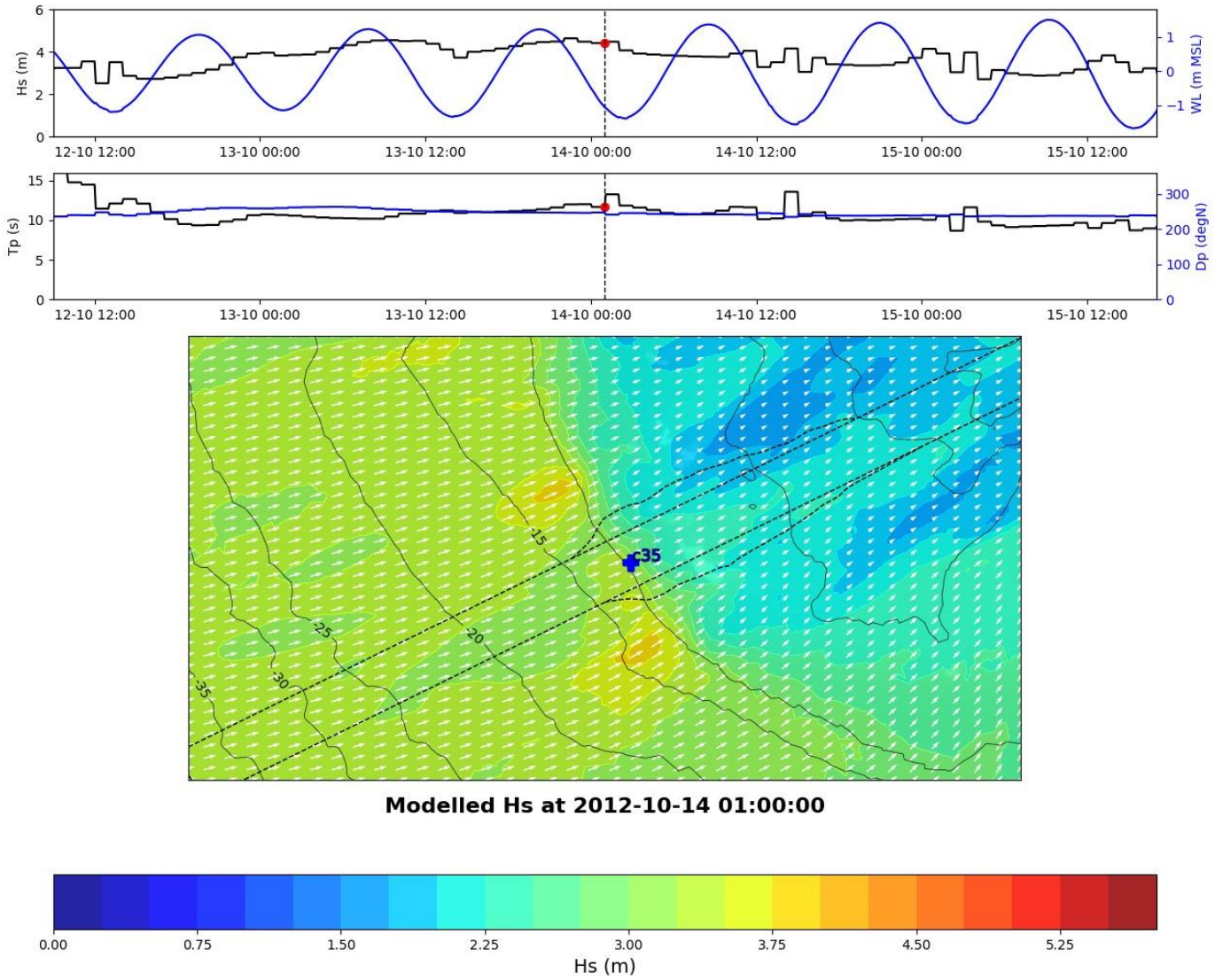

Figure 5-31 Modelled wave heights for the 'existing' simulation over Manukau bar during a wave event. The top panels present the significant wave height, water levels, peak wave period and wave direction timeseries at the location shown as a blue cross on the map.

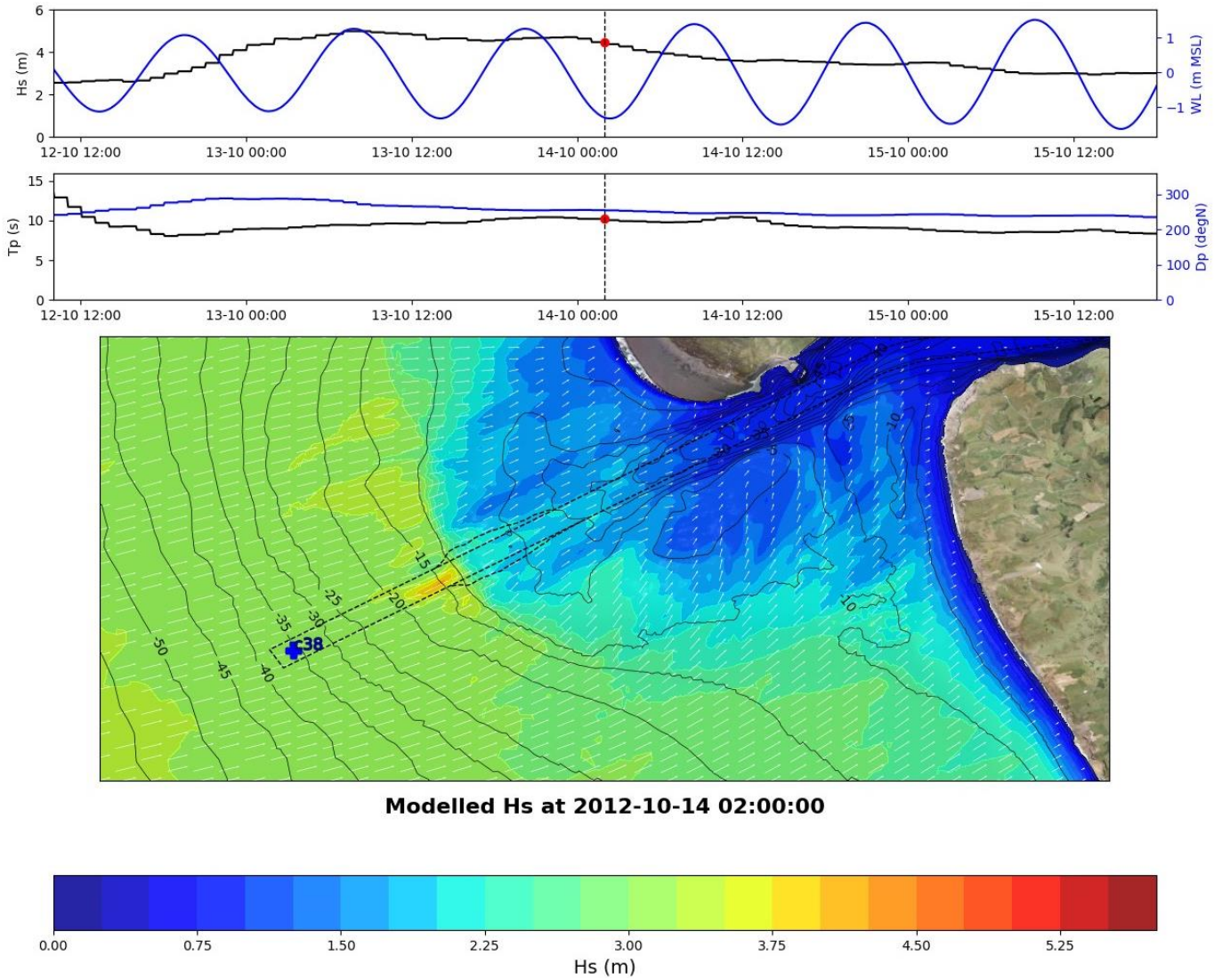

Figure 5-32 Modelled wave heights for the 'existing' simulation over Manukau bar during a wave event. The top panels present the significant wave height, water levels, peak wave period and wave direction timeseries at the location shown as a blue cross on the map.

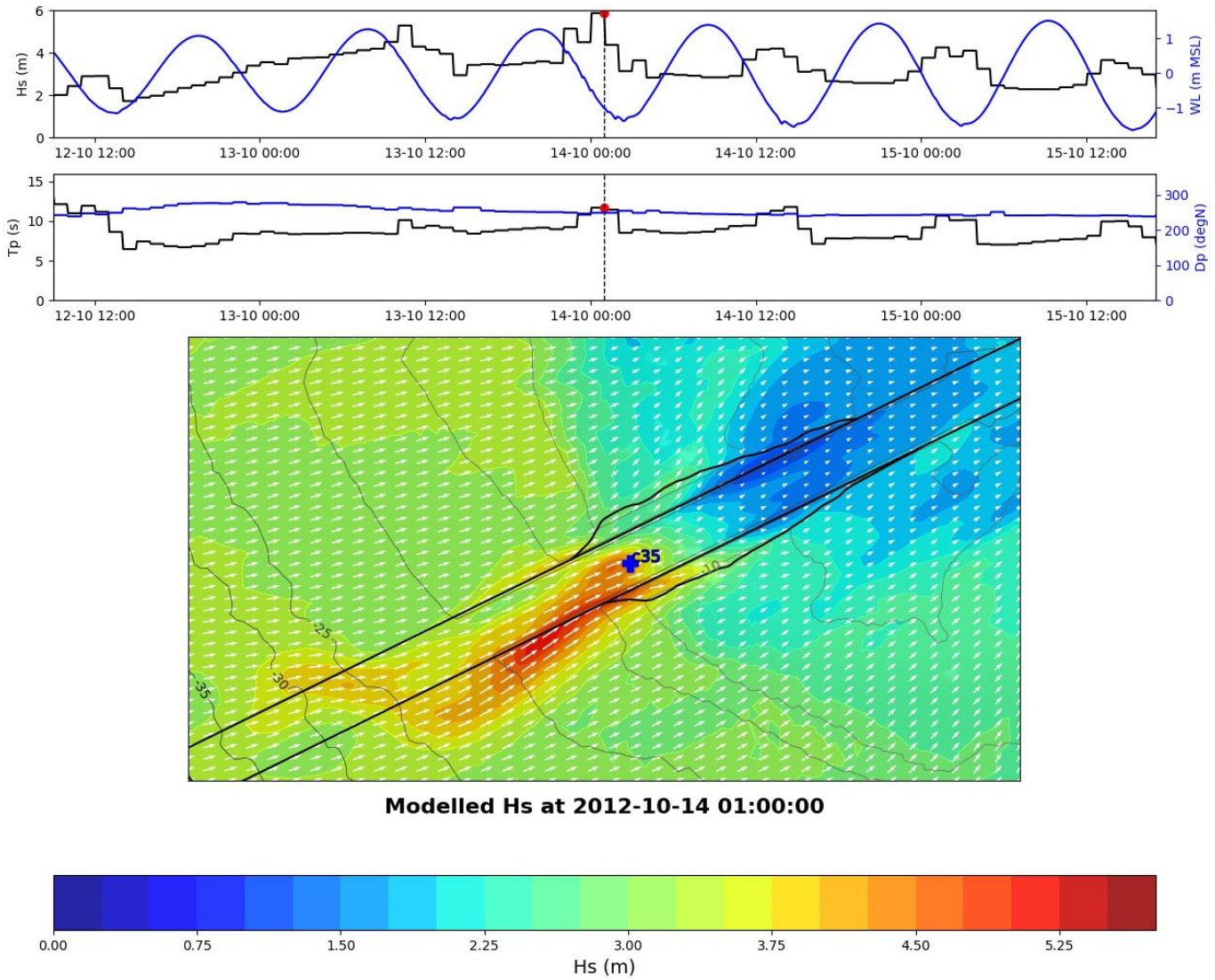

Figure 5-33 Modelled wave heights for the channel 'design' simulation over Manukau bar during a wave event. The top panels present the significant wave height, water levels, peak wave period and wave direction timeseries at the location shown as a blue cross on the map.

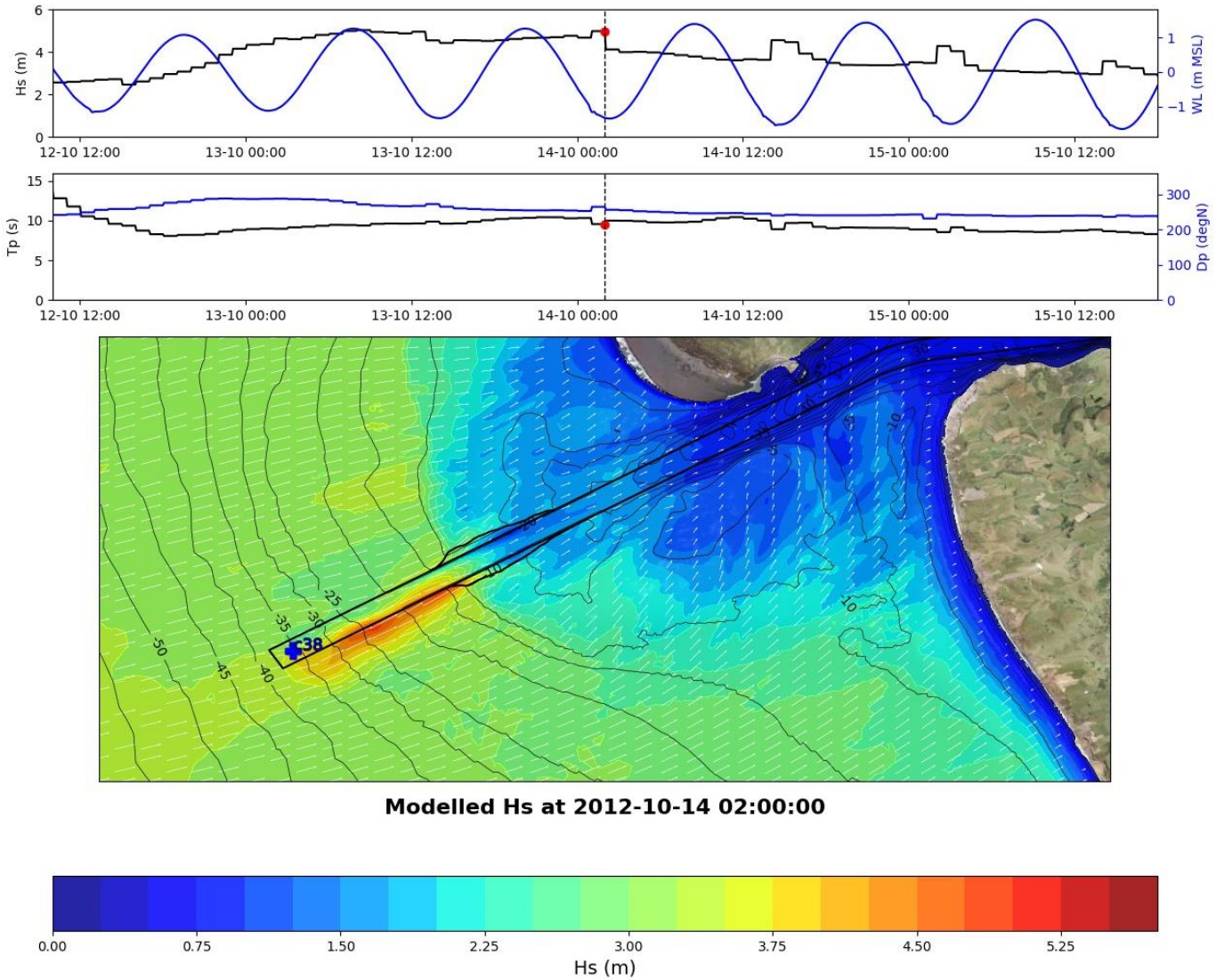

Figure 5-34 Modelled wave heights for the channel 'design' simulation over Manukau bar during a wave event. The top panels present the significant wave height, water levels, peak wave period and wave direction timeseries at the location shown as a blue cross on the map.

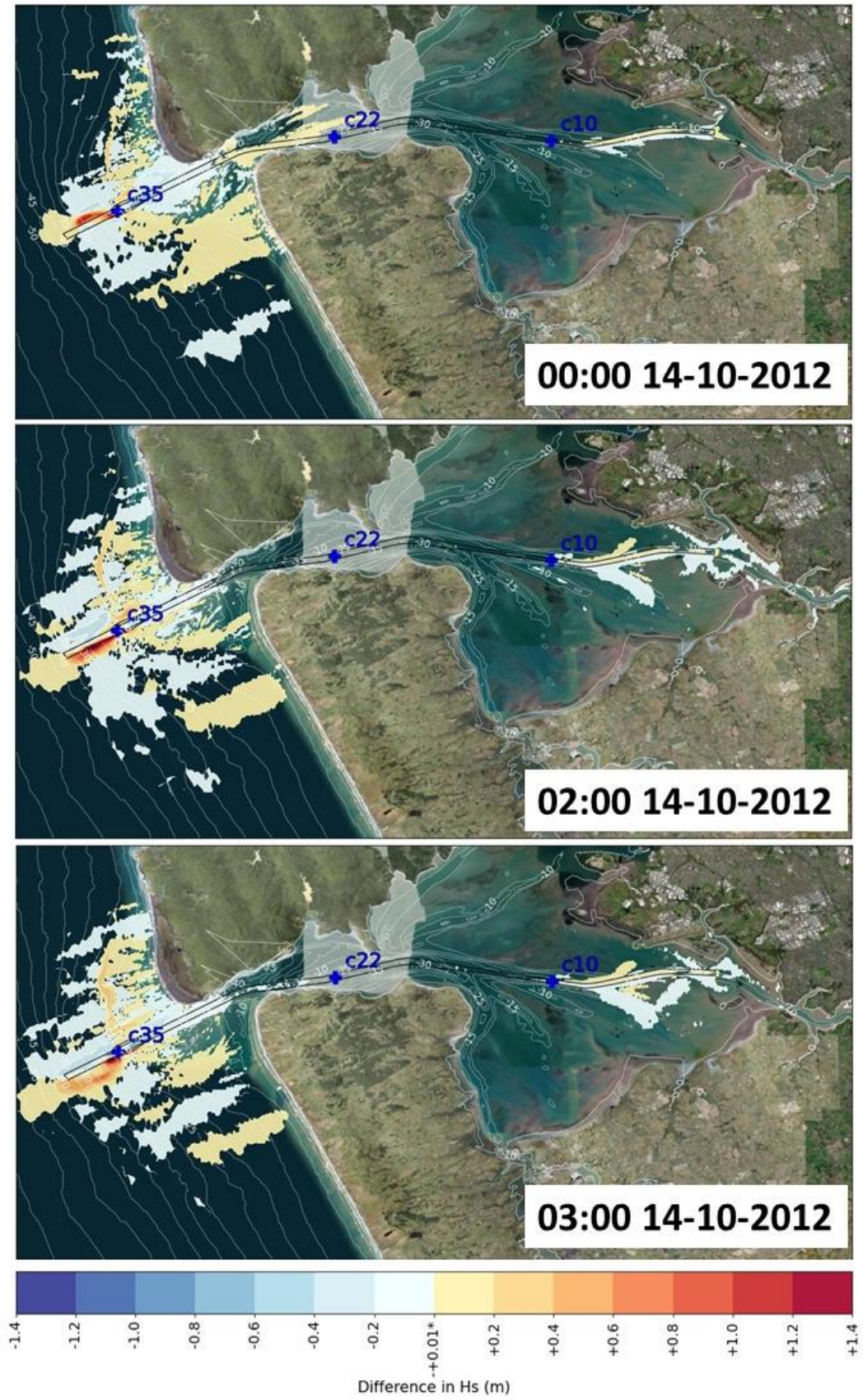

Figure 5-35 Difference in modelled H_s between the 'existing' and channel 'design' simulation within Manukau Harbour over a few representative timesteps during a high energy event. Red indicates and area of increased wave heights and blue indicates an area of decreased wave heights from 'existing' conditions.

5.3.8 Annual simulation outputs

Time series outputs of current speed, direction (going to), u and v components and water levels were provided at a five-minute interval at every 1 km along the channel. At C6 which is located in the upper Papakura Channel, examples of the water level and currents at for the 'existing' are displayed in Figure 5-36 and in Figure 5-37 for the channel 'design'. At C36 which is located immediately outside of the bar, the timeseries for the 'existing' is displayed in Figure 5-38 and the channel 'design' in Figure 5-39.

A separate file with significant wave height, peak wave period extracted from the wave spectra, wave direction (coming from) and water depth at a one hourly interval were also provided at the 38 channel locations. Examples of the wave parameters at C6 for the 'existing' are displayed in Figure 5-40 and in Figure 5-41 for the channel 'design'. At C36 the wave parameters for the 'existing' are displayed in Figure 5-42 and the channel 'design' in Figure 5-43.

One hourly wave spectra were also prepared. NetCDF files were provided for the 2D spectra at the 38 channel locations for the full annual simulation. The 1D spectra was extracted from the 2D spectral model outputs and provided as text files. The energy densities are reported in 25 frequency bins and 36 directional bins.

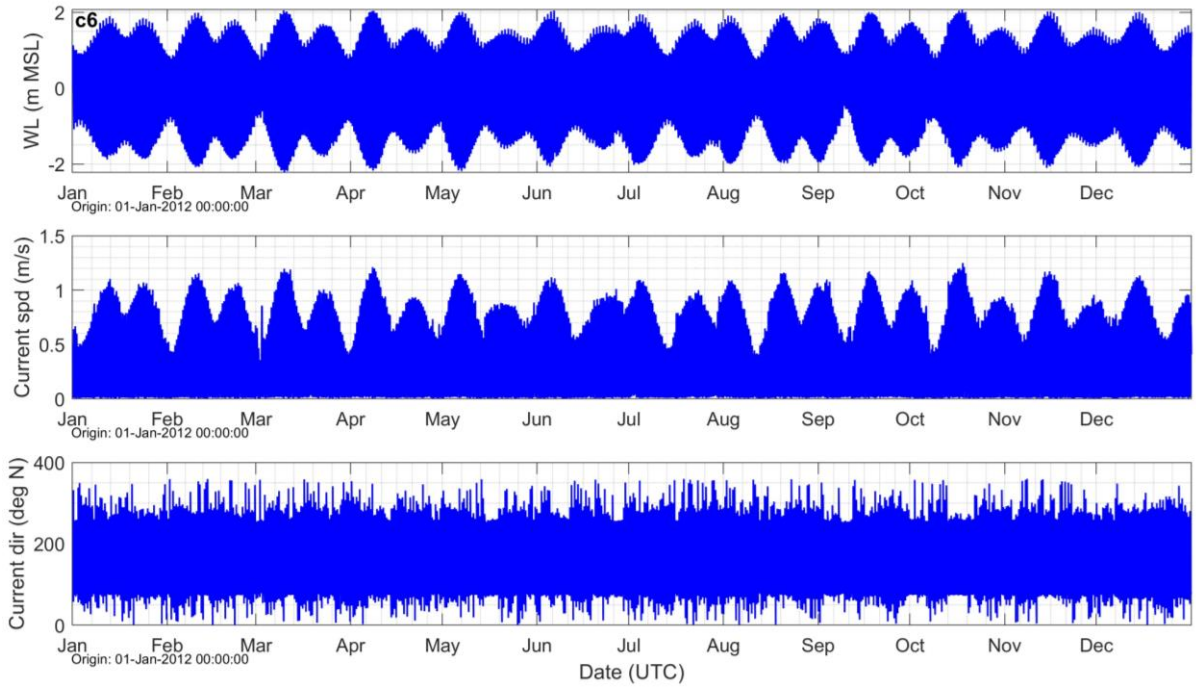

Figure 5-36 Modelled water levels and currents for the 'existing' simulation at C6.

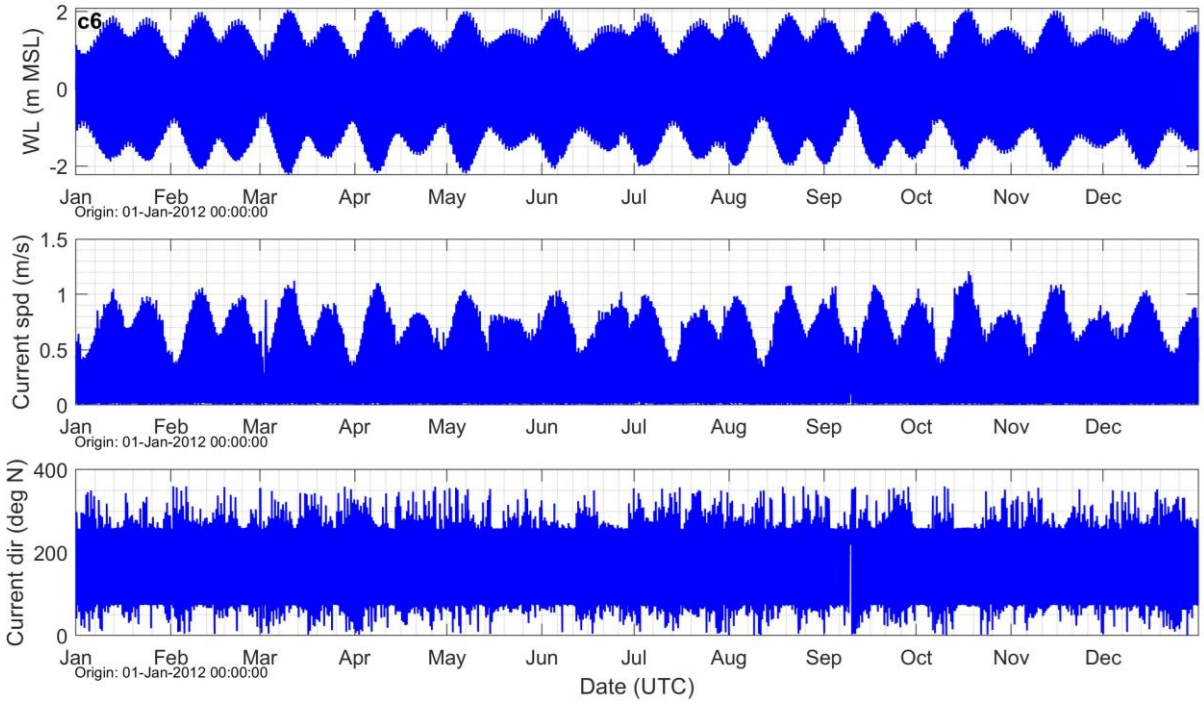

Figure 5-37 Modelled water levels and currents for the channel 'design' simulation at C6.

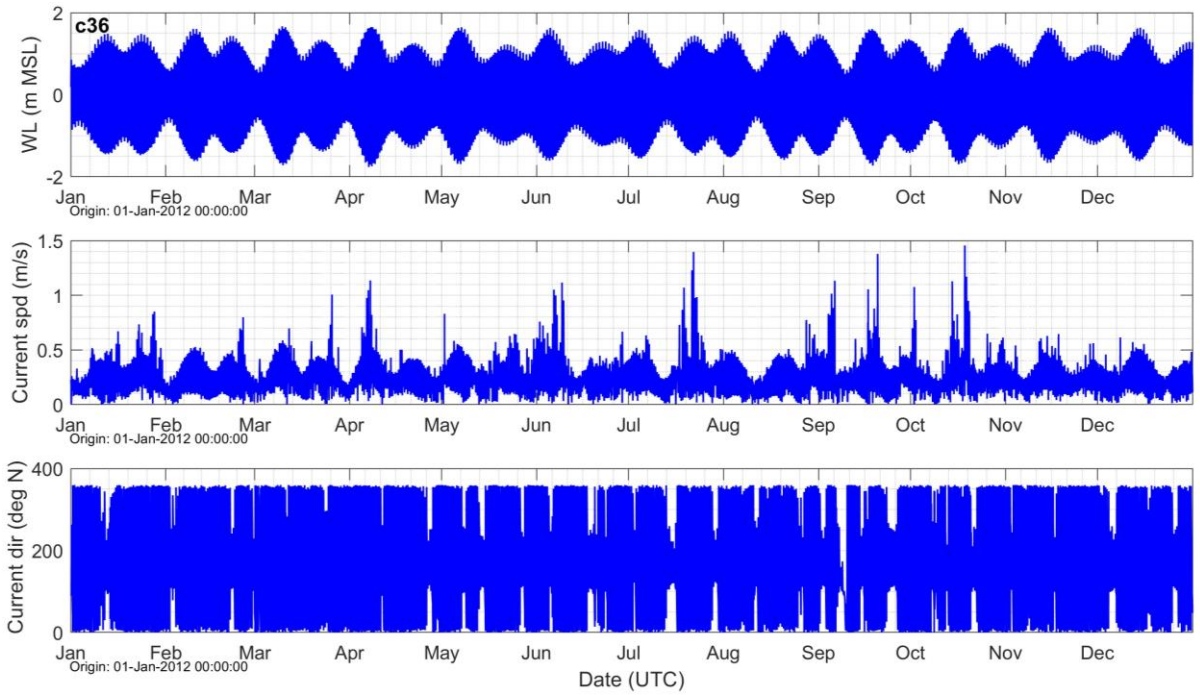

Figure 5-38 Modelled water levels and currents for the 'existing' simulation at C36.

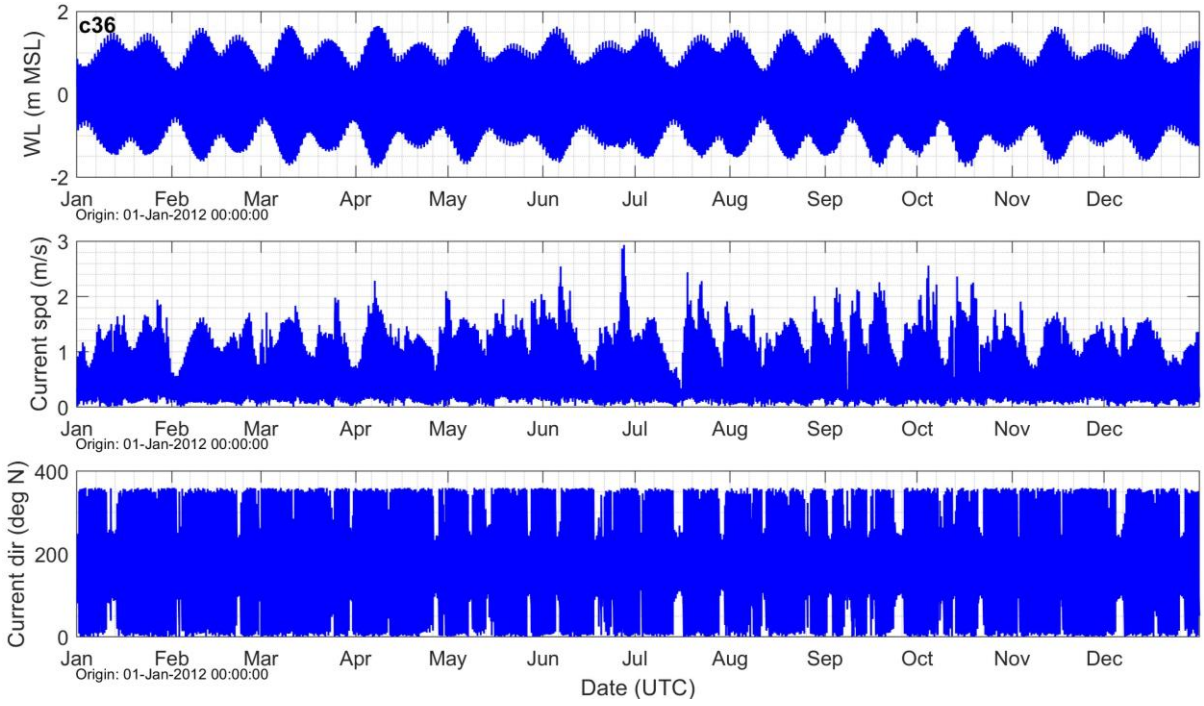

Figure 5-39 Modelled water levels and currents for the channel 'design' simulation at C36.

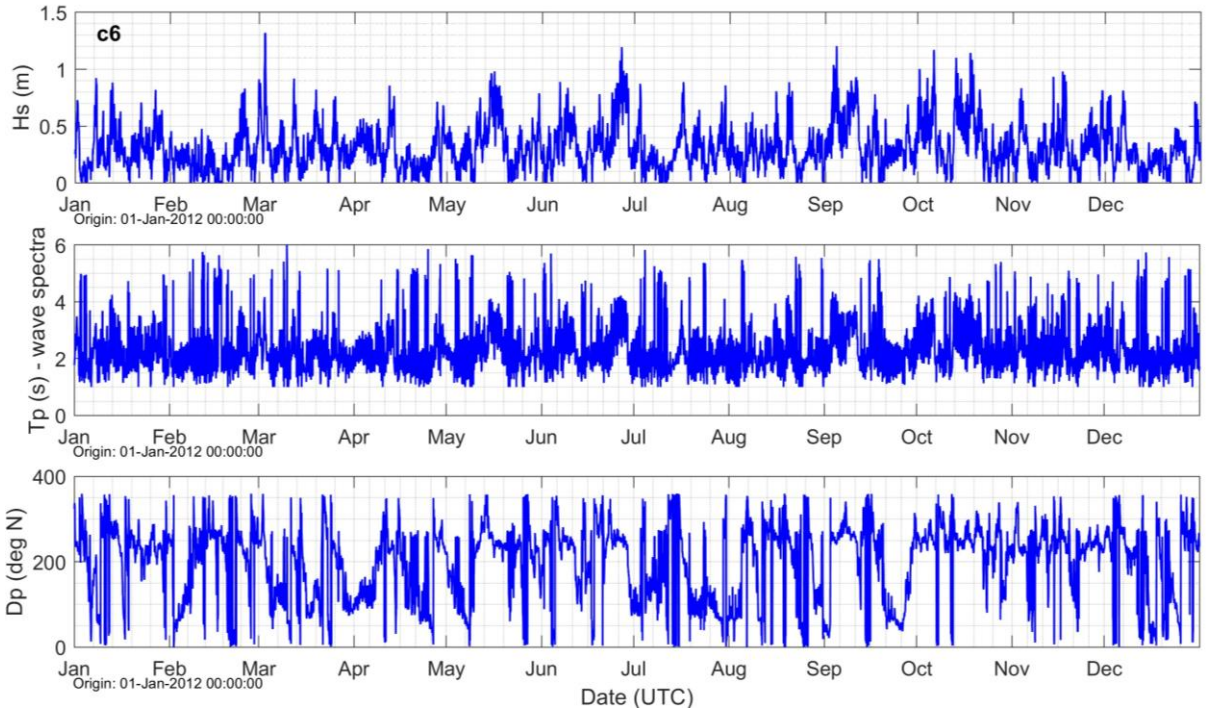

Figure 5-40 Modelled wave parameters for the 'existing' simulation at C6.

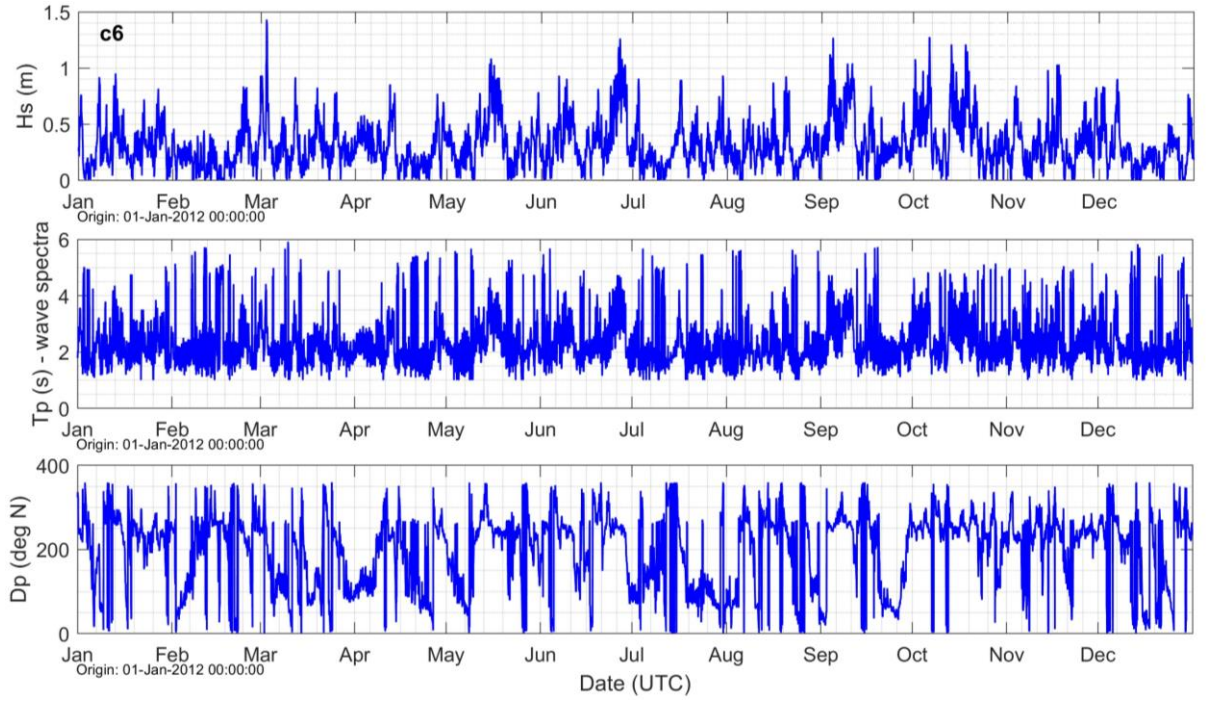

Figure 5-41 Modelled wave parameters for the channel 'design' simulation at C6.

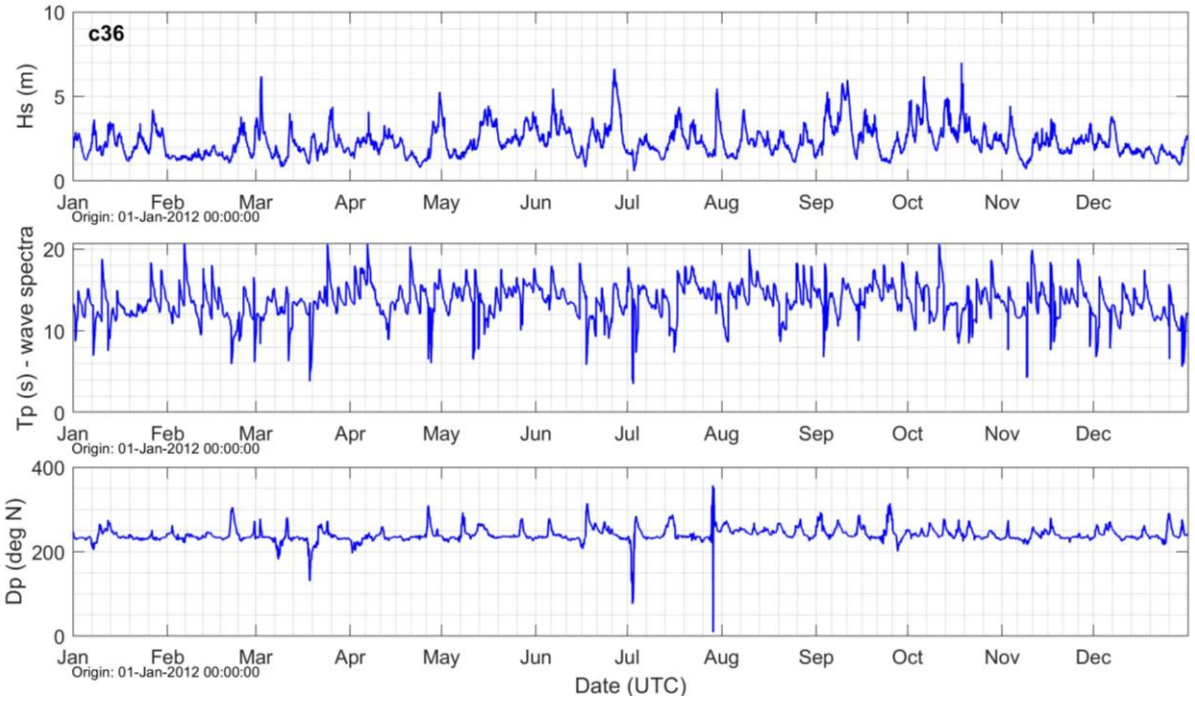

Figure 5-42 Modelled wave parameters for the 'existing' simulation at C36.

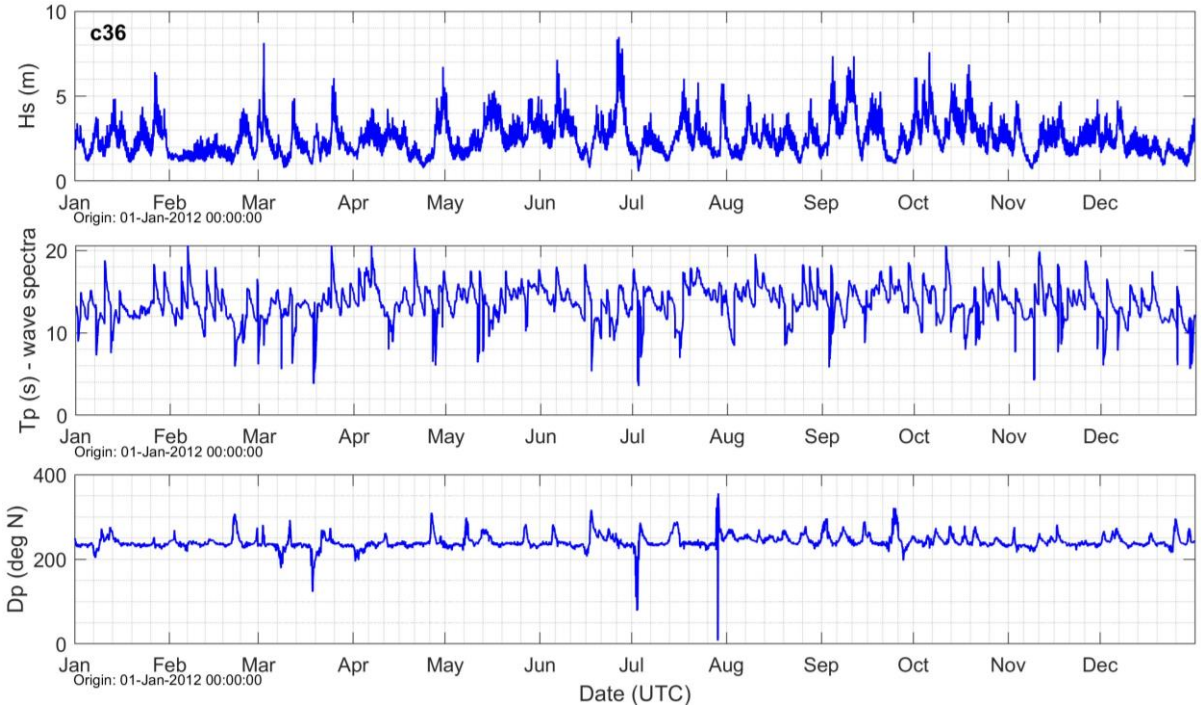

Figure 5-43 Modelled wave parameters for the channel 'design' simulation at C36.

5.3.9 Annual simulation statistics

Site output statistics were produced every ~ 2 km, i.e., for sites C1, C3, C5 to C37 (see Figure 5-1) from the model simulation over the full year 2012. In this section, wave and current statistics are provided for site C35 at the entry of the harbour. All site results are provided in Excel/PNG formats in the attached zipped folder labelled "Reporting_site_stats".

5.3.9.1 Wave statistics

The annual joint probability distribution of the total significant wave height (H_s) and mean wave direction at peak energy (D_{pm}) at C35 for the 'existing' and channel 'design' scenarios are presented in Table 5-15 and Table 5-16, respectively. Variation between the 'existing' and channel 'design' scenarios are up to 11.5% for each H_s/D_{pm} bin considered.

The annual joint probability distribution of the total significant wave height and peak period at C35 for the 'existing' and channel 'design' scenarios are presented in Table 5-17 and Table 5-18, respectively. Peak periods are from the wave spectra. Variation between the 'existing' and channel 'design' scenarios are up to 8.6% for each H_s/T_p bin considered.

Wave rose for the annual total significant wave height for the 'existing' and channel 'design' scenarios at C35 are presented in Figure 5-44 and Figure 5-45, respectively, showing the predominance of waves incoming from the SW and WSW sectors for the 'existing' and channel 'design' scenarios, respectively.

Table 5-15 Annual joint probability distribution (in %) of the total significant wave height and mean wave direction at peak energy at C35 for 'existing' scenario.

H_s (m)	Mean wave direction at peak energy (degree True North, coming from)									
	337.5-22.5	22.5-67.5	67.5-112.5	112.5-157.5	157.5-202.5	202.5-247.5	247.5-292.5	292.5-337.5	Total	Exceed%
0-0.5	-	-	-	-	-	-	-	-		100.00
0.5-1	-	-	-	-	-	0.58	0.05	-	0.63	100.00
1-1.5	-	-	0.03	0.06	0.13	7.30	1.39	0.09	9.00	99.37
1.5-2	0.02	-	0.05	0.01	0.10	15.86	2.66	0.07	18.77	90.38
2-2.5	-	-	-	-	0.03	20.31	3.16	-	23.50	71.61
2.5-3	-	-	-	-	-	17.62	3.09	-	20.71	48.10
3-3.5	-	-	-	-	-	11.63	1.68	-	13.31	27.39
3.5-4	-	-	-	-	-	6.72	1.20	-	7.92	14.07
4-4.5	-	-	-	-	-	3.18	0.28	-	3.46	6.16
4.5-5	-	-	-	-	-	1.79	0.15	-	1.94	2.70
5-5.5	-	-	-	-	-	0.66	0.02	-	0.68	0.76
5.5-6	-	-	-	-	-	0.08	-	-	0.08	0.08
Total	0.02	-	0.08	0.07	0.26	85.73	13.68	0.16	100.00	

Table 5-16 Annual joint probability distribution (in %) of the total significant wave height and mean wave direction at peak energy at C35 for 'design' scenario.

H_s (m)	Mean wave direction at peak energy (degree True North, coming from)									
	337.5-22.5	22.5-67.5	67.5-112.5	112.5-157.5	157.5-202.5	202.5-247.5	247.5-292.5	292.5-337.5	Total	Exceed%
0-0.5	-	-	-	-	-	0.01	0.01	-	0.02	100.00
0.5-1	0.01	-	-	0.03	0.08	5.20	0.77	0.09	6.18	99.98
1-1.5	0.14	0.05	0.14	0.08	0.43	18.80	5.53	0.89	26.06	93.78
1.5-2	0.03	0.02	0.03	0.01	0.17	19.26	6.81	0.31	26.64	67.74
2-2.5	-	-	-	-	0.13	12.10	5.31	0.02	17.56	41.09
2.5-3	-	-	-	-	-	7.82	3.16	-	10.98	23.53
3-3.5	-	-	-	-	-	4.17	1.84	-	6.01	12.55
3.5-4	-	-	-	-	-	2.23	0.74	-	2.97	6.53
4-4.5	-	-	-	-	-	1.51	0.44	-	1.95	3.56
4.5-5	-	-	-	-	-	0.73	0.18	-	0.91	1.61
5-5.5	-	-	-	-	-	0.32	0.07	-	0.39	0.69
5.5-6	-	-	-	-	-	0.16	0.02	-	0.18	0.31
6-6.5	-	-	-	-	-	0.09	-	-	0.09	0.13
6.5-7	-	-	-	-	-	0.01	-	-	0.01	0.03
7-7.5	-	-	-	-	-	-	-	-		0.02
7.5-8	-	-	-	-	-	0.02	-	-	0.02	0.02
Total	0.18	0.07	0.17	0.12	0.81	72.43	24.88	1.31	100.00	

Table 5-17 Annual joint probability distribution (in %) of the total significant wave height and peak period at C35 for 'existing' scenario.

H_s (m)	Peak period (s)											
	0-2	2-4	4-6	6-8	8-10	10-12	12-14	14-16	16-18	18-20	Total	Exceed%
0-0.5	-	-	-	-	-	-	-	-	-	-		100.00
0.5-1	-	-	-	-	-	0.20	0.40	0.02	-	-	0.62	100.00
1-1.5	-	-	0.03	0.16	0.09	2.45	3.45	2.50	0.23	0.08	8.99	99.37
1.5-2	-	-	0.03	0.15	0.41	3.05	8.41	5.24	0.97	0.46	18.72	90.38
2-2.5	-	-	-	0.28	0.32	2.50	11.07	7.50	1.37	0.43	23.47	71.61
2.5-3	-	-	0.01	0.15	0.63	3.21	7.43	7.25	1.51	0.43	20.62	48.10
3-3.5	-	-	-	0.03	0.47	1.64	4.49	4.88	1.42	0.35	13.28	27.39
3.5-4	-	-	-	0.01	0.33	1.05	2.58	2.80	0.98	0.16	7.91	14.07
4-4.5	-	-	-	-	0.01	0.35	0.91	1.58	0.58	0.02	3.45	6.16
4.5-5	-	-	-	-	-	0.11	0.26	1.21	0.33	0.02	1.93	2.70
5-5.5	-	-	-	-	-	0.05	0.03	0.42	0.18	-	0.68	0.76
5.5-6	-	-	-	-	-	-	-	0.07	0.01	-	0.08	0.08
Total	-	-	0.07	0.78	2.26	14.61	39.03	33.47	7.58	1.95	100.00	

Table 5-18 Annual joint probability distribution (in %) of the total significant wave height and peak period at C35 for channel 'design' scenario.

H_s (m)	Peak period (s)											
	0-2	2-4	4-6	6-8	8-10	10-12	12-14	14-16	16-18	18-20	Total	Exceed%
0-0.5	-	-	-	-	-	-	0.02	-	-	-	0.02	100.00
0.5-1	-	-	0.01	-	0.01	1.72	2.63	1.64	0.16	0.02	6.19	99.98
1-1.5	-	-	0.01	0.14	0.25	3.70	12.03	8.11	1.22	0.55	26.01	93.78
1.5-2	-	-	0.02	0.23	0.39	2.66	10.71	9.72	2.27	0.59	26.59	67.74
2-2.5	-	-	0.01	0.24	0.41	2.96	6.51	5.58	1.47	0.31	17.49	41.09
2.5-3	-	-	-	0.10	0.60	1.62	3.69	3.76	0.92	0.28	10.97	23.53
3-3.5	-	-	-	-	0.28	1.08	2.03	1.96	0.58	0.07	6.00	12.55
3.5-4	-	-	-	0.01	0.07	0.52	0.80	1.21	0.32	0.05	2.98	6.53
4-4.5	-	-	-	-	0.06	0.20	0.42	0.94	0.28	0.05	1.95	3.56
4.5-5	-	-	-	-	-	0.10	0.26	0.35	0.19	-	0.90	1.61
5-5.5	-	-	-	-	-	0.03	0.07	0.23	0.06	-	0.39	0.69
5.5-6	-	-	-	-	-	0.01	0.05	0.10	0.02	-	0.18	0.31
6-6.5	-	-	-	-	-	-	0.01	0.08	-	-	0.09	0.13
6.5-7	-	-	-	-	-	-	-	0.01	-	-	0.01	0.03
7-7.5	-	-	-	-	-	-	-	-	-	-		0.02
7.5-8	-	-	-	-	-	-	-	0.02	-	-	0.02	0.02
Total	-	-	0.05	0.72	2.07	14.60	39.23	33.71	7.49	1.92	100.00	

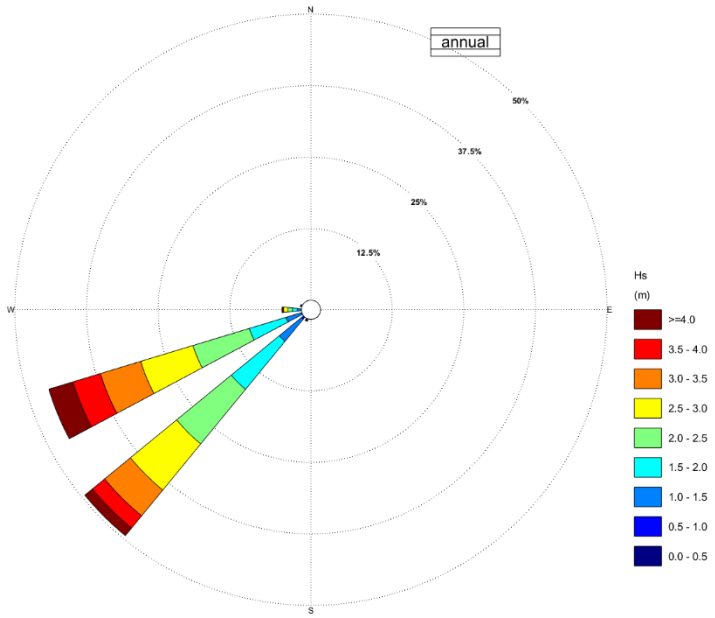

Figure 5-44 Annual wave rose plot for the total significant wave height at C35 for 'existing' scenario. Sectors indicate the direction from which waves approach.

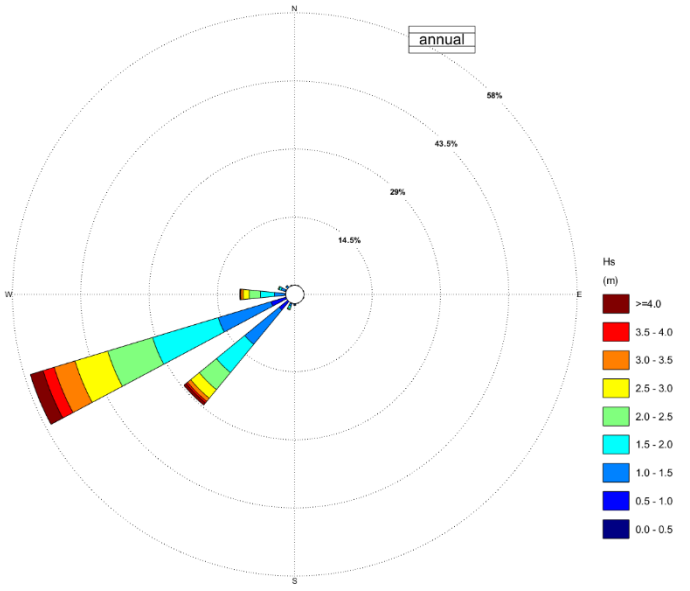

Figure 5-45 Annual wave rose plot for the total significant wave height at C35 for channel 'design' scenario. Sectors indicate the direction from which waves approach.

5.3.9.2 Current statistics

The annual joint probability distribution of current speed and direction for the 'existing' and channel 'design' scenarios at C35 are presented in Table 5-19 and Table 5-20, respectively. Results indicate variation between the existing and design scenarios of up to 5.66% change for each current speed/direction bin considered. Stronger SW currents are noted for the channel 'design' scenario.

Annual current roses for the 'existing' and channel 'design' scenarios at C35 are presented in Figure 5-46 and Figure 5-47, respectively, showing the predominance of currents flowing towards the SW sector.

Table 5-19 Annual joint probability distribution (in %) of depth-averaged current speed and direction at C35 for 'existing' scenario.

Cspd ($m.s^{-1}$)	Mean current direction (degree True North, going to)									
	337.5-22.5	**22.5-67.5**	**67.5-112.5**	**112.5-157.5**	**157.5-202.5**	**202.5-247.5**	**247.5-292.5**	**292.5-337.5**	**Total**	**Exceed%**
0-0.2	2.13	1.72	0.79	1.07	0.98	0.58	1.32	1.93	10.52	100.00
0.2-0.4	1.36	7.80	5.16	0.93	1.34	2.70	3.67	0.60	23.56	89.48
0.4-0.6	0.17	8.56	12.36	0.18	0.50	6.00	2.69	0.06	30.52	65.92
0.6-0.8	0.05	3.11	7.15	0.05	0.23	8.21	0.55	0.02	19.37	35.39
0.8-1	0.03	0.77	0.29	0.02	0.09	7.30	0.14	0.01	8.65	16.02
1-1.2	0.01	0.11	0.04	*	0.02	4.67	0.08	0.01	4.94	7.37
1.2-1.4	*	0.07	0.01	*	0.01	1.92	0.07	0.01	2.09	2.43
1.4-1.6	*	0.02	*	-	*	0.24	0.02	-	0.28	0.35
1.6-1.8	*	*	-	-	*	0.04	0.01	-	0.05	0.07
1.8-2	-	*	-	-	-	0.01	-	-	0.01	0.01
2-2.2	-	-	-	-	-	*	-	-		
Total	3.75	22.16	25.80	2.25	3.17	31.67	8.55	2.64	100.00	

Notes: * represents less than 0.005%.

Table 5-20 Annual joint probability distribution (in %) of depth-averaged current speed and direction at C35 for channel 'design' scenario.

Cspd ($m.s^{-1}$)	Mean current direction (degree True North, going to)									
	337.5-22.5	**22.5-67.5**	**67.5-112.5**	**112.5-157.5**	**157.5-202.5**	**202.5-247.5**	**247.5-292.5**	**292.5-337.5**	**Total**	**Exceed%**
0-0.2	1.34	3.98	1.74	0.51	0.76	1.05	2.70	0.99	13.07	100.00
0.2-0.4	0.08	9.32	6.95	0.12	0.21	3.39	1.95	0.04	22.06	86.94
0.4-0.6	*	7.67	12.07	0.03	0.09	4.28	0.77	0.01	24.92	64.87
0.6-0.8	-	0.70	1.32	*	0.02	4.87	0.54	*	7.45	39.95
0.8-1	-	-	-	-	0.01	5.70	0.40	-	6.11	32.51
1-1.2	-	-	-	-	*	6.54	0.33	*	6.87	26.40
1.2-1.4	-	-	-	-	*	6.43	0.26	-	6.69	19.52
1.4-1.6	-	-	-	-	-	5.90	0.23	-	6.13	12.83
1.6-1.8	-	-	-	-	-	4.03	0.19	-	4.22	6.70
1.8-2	-	-	-	-	-	1.90	0.09	-	1.99	2.49
2-2.2	-	-	-	-	-	0.38	0.03	-	0.41	0.50
2.2-2.4	-	-	-	-	-	0.06	0.02	-	0.08	0.09
2.4-2.6	-	-	-	-	-	0.01	-	-	0.01	0.01
2.6-2.8	-	-	-	-	-	*	-	-		
Total	1.42	21.67	22.08	0.66	1.09	44.54	7.51	1.04	100.00	

Notes: * represents less than 0.005%.

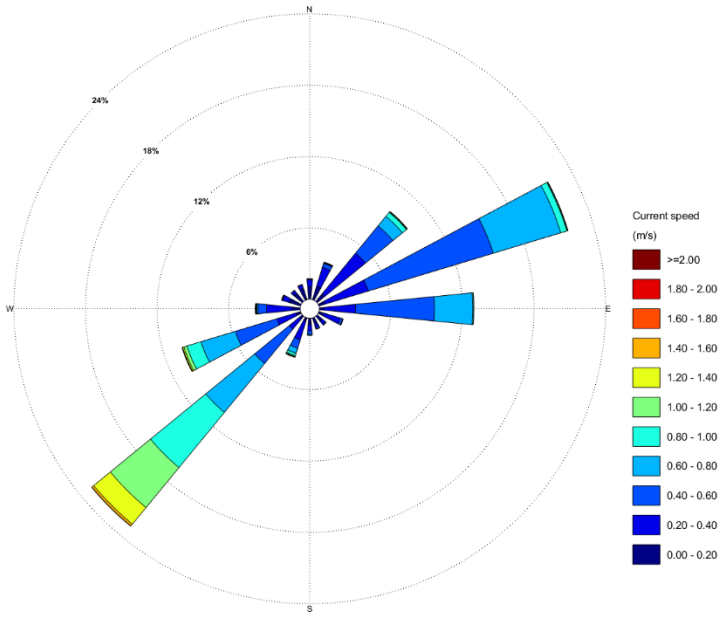

Figure 5-46 Annual depth-averaged current rose plot at C35 for 'existing' scenario. Sectors indicate the direction toward which currents flow.

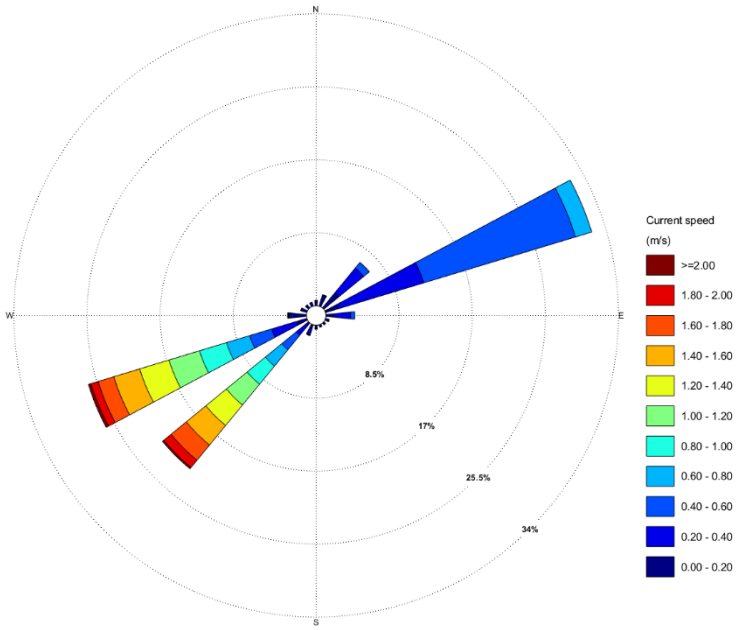

Figure 5-47 Annual depth-averaged current rose plot at C35 for channel 'design' scenario. Sectors indicate the direction toward which currents flow.

5.4 CFSR model – 41 years wind hindcast

A summary of wind speed statistics (*Wspd*) at O1 is provided in Table 5-21.

The annual joint probability distribution of the wind speed and direction are presented in Table 5-22.

Monthly and annual exceedance statistics for wind speed are presented in Table 5-23.

The annual and seasonal non-exceedance persistence probabilities for wind speed at O1 (Table 5-24 to Table 5-29) can be used to estimate the operational uptime for tasks with wind speed limitations of variable duration. For example, at O1 on average in autumn, wind speed are less than 10.0 m/s for durations of 24 hours and greater for 79.04% of the time (Table 5-26).

Wind rose for annual wind speed is presented in Figure 5-48, showing the predominance of winds incoming from the SW sector.

The directional return period values for wave extremes are given in Table 5-30 for 1, 10, 25, 50 and 100-year return periods (see Appendix A for details on the extreme value analysis). Note an adjustment factor of 1.16 is considered for wind extreme value analysis (see Section 4.1.1).

Note the climate change projections for New Zealand suggest that westerly flow will increase in frequency in spring (up to 20%) and winter (up to 70%) and to decrease in summer and autumn (up to 20%) (Mullan et al., 2011; Field, 2014; Rouse et al., 2017). Furthermore, projected increase in conditions conducive to storm development are estimated to reach 3%–6% by 2070–2100 relative to 1970–2000 (Mullan et al., 2011; Field, 2014; Rouse et al., 2017). A 2.4% averaged increase in the maximum wind speed, considering the period 1961-2100 relative to 1961-2000, is suggested by Mullan et al. (2011, Table 8) and is indicated as a reference in Table 5-31.

Table 5-21 Annual and monthly wind speed statistics at O1 for 'existing' scenario.

Period (01 Jan 1980 – 31 Dec 2020)	Wind speed statistics [1]															
	Wind speed (m/s)				Exceedance percentile for wind speed (m/s)											Main [2] Direction(s)
	min	max	mean	std	p1	p5	p10	p50	p70	p75	p80	p90	p95	p98	p99	
January	0.01	21.92	6.04	2.96	0.73	1.71	2.43	5.72	7.33	7.83	8.44	10.06	11.40	13.09	14.05	SW
February	0.07	18.63	5.68	2.81	0.70	1.60	2.23	5.43	6.92	7.39	7.88	9.37	10.76	12.53	13.55	SW
March	0.03	25.02	6.08	2.95	0.74	1.68	2.43	5.86	7.43	7.89	8.44	9.95	11.36	13.06	14.17	S SW
April	0.00	22.09	6.28	3.09	0.79	1.78	2.51	5.97	7.74	8.28	8.85	10.47	11.78	13.40	14.58	SW
May	0.02	21.56	7.06	3.37	0.97	2.05	2.86	6.74	8.70	9.30	10.02	11.82	13.13	14.49	15.23	SW W
June	0.08	21.02	7.50	3.38	1.05	2.34	3.22	7.25	9.23	9.77	10.39	12.11	13.44	14.96	15.91	SW W
July	0.07	21.82	7.52	3.59	0.98	2.16	3.09	7.12	9.24	9.88	10.60	12.47	14.04	15.66	16.67	SW W
August	0.05	21.27	7.27	3.31	1.01	2.19	3.06	7.04	8.95	9.51	10.15	11.72	13.03	14.46	15.40	SW W
September	0.05	24.92	7.28	3.30	1.02	2.28	3.15	7.03	8.88	9.43	10.05	11.72	13.20	14.74	15.67	SW W
October	0.06	23.47	7.20	3.20	1.03	2.24	3.12	7.04	8.74	9.24	9.81	11.31	12.73	14.65	15.68	SW W
November	0.03	21.36	6.74	3.03	0.91	1.96	2.81	6.65	8.32	8.78	9.32	10.76	11.97	13.32	14.17	SW W
December	0.05	18.31	6.15	2.84	0.80	1.78	2.54	5.98	7.55	8.01	8.53	9.91	11.10	12.57	13.52	SW W
Winter	0.05	21.82	7.43	3.43	1.01	2.23	3.12	7.13	9.14	9.71	10.37	12.09	13.48	15.09	16.06	SW W
Spring	0.03	24.92	7.08	3.19	0.98	2.14	3.02	6.91	8.64	9.14	9.72	11.26	12.66	14.27	15.31	SW W
Summer	0.01	21.92	5.97	2.88	0.74	1.69	2.40	5.72	7.28	7.75	8.29	9.82	11.11	12.73	13.74	SW
Autumn	0.00	25.02	6.48	3.17	0.82	1.83	2.59	6.18	7.94	8.47	9.08	10.82	12.25	13.81	14.84	SW
All	0.00	25.02	6.74	3.22	0.87	1.94	2.74	6.45	8.26	8.80	9.42	11.11	12.54	14.16	15.22	SW W

Notes: (1) All statistics derived from hindcast wind data for the period 01 January 1980 to 31 December 2020.

(2) Main directions are those with greater than 15% occurrence and represent incoming wind directions.

Table 5-22 Annual joint probability distribution (in %) of wind speed and direction at O1.

Wspd (m/s)	Mean wave direction at peak energy (degree True North, coming from)									
	337.5-22.5	22.5-67.5	67.5-112.5	112.5-157.5	157.5-202.5	202.5-247.5	247.5-292.5	292.5-337.5	Total	Exceed%
0-2	0.58	0.67	0.70	0.71	0.72	0.73	0.61	0.58	5.30	100.00
2-4	1.65	1.96	1.90	1.76	2.55	2.67	1.95	1.47	15.91	94.70
4-6	2.31	2.81	2.35	1.46	3.41	5.20	3.35	2.36	23.25	78.80
6-8	2.09	2.66	1.93	1.16	2.67	6.08	3.73	2.69	23.01	55.54
8-10	1.41	1.71	1.13	0.75	1.54	4.98	2.94	2.10	16.56	32.53
10-12	0.74	0.93	0.63	0.35	0.76	2.74	2.03	1.25	9.43	15.98
12-14	0.26	0.42	0.33	0.14	0.28	1.24	1.11	0.58	4.36	6.55
14-16	0.07	0.16	0.16	0.04	0.09	0.48	0.46	0.17	1.63	2.19
16-18	0.02	0.04	0.06	0.02	0.04	0.12	0.11	0.04	0.45	0.56
18-20	0.01	*	0.02	*	0.01	0.03	0.03	0.01	0.11	0.13
20-22	*	*	*	*	*	0.01	*	*	0.01	0.02
22-24	*	-	-	*	*	*	-	*		
24-26	-	-	-	-	*	*	-	-		
Total	9.14	11.36	9.21	6.39	12.07	24.28	16.32	11.25	100.00	

*Notes: * represents less than 0.005%.*

Table 5-23 Monthly and annual wind speed exceedance probabilities (%) at O1.

Wspd (m/s)	Exceedance (%)												
	Jan	Feb	Mar	Apr	May	Jun	Jul	Aug	Sep	Oct	Nov	Dec	annual
>0	100.00	100.00	100.00	100.00	100.00	100.00	100.00	100.00	100.00	100.00	100.00	100.00	100.00
>2	93.24	92.11	93.12	93.79	95.24	96.45	95.71	95.91	96.14	96.02	94.73	93.80	94.70
>4	73.59	70.46	73.75	74.65	80.05	84.47	83.13	82.77	83.43	83.19	79.85	75.72	78.80
>6	46.34	41.95	48.11	49.55	58.27	63.92	62.89	62.07	62.14	62.89	57.72	49.78	55.54
>8	23.56	18.97	23.99	27.47	36.70	42.01	41.03	39.71	39.15	38.36	33.55	25.04	32.53
>10	10.27	7.55	9.76	12.36	20.11	23.09	24.04	21.17	20.40	18.39	14.59	9.46	15.98
>12	3.54	2.60	3.46	4.39	9.13	10.44	12.13	8.65	8.87	7.28	4.89	2.94	6.55
>14	1.04	0.75	1.09	1.38	2.80	3.66	5.07	2.68	3.18	2.70	1.16	0.69	2.19
>16	0.29	0.18	0.32	0.37	0.51	0.91	1.59	0.61	0.76	0.79	0.21	0.11	0.56
>18	0.07	0.02	0.10	0.14	0.06	0.19	0.40	0.14	0.19	0.16	0.02	0.00	0.13
>20	0.02	0.00	0.04	0.03	0.03	0.01	0.05	0.02	0.03	0.02	0.01	0.00	0.02
>22	0.00	0.00	0.01	0.00	0.00	0.00	0.00	0.00	0.01	0.01	0.00	0.00	0.00
>24	0.00	0.00	0.00	0.00	0.00	0.00	0.00	0.00	0.01	0.00	0.00	0.00	0.00

Table 5-24 Annual and seasonal non-exceedance persistence (%) for wind speed below 6.0 m/s at O1.

Wspd (m/s)	Duration (hours)											
	3	6	9	12	15	18	21	24	30	36	42	48
Summer	51.16	48.81	46.35	43.78	41.09	37.80	35.37	33.57	30.12	26.83	23.78	20.59
Autumn	45.44	43.12	40.66	38.90	36.94	34.89	32.96	30.77	27.52	24.72	22.04	19.15
Winter	34.27	31.77	29.79	27.53	25.47	23.73	21.98	20.37	17.08	14.39	11.64	9.53
Spring	36.29	33.81	31.56	29.54	27.48	25.51	23.65	21.62	19.14	15.79	13.88	12.06
Annual	41.78	39.39	37.13	35.00	32.81	30.58	28.57	26.68	23.57	20.57	17.94	15.53

Table 5-25 Annual and seasonal non-exceedance persistence (%) for wind speed below 8.0 m/s at O1.

Wspd (m/s)	Duration (hours)											
	3	6	9	12	15	18	21	24	30	36	42	48
Summer	75.69	74.34	73.06	71.86	70.50	69.20	67.98	66.85	64.76	62.07	59.94	57.42
Autumn	68.69	67.01	65.41	63.82	62.37	61.09	59.82	58.72	56.55	53.66	50.84	48.35
Winter	56.65	54.82	53.13	51.49	49.76	47.85	45.97	44.06	40.58	38.11	34.19	31.12
Spring	60.66	58.64	56.49	54.75	52.82	51.26	49.51	47.84	44.58	41.11	38.14	35.39
Annual	65.40	63.70	62.06	60.58	58.99	57.52	56.03	54.56	51.83	49.00	46.16	43.42

Table 5-26 Annual and seasonal non-exceedance persistence (%) for wind speed below 10.0 m/s at O1.

Wspd (m/s)	Duration (hours)											
	3	6	9	12	15	18	21	24	30	36	42	48
Summer	90.09	89.50	88.82	88.27	87.81	87.14	86.62	86.17	85.23	84.31	83.14	81.90
Autumn	84.62	83.73	83.00	82.24	81.55	80.68	79.89	79.04	77.94	76.57	75.05	73.55
Winter	75.40	74.11	72.77	71.86	70.87	69.73	68.73	67.61	64.96	62.92	59.07	56.53
Spring	80.85	79.71	78.58	77.23	76.18	75.06	73.78	72.84	70.36	68.04	65.61	63.28
Annual	82.71	81.75	80.80	79.94	79.17	78.30	77.43	76.69	74.96	73.32	71.20	69.46

Table 5-27 Annual and seasonal non-exceedance persistence (%) for wind speed below 12.0 m/s at O1.

Wspd (m/s)	Duration (hours)											
	3	6	9	12	15	18	21	24	30	36	42	48
Summer	96.70	96.56	96.43	96.23	96.06	95.94	95.76	95.60	95.34	95.07	94.56	93.99
Autumn	93.68	93.20	92.80	92.47	92.04	91.53	91.20	90.96	90.09	89.38	88.70	87.78
Winter	88.43	87.82	87.02	86.36	85.73	85.21	84.61	84.00	82.72	81.16	79.85	78.67
Spring	92.36	91.89	91.49	90.99	90.54	90.13	89.59	89.16	87.97	86.46	85.19	83.54
Annual	92.78	92.36	91.94	91.54	91.14	90.76	90.37	90.08	89.22	88.31	87.44	86.51

Table 5-28 Annual and seasonal non-exceedance persistence (%) for wind speed below 14.0 m/s at O1.

Wspd (m/s)	Duration (hours)											
	3	6	9	12	15	18	21	24	30	36	42	48
Summer	99.08	99.04	99.03	98.99	98.85	98.83	98.79	98.76	98.60	98.44	98.30	98.14
Autumn	98.00	97.86	97.78	97.61	97.46	97.34	97.21	97.07	96.70	96.42	96.07	95.87
Winter	95.75	95.43	95.16	94.88	94.50	94.25	94.18	93.94	93.57	93.22	92.68	92.22
Spring	97.37	97.25	97.09	96.95	96.87	96.71	96.54	96.39	96.02	95.48	95.17	94.74
Annual	97.55	97.40	97.27	97.12	96.94	96.81	96.71	96.58	96.32	96.05	95.75	95.47

Table 5-29 Annual and seasonal non-exceedance persistence (%) for wind speed below 16.0 m/s at O1.

Wspd (m/s)	Duration (hours)											
	3	6	9	12	15	18	21	24	30	36	42	48
Summer	99.79	99.78	99.78	99.78	99.78	99.78	99.78	99.78	99.78	99.75	99.70	99.65
Autumn	99.57	99.55	99.54	99.51	99.48	99.46	99.46	99.43	99.36	99.33	99.19	99.14
Winter	98.84	98.73	98.69	98.52	98.44	98.38	98.33	98.28	98.10	97.91	97.72	97.57
Spring	99.36	99.32	99.30	99.30	99.29	99.18	99.14	99.11	99.05	99.05	98.91	98.81
Annual	99.39	99.35	99.33	99.29	99.26	99.22	99.19	99.17	99.09	99.07	98.95	98.89

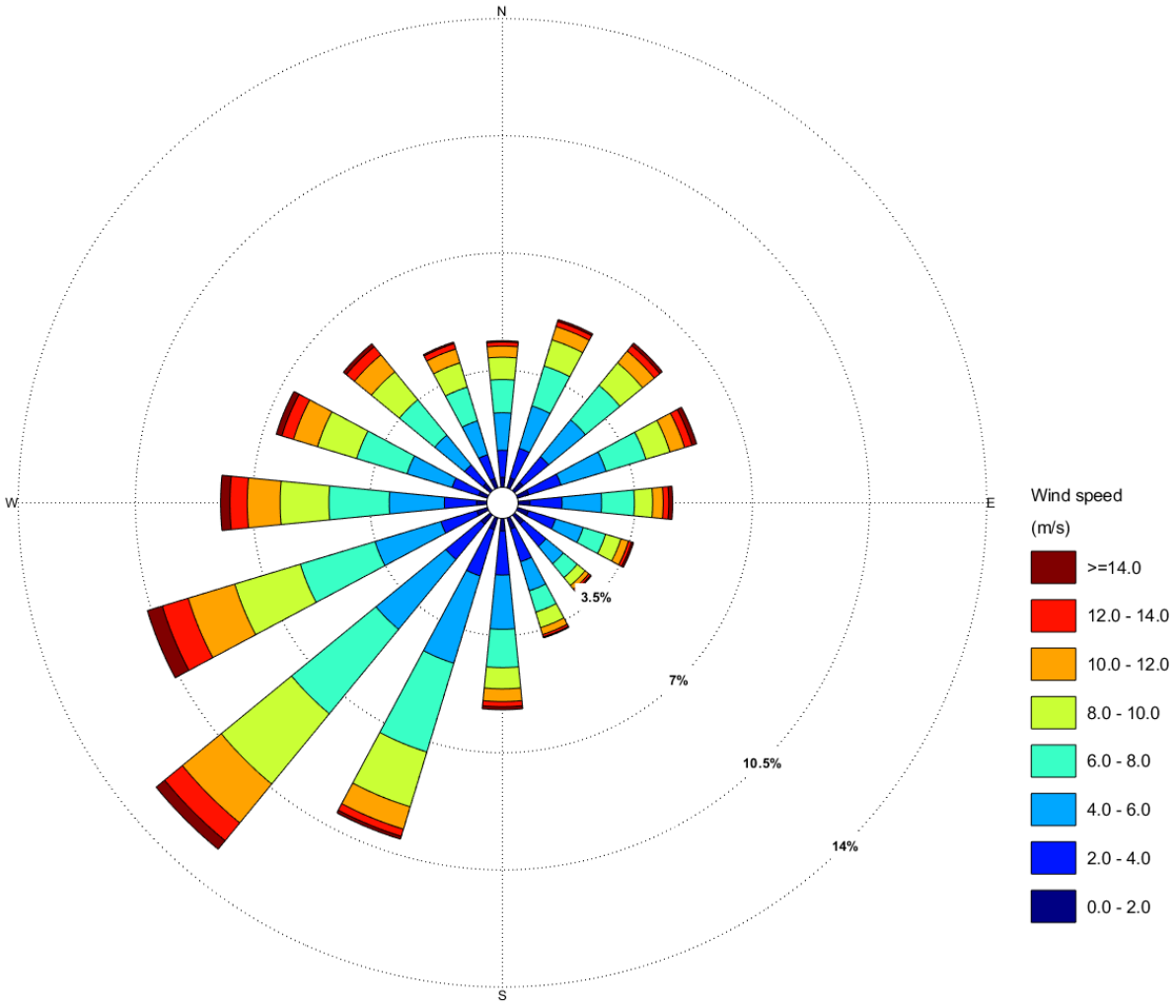

Figure 5-48 Annual wind rose at O1 given in 22.5-degree bins. Sectors indicate the direction from which wind comes from.

Table 5-30 Omni-directional extreme wind speed at O1.

ARI (years)	1	10	25	50	100
60-min wind speed	21.88	26.15	27.80	29.03	30.24
10-min wind	23.33	27.97	29.75	31.09	32.41
1-min wind speed	25.20	30.30	32.27	33.74	35.19
3-s wind gust	27.63	33.34	35.54	37.18	38.81

Table 5-31 Omni-directional extreme wind speed at O1 adjusted for climate change projection, i.e. + 2.4%, based on Mullan et al. (2011).

ARI (years)	1	10	25	50	100
60-min wind speed	22.41	26.78	28.47	29.73	30.97
10-min wind	23.89	28.64	30.46	31.84	33.19
1-min wind speed	25.80	31.03	33.04	34.55	36.03
3-s wind gust	28.29	34.14	36.39	38.07	39.74

5.5 Water levels

The representative site for water level statistics was chosen in front of the harbour entrance (O5) as the available ROMS Moana Backbone hydrodynamic model resolution is too coarse to resolve the inner harbour.

A summary of the tidal elevation statistics at O5 from the modelled tidal constituents is presented in Table 5-32. Also provided are the standard tidal levels for Onehunga from Land Information New Zealand (LINZ)[3], calculated from measured tide gauge data.

Extremes of still water elevation (combined tide+surge) are given in Table 5-33 for 1, 10, 25, 50 and 100-year return periods. Because significant differences were noted between the offshore modelled standard tidal levels and inner harbour LINZ measured levels, a 30% and 40% increase in amplitude of high and low tide, respectively, were applied to the modelled tidal data. The extreme value analysis was repeated with these increased tidal levels and the results are presented in Table 5-34 .

[3] https://www.linz.govt.nz/guidance/marine-information/tide-prediction-guidance/standard-port-tidal-levels

Table 5-32 Tidal water level parameters in front of the harbour entrance (as resolved from the modelled tidal constituents), and standard water levels for Onehunga Port Manukau (provided by LINZ).

Parameter	Description	Elevation (m MSL) at o5 (Moana model)	Elevation (m MSL) At OnehungaPort (LINZ data)
HAT	Highest Astronomical Tide	1.66	2.11
MHWS	Mean High Water Springs (M2+S2)	1.33	1.74
MHWN	Mean High Water Neaps (M2-S2)	0.78	0.89
MLWN	Mean Low Water Neaps (-M2+S2)	-0.78	-0.97
MLWS	Mean Low Water Springs (-M2-S2)	-1.33	-1.86
LAT	Lowest Astronomical Tide	-1.66	-2.31

Table 5-33 Extreme water level in front of the harbour entrance (Moana dataset).

ARI (year)	Maximum still water elevation (combined modelled tide+surge) (m MSL)	Minimum still water elevation (combined modelled tide+surge) (m MSL)
1	1.84	-1.80
10	2.06	-1.99
25	2.14	-2.06
50	2.20	-2.11
100	2.25	-2.16

Table 5-34 Extreme water level in front of the harbour entrance (adjusted to LINZ standard tidal water levels, i.e. +30% and +40% for high and low tide, respectively).

ARI (year)	Maximum still water elevation (combined modelled tide+surge) (m MSL)	Minimum still water elevation (combined modelled tide+surge) (m MSL)
1	2.31	-2.44
10	2.56	-2.67
25	2.65	-2.76
50	2.72	-2.83
100	2.78	-2.89

5.6 South Channel Assessment

Early in the project, several key stakeholders' consultations (e.g. vessel pilots) and initial dredging volume estimates indicated that the natural South West channel is the preferred alignment for the proposed concept navigation channel. While all the modelling presented in this report is undertaken with the proposed South West navigation channel, a high-level assessment of an alternative concept navigation channel within the natural South Channel was undertaken. Further refinement of the Delft FM flexible mesh was required to accurately incorporate this proposed channel design. The South Channel bathymetry which was the existing 2023 bathymetry with the addition of the South Channel concept navigation Channel dredged design. The model mesh and bathymetry are displayed in Figure 5-49. The South Channel design bathymetry was also incorporated into the existing SWAN grids.

The fully coupled wave and hydrodynamic model was run for a month-long simulation (January 2012).

The modelled depth averaged currents for the South Channel simulation for the peak flood and peak ebb current vectors during a spring tide within Manukau Harbour are presented in Figure 5-50 to Figure 5-53. The difference between the modelled depth averaged currents during the 'existing' and design South Channel simulation (existing minus design) at various stages of the tidal cycle during a spring tide within Manukau Harbour are presented in Figure 5-54 to Figure 5-56. Red (positive speeds) indicates and area of increased current speeds and blue (negative speeds) indicates a decrease in current speeds from 'existing' conditions. Note that as the mesh are not the same between the simulations, model results were interpolated onto a regular grid for comparison.

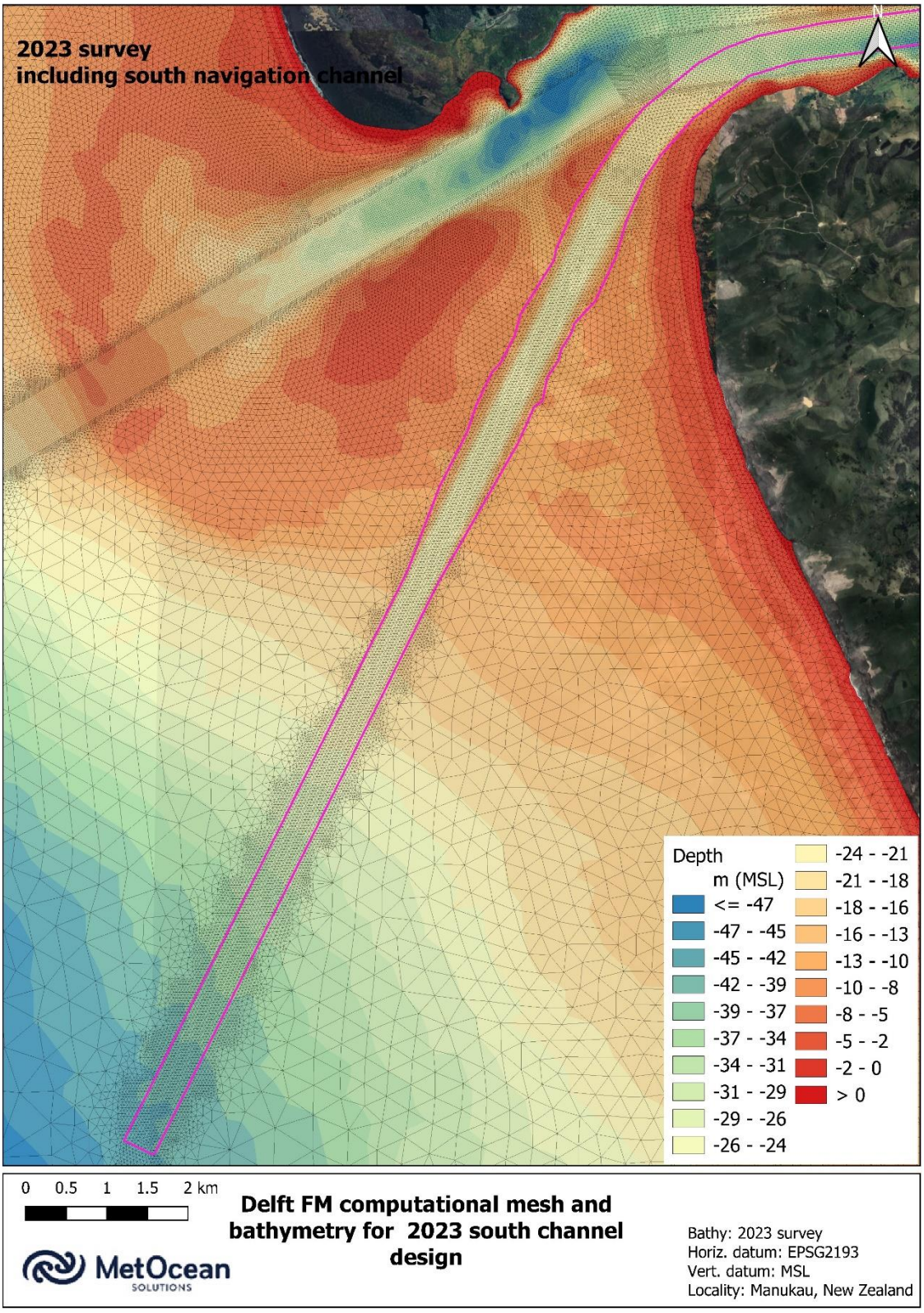

Figure 5-49 Bathymetry used in the assessment of the South Channel model simulations within the entrance channel and bar at Manukau Harbour where the pink is the South Channel outline.

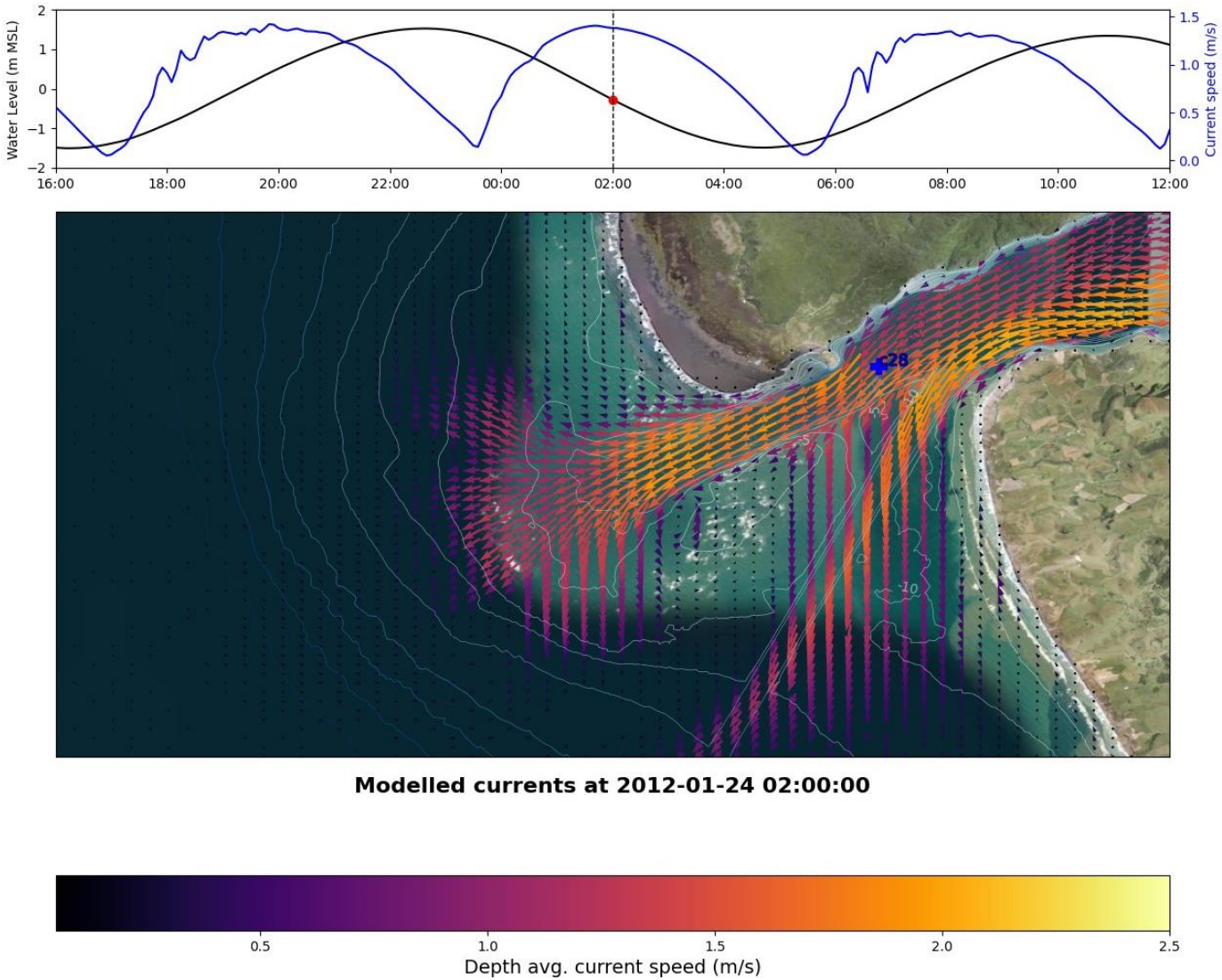

Figure 5-50 Modelled spring tidal current vectors for the design South Channel simulation over Manukau bar at peak ebb tide. The top panel presents the water level and depth averaged currents timeseries at the location shown as a blue cross on the map.

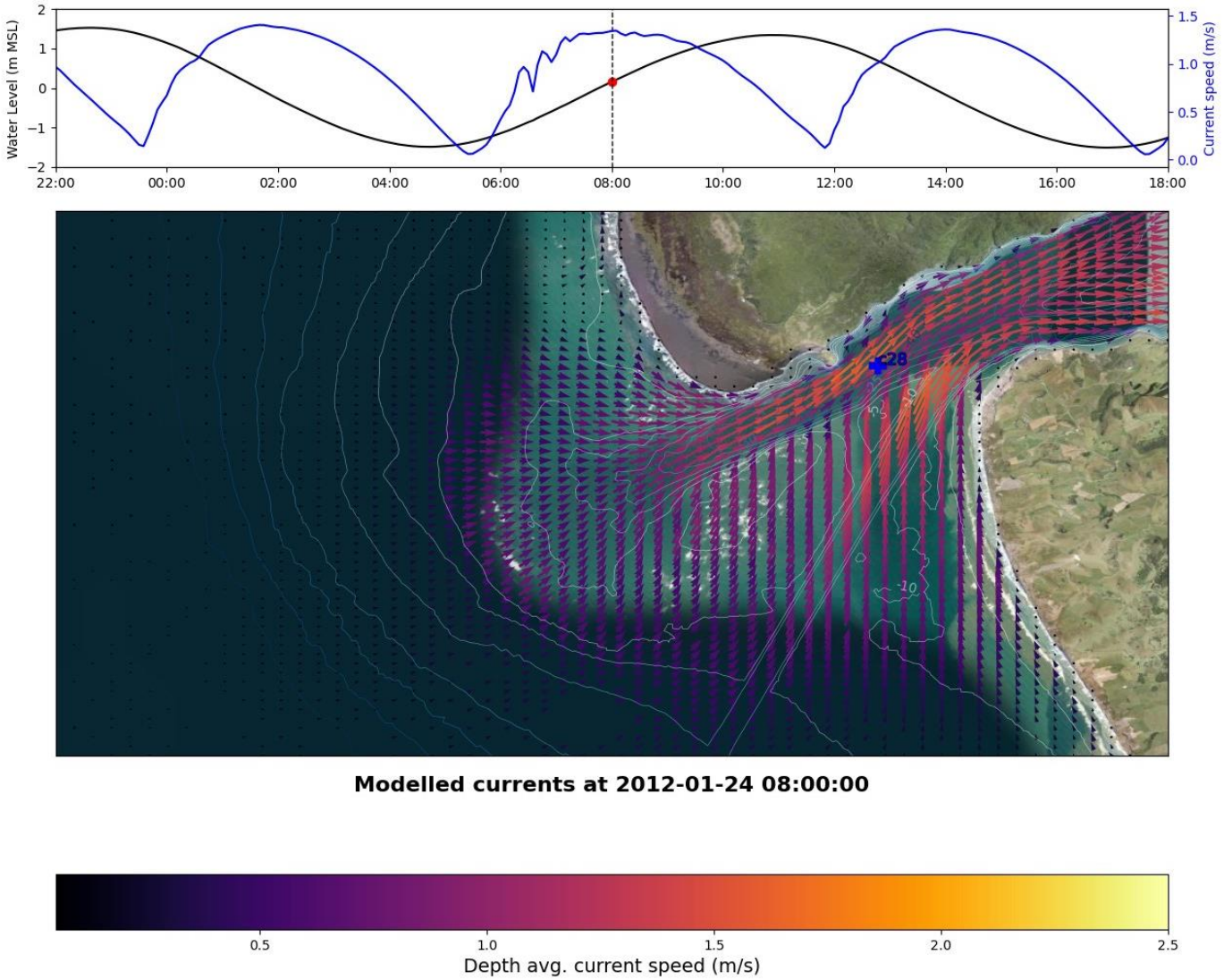

Figure 5-51 Modelled spring tidal current vectors for the design South Channel simulation over Manukau bar at peak flood tide. The top panel presents the water level and depth averaged currents timeseries at the location shown as a blue cross on the map.

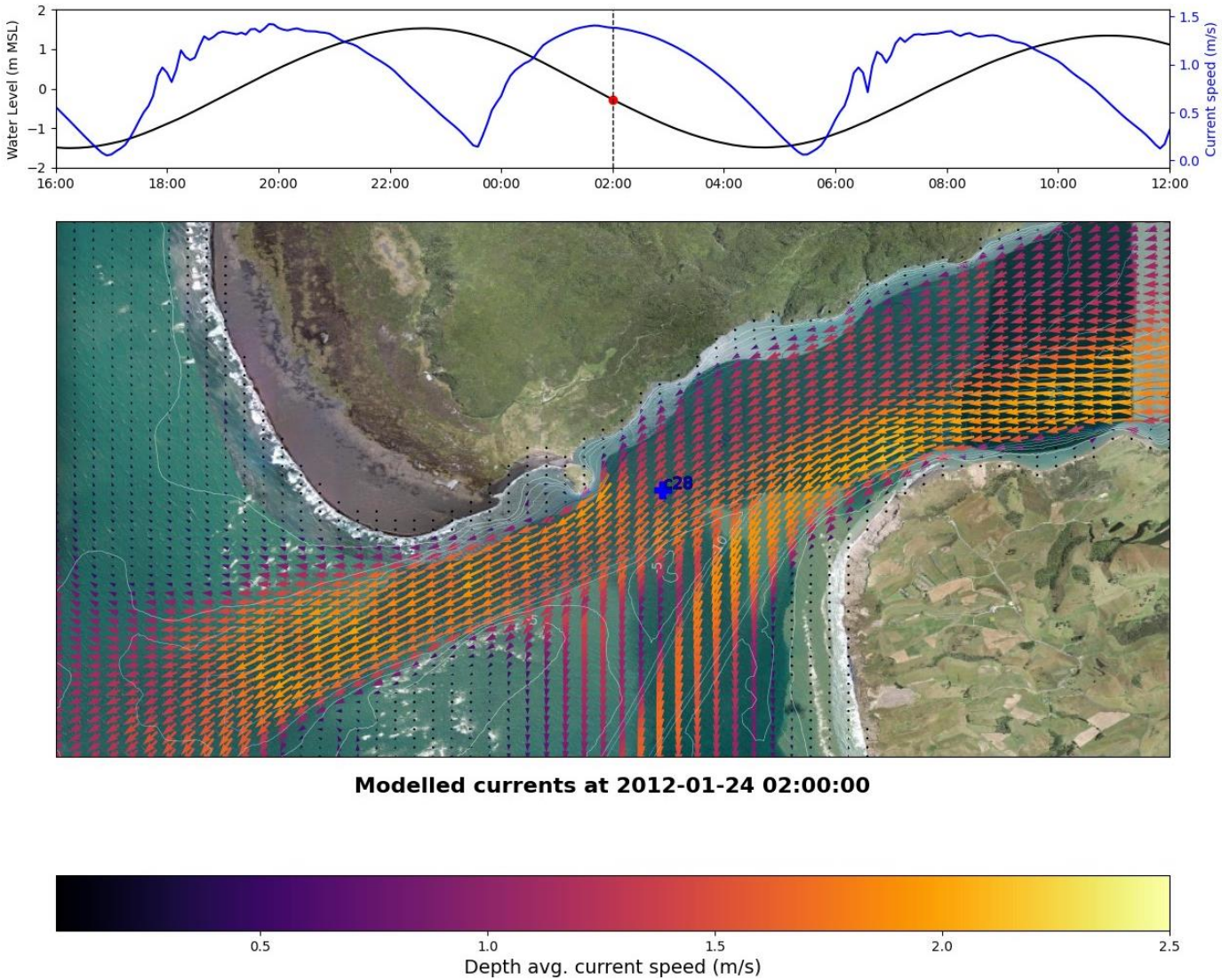

Figure 5-52 Modelled spring tidal current vectors for the design South Channel simulation over Manukau entrance at peak ebb tide. The top panel presents the water level and depth averaged currents timeseries at the location shown as a blue cross on the map.

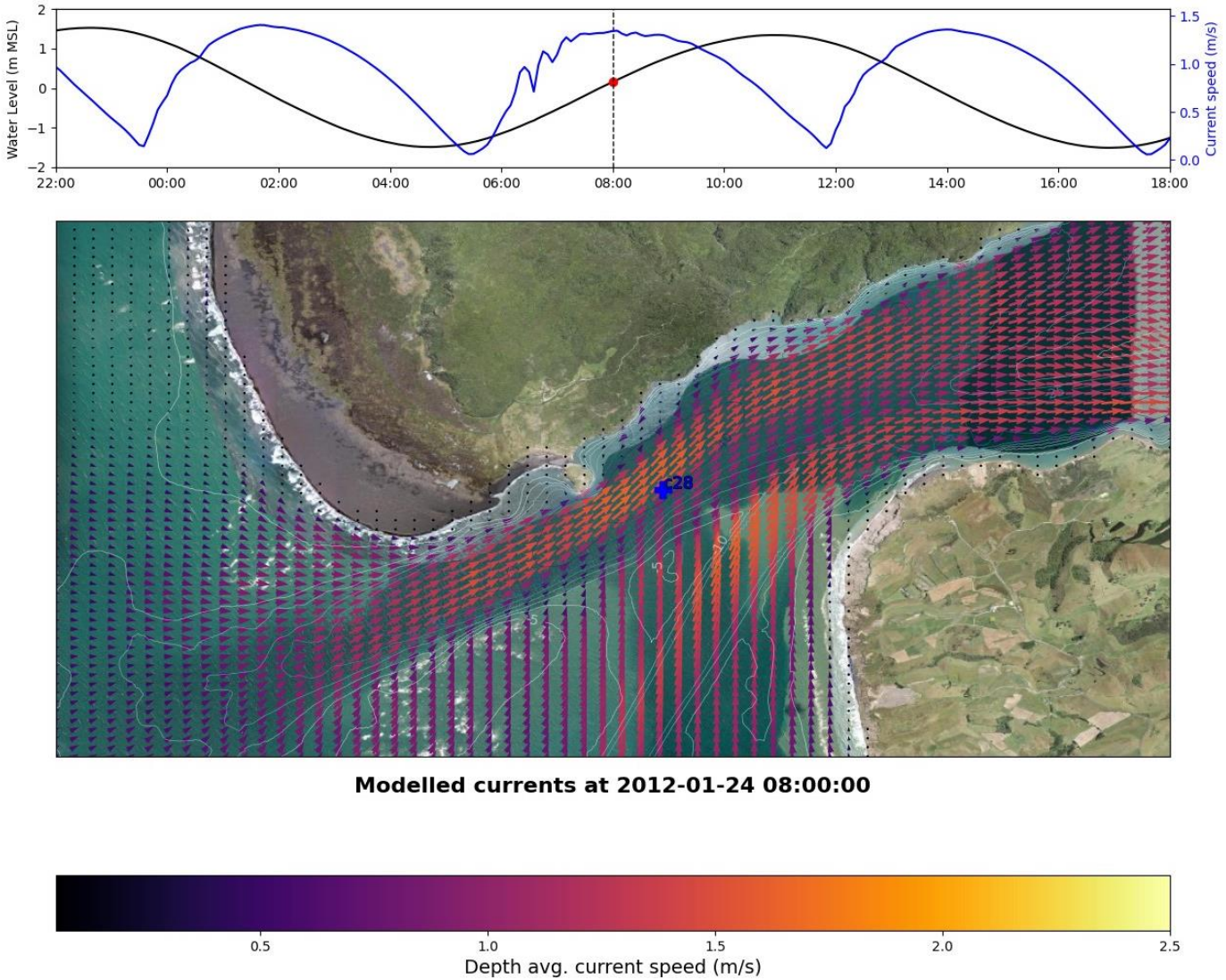

Figure 5-53 Modelled spring tidal current vectors for the design South Channel simulation over Manukau entrance at peak flood tide. The top panel presents the water level and depth averaged currents timeseries at the location shown as a blue cross on the map.

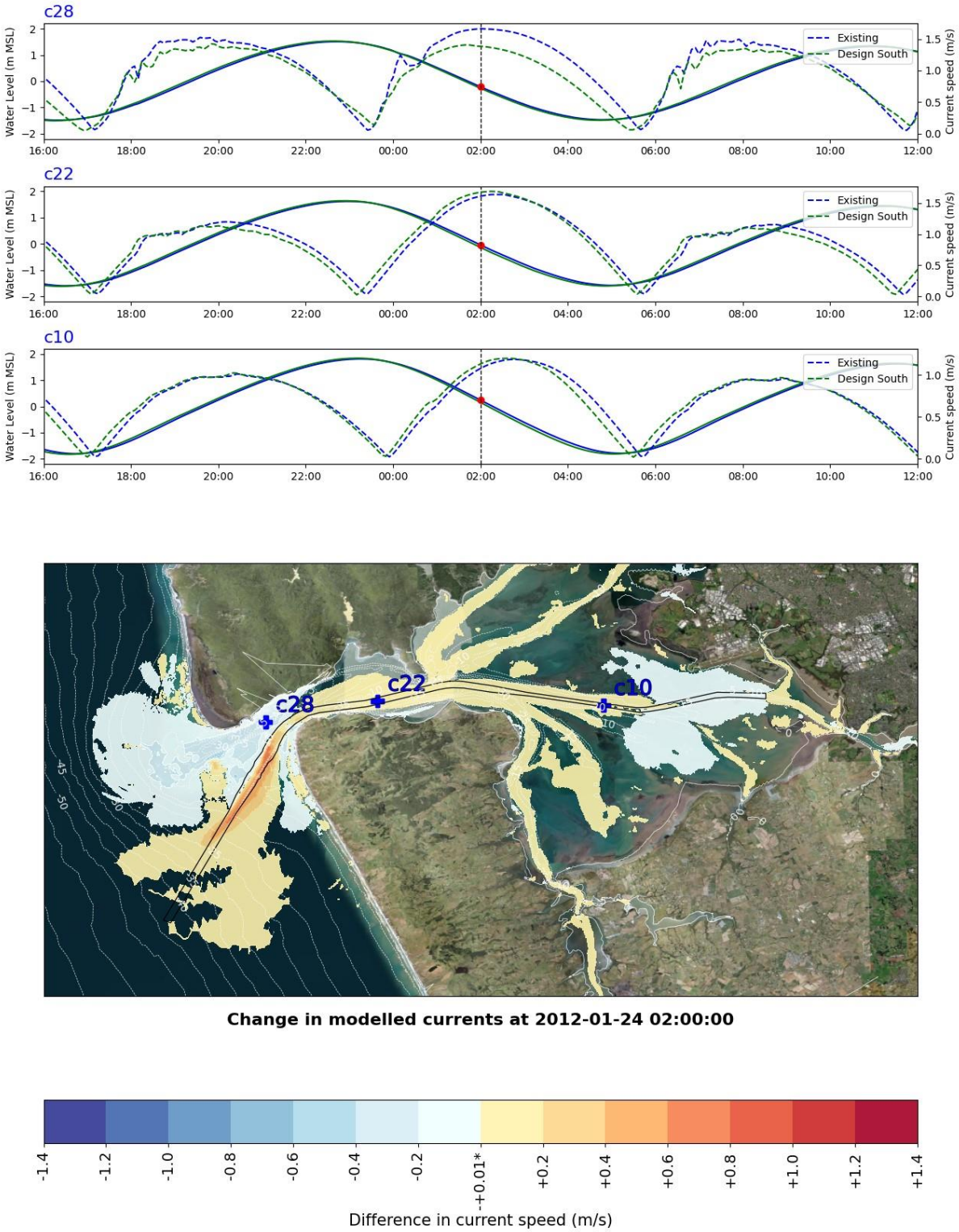

Figure 5-54 Difference in modelled spring tidal current magnitudes between the 'existing' and design South Channel simulation within Manukau Harbour during a peak ebb tide. Red indicates and area of increased current speeds and blue indicates an area of decreased current speeds from 'existing' conditions. The top panel presents the water level and depth averaged currents timeseries at the locations shown as blue crosses on the map.

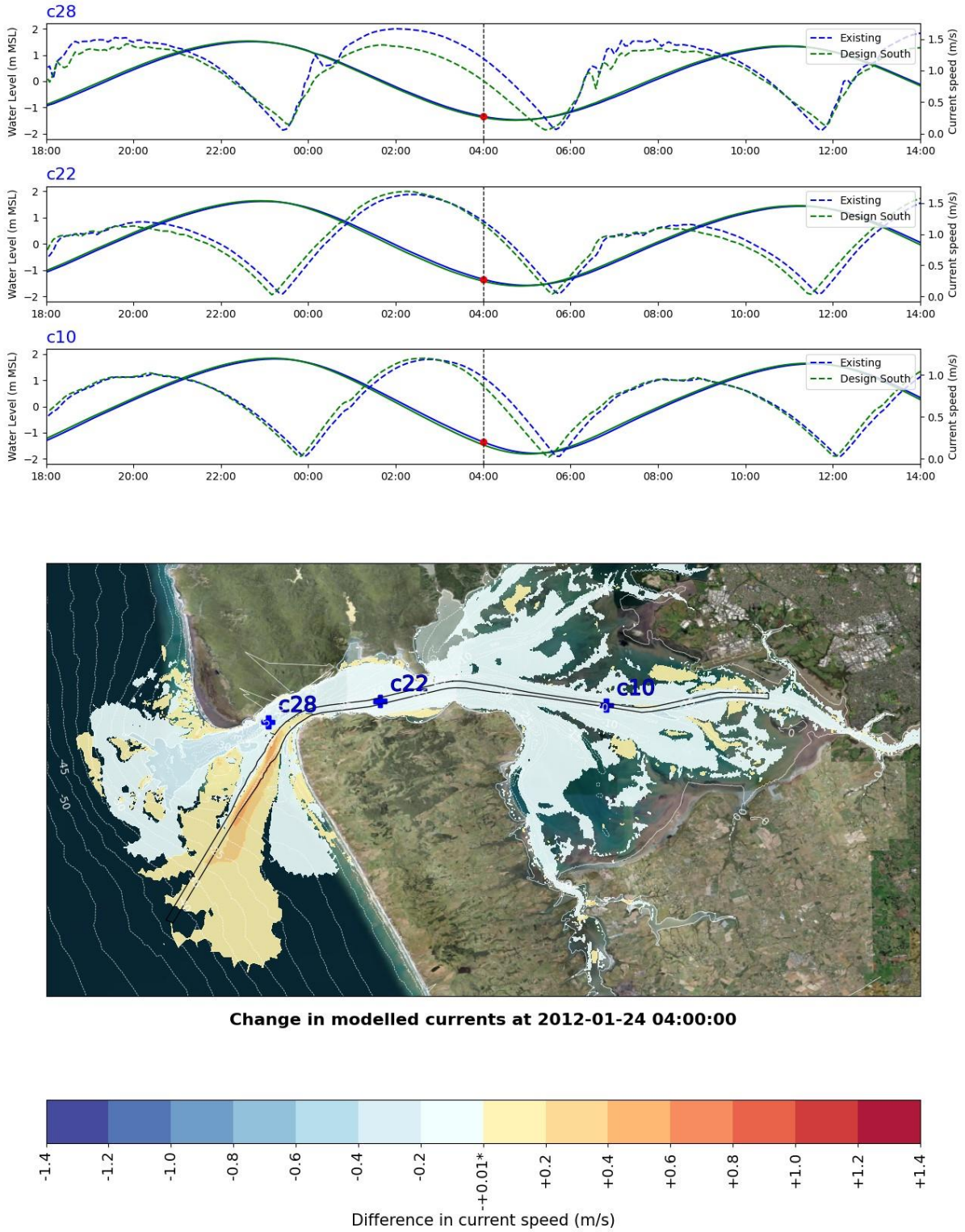

Figure 5-55 Difference in modelled spring tidal current magnitudes between the 'existing' and design South Channel simulation within Manukau Harbour during an ebb tide. Red indicates and area of increased current speeds and blue indicates an area of decreased current speeds from 'existing' conditions. The top panel presents the water level and depth averaged currents timeseries at the locations shown as blue crosses on the map.

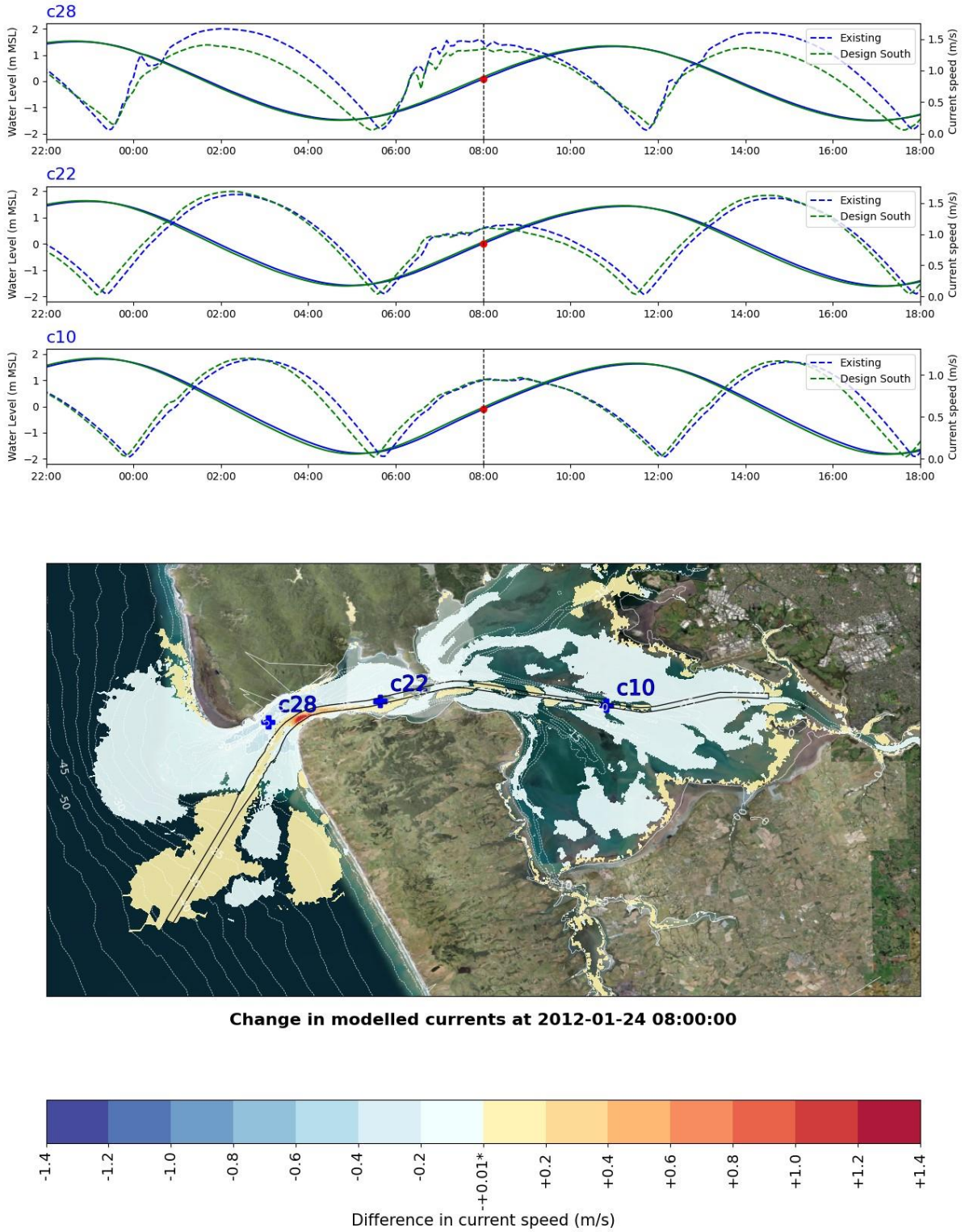

Figure 5-56 Difference in modelled spring tidal current magnitudes between the 'existing' and design South Channel simulation within Manukau Harbour during a peak ebb tide. Red indicates and area of increased current speeds and blue indicates an area of decreased current speeds from 'existing' conditions. The top panel presents the water level and depth averaged currents timeseries at the locations shown as blue crosses on the map.

6.References

Ardhuin, F., Rogers,E., Babanin, A. V., Filipot, J. F., Magne, R., Roland, A., Van Der Westhuysen, A., Queffeulou, P., Lefevre, J. M., Aouf, L., & Collard, F. (2010). Semiempirical dissipation source functions for ocean waves. Part I: Definition, calibration, and validation. *Journal of Physical Oceanography*, *40*(9), 1917–1941.

Battjes, J. A., & Janssen, J. P. F. M. (1978). Energy loss and set-up due to breaking random waves. *Coastal Engineering Proceedings*, *1*(16). https://icce-ojs-tamu.tdl.org/icce/index.php/icce/article/view/3294

Booij, N., Ris, R. C., & Holthuijsen, L. H. (1999). A third-generation wave model for coastal regions: 1. Model description and validation. *Journal of Geophysical Research: Oceans*, *104*(C4), 7649–7666.

Collins, J. (1972). Prediction of Shallow Water Spectra. *Journal of Geophysical Research*, *77*(15), 2693–2707.

Deltares. (2020a). *D-Flow Flexible Mesh, Computational Cores and User Interface. User Manual* (Version: 0.9.1).

Deltares. (2020b). *D-Flow Flexible Mesh, Technical Reference Manual* (Version: 1.1.0).

Deltares. (2020c). *D-Wave, Simulation of short-crested waves with SWAN. User Manual* (Version: 1.2).

Deltares. (2022). *Delft3D FM Suite 2D3D. D-Morphology. User Manual* (Version: 2023).

Dingemans, M., W. (1987). *Verification of numerical wave propagation models with laboratory measurements: HISWA verification in the directional wave basin* (Hydraulic Engineering Reports). Deltares (WL). https://repository.tudelft.nl/islandora/object/uuid:ee1211e7-3b12-430c-99e9-b0bf2db295a8?collection=research

Egbert, G. D., & Erofeeva, S. Y. (2002). Efficient inverse modelling of barotropic ocean tides. *Journal of Atmospheric and Oceanic Technology*, *19*(2), 183–204.

Field, C. B. (2014). *Climate change 2014–Impacts, adaptation and vulnerability: Regional aspects*. Cambridge University Press.

Forristall, G. Z. (1978). On the statistical distribution of wave heights in a storm. *Journal of Geophysical Research: Oceans*, *83*(C5), 2353–2358.

Forristall, G. Z. (2000). Wave Crest Distributions: Observations and Second-Order Theory. *Journal of Physical Oceanography*, *30*(8).

Hemer, M. A., Fan, Y., Mori, N., Semedo, A., & Wang, X. L. (2013). Projected changes in wave climate from a multi-model ensemble. *Nature Climate Change*, *3*(5), 471–476.

Holthuijsen, L. H. (2007). *Waves in oceanic and coastal waters*. Cambridge University Press.

Hoogeveen, S. J. W. (2020). *Mangrove dynamics in the Richmond River's estuary*. Faculty of Engineering Technology, University of Twente.

HSE. (2002). *Environmental considerations. Offshore technology report 2001/010* (p. 82). Prepared by Bomel Ltd for the Health and Safety Executive.

ISO. (2015). 19901-1:2015(en) Petroleum and natural gas industries—Specific requirements for offshore structures—Part 1: Metocean design and operating conditions. *British Standards Institute*.

Mullan, B., Carey-Smith, T., Griffiths, G., & Sood, A. (2011). Scenarios of storminess and regional wind extremes under climate change. *NIWA Client Report WLF2010-31 Prepared for the Ministry of Agriculture and Forestry*.

Rapizo, H., Babanin, A. V., Provis, D., & Rogers, W. E. (2017). Current-induced dissipation in spectral wave models. *Journal of Geophysical Research: Oceans*, *122*(3), 2205–2225. https://doi.org/10.1002/2016JC012367

Repko, A., Van Gelder, P., Voortman, H. G., & Vrijling, J. K. (2005). Bivariate description of offshore wave conditions with physics-based extreme value statistics. *Applied Ocean Research*, *26*(3–4), 162–170.

Ribal, A., & Young, I. R. (2019). 33 years of globally calibrated wave height and wind speed data based on altimeter observations. *Scientific Data*, *6*(1), 77. https://doi.org/10.1038/s41597-019-0083-9

Ris, R. C., Holthuijsen, L. H., & Booij, N. (1999). A third-generation wave model for coastal regions: 2. Verification. *Journal of Geophysical Research: Oceans*, *104*, 7667–7681.

Rouse, H. L., Bell, R. G., Lundquist, C. J., Blackett, P. E., Hicks, D. M., & King, D. N. (2017). Coastal adaptation to climate change in Aotearoa-New Zealand. *New Zealand Journal of Marine and Freshwater Research*, *51*(2), 183–222.

Saha, S., Moorthi, S., Pan, H.-L., Wu, X., Wang, J., Nadiga, S., Tripp, P., Kistler, R., Woollen, J., Behringer, D., Liu, H., Stokes, D., Grumbine, R., Gayno, G., Wang, J., Hou, Y.-T., Chuang, H.-Y., Juang, H.-M. H., Sela, J., … Goldberg, M. (2010). The NCEP Climate Forecast System

Reanalysis. *Bulletin of the American Meteorological Society*, *91*(8), 1015–1057. https://doi.org/10.1175/2010BAMS3001.1

Tolman, H. L. (1991). A Third-Generation Model for Wind Waves on Slowly Varying, Unsteady, and Inhomogeneous Depths and Currents. *Journal of Physical Oceanography*, *21*(6), 782–797. https://doi.org/10.1175/1520-0485(1991)021<0782:ATGMFW>2.0.CO;2

Tonkin & Taylor Ltd. (2024). *Manukau Harbour Port Feasibility Study: Fieldwork Techincal Working Paper* (TWP02). Report prepared for Ministry of Transport.

Tromans, P., & Vanderschuren, L. (1995, May). *Response Based Design Conditions in the North Sea: Application of a New Method*. https://doi.org/10.4043/7683-MS

Winterstein, S. R., Ude, T. C., Cornell, C. A., Bjerager, P., & Haver, S. (1993). Environmental parameters for extreme response: Inverse FORM with omission factors. *Proc., ICOSSAR-93, Innsbruck*. http://www.rms-group.org/RMS_Papers/pdf/Todd/innsbruck.pdf

Wolanski, E., Mazda, Y., & Ridd, P. (1992). Mangrove hydrodynamics. In *Coastal and estuarine studies: Tropical mangrove ecosystems* (Vol. 41). American Geophysical Union.

Appendix A: Extreme value analysis

Return period values (RPVs) have been calculated from the hindcast time series of wave, wind and water level.

A *Peaks over Threshold* (POT) sampling method is used for event selection, applying the 95th percentile exceedance levels as the threshold with a 24-hour window. For wind and wave extreme value analysis (EVA), the 3-parameter Weibull distribution were applied, with Maximum Likelihood Method (MLM) used to find the best-fit of the sampled events to the model distribution.

Bivariate return period values were calculated for significant wave height and peak period. The method of Repko et al. (2005) was employed, which considers the distribution of H_s and wave steepness, s. A joint probability distribution function (PDF) is calculated by multiplying marginal distributions of H_s and s (thus assuming they are independent), after which the PDF is transformed back into H_s/T_p space. In addition, a minimum wave steepness threshold of 0.005 is applied to exclude events with very long wave periods, which are not believed to be representative of extreme conditions.

The marginal distributions for H_s and s are estimated by fitting the POT values to a Weibull distribution using the maximum likelihood method (as implemented in the WAFO toolbox). Contours of the return period values were constructed from the joint PDF using the Inverse FORM method (Winterstein et al., 1993) at the return year levels.

The methods used to estimate extreme maximum individual wave height (H_{max}) and maximum wave crest (C_{max}) account for the long-term uncertainty in the severity of the environment and the short-term uncertainty in the severity of the maximum wave of a given sea state, as suggested by Tromans and Vanderschuren (1995) and recommended by ISO (2015). The most probable value of the extreme individual wave height (H_{mp}) of each storm is obtained from the product of the Foristall distributions of individual wave height in each hindcast interval within the storm duration (Forristall, 1978; ISO, 2015). The same technique is used for the most probable value of the extreme individual wave crest (C_{mp}) but using the Weibull distribution with scale and shape parameters dependent on the wave steepness and the Ursell number (ISO, 2015; Forristall, 2000). Note that the resulting short-term distributions for each storm are dependent on the number of intervals with H_s values near the region of maximum peak H_s. The uncertainty in the height and crest of the maximum wave of any storm is represented as a short-term probability distribution conditional on H_{mp} and C_{mp}, respectively (Tromans and Vanderschuren, 1995). The long-term distributions of H_{mp} and C_{mp} are then fitted to Pareto distributions. Finally,

the convolutions of the short- and long-term distributions give the complete long-term distributions of H_{max} and C_{max} (Tromans and Vanderschuren, 1995; ISO 2015).

Note the Tromans and Vanderschuren (1995) method described above can fail to find associated H_{max}, or C_{max} (typically when the selected H_s storm events are small and distributed within a narrow H_s range). In such cases, the standard conventional value of H_{max} = 1.86 H_s (assuming Rayleigh distribution of individual wave heights) and C_{max} = 1.05 H_s (HSE, 2002) are adopted.

Note an arbitrary minimum number of 10 storm peaks has been chosen for reliable distribution fitting. This resulted in specific directional return period values being omitted.

The still water elevation (i.e. combined tidal level and storm surge) return period values are estimated by fitting a Weibull distribution to the empirical distribution obtained by combining the frequency distribution of tidal and surge elevations, recommended by ISO (2015).